REPORT NO.
UCB/EERC-79/23
SEPTEMBER 1979

EARTHQUAKE ENGINEERING RESEARCH CENTER

SHAKING TABLE STUDY OF SINGLE-STORY MASONRY HOUSES VOLUME 1: TEST STRUCTURES 1 and 2

by

POLAT GÜLKAN
RONALD L. MAYES
RAY W. CLOUGH

Report to Department of Housing and Urban Development

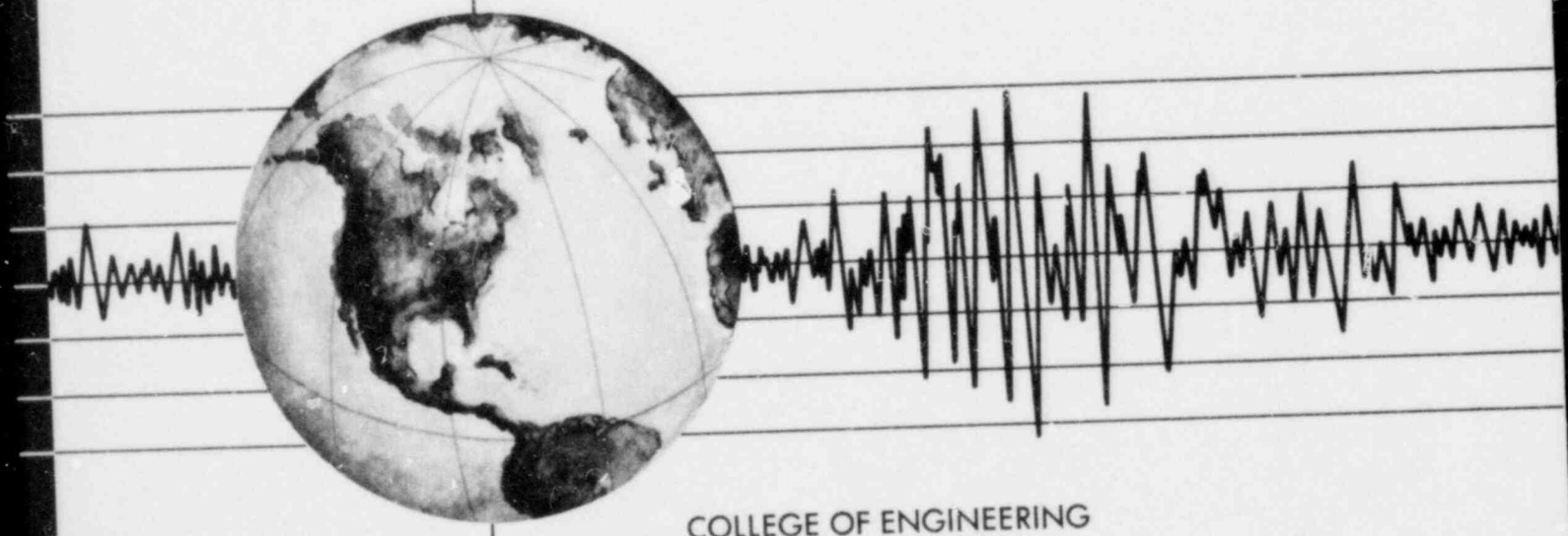

COLLEGE OF ENGINEERING
UNIVERSITY OF CALIFORNIA · Berkeley, California

SHAKING TABLE STUDY OF SINGLE-STORY MASONRY HOUSES

VOLUME 1: TEST STRUCTURES 1 AND 2

by

Polat Gülkan
Ronald L. Mayes
Ray W. Clough

Report to

Department of Housing and Urban Development

Report No. UCB/EERC-79/23
Earthquake Engineering Research Center
College of Engineering
University of California
Berkeley, California

September, 1979

ABSTRACT

Earthquake damage to masonry construction during recent years underscores the need for a better understanding of the seismic response of these structures, and the establishment of rational reinforcement requirements. An experimental investigation aimed at determining reinforcement requirements for single-story masonry dwellings in Uniform Building Code Seismic Zone 2 areas of the United States has been completed at the University of California, Berkeley. The experimental results of the investigation are presented in Volumes 1 and 2 of a series of three reports, while Volume 3 contains conclusions from the tests as well as recommendations for reinforcement requirements for masonry houses based on realistic seismic conditions for Zone 2.

The overall study included the testing of four masonry houses, with both unreinforced and partially reinforced wall panels, assembled to form 16 ft square models of typical masonry houses. The masonry units utilized in the construction of all test structures were full-sized units. Each house was provided with a timber truss roof structure to which weights were attached so as to obtain realistic loads on the bearing walls.

Methods, models and test facilities utilized in the study are described. A detailed description of the measured response of each test structure is provided, and a quantitative assessment of parameters affecting the response is presented, in this volume for Houses 1 and 2, and in Volume 2 for Houses 3 and 4.

The tests show that partially reinforced walls demonstrate excellent behavior under all levels of base excitation applied during the tests.

ACKNOWLEDGMENTS

The investigation described in this report is part of a research program entitled "Laboratory Studies of the Seismic Behavior of Single-Story Masonry Buildings in Seismic Zone 2 of the U.S.A.", sponsored by the Department of Housing and Urban Development under Contract No. H2387. The authors would like to acknowledge the support they have received from HUD which made the study possible. The concrete block units were donated by the California Concrete Masonry Technical Committee, and are gratefully acknowledged. D.A. Sullivan Co. fabricated the masonry walls. Planning and implementation of the tests were carried out with the suggestions of the Applied Technology Council (ATC) Advisory Panel consisting of J. Gervasio, J. Kesler, O.C. Mann, L. Pritchard and R.L. Sharpe; and ATC's subcontractor R.D. Benson. The government technical representatives on the project were R. Moroney and the late W. J. Werner. Additional coordination with the Department of HUD was provided by L. Chang and A. Gerich. W.L. Dickey, consulting engineer, was present during all experiments and offered numerous helpful suggestions and background information. Student assistants P. Buscovich and T. Nearn did the laboratory work, D. Steere implemented the data acquisition setup in addition to running the earthquake simulator, and the personnel of the Structural Research Laboratory headed by I. Van Asten contributed to every phase of the experimental work. Initial phases of the study were done under the supervision of Y. Omote and R. Hendrickson.

The drafting was done by G. Feazell, and the typing by Shirley Edwards. The authors also wish to thank B. Bolt who reviewed the text and offered valuable editorial suggestions.

TABLE OF CONTENTS

LIST OF TABLES

LIST OF FIGURES

1. INTRODUCTION

1.1 Background

The investigation described in this report is a major part of a research program entitled "Laboratory Studies of the Seismic Behavior of Single-Story Residential Masonry Buildings in Seismic Zone 2 of the U.S.A.", which has been in progress at the Earthquake Engineering Research Center (EERC) of the University of California in Berkeley since April 1976. The study was undertaken to evaluate U.S. Department of Housing and Urban Development (HUD) criteria for single-story masonry dwellings in Seismic Zone 2 areas of the Uniform Building Code (UBC).

The HUD Minimum Property Standards (MPS) for housing apply to dwellings containing one or two living units, and to the sites upon which they are located. The buildings may be detached, semi-detached, duplex or row houses. They may be site built or factory produced. Several purposes of the MPS in housing construction are cited in the MPS Introductory Statement as follows:

(1) To combine the diverse standards for mortgage insurance financing of private housing with those for low rent public housing into a single set of unified standards;

(2) To update the various minimum property standards and related guide material following a careful review and analysis of past provisions;

(3) To provide improved design and construction standards based more on performance than has been true in the past, with appropriate flexibility to meet local conditions;

(4) To encourage design innovations and improved building technologies giving promise of increased quality and reduced costs; and

(5) To aid national and local efforts being made to improve the environmental factors of urban areas.

The MPS are considered essentially minimum requirements in housing and design and construction. Consequently, where local codes or requirements permit lower standards than the MPS, the latter shall apply. However, all housing construction must comply with local ordinances, codes and regulations in addition to the MPS. This is required for all housing financed under HUD mortgage insurance programs.

The promulgation of "Local Acceptable Standard No. 2", dated August 1974, by the HUD Phoenix, Arizona office was questioned by individuals associated with the local industry on the grounds that compliance with its requirements would lead to increased costs and unnecessarily high factors of safety for earthquake loads. To address this question, the research program undertaken at the request of HUD was designed to yield information in the following areas:

(1) The dynamic behavior of simple masonry structures constructed with full-scale components when subjected to simulated earthquake motions;

(2) Reinforcement requirements, if any, for adequate out-of-plane and in-plane resistance of typical masonry housing construction for the level of seismic activity expected in UBC Zone 2 areas of the U.S.;

(3) Adequacy of typical roof connection details of masonry housing construction in withstanding the forces developed during earthquakes.

The third item above has been discussed in reference (1). This report contains results of simulated earthquake tests on two test specimens which formed the first phase of the program for items 1 and 2. The entire test program involved a total of four different test structures. The results for the next two test specimens and the final recommendations will be presented in future reports.

1.2 Current Design Codes and Construction Practices for Masonry Dwellings

In many regions, local building codes provide the governing regulations for the design and construction of houses. These are based on local requirements and environmental conditions. For instance, the Phoenix Building Code emphasizes wind-resistant construction details for dwellings. These are based on recommendations by the Residential Construction Committee of Structural Engineers Association of Arizona and the revised code regulation of Section 2802.6. The impetus for this major revision of the code requirements for wind resistance stemmed from extensive damage to homes in the Phoenix metropolitan area in 1972 and 1973.

The Uniform Building Code (UBC) provides most of the basic regulations for local building codes in the western states. As noted in the previous section, for homes financed under the mortgage insurance programs of the Department of Housing and Urban Development, the design and construction details must also comply with the HUD Minimum Property Standards (MPS) if these are more stringent than the local codes.

Generally the details of masonry construction, i.e. masonry units, mortar, grout, joint connections, bond patterns, splices for reinforcements, high or low-lift grouted construction, etc., are controlled by UBC, MPS or other building code requirements. To ensure that these regulations are complied with, local building authorities administer field inspections which occur at several different phases depending on the size of the project and the complexity of the design. Unless otherwise indicated, only specific items of work mentioned in the requirement need be inspected. As applicable, the requirement typically involves checking to see if materials are as specified; to see that materials are combined as specified; that specified procedures are followed; that proper sizes are used; that tolerances are maintained; and in general, that the quality of workmanship and details of construction are as specified.

Special inspections are required for other cases which may include the following:

(1) Examination of materials and/or material certifications for compliance,

(2) Observation of the bonding of units in the walls between wythes and at corners and intersections.

(3) The proper placement of reinforcement, including splices, holding reinforcement in place and clearances,

(4) Inspection of grout spaces immediately prior to grouting including the removal of mortar fins, dirt and debris, and conditions at the bottom of the grout space,

(5) Observation of grout placement with special attention to procedures to obtain complete filling of required spaces, avoidance of segregation, and proper consolidation.

The analysis and design of reinforced masonry systems have traditionally been by the working stress method. This procedure is comparable to the design of reinforced concrete systems because both materials are heterogeneous, and have low tensile strength.

In the working stress method the limits of allowable stress for the material are based on the properties of the material. Assumed design earthquake and wind forces are determined by local building codes or the MPS. The flexural and shear stresses are then checked for all structural elements. The minimum wall thickness and reinforcement are then determined. After each of the individual structural elements is designed, the total structure must be checked and designed for lateral seismic or wind forces. Construction details including roof connections, footing connections, etc., must be designed to satisfy the lateral forces.

In some areas of the United States the design of single-family masonry dwellings is governed by lateral forces due to wind. Local conditions may allow the use of partially reinforced masonry walls which are basically designed as unreinforced masonry, and the masonry and mortar joints are assumed to resist the tensile forces. The minimum reinforcement for partially reinforced masonry structures is specified by the local code. For fully reinforced masonry walls the minimum area of reinforcement is obtained either by design or by minimum code provisions, whichever is larger. Frequently in the design of single-family masonry houses the minimum reinforcement requirement is governed by code provisions.

Commonly each house is designed by an architect. The use of a structural engineer depends upon the complexity of the design. Whenever a structural engineer is not engaged for the design, minimum reinforcement requirements provided in local building codes or MPS are followed. In many cases of subdivision development, a house design may be used repeatedly for several dwellings in the same project. Quite often this repeated house receives a more careful structural analysis and design. For a repetitive basis project under the HUD mortgage insurance program, variations of design and planning standards or construction methods and materials demonstrating equivalency are approved by the HUD field office through the regional office and finally by the HUD central office.

1.3 Object and Scope

Current design provisions for masonry construction are derived from experimental data obtained mainly from static, monotonically conducted experiments on masonry components and accumulation of long experience, collective judgment and concensus of code writing bodies. These provisions are particularly stringent where they apply to lateral load conditions since the lateral load performance of unreinforced or inadequately reinforced masonry construction has, in the past, been inadequate. Although there have been notable instances of masonry construction behaving quite well under earthquake conditions, significant amounts of damage and loss of life have been associated with failure of unreinforced masonry.

The overall objective of this phase of the investigation was to subject components of typical masonry houses to carefully controlled simulated earthquakes and to observe their structural behavior. Both

partially reinforced and unreinforced wall panels, fabricated using 6x4x16 in. hollow concrete masonry units, were tested. This report presents a discussion of the results obtained from the first two test specimens of the program which in total consisted of testing four specimens. Both test specimens measured 16x16 ft in plan and had 8 ft 8 in. high walls. In addition to varying the basic geometry and amounts of reinforcement in the panels, the effects of roof truss orientation, base fixity conditions and repairs between tests were considered. The houses were subjected to three different simulated earthquakes the intensity of which (measured in terms of peak base acceleration) varied by as much as an order of magnitude.

In the following two chapters, a description of the material properties of the test specimens, procedures and instrumentation details is provided. Chapter 4 presents an overview of the test facility and provides a brief background for earthquake simulation. Selected results from the earthquake simulator experiments are presented in Chapter 5. The interpretation of test results and the analytical approach for predicting the strength of out-of-plane and in-plane walls are given in Chapter 6. Conclusions and a summary of findings constitute Chapter 7. Two additional reports will contain results obtained from the remaining two test specimens and recommendations regarding reinforcement requirements for simple masonry houses.

1.4 Literature Survey

Although it is not within the purview of this section to present a comprehensive and detailed summary of all related work, an overview of some relevant research will be provided. In recent years, because of a renewed surge of interest in masonry construction particularly as it relates to earthquake resistant construction, several literature

surveys have been published [2,3,4,5]. A frequent concensus of such overviews is that although masonry has been used for millenia its development has evolved more from an intuitive basis than a purely scientific one. The lack of a strong centralized organization for masonry research and development (as has been the case for concrete and steel, for example,) has caused the introduction of contradictory and sometimes overly cautious requirements in building codes and regulations. The generally poor earthquake resistance of masonry structures, abetted no doubt by an awareness that "field" conditions are liable to be very uneven, has resulted in the application of wider margins of safety for masonry construction. Even so, there are many cases where the trend towards increasing conservatism concerning earthquake requirements for masonry structures may be justifiable, particularly for medium to high rise buildings[6].

The development of a rational basis for earthquake response analysis of masonry structures has begun to receive increasing attention from research organizations, as indicated in references (7) and (4). The masonry industry is actually quite young in the field of "rational design". The first completely rational design procedure in the United States dates back to 1966[8] and it was, as it still is, a working stress design. Other design procedures currently in use,such as the Uniform Building Code and the American National Standards Institute (ANSI) Codes for unreinforced or reinforced masonry construction,contain a good many empirical requirements. Although efforts are currently under way to bring masonry design procedures to a rational basis [9,10], it appears that a substantial amount of research must yet be conducted before that can be accomplished.

Studies on the post-elastic cyclic behavior of masonry cantilever shear walls and piers have been performed by Williams[11], Meli[12], and Priestley and Bridgeman[13]. A major program designed to obtain a better understanding of the cyclic behavior of masonry piers is currently underway at the Berkeley[15,16] and the San Diego[8] Campuses of the University of California. These tests are directed toward providing a better basis for code requirements for multistory masonry buildings. A general procedure for computing the out-of-plane strength of masonry walls subjected to vertical compression has been presented in references (16) and (17), and is reviewed in reference (5). However, to date, no results are available on the structural performance of masonry buildings subjected to simulated earthquakes.

2. MATERIAL PROPERTIES

2.1 Introduction

The basic purpose of this study was to evaluate experimentally the seismic resistance of masonry dwellings with construction details typically used in less active seismic regions of the United States. As stated earlier, no experimental study has been reported to date for masonry structures or components subjected to simulated earthquakes, although the inadequate seismic resistance of poorly designed or constructed masonry buildings has traditionally been given heavy emphasis in post-earthquake survey reports. During the planning phase of this investigation, the primary objective was to define structures which were simple in concept and yet contained the most significant components, such as wall panels with or without openings, corners and wall-footing and roof-wall connections. Because the main objective was to determine the minimum reinforcement requirements for Seismic Zone 2, no attempt was undertaken to include a large array of variables in the test specimens. Hence both house models were made from the same type of block, and the same roof structure was used for both. In this chapter, the material properties are described. Test specimens, procedures, and instrumentation are discussed in the next chapter.

2.2 Materials

All materials used in the construction of the test specimens are commercially available and are typical of those commonly used in building construction in Arizona.

2.2.1 Concrete Block Units

The concrete block units were two-core hollow block with nominal dimensions of 6x4x16 in.* The units are shown in Fig. 2.1 and their dimensions and other physical properties are listed in Table 2.1. Two different shapes of hollow units were used in both specimens. In House 1 corner return units were used in the corner walls in addition to the standard units that were also used for House 2. A number of open end units were used in House 2 since the manufacturer could not supply regular blocks at the time of construction. However, all units were mortared across the face shells in the head joints so that the use of open end blocks produced no detrimental effects on strength. Whenever a given course called for a half unit, standard units were cut in two.

2.2.2 Mortar

The mortar used in both test specimens was specified as type S mortar, proportioned in accordance with the specifications of ASTM C 270[18]. Type I Portland cement, (ASTM C 150)[19], Type S hydrated lime, (ASTM C 207)[20], and sand were proportioned 1:1/2:4½ by volume and mixed in a motor-driven mixer with blades rotating in a horizontal axis. The construction of the wall panels and the control prisms typically took one working week and required the mixing of more than one batch of mortar. For each batch, two mortar samples were taken in 2x4 in. cylinders and air cured in the laboratory under the same conditions as the wall panels. The mortar cylinders for both houses were tested at 29 days. Compressive strengths of the mortar samples are given in Table 2.2. Although the average strength of mortar for

---

*At the present, the international system of units has made no inroads into the masonry industry of the United States. For consistency, the traditional British units are used throughout this report.

House 1 is what one would expect to find in good quality field workmanship conditions, the high strength obtained for House 2 is not typical. Also, since several batches of mortar were required during the construction of the walls, mortar strength probably varied at different levels in the walls as well as between different wall panels of the same house.

2.2.3 Grout

For both test specimens fine grout was used in the partially reinforced wall panels. This consisted of 1 part Type I cement and 3 parts top sand mixed with water to achieve the required consistency. Control specimens of grout were cast inside the cells of the concrete blocks placed on a non-absorbent base, and stored in the laboratory under the same conditions as the wall panels. The compressive strength of grout was determined by cutting the filled cells into 2 in. cubes which were then tested in a standard testing machine. Average compressive strengths for the grout in the two house models are indicated in Table 2.2; the minimum acceptable strength requirement of 2,000 psi was met for both houses.

2.2.4 Reinforcement

Both houses had panels which were partially reinforced with #4 bars. The reinforcement used in House 1 had average yield and ultimate strengths of 54,000 and 80,000 psi, respectively. The corresponding values for House 2 were 59,250 and 86,000 psi. In each case the figures are averages determined from three bar specimens. No attempt was made to obtain additional mechanical properties of the reinforcement, because there was no indication that stress levels in the reinforcement were significant in determining structural response.

2.2.5 Joint Reinforcement

The top two bed joints of each wall and corner unit of House 1 were reinforced with 9-gage wire joint reinforcement which was of a continuous truss design and consisted of two parallel longitudinal wires, 5.5 in. apart, welded to a continuous, diagonally-folded cross wire. Joint reinforcement was omitted from House 2.

2.2.6 Prisms

Test prisms and wall panels for the houses were fabricated in the same laboratory using similar construction methods and workmanship. For each house specimen, a number of control prisms were fabricated with the same nominal cross-sectional dimensions as the masonry units. All prisms were constructed in stacked bond and tested according to ASTM E 447[21] requirements. The results obtained from the prism tests are listed in Table 2.3. For these values, no corrections have been made to consider the effects of the so-called "h/t" ratios[22].

2.2.7 Shear Strength

It is commonly agreed that shear failure may be initiated in masonry assemblages when the principal tensile stress reaches a critical value. In reference (3), a critical review is presented to evaluate the current methods for shear strength determination. For both test specimens, a number of 4x4 ft square panels constructed with the remaining control prisms were tested in diagonal compression. The so-called critical tensile strength, after Blume and Proulx[23], is determined from the equation

$$\sigma_{tcr} = \sqrt{2.424\tau^2 + \left(\frac{\sigma_c}{2}\right)^2} - \left(\frac{\sigma_c}{2} + 0.823\tau\right) \qquad (2.1)$$

where

$$\tau = 0.707 \frac{P}{A} \qquad (2.2)$$

and

P = maximum diagonal compressive load

σ_c = compressive stress on square panel (equal to zero in the present case)

A = net cross-sectional area of panel.

In Table 2.4 a summary of the indicated critical tensile strengths is presented for both houses. The lower mortar strength of the first house as well as the lower quality of its blocks is reflected in the entries of this table. The correlation between index values such as the critical tensile stress and the strength of masonry assemblage is a subject of current investigation. Consequently, the values in Table 2.4 should be judged on a comparative basis rather than as absolute values for the estimation of maximum lateral forces on full-scale masonry elements. Further reference will be made to Eq. (2.1) in Chapter 6.

2.2.8 Roof Components

The truss roof structure used in the testing of both house specimens consisted of nine pre-made grade 1 Douglas Fir trusses with a span of 16 ft (plus 1 ft overhangs on either side) at a slope of 4:12. Joints for the 2x4 in. truss elements were made by pressing metal plate fasteners on either side of the joints. The design load for the roof was taken as 125 psf when the distance between the trusses was 2 ft. Roof sheathing consisted of 1/2 in. thick plywood (grade CD-X) nailed to the sloping edges of the trusses with 6d-nails

at 8 in. spacing at the edges of the sheets and 12 in. spacing at intermediate locations. The plywood sheets were staggered at the roof surface so that there would be no "weak planes" to reduce diaphragm stiffness.

The trusses were toe-nailed at a spacing of 2 ft to a single 2x6 in. top plate (Douglas Fir select structural grade) with three 16d-nails at either end. Additionally, every other truss was attached to the top plate with a proprietary metal framing anchor. The two trusses at the gable ends of the roof directly above the non-bearing walls were connected to the top plate by three 1 ft long 2x4 in. blocks. These boards were symmetrically placed and then nailed down into the top plate by four 16d-nails in contact with the inside edge of the bottom rafters of the two trusses. Three 16d-nails were then driven horizontally through the bottom rafter into the boards to complete the attachment. Strength and cyclic behavior of these connections are contained in reference (1). Connection of the plates to the wall was achieved by means of 10½ in. long 5/8 in. diameter anchor bolts embedded 8 in. into the masonry and used in conjunction with 3x3x1/4 in. plate washers.

Standard 1/2 in. thick drywall sheets were nailed to the lower edge of the bottom chords of the trusses using "dry tite" nails to form the "ceiling" of the house. No quality control tests were conducted on the items which formed the roof.

TABLE 2.1

DIMENSIONS AND PHYSICAL PROPERTIES OF CONCRETE MASONRY UNITS[a]

House Unit	Width in.	Height in.	Length in.	Minimum Thickness, in.		Gross Area $in.^2$	Net Area Percent	Compressive Strength, psi		Oven Dry Weight lb	Concrete Weight lb/cu ft
				Face Shell	Web			Gross Area	Net Area		
1	5.61	3.62	15.60	1.37	1.50	87.5	64	980	1,530	10.9	92.9
2[b]	5.60	3.62	15.60	1.12	1.12	87.4	56	1,110	1,983	11.0	107.3

(a) Concrete masonry units were tested in accordance with appropriate UBC requirements. Each value in the table represents the average of results from five specimens.

(b) Open end units are excluded from this listing.

TABLE 2.2

COMPRESSIVE STRENGTH OF MORTAR CYLINDERS AND GROUT CUBES

House Unit	Mortar			Grout		
	Number of Specimens	Age Days	Compressive Strength, psi	Number of Specimens	Age Days	Compressive Strength, psi
1	6	29	2,650	3	43	6,300
2	6	29	4,730	3	41	3,360

TABLE 2.3

SUMMARY OF VERTICAL COMPRESSION TESTS OF HOLLOW BLOCK PRISMS

House Unit	Nominal Height, in.	Prism No.	Age Days	Maximum Load, lb	Compressive Strength[(a)], psi
1	16	1	28	76,000	1,350
		2	28	72,600	1,300
					Avg. = 1,325
	24	1	29	51,700	920
		2	29	64,200	1,140
					Avg. = 1,030
	40	1	28	56,200	1,000
		2	28	54,800	970
					Avg. = 985
2	8	1	79	110,000	2,247
		2	79	84,000	1,716
		3	79	106,400	2,174
		4	79	87,800	1,794
					Avg. = 1,983
	40	1	78	105,000	2,145
		2	78	124,500	2,544
		3	78	103,500	2,115
		4	78	95,000	1,941
					Avg. = 2,186

(a) Based on net area of hollow concrete block units.

TABLE 2.4

SUMMARY OF DIAGONAL COMPRESSION TESTS OF SQUARE HOLLOW BLOCK PANELS

House Unit	Panel No.	Age Days	Maximum Load, lb	Critical Tensile Strength, psi [a]
1	1	28	13,000	57.8
	2	28	32,000	142.2
	3 [b]	28	18,500	82.2
	4 [b]	28	33,600	149.3
				Avg. = 107.9
2	1	80	54,000	286.3
	2	80	47,300	250.8
	3	80	53,600	284.7
	4	80	63,000	334.
				Avg. = 288.8

(a) Based on Eq. (2.1) and net area of hollow concrete block units.

(b) End cells grouted

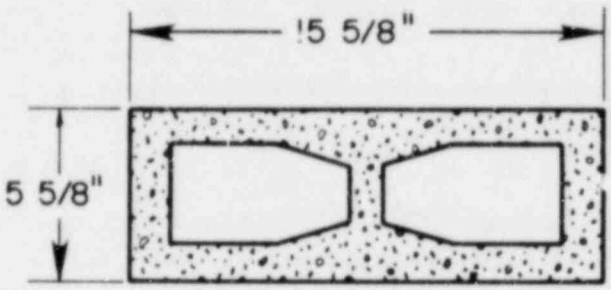

STANDARD UNIT
HOUSES I AND 2

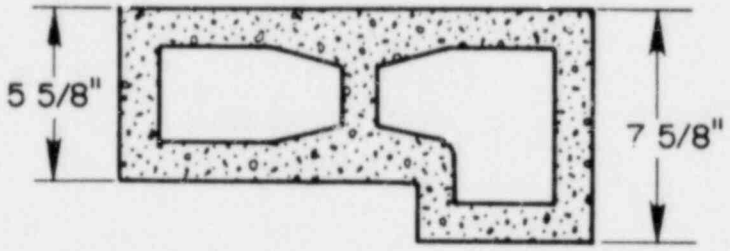

CORNER RETURN UNIT
HOUSE I

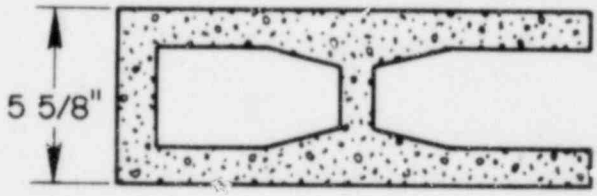

OPEN END UNIT
HOUSE 2

FIGURE 2.1 MASONRY UNITS

3. TEST SPECIMENS, PROCEDURES AND INSTRUMENTATION

3.1 Description of the Test Structures

The first test structure was viewed as an exploratory test for observing the behavior of masonry buildings under realistic earthquake loads. The requirement of including typical components of a masonry house and the shaking table size limitation resulted in the design and fabrication of the structure shown in Fig. 3.1. The specimen consisted of four 8 ft long wall panels designated as W1, W2, W3, and W4 and four L-shaped corner units designated as C1, C2, C3, and C4. Wall panels W1 and W2 and corner units C1 and C3 were partially reinforced. In the walls, partial reinforcement consisted of two #4 bars (area 0.2 sq in.) placed in the end cells. For the corners, three similar bars were located as shown in Fig. 3.1. Similar walls or corners were placed at right angles to one another so that under the uniaxial motion of the shaking table,both in-plane and out-of-plane behavior could be determined simultaneously. All reinforcement was lapped into 20 in. long dowels embedded in the 7½x16 in. footings. The horizontal translation and rotation of each individual wall footing could be controlled through a specially designed attachment system (Fig. 3.1). The system consisted of three 4 ft long 1½x5½ in. flat bars placed in matching grooves on the bottom side of the 8 ft 8 in. long footings at a spacing of 3 ft. The bars were stressed to the surface of the shaking table by high strength rods. The footings could then be bolted to the flat bars by 3/4 in. diameter bolts through holes in the footings on either side of the walls. To increase the resistance against translation of the footings, particularly underneath the out-of-plane walls W2 and W4, angles snugly fitted against either side of the footing were

also bolted to the flat bars. With the 3/4 in. bolts loose, the angles provided resistance against translation but some rotation could take place.

With the angles loose but bolts tightened, the rotation of the footings was greatly reduced. It is difficult to quantify how much foundation flexibility actual masonry structures have. At the beginning of the testing program only footing translations of the walls were prevented. During later stages the footings of the in-plane walls W1 and W3 were bolted to prevent the uplift observed at these footings. Out-of-plane walls W2 and W4 were, however, left free to rotate at the footing level at all times on the assumption that this more closely approximated actual site conditions. The footings under all four corner units were prestressed against the table during the entire testing sequence. In Fig. 3.2 the attachment details of the footing are shown before the angles were attached.

For House 1, the roof was anchored to the masonry components by means of three symmetrically placed bolts in the wall panels and the corner units. The overall structural integrity was provided by the diaphragm action of the roof assembly; this system was probably stiffer in the vertical direction than a full-size house roof because of its shorter span.

Because of the small area of the roof system in the test structure, it was necessary to add weight to it to simulate the shear forces generated during earthquake excitation. The criterion used to determine the additional weight was the dead load per foot of wall support length; i.e. the dead weight per unit length of wall should be similar in both the model and the prototype house. Assuming a prototype total roof load of 20 psf and a house with roof trusses spanning 48 ft the

dead load per unit length of the bearing walls, ignoring openings, would be 480 lb/ft. To achieve a similar dead load per unit length of wall in the test specimens the roof weight had to be approximately 15,000 lb. As the roof structure only weighed 3,000 lb six concrete slabs with a combined weight of 12,000 lb were bolted on top of the roof plywood sheathing during the simulated earthquake tests for both houses. An implication of this model scaling is that for the same acceleration at the roof level for both model and prototype similar nominal shear stress would be obtained in the panels. However, because wall heights were not reduced in the model structure (8 ft 8 in.) overturning effects were slightly amplified because the center of gravity of the concrete slabs was nearly 12 ft above the shaking table. A quantitative assessment of the effect of overturning will be made in Chapter 6.

Compared with current masonry dwelling construction practice, the geometry of the first test specimen shown in Fig. 3.1 was a great simplification. Depending on development preferences and architectural requirements, there are a large number of possible configurations for masonry dwellings which could be adopted for testing. After considerable consultation with professional engineers and home developers in Arizona where 6 in. concrete block is widely used, it was decided to adopt the configuration shown in Fig. 3.3 for the second house of the test series. This specimen consisted of four independent wall panels which contained either a door and a window opening designated as A(in-plane) and A1(out-of-plane) or a single large door opening designated as B and B1, placed parallel and transverse to the table motion. The in-plane walls were 16 ft in length, and the out-of-plane walls were 14 ft long. Walls with similar geometry were again placed

at right angles to one another so that both in-plane and out-of-plane types of behavior could be observed simultaneously. As seen in Fig. 3.3, minor changes were made in the dimensions of walls A1 and B1 to obtain overall lengths within multiples of the half block dimension of 8 in.

Walls A and A1 were unreinforced. The lintels above the doors and the windows consisted of double angles ($2\frac{1}{2}$x$2\frac{1}{2}$x3/16 in. for the doors and 3x$2\frac{1}{2}$x3/16 in. with the long sides up for the windows) with an end bearing of 4 in. on either side. Partial reinforcement for walls B and B1 consisted of one #4 bar placed in each end cell. The lintel beam for the large opening in either panel consisted of a W6x8.5 section for which the top flange was trimmed to a width of $2\frac{1}{2}$ in. and a 5x1/8 in. plate was welded underneath the bottom flange. End bearing for these beams was 6 in. on both sides. The masonry units placed around all lintel beams were "slushed" solidly with mortar. Footings for all wall panels measured $7\frac{1}{2}$x16 in. in cross-section, and were bolted to the shaking table at two points 5 ft from either end of the in-plane walls and 4 ft from the ends of the out-of-plane walls.

Corner units were not included in this house model in order to avoid the interaction of in-plane and out-of-plane walls. To the extent possible, the wall elements were designed to represent the center parts of longer panels in a prototype structure. The same roof structure used in testing House 1 was used again to provide the diaphragm action through which the panels were forced to behave as an assembly rather than as separate components. Each panel had five anchor bolts for attachment of the timber plate, spaced at about 3 ft and staggered so that roof trusses would not interfere with their being tightened.

Figure 3.4 shows the second house specimen placed on the shaking table and ready for testing.

3.2 Fabrication of House Models

House 1 was constructed and air cured outside the laboratory area. Although there were the normal daily variations in temperature and relative humidity conditions, no rain was recorded during the 52 days it was stored outside.

Because of difficulty in transporting unreinforced wall panels from the construction area to the earthquake simulator, it was decided to fabricate the second and later specimens in the same laboratory as the shaking table. This practice also served to protect the specimens from extreme variations in weather conditions and reduced the likelihood of cracking the fragile components. All specimens were constructed by the same experienced mason/contractor using practices of good workmanship and supervision. Mortar joints were carefully tooled on both faces of all the walls and the control prisms. All walls for both specimens were laid in running bond with mortar across the face shells only, except for cells where grouting would be done for which the webs also were mortared. Grouting was done several days after the completion of walls so that the mortar would be able to withstand the hydrostatic pressure at the lower corners. The height of the mortar joints was carefully controlled so that all panels would be within acceptable limits of the required 8 ft 8 in. panel height.

3.3 Test Procedure and Instrumentation

The primary research tool used in this investigation was the Earthquake Simulator Facility of the University of California, Berkeley. The test facility and its capabilities are described in greater detail

in Chapter 4. Both test houses discussed in this report were subjected to a series of single horizontal component base motions which varied in intensity from just barely perceptible (peak base acceleration less than 0.05 g) to extremely severe (in which the base acceleration exceeded 0.5 g). Three different types of earthquakes were simulated within this spectrum of intensities. These were the N-S component of the 1940 El Centro, S69E component of the 1952 Kern County (Taft), and the S74W component of the 1971 San Fernando earthquake recorded at Pacoima Dam.

During erection the walls or corner panels which comprised a given house specimen were subjected to compressive forces by means of externally applied prestressing rods so that slight out of plumb conditions or bumps would not cause cracks. Once the footing was placed on the shaking table and lined up with the anchor rod locations, perfect vertical and horizontal alignment was assured by inserting wedges at the bottom side of the footings as needed, and then filling the empty spaces with a quick-setting gypsum compound. The roof structure, without the added weights which were attached later, was then carefully lowered on the wall segments to mark the anchor bolt location on the top plates. These bolt holes were drilled anew for each house specimen. After the roof was set in place, the anchor bolts were tightened with 3x3x1/4 in. washer plates. Next, the concrete slab weights were lowered to their locations on the roof. These were attached to the plywood sheathing through 1x6 in. metal bands which straddled the entire roof width on either side of the ridge line (see Figs. 3.5, 3.6). No slip was observed between the concrete slabs and the roof sheathing during any test.

The response of the test structure was measured by means of an array of displacement or acceleration measuring devices. Displacements were monitored with either direct current displacement transducers (DCDTs, or potentiometers, and accelerations with either strain gage or force-balance type accelerometers. The ranges of the transducers were selected so that the signal would not be saturated at the maximum expected response peak. In Figs. 3.5 and 3.6, the instrument locations for Houses 1 and 2 are shown in an isometric view of the corresponding specimen. Appendix A provides a complete listing of the transducer channels whose outputs were monitored through the recording system. The channel number of a given instrument listed in the Appendix matches the number in Fig. 3.5 or 3.6 so that the actual location can be visualized. The concrete block pattern indicated in each diagram is exact; therefore, given the nominal dimensions of the blocks, the exact coordinates of all transducers can be determined from these figures. Further references will be made to these locations in Chapter 5 which presents a discussion of the measured responses.

Displacements of the structures relative to the shaking table were measured from the rigid octagonal reference frame, located inside the walls, which measured approximately 12 ft across. The frame was well braced, and when fully assembled it was extremely stiff. Its natural frequencies (around 30 Hz for the "first" mode), observed by free vibration tests and also predicted by dynamic analysis, were considerably higher than any significant response frequencies of the test structures. The presence of the braced frame inside the test models also provided a possible support for the concrete weights in case of structural failure, although this was a function which the frame was never called upon to perform.

The houses were tested under a wide spectrum of conditions. In addition to variations in the type and intensity of the applied base motions, the structure itself was modified by repairing cracks which formed during some of the tests. Repairs were made by plastering the affected masonry walls with a fiberglass based surface bonding mortar on both surfaces. The roof truss orientation also was changed in some tests and the base fixity of the footings of the in-plane walls was modified. A general description of the response is provided in Chapter 5.

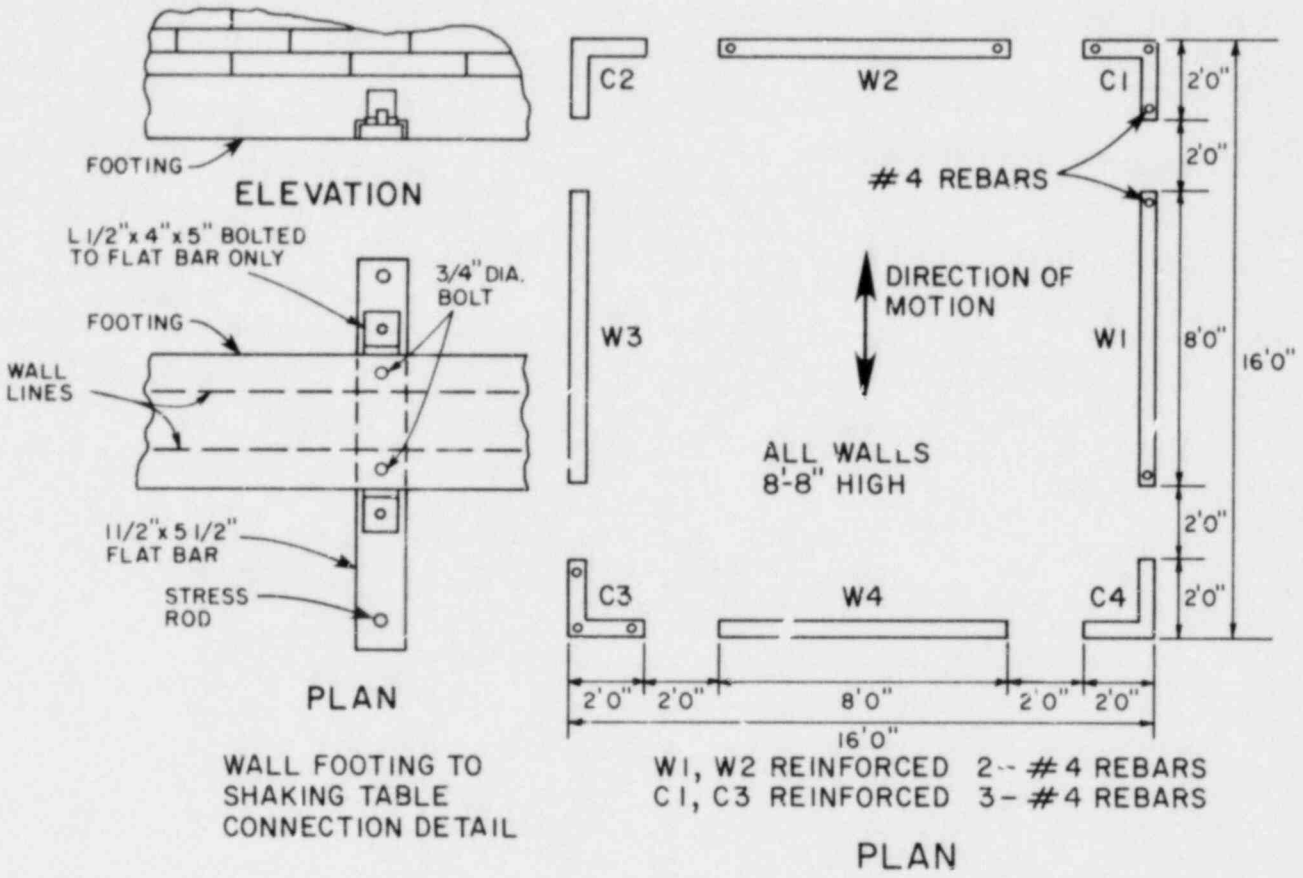

FIGURE 3.1 HOUSE 1

FIGURE 3.2 FOOTING CONNECTION DETAIL FOR HOUSE 1

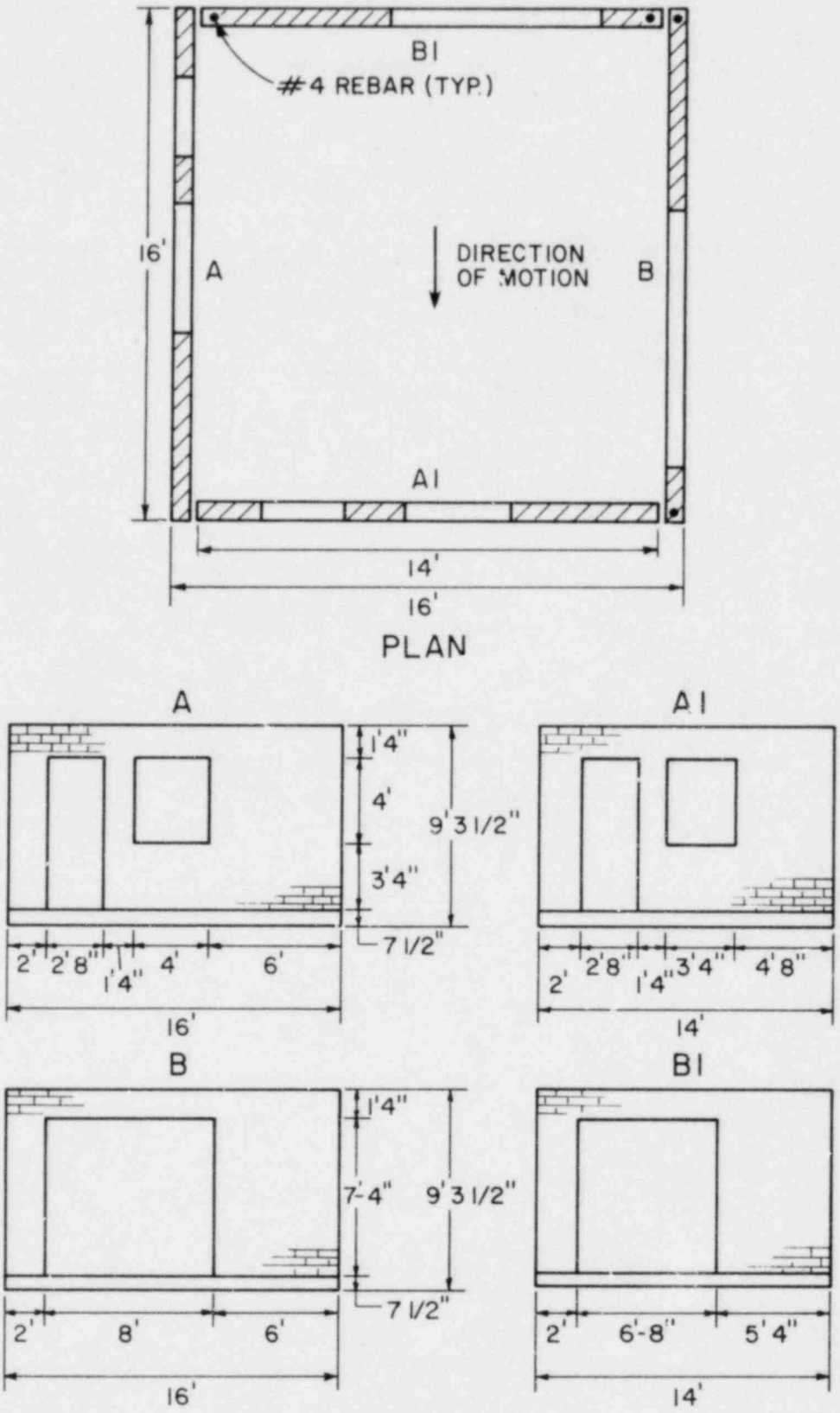

FIGURE 3.3 HOUSE 2

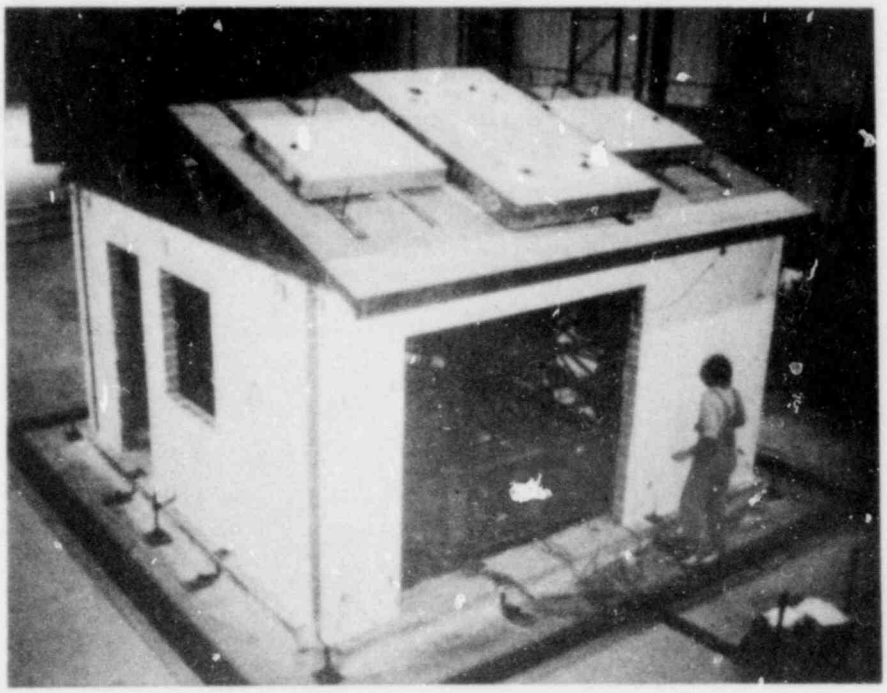

FIGURE 3.4 OVERALL VIEW OF HOUSE 2

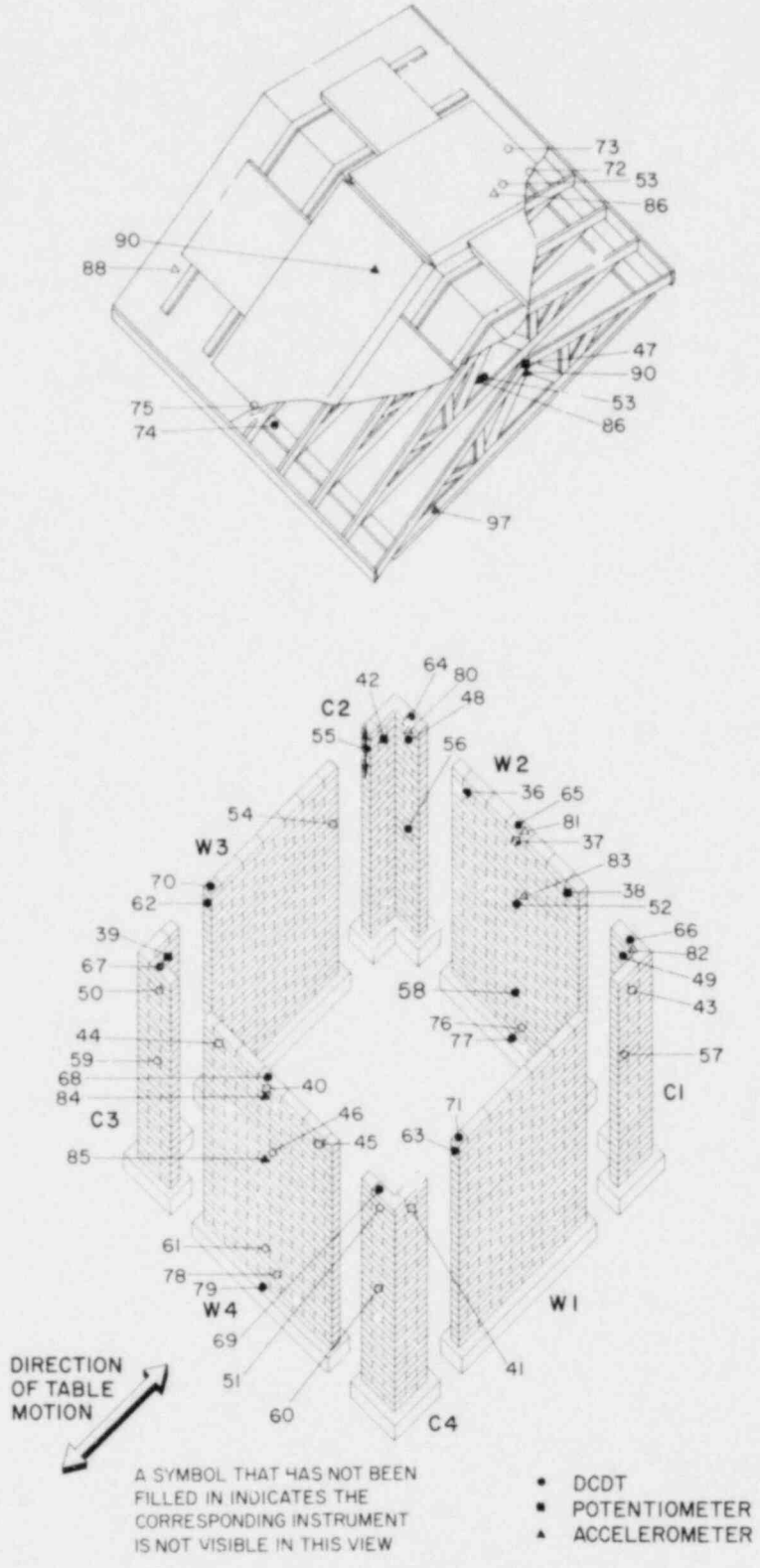

FIGURE 3.5 INSTRUMENTATION FOR HOUSE 1

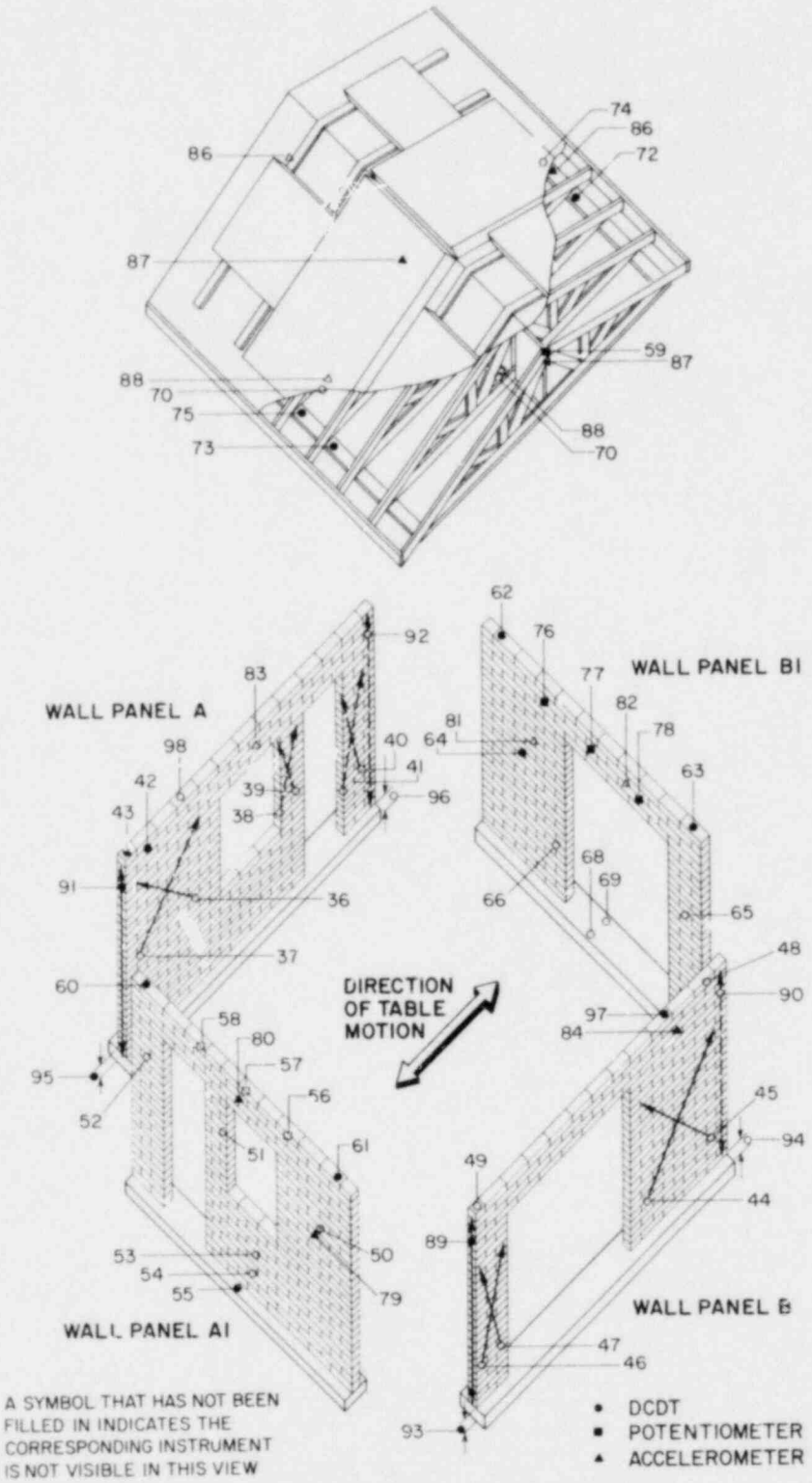

FIGURE 3.6 INSTRUMENTATION FOR HOUSE 2

4. TEST FACILITY

4.1 Earthquake Simulator

The Earthquake Simulator Laboratory is located at the Richmond Field Station of the University of California at Berkeley. The main part of the test facility is a 20x20 ft shaking table with associated control and data acquisition equipment. The system was designed by faculty and staff of the Department of Civil Engineering, and the hydraulic actuator and control systems were manufactured by MTS Corporation. Figure 4.1 shows the shaking table and the control room.

The shaking table is essentially a square concrete slab which is heavily reinforced and post-tensioned in both directions and has a dead weight of about 100,000 lb. It is supported by four vertical actuators in a concrete foundation pit (which resembles an open-top box) in such a manner that the top of the table is flush with the laboratory floor. In addition to the vertical actuators, three horizontal actuators provide motion in one horizontal direction. Vertical and horizontal motion can be imparted to the table separately or simultaneously. During operation the weight of the table plus that of the test structure it carries is supported by differential air pressure applied in the test pit. This relieves the vertical actuators of the static load carrying function and virtually eliminates all friction.

The table may be controlled to produce any desired motion. The usual procedure is to select an accelerogram recorded during some past earthquake, although "artificial" earthquakes or steady-state motions are also possible. In the case of earthquake motions, the digitized accelerogram is input to a mini-computer and passed through a

digital-to-analog converter. The resulting analog acceleration signal is then integrated electronically twice to obtain an analog displacement signal. This signal recorded on magnetic tape serves as input to the earthquake simulator and a feed-back system provides accurate control of actual table motion. The limits of table motion with zero payload are shown in Fig. 4.2 which also gives plan and elevation views of the table itself. The displacement limits arise from the actuator strokes; the velocity limits result from oil pumping capacity, the acceleration limits are controlled by the actuator force capacities and the frequency is limited by the oil column resonance of the drive system. With a full payload (110,000 lb) on the table, the acceleration limits will be reduced to 0.67 g and 0.45 g, respectively; the other limits are not affected significantly. Further details of the earthquake simulator characteristics are provided in reference (24).

4.2 Data Acquisition and Processing

The data acquisition system, centered on a NOVA 1200 minicomputer equipped with a Diablo 31 magnetic disk unit, is capable of sampling up to 128 channels at rates of up to 100 samples per second per channel. The analog signals from the various transducers pass through a NEFF System 620 Analog Digital processor. The digitized data are then temporarily stored on the magnetic disk before being transferred to tape for permanent storage by a Wang 9-track magnetic tape drive.

Some preliminary data reduction can be performed on the minicomputer but the bulk of subsequent data processing is done on the CDC 6400 system of the Berkeley Campus. In order to be compatible with the CDC system, the 9-track tapes are first scanned and the desired

information is converted to a 7-track tape form. Once reduced to this form, the data are generally converted into graphical display format utilizing the plotting facility coupled to the CDC system.

4.3 Repeatability and Accuracy of Simulated Earthquake Motions

Earthquake simulation in the laboratory can be defined as the process of moving, at prescribed rates of speed, the base of a test structure through a displacement program representing one or two components of a representative earthquake motion. The energy and control requirements for such an undertaking, as well as the cost of the structures, tend to limit the size of the test structure and the number of base motion components that can be applied to it. Although the first attempts at earthquake simulation were made at the turn of the century[25], the earthquake simulator has become a tool for structural research only within the last decade[26,27] because of its dependence on advanced technology in electronic controls, data acquisition and management. The first and most obvious question asked regarding any earthquake simulator concerns the quality of the earthquake motion it purports to reproduce. This quality can be judged on two grounds. The first is the fidelity of the motion to that of any past earthquake of which an analog record has been fed into the control devices of the facility. The second is the repeatability of the resulting motion at different prescribed levels of intensity, so that a given test structure can be subjected to a particular base motion at various intensity levels. Obviously, perfect quality is unattainable within current technological capability. Hence a compromise is necessary between what is attainable and what is acceptable.

As numerous subsequent diagrams will verify, the type of motion produced by the simulator does resemble real earthquakes. A visual

inspection of the different accelerograms generated by the shaking table reveals a high-frequency, low-amplitude "noise" at the leading and trailing portions of the average table acceleration. This is a characteristic feature of the system and is recorded by all measuring devices when the shaking table is fully pressurized and ready for operation. Generally such noise levels are low, and tend to remain below 0.5 percent of the recorded data peaks. A less apparent feature of the table motion is the "clipping" of long period displacements so that the table will not exceed the limits of the actuators. This tends to distort the resulting motions somewhat, but the distortion is not significant in the range of frequencies of the test structures considered here. Furthermore, the platform is a structure with six degrees of freedom so that it may execute small amplitude motions laterally as well as rotate about three perpendicular axes. Hence, although only the average motions are reported, it should be understood that motion may not be exactly the same at all points of the 20 ft square table.

If the premise is adopted that visual similarity between actual and reproduced earthquakes is a weak criterion for acceptance, the next step is to base judgment on the similarity of the response spectra for both. This is where repeatability enters as a parameter since in the laboratory environment there exists the capability of reproducing approximately the same wave form at different amplitudes and at different times. In this study, three different simulated earthquakes were run on the shaking table without time scaling. These motions will be referred to as the Taft (T), El Centro (E) and Pacoima (P) earthquakes, and were actually derived from the original digitized records. Inasmuch as nearly the same motion was reproduced at several different amplitudes for the two houses, a basis of comparison was sought by

normalizing the maximum peak accelerations of each recorded motion to unity before computing its response spectrum. In Figs. 4.3(a) and (b) the upper and lower bounds for the resulting acceleration spectra computed for 2 percent damping are shown for the two series of tests. The amplification of base acceleration is essentially unity in the period range 0.01 to 0.05 second and varies between 3 and 5 in the 0.2 to 0.6 second interval. Also for comparison the response spectra of the corresponding original motions for 2 percent damping are superposed on these diagrams. In general, the trends in the two sets of curves are similar although there are differences between the individual peaks. Since the upper and lower bounds for the simulated earthquake responses represent a severe test for the quality of the reproduced motions and since the response spectra provide no information on the sequence of events for the single degree of freedom oscillators represented in these diagrams, the reproduced motions can be claimed to mimic the original motions satisfactorily. Actually, there is no need to reproduce any given earthquake motion exactly, because no past earthquake will ever occur again. It is necessary only that the simulator motions contain the essential characteristics of actual earthquakes, and it may be concluded that these motions meet that requirement.

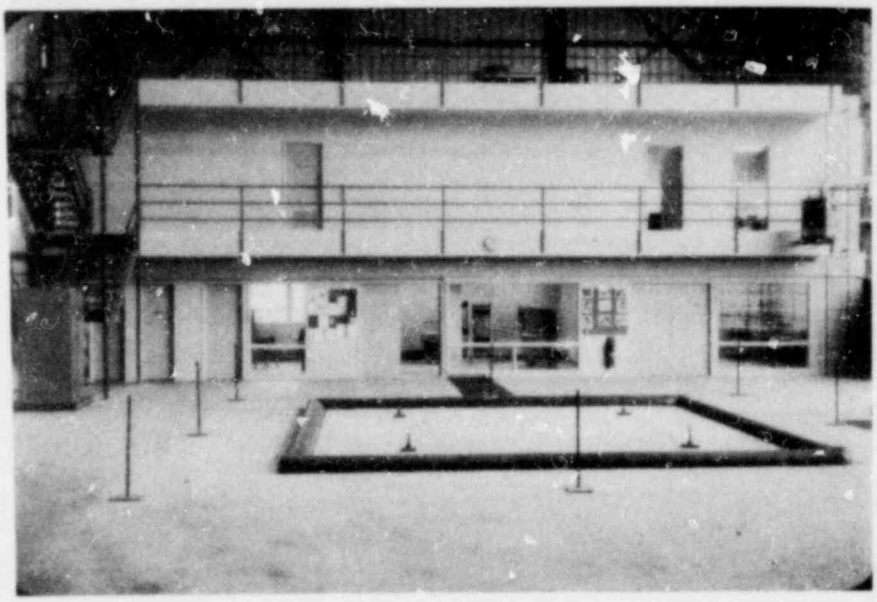

(a) Shaking Table

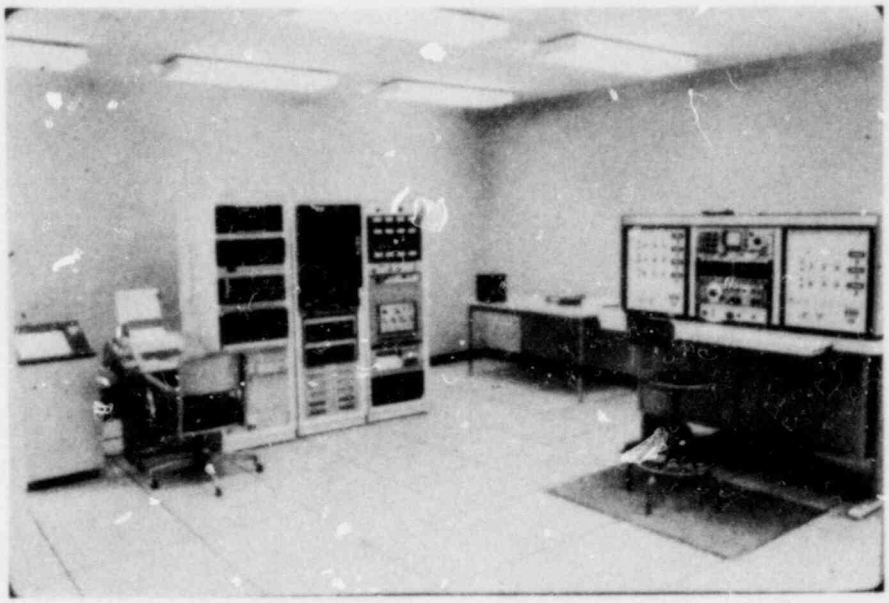

(b) Control Room

FIGURE 4.1 OVERALL VIEW OF THE TEST FACILITY

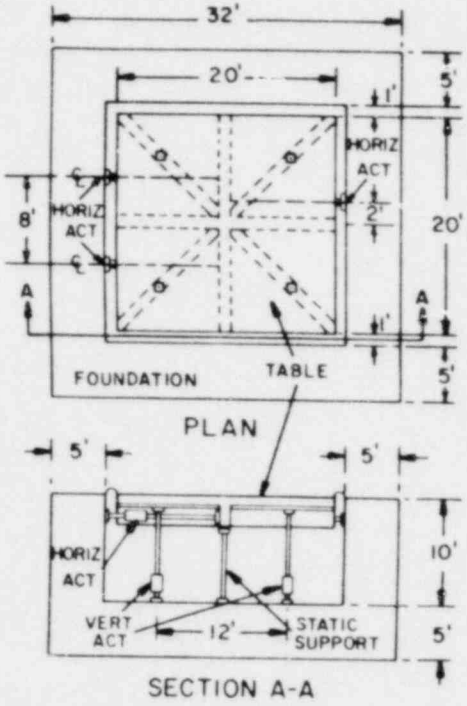

ACTUATOR LOCATIONS

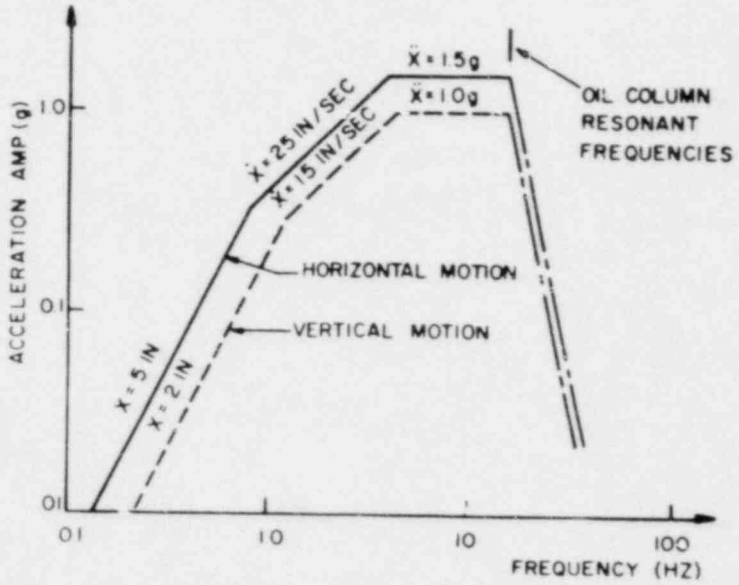

LIMITATIONS OF DYNAMIC PERFORMANCE

FIGURE 4.2 SHAKING TABLE MOTION LIMITS

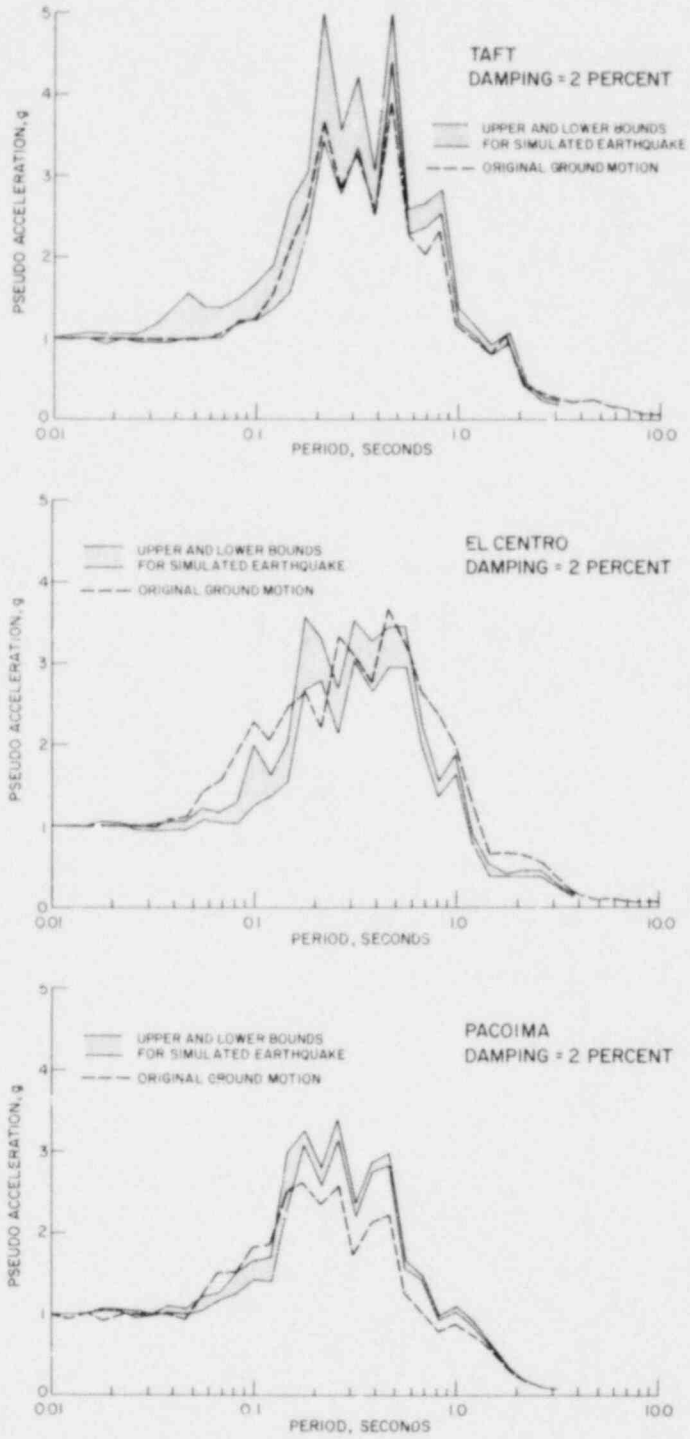

(a) Motions Applied to House 1

FIGURE 4.3 NORMALIZED RESPONSE SPECTRA

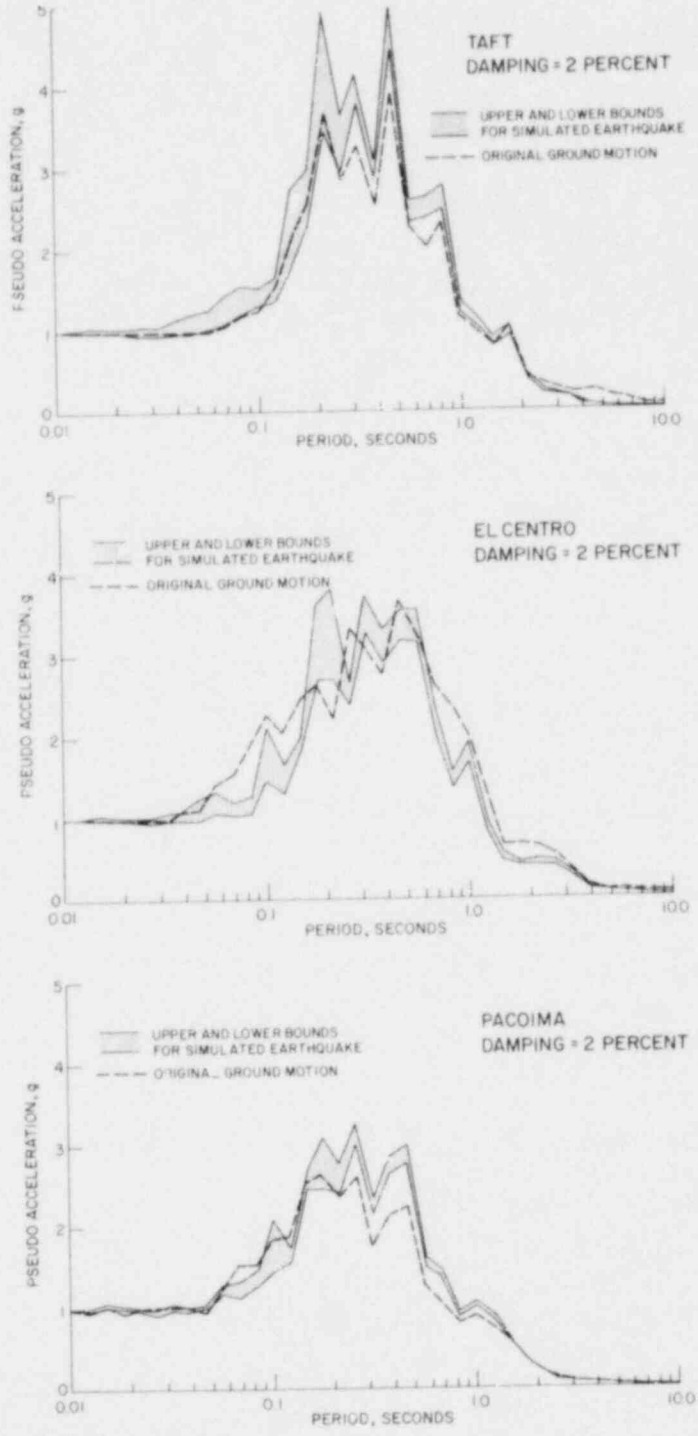

(b) Motions Applied to House 2

FIGURE 4.3 (CONT.) NORMALIZED RESPONSE SPECTRA

5. TEST RESULTS

5.1 Introduction

The present research was conducted to provide a basis for the evaluation of the strength of masonry houses in a seismic environment. Because of practical limitations in the implementation of typical details in the test structures, only a limited number of parameters could be included in the investigation. The variables considered in the program were

a) Unreinforced and partially reinforced walls

b) Variations in the geometry of the walls

c) Variations in the type of excitation

d) Variations in the orientation of the roof structure

e) Variations in base fixity (House 1 only)

f) Repair of damaged walls.

As described in Chapter 3, the models were tested under a variety of conditions in which one or more of the above parameters was considered. Undoubtedly, there are interactions between these parameters and consequently the determination of the effects of a specific variable is difficult. One must therefore generalize in order to bring out the more prominent features of the response characteristics. In this chapter, data related to the measured response is presented in graphical display form in three levels of increasing sophistication. At the simplest level, time history plots of data recorded in single or grouped transducer channels are considered. With such a display, it becomes possible to study the amplitude and phase relationship between input and response. At the next level, selected portions of

some data channels are presented in amplified time scales so that the response can be studied in greater detail. Finally, the displacement patterns of the out-of-plane walls (W2 and W4 for House 1 and A1 and B1 for House 2) are shown at selected time intervals in order to assess better the effect of reinforcement and progressive cracking. Chapter 6 presents an analysis of the results described in the following sections.

5.2 Response of House 1

The measured response of a masonry house can not be described adequately by discussing only a few selected results; the whole sequence of testing must be described in detail. Masonry is a material with memory; response in a particular test reflects the previous loading history because existing cracks influence the subsequent response. As stated earlier, tests were generally conducted in increasing intensity, applying a particular base motion with both roof orientations. A total of 29 test runs were conducted on House 1 during a two-week period, with roughly an equal number of tests in each orientation. A summary of the dynamic tests and testing conditions is provided in Table 5.1. In the next paragraphs, a description of the entire test series is given; a qualitative discussion of the response then follows. It should be noted that House 1 was viewed as an exploratory test specimen. Deducing the effects of some of the variables on this structure is difficult because at one stage in the test sequence the footing attachment of the in-plane walls was changed from free to fixed conditions; in addition the in-plane and out-of-plane walls were repaired at different times to permit continuation of testing.

5.2.1 Test Sequence

Careful examination of the wall segments after the roof structure was in place, but not yet bolted, revealed hairline cracking in the eighth course from the base of the unreinforced wall W3, shown in Fig. 5.1(a). This was believed to have initiated as a shrinkage crack during the curing period, but was probably extended somewhat during the installation of the roof. In Figs. 5.1(a) to 5.1(h) and similar drawings, the perimeter of the structure is unfolded as one would see the walls when walking around the structure counterclockwise. As Fig. 3.1 and Table 5.1 indicate, the sequence of tests was started with the roof trusses oriented parallel to the table motion so the in-plane walls were non-load bearing. When the anchor bolts were tightened to offset the negative camber of the truss above C2, W3, and C3, cracking in the unreinforced units C2 and W3 occurred as shown in Fig. 5.1(b). Apparently the tensile strength of the masonry bed joint was not sufficient to sustain the tension forces applied by the bolts which were provided with 8 in., or two course, embedment depths. This second set of cracks was wide enough to warrant the application of quick curing structural epoxy to the affected areas. Measurements indicated the width of the cracks to vary from hairline to 1/8 in. However, the applied apoxy gave enough strength to the repaired joints so that until the end of the tests no further cracking or slippage occurred at these joints. In subsequent crack distribution diagrams, therefore, this set of cracks is not indicated.

The first three test runs were conducted before the concrete weights were added to the roof in order to ensure that the instrumentation functioned properly. Also, the footings under W1 and W3, both parallel to the table motion, were anchored so that uplift was possible

but sliding was prevented. (These were later restrained against uplift.) Following the addition of the 12,000 lb concrete slabs to the roof, eight runs (number 4 through 11) were conducted with the Taft signal. During Test 9, (T-0.21 g) rocking was observed at the mortar joint in the eighth course of W3 where hairline cracks had been noted earlier. The fully opened width of these cracks during the test could not be established, only their residual width afterwards. The relative width of the lines with which cracks in Fig. 5.1 are indicated, is intended to indicate the estimated amount of opening. Further shaking during Test 10 (T-0.27 g) resulted in crushing at both ends of this crack as shown in Fig. 5.1(c). At this point, the lateral stiffness of wall panel W3 was theoretically reduced to near zero, and the only resistance to imposed forces was from friction along the crack. However, as subsequent discussions will indicate, there was no great disparity between the measured in-plane displacement amplitudes for W1 and W3, apparently because W1 was rocking at its base.

The only damage in the test structure up to Test 11 (T-0.29 g) was in W3 and was confined to a single continuous, horizontal crack. Rather than resorting to an epoxy repair it was decided that slippage of the wall at this level should be prevented by prestressing the wall horizontally between structural tubing placed vertically on either side. Figure 5.2 shows this arrangement. However, during Test 11 (T-0.29 g), a new horizontal joint crack developed at the second joint from the base of the wall, Fig. 5.1(d).

The last two tests with the trusses oriented parallel to the table motion were conducted with the El Centro motion. During Test 12 (E-0.14 g) noticeable uplift of the footing under W1 occurred. Therefore, after this particular test run, the footing of W1 was bolted to

the shaking table so that uplift would be prevented. When the El Centro motion was applied at double the intensity during Test 13 (E-0.28 g), additional cracks in the fifth and sixth joints from the bottom occurred in W3 as indicated in Fig. 5.1(e). Also, a continuous crack at the first joint from the base was observed in W4.

After this sequence of runs, the roof structure was rotated 90 degrees so that the trusses were transverse to the table motion and the in-plane walls were load bearing. Further, a general repair for W3 was provided by coating the wall on both surfaces with a 1/8 in. thick layer of fiberglass reinforced plaster. The unreinforced corner unit C4 which had cracked at the first course from the bottom during Test 10 (T-0.27 g) was repaired locally with the same plaster applied to the bottom two courses of block. The footing under W3 was bolted down to provide a base condition similar to W1.

The second series of tests was started with the Taft signal, which controlled the table motion during Tests 14 through 19. During Test 20 (E-0.21 g), the El Centro earthquake was applied at 0.21 g intensity, a second structural crack was noted in W4 at the sixth course from the top, Fig. 5.1(f). Observations during Test 21 (E-0.31 g) indicated that significant hinging was occurring at the cracked joint with an out-of-plane displacement of 2 in. at 2/3 the wall height. Concern about the stability of the wall led to the application of the same surface bonding plaster along the length of the crack on both sides of the wall. Cracking which occurred during the last eight tests is indicated in Fig. 5.1(g) for Test 24 (E-0.46 g) and Fig. 5.1(h) for Test 28 (P-0.63 g). The structure withstood the final test run (E-0.59 g) without collapsing; however, the extent and degree

of damage both in the masonry as well as in the roof assembly made it advisable to stop the testing.

Of the 29 tests conducted on House 1, 15 were selected for detailed data reduction. These are indicated with asterisks in Table 5.1; double asterisks signify that amplified time plots were also obtained for some of the data channels. The following response quantities will be discussed:

(1) Input table motion

(2) Out-of-plane displacements of the reinforced wall W2 (transducers numbered 36, 37, 38, 52, 58 in Fig. 3.5) and the unreinforced wall W4 (transducers 44, 40, 45, 46, 61)

(3) In-plane displacements of W1 (reinforced) and W3 (unreinforced) as measured by transducers 63, 62, respectively.

(4) Displacements of the reinforced corner unit C1 (transducers 49, 57) and the unreinforced corner unit C2 (transducers 48, 56)

(5) Roof displacement (transducer 53)

(6) Slip of the top plate relative to W1 and W3 (transducers 71, 70)

(7) Out-of-plane accelerations of W2 (transducers 81, 83) and W4 (transducers 84, 85)

(8) Roof acceleration above W1 and W3 (transducers 97, 88)

(9) Roof acceleration at weight and drywall levels (transducers 90, 86).

In order to present the data more compactly, certain response quantities are omitted in the groups of figures; however little information of interest is excluded.

In evaluating response quantities presented either in graphical form or from the tables, the orientation and location of transducers indicated in Fig. 3.5 should be consulted. For example, the displacements of out-of-plane walls W2 and W4 were measured relative to the steel frame inside the house, and therefore when one wall moved towards the reference frame the other moved away from it. This resulted in opposite signs for the signals as may be seen in the figures or tables. Likewise, a 180-degree phase difference is seen for accelerations of panels W2 and W4. The displacements at the top of walls W2 and W4 were averaged from the three instruments at that level because they were usually within a few percent of each other for a given wall. Table 5.2 summarizes the peak recorded values for those transducers which characterize five selected tests. The two numbers given for each entry denote the measured "positive" and "negative" extremes. It is stressed that the directional orientation of the instruments is reflected in these numbers. For example, a "positive" extreme deflection or acceleration for W2 is comparable to a "negative" quantity for W4.

5.2.2 Overview of Structural Response

A detailed description of the effects of various parameters is given in the following subsections; this subsection provides an overview of the response of the structure as a framework for the more detailed descriptive information that follows.

(a) None of the partially reinforced walls and corner units (W1, W2, C1, and C3) were damaged throughout the entire test sequence.

This included base motions of the order 0.3 g when the in-plane walls were non-load bearing and 0.6 g when they were load bearing.

(b) The unreinforced in-plane wall W3 cracked as a result of overturning effects at the eighth course from the bottom during Test 9 (T-0.21 g) when it was non-load bearing. This cracking was partially attributed to a preexisting shrinkage crack along this bed joint. After the wall was repaired and became load bearing, it cracked again as a result of overturning effects along the first bed joint from the bottom during Test 27 (P-0.49 g).

(c) The unreinforced out-of-plane wall W4 had only a minor crack along the first bed joint from the bottom when it was load bearing. In this condition it was subjected to base motions of the order of 0.3 g. When it was non-load bearing it cracked along the sixth bed joint from the top during Test 19 (T-0.25 g) although the crack was not visually evident until after Test 20. After it was repaired it cracked again at the same joint during Test 27.

(d) The effect of the roof truss orientation was not clear from this series of tests because the anchorage of the footings of the in-plane walls changed just before the roof truss orientation changed. It was clear that the roof structure was much stiffer when the trusses were parallel to the base motion than when they were oriented transversely. In the transverse orientation visual observations indicated sizable displacements of the top of the roof relative to the bottom of the roof trusses.

(e) When the trusses were transverse to the base motion the deformation at the center of the roof structure relative to its ends was of the order of 0.05 in. during base motions having a peak

acceleration of the order of 0.25 g. When the trusses were parallel to the base motion the relative deformations were much smaller.

(f) The fiberglass-based plaster that was used to repair the unreinforced walls appeared to be capable of at least restoring the original strength of the walls.

(g) Restraining the footings of the in-plane walls to prevent uplift decreased the displacement of the reinforced in-plane wall from 0.03 in. to 0.05 in. The out-of-plane walls were permitted to uplift throughout the tests; however no uplift was observed or recorded.

5.2.3 Structural Response

(A) Effect of Type of Excitation

As indicated in Chapter 4, horizontal components of three different earthquakes with varying peak accelerations were used in the test program. Normalized response spectra shown in Fig. 4.3 indicate that the simulated base motion closely matched the original records in the frequency range of interest.

In general the response of House 1 was similar for all three types of base motions. To illustrate this effect, three reasonably similar tests were selected. These are Test 19 (T-0.25 g), Test 21 (E-0.31 g) and Test 25 (P-0.25 g) In all three tests the in-plane walls were load bearing. However, during Test 20 (E-0.21 g) W4 cracked and was repaired after Test 21. Therefore, the state of the unreinforced out-of-plane wall was different in Test 21 from that in Tests 19 and 25. The recorded response quantities for these tests are presented as time histories in Figs. 5.3 to 5.5. These should be studied in conjunction with Tables 5.1 and 5.2.

For the out-of-plane walls, the out-of-plane displacements at the top of W2 and W4 (with the exception of W4 in Test 21) were similar for all three base motions and were of the order of 0.05 to 0.08 in. as shown in Figs. 5.3(b) and (c), 5.4(b) and 5.5(b) and (c).

For the in-plane walls W1 and W3, the displacements were of the order of 0.01 to 0.02 in., and again the response was similar for each of the three base motions as shown in Figs. 5.3(d), 5.4(d) and 5.5(d). In each case, the response was in phase with the applied base motion indicating a stiff structure type of response.

Selected acceleration readings complete the description of the response. Absolute accelerations of the out-of-plane walls W2 and W4 are shown in Figs. 5.3(g) and (h), Figs. 5.4(g) and (h), Figs. 5.5(h) and (i). It is seen that at elevations corresponding to the full or 2/3 wall height, acceleration limits are closely matched both in amplitude and frequency; however, the wall failure for W4 resulted in the totally different history of Fig. 5.4(h).

(B) Effect of Roof Truss Orientation

A direct assessment of the effects of roof truss orientation was complicated by the fact that the anchorage of the footings of the in-plane walls changed before Test 13 which was just before the roof orientation changed. As a result the in-plane walls changed from non-load bearing to load bearing one test after their footings were restrained against uplift. Both these factors decreased the displacement response of the in-plane walls and the overall response of the test specimen. For the out-of-plane walls the response characteristics were different for the two roof truss orientations. This is attributed to the difference in the response of the in-plane walls for the two roof orientations.

The major effect of roof orientation in this series of tests was in the response of the roof structure itself. When the trusses were parallel to the base motion the roof structure responded essentially as a rigid system. When the trusses were perpendicular to the base motion there was relative motion and some energy dissipation between the ridge line and the bottom of the trusses. This clearly affected the force levels transmitted to the in-plane walls, but to what degree is a matter of judgment since no force measuring devices were placed under the roof structure.

A detailed assessment of the different modes of response influenced by roof orientation can be obtained from a comparison of Tests 10 (T-0.27 g) and 19 (T-0.25 g). In Test 10, walls W2 and W4 were load bearing while during Test 19 walls W1 and W3 were load bearing. An additional difference existed in the fixity of the in-plane walls: in Test 19 walls W1 and W3 were restrained from uplift, while during Test 10 only lateral sliding was prevented. Selected quantities illustrating the behavior of the test specimen during Test 10 are displayed in Fig. 5.6; note that the arbitrary window times for the plots have been selected such that a given point in the response is reached roughly 1 second earlier during Test 10.

The out-of-plane walls cracked when they were non-load bearing - Test 19 (T-0.25 g), but resisted a similar base motion when they were load bearing - Test 10 (T-0.27 g). Clearly the vertical load affected the strength of the walls and this is discussed in detail in Chapter 6. The response characteristics of the out-of-plane walls of the two tests also differed as discussed in the following paragraph.

The displacement histories during Test 10 for the reinforced and unreinforced out-of-plane load bearing walls W2 and W4, respectively,

indicate very closely matched response which was in phase with the base motion. By superimposing the transverse displacements of these walls measured at the top as well as the middle one-third points, an estimate of the deflected shape can be obtained. Inspection of Figs. 5.6(b) and (c) reveals that both out-of-plane walls vibrated at the frequency of the structure as a whole in the "cantilever" mode, and that both had the same peak displacements; 0.42 in. at the top, 0.28 in. at two-thirds the wall height, and 0.12 in. at one-third the wall height. Also, these peaks are reached simultaneously. This picture is altered for Test 19, as shown in Figs. 5.3(b) and (c), when the walls were non-load bearing. In addition to the significant decrease in displacement amplitudes (note that the scales for out-of-plane displacements are not the same in Figs. 5.3 and 5.6), there appears to be a slight increase in the frequency of response. Also, peak displacements are no longer attained simultaneously along the height, especially for W4 for which the peak displacement amplitudes at the top and the two-thirds point are both 0.65 in. From about 9.2 seconds into the response, the displacement at the top is less in magnitude than that at the two-thirds wall height, indicating horizontal cracking and hinging at the crack location. This deviation from a cantilever shape is also evident for wall W2 which is illustrated in Fig. 5.3(b). Isometric views of the deformed shapes of the two walls are shown in Figs. 5.7 and 5.8 for Tests 10 and 19, respectively. Although these figures are based on the same data presented as time history plots, they afford a more convenient means of describing the deflected shapes.

The difference in the response characteristics of the in-plane walls when they were non-load bearing and load bearing is significant. However, since the footings of the walls were restrained against uplift

almost at the same time as the roof orientation change ! ..h factors contributed to the significant decrease in displacement amplitude of response.

With the trusses parallel to the table motion, Test 10 (T-0.27 g) Fig. 5.6(d), the in-plane displacements measured at the top are of the same order of magnitude as the out-of-plane wall displacements. Inasmuch as wall W3 developed a continuous horizontal crack along the entire length of the wall at the eighth joint from the bottom, the wall displacement at the top was probably largely due to rocking on this plane. Also, the footing uplift of W1 accounted for most of its top displacement. (Both walls had been bolted to the table after Test 13.) Because of the great difference in the stiffnesses of W1 and W3, relative slip readings of the top plate showed significant differences also, as illustrated in Fig. 5.6(g). After the rotation of the roof when W1 and W3 became load-bearing walls and their footings were restrained against uplift, the magnitudes of these displacements as well as the slip readings were reduced to only a fraction of their previous values. The substantial decrease in the overall displacement amplitude of the structure is also illustrated in Figs. 5.3(e) and (f), and 5.6(e) and (f).

The difference in the roof response mechanisms is contained in Figs. 5.3(j) and 5.6(k). In the former, when the trusses are perpendicular to the table motion, peaks of the acceleration measured at the "weight level" (see Fig. 3.5 for the exact location) are generally greater than the peaks at the "ceiling" or drywall level indicating relative motion of the roof between these two elevations. By contrast, the roof respond- ssentially as a rigid system when the trusses are

oriented parallel to the table motion. A tabulation of the measured peak accelerations at the different levels is given in Table 6.3.

(C) Effect of Base Fixity for In-Plane Walls

The representation of foundation flexibility under laboratory conditions is difficult and is a factor that must be accounted for when the laboratory results are extrapolated to field conditions. Under site conditions the degree of foundation flexibility and its effect on the response of the superstructure depends on the length, size and continuity of the foundation, the nature of the soil, and the geometry and strength of the walls which are attached to it.

For House 1 both in-plane walls were initially free to uplift from the shaking table. Because of visible uplift at the footing-shaking table interface during excitation, the footing under the reinforced panel W1 was bolted to a prestressed metal plate at two symmetrical locations 6 ft apart after Test 12, while that under W3 was similarly bolted following the repairs after Test 13.

The decision to restrain the in-plane footings against uplift was made because it was felt that the continuous and interconnected footings commonly used in house construction would not permit the order of magnitude of uplift that was observed. The obvious effect of restraining the footings against uplift was a significant decrease in the displacement of the restrained walls, and this is illustrated by comparing the results of Tests 10 and 13. Recorded response quantities for Tests 10 and 13 are presented in Figs. 5.6 and 5.9, respectively.

In both tests wall W3 was cracked along a bed joint and consequently had a similar mode of response in both tests. In Test 10 (T-0.27 g) when W1 was free to uplift, the in-plane displacement at the

top of the two walls was similar and of the order of 0.4 in., and the structural response was reasonably symmetric as shown in Fig. 5.6(d). When W1 was restrained against uplift in Test 13 (E-0.28 g) the decrease in the response of W1 was dramatic as shown in Fig. 5.9(d) where the maximum displacement decreased to 0.05 in., whereas W3 had peak displacements comparable to Test 10. This difference in response of the in-plane walls caused asymmetrical response of the test structure, as shown in Figs. 5.9(e)-(h).

It is clear from this one comparison that restraining it against uplift affected the displacement at the top of the in-plane wall W1 by an order of magnitude. As stated this result will have to be carefully assessed when extrapolating the behavior to field conditions because the footings of the in-plane walls of Houses 2, 3 and 4 were all restrained against uplift. For the out-of-plane walls W2 and W4 which were only restrained against lateral translational movement, base fixity had no influence; the walls were not capable of causing rotation of the footing.

(D) Effect of Repair

During the tests on House 1 the unreinforced components failed at different stages in the test sequence. Perhaps the most significant of these was the failure of W3 during Test 9 (T-0.21 g), and its gradual deterioration until after Test 13 (E-0.28 g) when it was repaired with a fiberglass-based plaster. The repair material was applied at an average thickness of 1/8 in. on both surfaces of the wall and was allowed to cure for several days. Failure of W3 did not occur again until Test 27 (P-0.49 g). In the case of the out-of-plane wall W4 the same repair process was used after Test 21 (E-0.31 g). It is

noteworthy that the recorded peak displacements for W4 are less than those for W2 during Test 25 indicating a greater initial stiffness after it was repaired. In the case of W4, failure reoccurred at the location of the previous crack during Test 27 (P-0.49 g). A sequence of deflected shapes for W2 and W4 is shown in Figs. 5.10 and 5.11 for Tests 21 and 25. It is seen that W2 was apparently slightly more flexible during Test 25 (with W4 repaired), whereas the reverse was true during Test 21.

In summary, the repair method restored the strength of both the in-plane and out-of-plane walls so that they were capable of resisting base motions significantly greater than those that caused the original damage.

(E) Summary

Evaluation of selected quantities describing the behavior of House 1, which was simple in plan but which contained significant components of a masonry structure, indicates the following:

(1) The response of the test specimen to the base motions was complex and was affected by the orientation of the roof structure, by base fixity of the in-plane walls and by the cracks that formed in the unreinforced walls.

(2) With the roof trusses oriented in the direction of the table motion, the house was subjected to twelve simulated earthquakes patterned after either the Taft or the El Centro accelerograms. During this series, the maximum peak table accelerations were of the same order of magnitude as the corresponding actual earthquake motion (0.25 to 0.30 g). After the roof structure was rotated through 90 degrees,

the house was subjected to sixteen additional motions which included the simulated Pacoima earthquake. The peak table accelerations recorded during these tests reached 0.60 g. These were considerably larger than the corresponding actual ground motions with the exception of the Pacoima signal.

(3) The first observed structural damage in the unreinforced walls occurred in the in-plane wall W3 when the house was subjected to the Taft motion with a peak acceleration of 0.21 g during Test 9. It is likely that this failure was initiated from a shrinkage crack that existed in the wall panel prior to testing. The out-of-plane unreinforced wall W4 was essentially undamaged during the initial sequence of tests when it was a load bearing wall. When it was non-load bearing it remained undamaged until Test 18 (T-0.19 g) and cracked during Test 19 (T-0.25 g). The crack did not become visible until after Test 20 (E-0.21 g). During the next test, Test 21 (E-0.31 g), the wall hinged significantly at the crack location, but did not collapse.

(4) The nominal amount of vertical reinforcement used in the wall segments (W1 and W2) and corner units (C1 and C3) was sufficient to prevent the occurrence of any significant damage to these components throughout all the tests.

(5) The surface bonding material used to repair the cracked unreinforced walls appeared to be effective for this house. Following repair, the test specimen had to be subjected to increased base motions before cracking reoccurred.

5.3 Response of House 2

The discussion of the behavior of House 2 will be presented in the same format as House 1. The major difference in the tests of the two specimens was that change of the fixity conditions of the footings and progressive repair of the walls were not factors for House 2. An overview of the structural response is presented at the beginning of the detailed discussion of the results in order to provide a framework for the more detailed information that follows.

5.3.1 Test Sequence

As with House 1, this specimen was also tested over a two-week long period during which the magnitude of the applied base motions varied significantly. A major change from House 1 was the sequence of orientation of the roof structure; the test sequence began with the roof trusses oriented perpendicular to the table motion so that the in-plane walls were initially load bearing. For House 2 the more unfavorable truss orientation was implemented during the second phase of the tests so that more severe base motions could be applied during the first phase, without running a serious risk of causing significant structural failure. A chronological listing of the 32 test runs conducted on this specimen is provided in Table 5.3.

The second house was fabricated and stored indoors until the time of testing. However, possibly because of the openings in the panels and the lack of joint reinforcement in the top two bed joints, shrinkage led to the formation of hairline cracking which is shown in Fig. 5.12(a). These cracks were generally initiated at the corners of the panel openings. Figures 5.12(b) through (i) should be considered simultaneously with Table 5.3 in order to understand the effect of the

applied base motions on the structural behavior. In these figures the local surface bonding repair that was applied (following Test 19) on each side of the spandrel beam above the large opening for panel B has not been indicated; additional cracks formed at more or less the same locations in the repaired sections.

The bolt hole pattern of the shaking table dictated that the footings under the in-plane panels A and B be bolted at two symmetrical locations 6 ft apart and 5 ft from either end. Similarly, footings of the out-of-plane panels were fixed to the table at two locations 4 ft from the ends. Although measurements indicated that the footings of the out-of-plane walls underwent no sliding or rotation, it was evident that both ends of the footings under walls A and B tended to uplift from beyond the bolt locations. In particular, the right end of the footing below wall B could be observed to undergo significant upward motion during the stronger simulated earthquakes. After Test 16 when the spandrel beam was fully cracked at the ends, this tendency was further accentuated. From Test 27 on, displacement measuring devices were attached to the ends of these footings to measure the uplift (see Table 6.12). Since the in-plane displacements at the tops of the panels A and B were measured at the corners of these walls (instruments 42 and 48, respectively, in Fig. 3.6) the magnitudes of these displacements were amplified on account of uplift. However, as the subsequent discussion will emphasize, the footing under B where the wall reinforcement was doweled at both ends was more prone to this uplift action than the footing under A which was unreinforced.

A description of the behavior of the house will be presented with reference to the following measured quantities illustrated in Fig. 3.6:

(1) Input table motion

(2) In-plane displacements of the unreinforced wall panel A (transducer 42) and the reinforced wall B (instrument 48)

(3) Out-of-plane displacements of the unreinforced panel A1 (instruments 56, 57, 58, 50, 51, 52 and 53) and the reinforced panel B1 (instruments 76, 77, 78, 64, 65 and 66)

(4) Uplift of in-plane walls A and B from their footings (instruments 91, 92 and 89, 90, respectively)

(5) Rotation of the truss rafters above the top plate when the trusses were oriented transverse to table motion (transducers 72, 73, 74 and 75)

(6) Roof displacement (instrument 70)

(7) Accelerations at top of A and B (instruments 83 and 84)

(8) Accelerations of A1 (instruments 80 and 79) and B1 (instruments 82 and 81)

(9) Roof accelerations at weight and drywall ceiling levels (instruments 87 and 88).

In describing the response of House 2 by time history plots, references are made to the "right" and "left" sides of walls. For a consistent definition of these directions the following convention was adopted (see Fig. 3.6): For in-plane walls A and B, "right" is the side common to wall B1 while "left" denotes the side common to wall A1. For the out-of-plane walls, right is always the side common to the in-plane wall B and left is the side common to wall A.

Unlike House 1, total structural failure in this specimen occurred essentially during a single test, Test 32 (P-0.52 g); therefore

extensive repairs were not required as testing progressed. Following Test 19 (P-0.51 g), both ends of the spandrel beam in panel B (Fig. 5.12(e)) were locally repaired with the surface bonding plaster, but these cracks reappeared quickly at their previous locations during the second series of tests when the roof structure was rotated. This cracking was due to the fact that the 16 in. deep unreinforced spandrel beam was subjected to significant reversed flexure because the two piers it connected tended to undergo rocking. Once both ends of the spandrel beam were fully cracked (see Fig. 5.12(c)), this beam served as a strut to maintain a constant distance between the two piers.

Selected extreme readings from five representative test runs are listed in Table 5.4. On account of the fundamental similarities between the response mechanisms of House 1 and House 2, only three of these tests will be presented in graphical display form and the discussion will be limited to the effects of base motion characteristics and roof orientation.

5.3.2 Overview of Structural Response

House 2 was viewed as a test structure with wall panels representative of typical construction in UBC Zone 2. The walls were intended to represent central segments of longer walls away from the influence of interaction between out-of-plane and in-plane walls, which would have been produced by corners. The geometry of the walls indicated in Fig. 3.3 became a standard for the entire experimental program because Houses 3 and 4 which are discussed in a subsequent report had basically the same geometry as House 2. A detailed discussion of the response is given in the following subsections, and a summary is provided at the end of the chapter. For emphasis, and to

establish a framework for the subsequent discussion, the important features of the observed response are listed below:

(a) The displacement amplitudes of response were more strongly dependent on the peak table acceleration than on the types of earthquakes used as base motions.

(b) Comparison of response amplitudes between Houses 1 and 2 demonstrated the much greater overall rigidity of the latter. No variations of footing fixity were made for House 2; the footings were bolted to the test table throughout the test sequences; however, experimental evidence showed that the in-plane walls tended to uplift the ends of their footings because the hold-down bolts were located 5 ft from each end. This uplift was more pronounced for the reinforced in-plane wall because of the dowels located near the ends of the footings.

(c) The roof orientation when the trusses were parallel to the table motion (in-plane walls being non-load bearing) was clearly the more severe loading condition for a given base acceleration. Irreparable damage to the two unreinforced walls occurred during a test with this orientation; the same motion applied previously with the transverse truss orientation had not caused any significant damage.

(d) The difference in the geometry of the in-plane walls was the source of an inherent eccentricity in the response. The reinforced in-plane wall B was more flexible and consequently the out-of-plane walls were forced to undergo simultaneous bending and twisting.

(e) The largest table acceleration applied to the structure was approximately 0.5 g in each truss orientation. Both the in-plane

and out-of-plane unreinforced walls were damaged at this level of excitation when the roof trusses were parallel to the table motion. The reinforced walls demonstrated the effectiveness of nominal partial reinforcement since they remained essentially uncracked throughout the test sequence.

5.3.3 Structural Response Details

(A) Effect of Type of Excitation

The effect of the type of excitation will be discussed with respect to Tests 14 (E-0.33 g) and Test 17 (P-0.27 g). The time histories of the measured quantities for these tests are given in Figs. 5.13 and 5.14, respectively. In general there were no significant differences in the response of the test structure to the two different base motions; the detailed discussion that follows will compare the more important aspects of the observed response when the in-plane walls were load bearing.

First an examination of Tables 5.2 and 5.4 indicates that House 2 was more rigid than House 1; for comparable base motions and roof orientations in the absence of significant cracking, the displacement limits for House 2 are smaller than House 1. In addition, there was significant torsional response in House 2 because of the difference in rigidity between Walls A and B. Figures 5.13(b) and 5.14(b) graphically illustrate this difference in addition to showing the bias of wall B towards greater "negative" displacements. The difference in the displacement amplitudes of A and B were reflected in the out-of-plane displacements for walls A1 and B1. Frames (c) through (h) of Figs. 5.13 and 5.14 illustrate the deformation pattern for these walls. Several features of this pattern are evident in these figures. First,

magnitudes of the displacements at the top of the out-of-plane walls are slightly greater than the displacements of the in-plane walls. This is due to out-of-plane bending of the bottom rafters of the trusses. The second important feature illustrated in Figs. 5.13(d), (g) and 5.14(d), (g) is that the side of wall A1 and that of wall B1 adjacent to wall B underwent greater displacements than the side adjacent to wall A. This follows from the disparity of displacements for the in-plane walls, and indicates racking distortion of the roof system. Values listed in Table 5.4 also verify this trend. Finally, examination of the displaced "vertical profile" for both out-of-plane walls illustrated in Figs. 5.13(c), (f) and 5.14(c), (f) indicates that the basic cantilever (straight line) deflection shape for both walls was maintained at all times during excitation, even for the unreinforced panel A1 which was noted to have developed a horizontal crack in the main pier (Fig. 5.12(b)).

In view of the observed flexibility of the roof structure for House 1, a bracing system was devised (see Fig. 3.6) for House 2. This consisted of rectangular plywood sheets nailed on either side of 2 ft long 2x4 in. boards secured between each set of trusses along a vertical plane passing through the ridge line.

Even with this bracing system in the roof, the displacement of the roof structure in the direction of table motion shown in Figs. 5.13(i) and 5.14(i) was greater (by a factor of almost 2, see Table 5.4) than the top displacements for walls A1 and B1. Part of this flexibility resulted from rotation of the bottom rafters of the trusses as shown in Figs. 5.13(j) and 5.14(j). The difference in the rafter rotations with and without the metal framing anchors (referred to as straps in the figures) is not significant.

Accelerations recorded at various points of the test structure are presented in frames (k)-(n) of Figs. 5.13 and 5.14. The difference in displacement amplitudes for walls A and B is also evident in their accelerations (Figs. 5.13(k) and 5.14(k)). In both frames the signal for wall B contains some higher frequency peaks reflecting the impact with the table of the uplifting footing during every half cycle. Out-of-plane accelerations for panels A1 and B1 shown in frames (l) and (m) of both figures indicate higher frequency components not evident in the displacement measurements. Also, roof accelerations measured at two different levels and shown in Figs. 5.13(n) and 5.14(n) indicate the relative motion of the roof ridge line at the weight level with respect to the drywall level below the bottom truss chords.

An overall evaluation of Figs. 5.13 and 5.14 shows that for comparable peak base accelerations very similar response was obtained for two different table motion signals.

(B) Effect of Roof Truss Orientation

An assessment of the effect of the roof truss orientation will be made by comparing Test 30 (E-0.37 g) with Test 14 (E-0.33 g) and Test 17 (P-0.27 g). The recorded time histories for Tests 14, 17 and 30 are given in Figs. 5.13, 5.14 and 5.15, respectively. Figures 5.13 and 5.15 show a six-second segment of the total motion. It should be noted that the displacement scale in Fig. 5.15 is different from that in Figs. 5.13 and 5.14.

The major difference between Test 30 (in-plane walls being non-load bearing) and Tests 14 and 17 (in-plane walls being load bearing) is the significant increase in the displacements of walls A and B and especially that of wall B. These increased amplitudes are evident in

frames (b)-(i) of Fig. 5.15 when compared with Figs. 5.13 and 5.14. In addition, the difference between the displacements of walls A and B was also increased with the change in roof orientation. This torsional response of the house is also evident in the recorded displacements of the out-of-plane walls A1 and B1 shown in Figs. 5.15(c)-(h). The twist of both panels is due to the greater flexibility of wall B.

The increased displacements of the in-plane walls in Test 30 are attributed to two factors: the increased rigidity of the roof structure when the trusses are parallel to the table motion, and the restraining effect provided by the dead load. Also it should be noted that the roof inertia load follows a more circuitous path to the in-plane walls when they are non-load bearing.

Another difference attributable to the change in the roof orientation is the in-plane flexibility of the roof structure. In Tests 14 and 17 there was a noticeable difference between the displacements recorded at the center of the roof and those recorded at the center of the out-of-plane walls. In Test 30 this difference was not evident as the displacement measured at the center of the house (Fig. 5.15(i)) was almost identical to that measured at the center of the out-of-plane walls. This difference resulted from the reduced restraint provided at the top of the out-of-plane walls by the gable end of the roof.

Figure 5.16 shows the deflected shapes of the out-of-plane walls, A1 and B1, at selected instants of time. In these diagrams broken lines depict undeflected geometries for both panels while solid lines describe the scaled deflected shapes. Reference to Fig. 3.3 and the indicated greater flexibility for panel B explain the greater out-of-plane displacements at the corners common to panel B. It is noted from this

sequence of diagrams that substantial twisting accompanied the out-of-plane displacements because of the inherent eccentricity "built-in" to the structure.

(C) Description of Failure

The limiting state of the test structure was attained during Test 32 (P-0.52 g) as a result of the failure of the unreinforced in-plane wall A. The crack pattern shown in Fig. 5.12(i) indicates that significant damage was confined to the in-plane and out-of-plane unreinforced walls A and A1. The failure of the 2 ft wide door pier of the out-of-plane wall A1 was attributed to the failure of the in-plane wall A.

The inclined crack of wall A was initiated at the reentrant corner adjacent to the window opening and propagated through the masonry units as well as the bed and head joints. The permanent residual displacement at the top of wall A was 0.3 in. and the residual crack width averaged 0.5 in. The permanent inward displacement of the small door pier of the out-of-plane wall was 3 in. at the crack location.

An overall evaluation of the crack pattern indicates that the presence of even a very nominal quantity of reinforcement was sufficient to prevent damage in panels B and B1. The two doweled #4 bars at either end for wall B prevented any significant cracking even though the displacement amplitudes of wall B were consistently much larger than those of wall A because of rocking. Also, because the spandrel beam in panel B was not capable of resisting significant bending, the two piers in this wall were quickly forced to act as two partially-reinforced vertical columns connected at the top through the spandrel.

Panel B1 had a response similar to A1 in terms of displacement and acceleration, however the margin of strength provided by the two bars resulted in the formation of only a few structurally insignificant cracks in B1. Both out-of-plane walls were subjected to substantial out-of-plane displacements at the top of the walls, but apart from the damage to the door pier caused by wall A these displacements did not cause any significant cracking.

(D) Summary

Because of the different geometry of the in-plane walls the overall stiffness of House 2 was greater than that of House 1. This caused smaller displacement amplitudes to be recorded for similar base motions. Other significant observations are

(1) Because of the inherent eccentricity designed into the structure, out-of-plane walls A1 and B1 underwent simultaneous twisting and bending. These displacements did not cause substantial cracking during any of the tests.

(2) The non-load bearing unreinforced in-plane wall A failed during Test 32 (P-0.52 g). The house had been subjected to the same motion during an earlier test run without failure when the in-plane walls A and B were load bearing.

(3) Unreinforced out-of-plane wall cracking was due to lateral inertial forces which caused horizontal cracking at about the mid-height of the panel. However unlike House 1, significant hinging did not occur at this crack location. The fracture near the top of door pier in wall A1 was precipitated by the shear failure of wall A during Test 32.

(4) The failure pattern of wall A indicated both joint separation and splitting of masonry units. The tensile and bond strength of the material in House 2 was greater than in House 1 because of the very high mortar strength (Table 2.2), and resulted in House 2 being capable of resisting higher base motions before damage occurred.

TABLE 5.1

SUMMARY OF SHAKING TABLE TESTS AND TESTING CONDITIONS: HOUSE 1

Sequence Number	Reference Number	Base Motion/ Span Setting	Peak Base Acc., g	Remarks
1	230977.1	Taft/000	0.002[1]	No weights attached to the roof; trusses oriented in the direction of table motion; see Figs. 5.1(a) and (b).
2	230977.2	Taft/040	0.026	
3	230977.3	Taft/080	0.050	
4*	260977.1	Taft/100	0.066	Concrete weights totaling 12,000 lb attached to the roof assembly.
5	260977.2	Taft/150	0.081	
6*	260977.3	Taft/200	0.122	
7	260977.4	Taft/250	0.147	
8*	260977.5	Taft/300	0.190	
9	260977.6	Taft/350	0.214	W3 cracked along the mortar joint of the 8th course from bottom.
10**	260977.7	Taft/400	0.267	Crushing at ends of crack in W3; see Fig. 5.1(c).
11	270977.1	Taft/300[2]	0.285	Crack in W3 restrained by stressed metal tubing; new crack plane along 2nd course from bottom; see Fig. 5.1(d).
12	270977.2	El Centro/200	0.140	Footing under W1 bolted onto table after this test.
13	270977.3	El Centro/400	0.282	W3 cracked along 5th and 6th courses from bottom; W4 cracked at first course from bottom; see Fig. 5.1(e).
				Roof rotated 90 degrees; W3 and C4 repaired; footing under W3 bolted to table after this test.
14	290977.1	Taft/080	0.051	

15	290977.2	Taft/100	0.062	
16	300977.1	Taft/150	0.092	C2 repaired.
17	300977.2	Taft/200	0.119	
18*	300977.3	Taft/300	0.193	
19**	300977.4	Taft/400	0.248	
20	300977.5	El Centro/300	0.209	W4 cracked along 6th course from top; see Fig. 5.1(f).
21**	300977.6	El Centro/450	0.311	
22	041077.1	El Centro/300	0.214	W4 repaired
23**	041077.2	El Centro/450	0.323	
24*	041077.3	El Centro/600	0.455	C2 cracked at 7th course from top; see Fig. 5.1(g).
25*	041077.4	Pacoima/200	0.247	
26	041077.5	Pacoima/300	0.386	
27**	041077.6	Pacoima/400	0.492	W3 failed by cracking at 1st joint from bottom, W4 cracked at 6th course from top.
28*	041077.7	Pacoima/500	0.627	Compressive fracture at corner junction of C4.
29**	041077.8	El Centro/750	0.592	Imminent collapse of structure; reappearance or widening of all previous cracks; loosening of roof; see Fig. 5.1(h).

(1) This value represents the "noise" in the recorded signal, hence peak values given may include this amount.

(2) Command system malfunctioned, resulting in a significantly altered base motion of the table.

* Selected for data reduction.

** Selected for expanded time scale plots.

TABLE 5.2

RECORDED PEAK MEASUREMENTS: HOUSE 1

Test No. Base Motion Peak Acceleration	10 Taft 0.267 g	13 El Centro 0.282 g	19 Taft 0.248 g	21 El Centro 0.311 g	25 Pacoima 0.247 g
Base acceleration, g	0.267	0.282	0.248	0.311	0.230
	0.249	0.246	0.214	0.282	0.247
Out-of-plane displacement at top center for wall W2, in.	0.371	0.282	0.056	0.061	0.079
	0.423	0.262	0.078	0.118	0.073
Out-of-plane displacement at 2/3 height for wall W2, in.	0.240	0.185	0.043	0.053	0.063
	0.280	0.180	0.057	0.080	0.057
Out-of-plane displacement at top center for wall W4, in.	0.417	0.264	0.067	0.556	0.043
	0.368	0.275	0.002	0.69[illegible]	0.056
Out-of-plane displacement at 2/3 height for wall W4, in.	0.282	0.179	0.065	1.484	0.027
	0.249	0.180	0.046	1.961	0.035
In-plane displacement for W1, in.	0.344	0.047	0.018	0.022	0.021
	0.340	0.036	0.019	0.018	0.011
In-plane displacement for W3, in.	0.310	0.263	0.009	0.012	0.011
	0.397	0.277	0.014	0.013	0.009
Displacement at top of corner C1, in.	0.359	0.174	0.022	0.024	0.022
	0.385	—	0.024	0.024	0.019
Displacement at top of corner C2, in.	0.002	0.261	0.016	0.018	0.018
	0.206	0.306	0.026	0.023	0.014
Roof displacement at drywall level, in.	0.469	0.292	0.072	0.080	0.067
	0.404	0.307	0.053	0.069	0.075
Slip of top plate relative to W1, in.	0.077	0.099	0.003	0.003	0.002
	0.094	0.126	0.003	0.003	0.004

Slip of top plate relative to W3, in.	0.010	0.011	0.002	0.001	0.000
	0.028	0.028	0.000	0.001	0.000
Out-of-plane acceleration at top center for wall W2, g	0.406	0.563	0.344	0.438	0.514
	0.406	0.450	0.384	0.658	0.412
Out-of-plane acceleration at 2/3 height for wall W2, g	0.370	0.390	0.276	0.374	0.442
	0.367	0.350	0.309	0.563	0.328
Out-of-plane acceleration at top center for wall W4, g	0.493	0.428	0.352	0.398	0.381
	0.571	0.459	0.395	0.521	0.406
Out-of-plane acceleration at 2/3 height for wall W4, g	0.493	0.347	0.314	0.617	0.282
	0.597	0.340	0.271	0.559	0.334
Roof acceleration above W1, g	0.704	0.446	0.306	0.336	0.222
	0.583	0.619	0.225	0.306	0.279
Roof acceleration above W3, g	0.631	0.758	0.271	0.362	0.235
	0.640	0.662	0.227	0.293	0.251
Roof acceleration at drywall level, g	0.394	0.469	0.466	0.566	0.503
	0.403	0.538	0.431	0.488	0.376
Roof acceleration at weight level, g	0.415	0.556	0.539	0.622	0.564
	0.432	0.499	0.562	0.548	0.385

Note: The top value of each pair of measurements for each earthquake is the maximum positive value recorded for the particular instrument. The bottom value is the maximum negative value. The location of the instrument relative to the reference frame determines the positive and negative directions.

TABLE 5.3

SUMMARY OF SHAKING TABLE TESTS AND TESTING CONDITIONS: HOUSE 2

Sequence Number	Reference Number	Base Motion/ Span Setting	Peak Base Acc., g	Remarks
1	010378.1	Taft/000	0.004	Trusses transverse to motion
2	010378.2	Taft/050	0.030	
3	020378.1	Taft/100	0.059	
4*	020378.2	Taft/200	0.117	
5	030378.1	Taft/250	0.160	
6*	030378.2	Taft/300	0.178	
7	030378.3	Taft/350	0.232	
8**	030378.4	Taft/400	0.241	
9	030378.5	Taft/450	0.280	
10*	070378.1	El Centro/200	0.132	
11	070378.2	El Centro/250	0.168	
12*	070378.3	El Centro/300	0.207	
13	070378.4	El Centro/400	0.285	
14**	070378.5	El Centro/450	0.331	Crack distribution shown in Fig. 5.12(b)
15*	070378.6	El Centro/600	0.452	Crack distribution shown in Fig. 5.12(c)
16*	070378.7	Taft/600	0.400	Crack distribution shown in Fig. 5.12(d)
17**	070378.8	Pacoima/200	0.268	
18	070378.9	Pacoima/300	0.385	

19**	070378.10	Pacoima/400	0.505	Crack distribution shown in Fig. 5.12(e): Roof structure rotated 90 degrees; lintel ends for wall B repaired with surface bonding material
20	130378.1	Taft/100	0.059	
21	130378.2	Taft/150	0.076	Crack distribution shown in Fig. 5.12(f)
22*	130378.3	Taft/200	0.119	
23	130378.4	Taft/250	0.156	
24*	130378.5	Taft/300	0.188	
25	130378.6	Taft/350	0.227	
26**	130378.7	Taft/400	0.262	Crack distribution shown in Fig. 5.12(g)
27*	140378.1	El Centro/200	0.140	
28*	140378.2	El Centro/300	0.212	
29*	140378.3	El Centro/400	0.304	
30**	140378.5(1)	El Centro/500	0.370	Crack distribution shown in Fig. 5.12(h)
31*	140778.6	Pacoima/200	0.258	
32*	140378.7	Pacoima/400	0.519	Walls A and B seriously damaged, crack distribution shown in Fig. 5.12(i)

(1) Test 140378.4 was not recorded due to equipment malfunction

* Selected for data reduction

** Selected for expanded time scale plots

TABLE 5.4

RECORDED PEAK MEASUREMENTS: HOUSE 2

Test No. Base Motion Peak Acceleration	14 El Centro 0.331 g	17 Pacoima 0.268 g	19 Pacoima 0.505 g	30 El Centro 0.370 g	32 Pacoima 0.519 g
Base acceleration, g	0.331 0.284	0.228 0.268	0.471 0.505	0.370 0.334	0.476 0.519
In-plane displacement for panel A at top, in.	0.013 0.008	0.012 0.005	0.049 0.016	0.070 0.019	1.115 1.080
In-plane displacement for panel B at top, in.	0.028 0.056	0.033 0.054	0.284 0.400	0.350 0.308	1.067 1.061
Displacement at top right for panel A1, in.	0.103 0.079	0.180 0.105	0.446 0.394	0.304 0.350	2.794 1.566
Displacement at top left for panel A1, in.	0.076 0.066	0.076 0.090	0.313 0.309	0.173 0.238	3.072 1.642
Displacement at 2/3 height for panel A1 (window pier), in.	0.044 0.035	0.046 0.049	0.175 0.182	0.143 0.197	2.012 1.262
Displacement at top right for panel B1, in.	0.084 0.112	0.098 0.092	0.414 0.395	0.331 0.299	1.490 2.772
Displacement at top left for panel B1, in.	0.074 0.066	0.084 0.051	0.335 0.212	0.232 0.176	1.626 3.043
Displacement at 2/3 height for panel B1 (main pier), in.	0.044 0.036	0.053 0.032	0.212 0.128	0.147 0.106	1.135 2.048
Roof displacement at centerline (drywall level), in.	0.189 0.183	0.183 0.228	0.544 0.573	0.266 0.298	3.213 1.645
Acceleration at top of panel A, g	0.334 0.292	0.215 0.269	0.465 0.533	0.390 0.336	0.749 2.506

Acceleration at top of panel B, g	0.354	0.233	0.827	0.547	0.910
	0.338	0.331	1.773	0.861	1.077
Acceleration at top of panel A1, g	0.393	0.350	0.779	0.528	1.006
	0.389	0.587	1.450	0.687	0.853
Acceleration at 2/3 height of panel A1, g	0.369	0.259	0.660	0.576	1.110
	0.380	0.448	1.144	0.538	0.695
Acceleration at top of panel B1, g	0.510	0.570	1.145	0.621	0.680
	0.437	0.311	0.991	0.503	0.844
Acceleration at 2/3 height of panel B1, g	0.335	0.378	0.697	0.379	0.938
	0.332	0.284	0.719	0.445	0.861
Roof acceleration at gable (weight level), g	0.565	0.525	1.078	0.759	0.878
	0.550	0.369	0.825	0.527	0.651
Roof acceleration at centerline (drywall level), g	0.622	0.302	0.784	0.537	0.696
	0.450	0.428	2.170	0.735	0.817

Note: The top value of each pair of measurements for each earthquake is the maximum positive value recorded for the particular instrument. The bottom value is the maximum negative value. The location of the instrument relative to the reference frame determines the positive and negative directions.

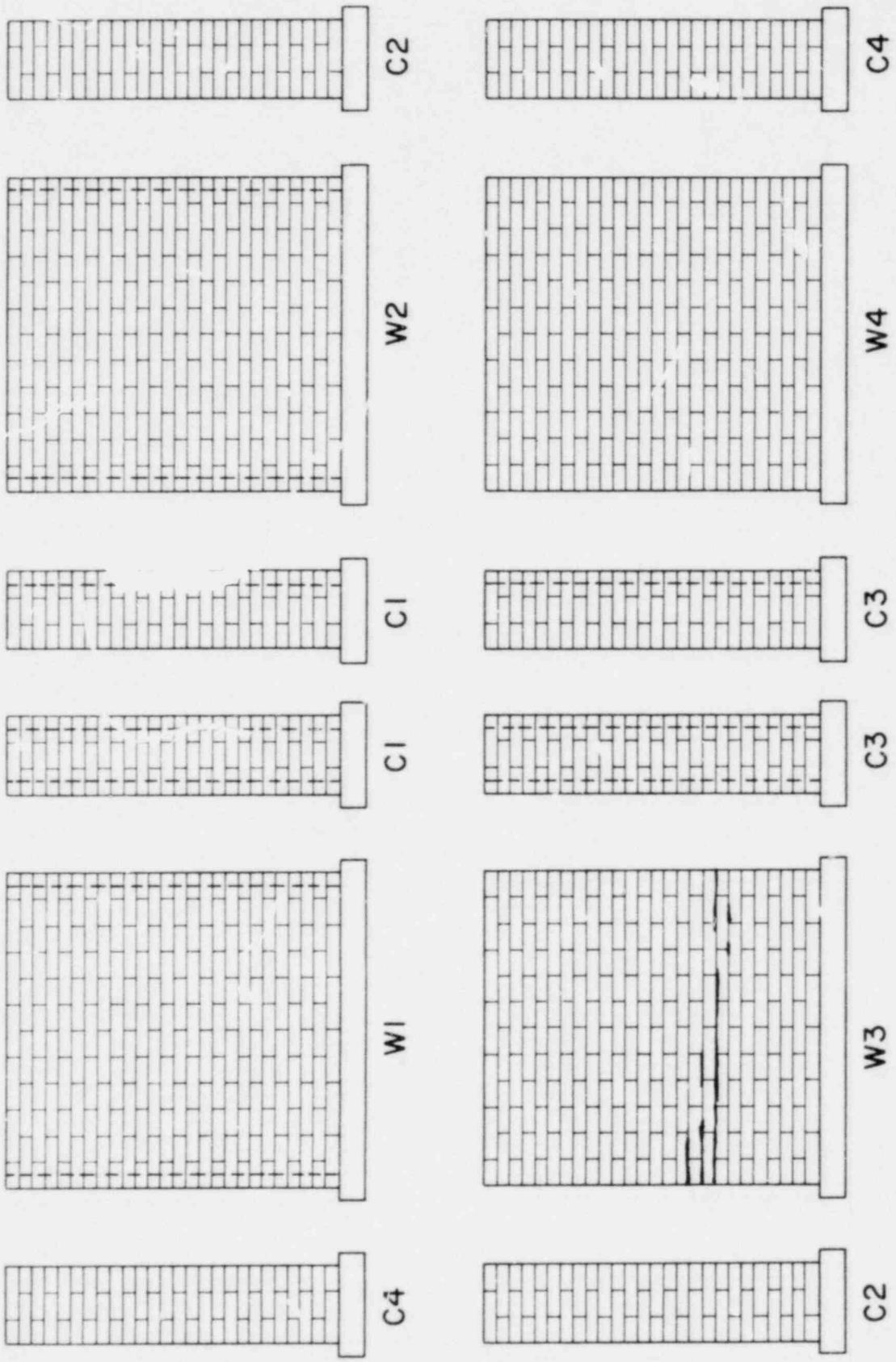

FIGURE 5.1(a) DISTRIBUTION OF CRACKS IN THE MASONRY COMPONENTS: HOUSE 1, BEFORE TESTING

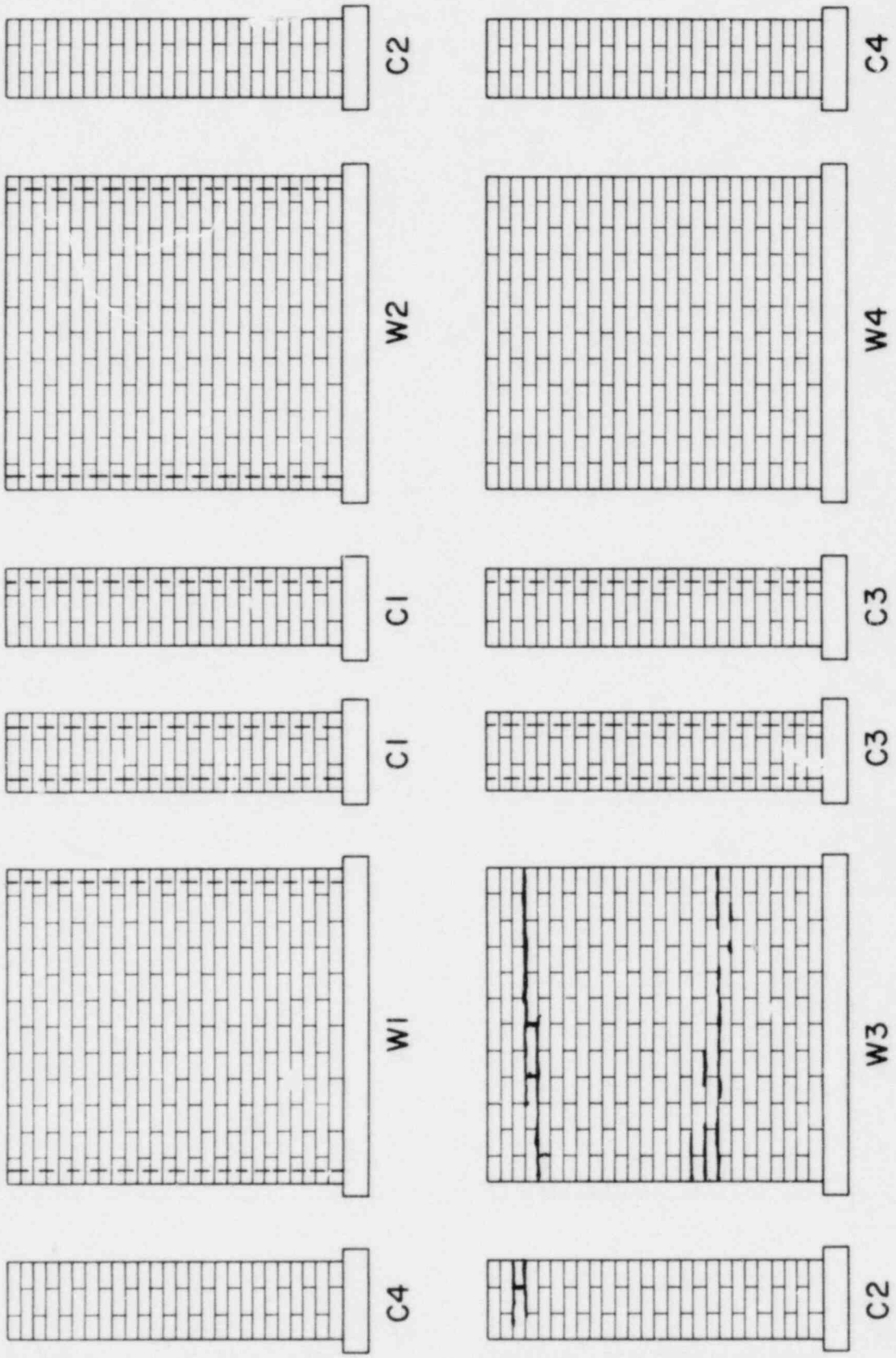

FIGURE 5.1(b) DISTRIBUTION OF CRACKS IN THE MASONRY COMPONENTS: HOUSE 1, AFTER ROOF STRUCTURE WAS INSTALLED

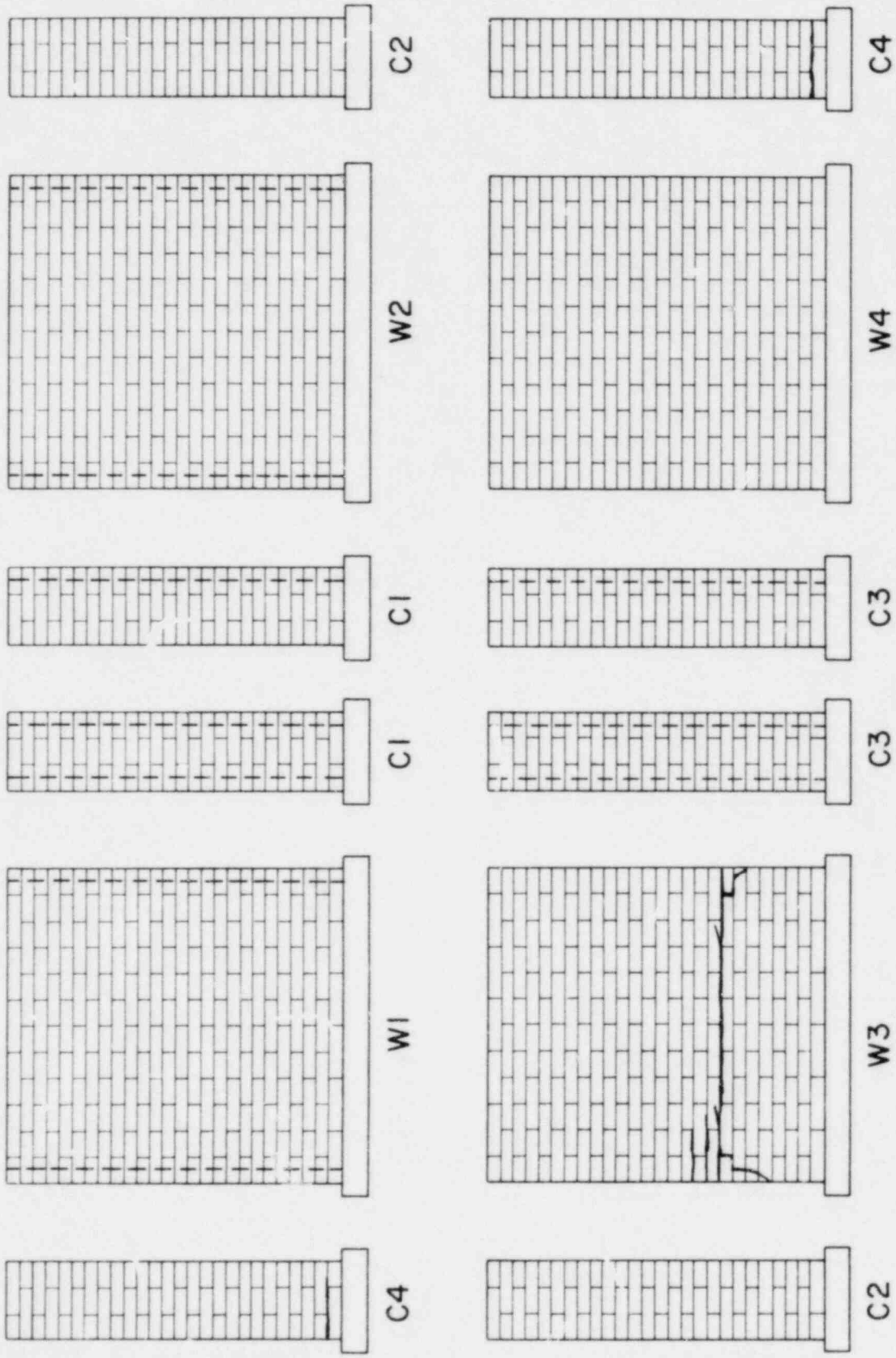

FIGURE 5.1(c) DISTRIBUTION OF CRACKS IN THE MASONRY COMPONENTS: HOUSE 1, AFTER TEST 10 (TAFT - 0.27 g)

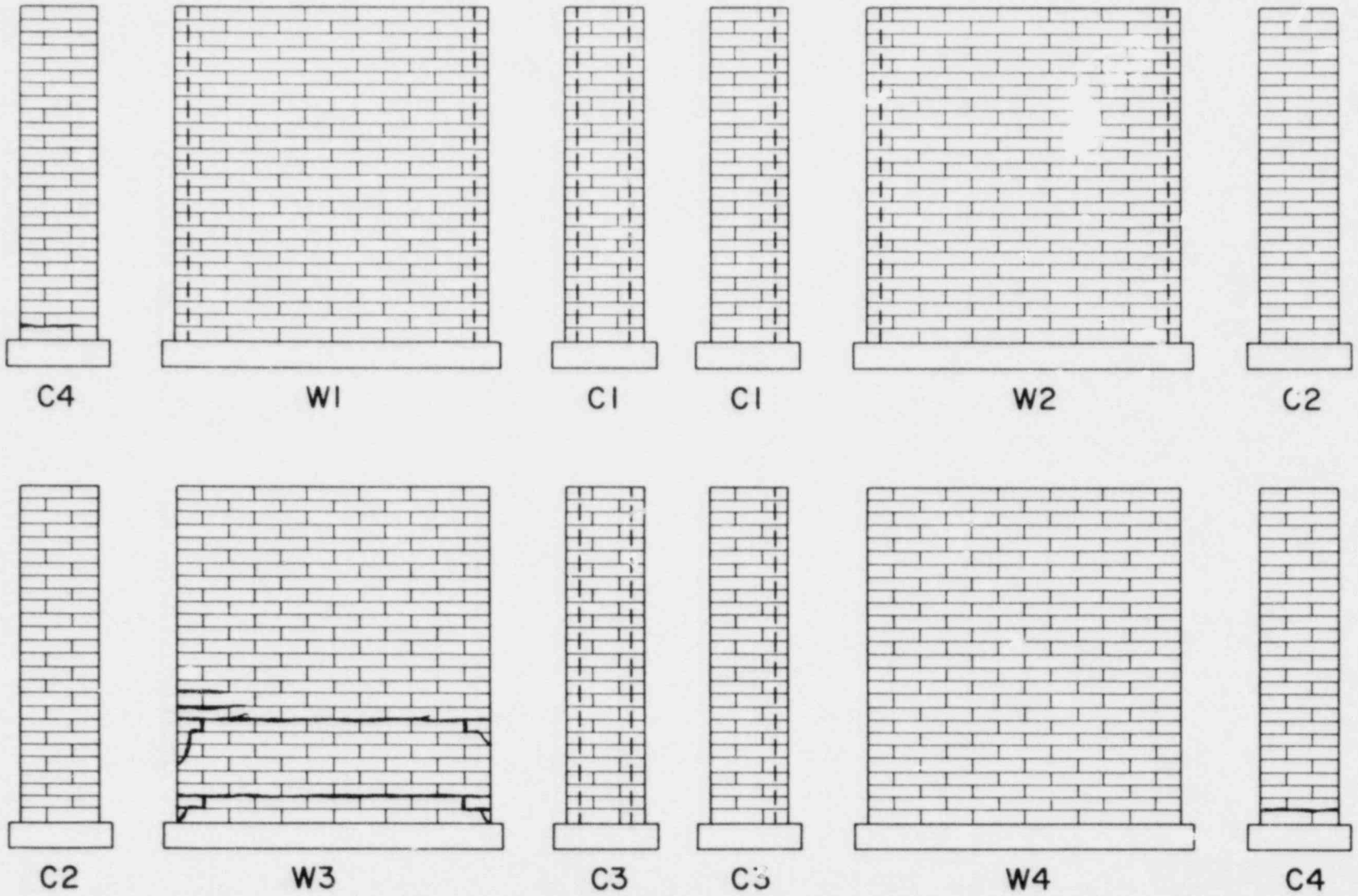

FIGURE 5.1(a DISTRIBUTION OF CRACKS IN THE MASONRY COMPONENTS: HOUSE 1, AFTER TEST 11 (TAFT - 0.29 g)

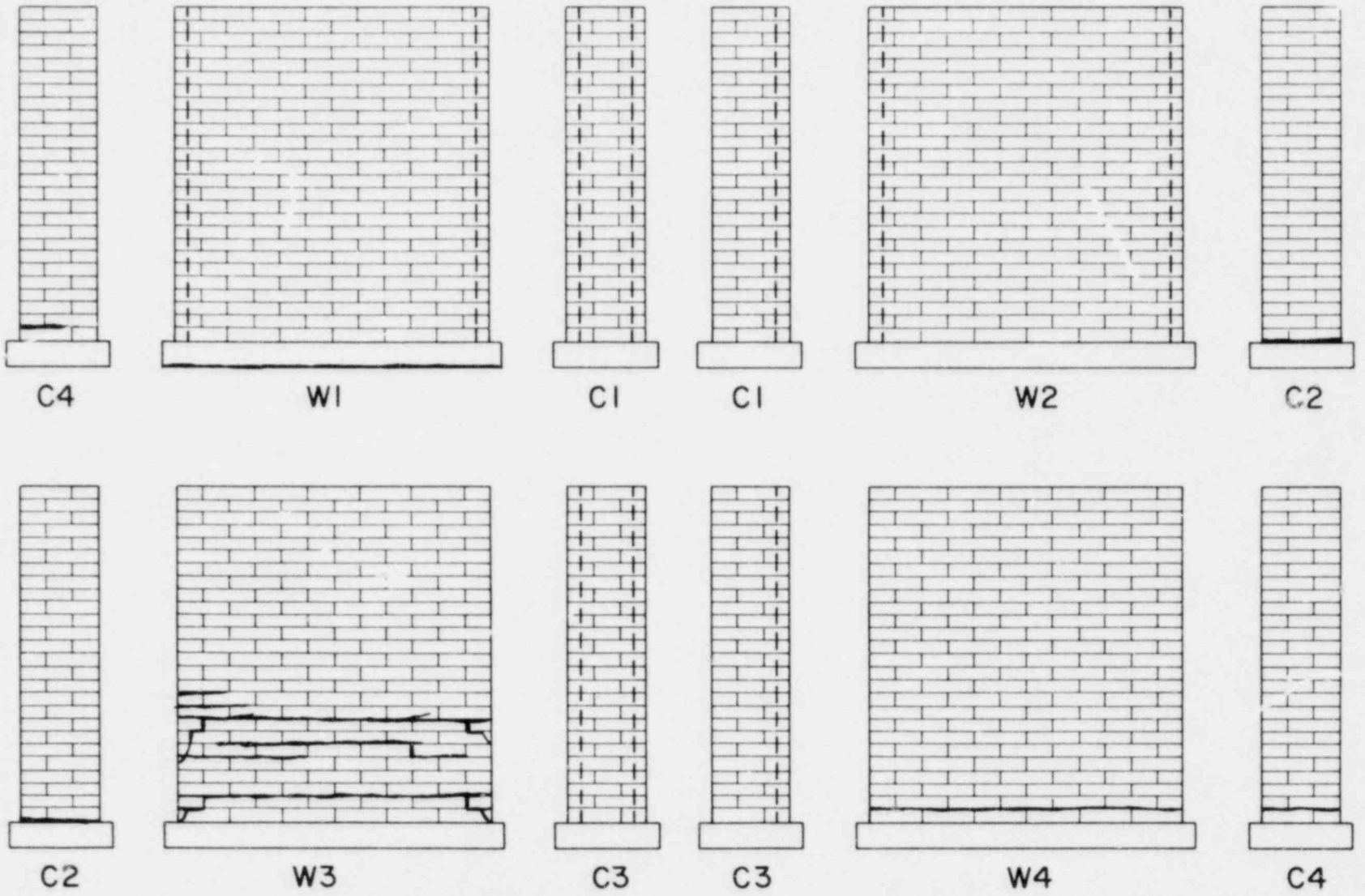

FIGURE 5.1(e) DISTRIBUTION OF CRACKS IN THE MASONRY COMPONENTS: HOUSE 1, AFTER TEST 13 (EL CENTRO - 0.28 g)

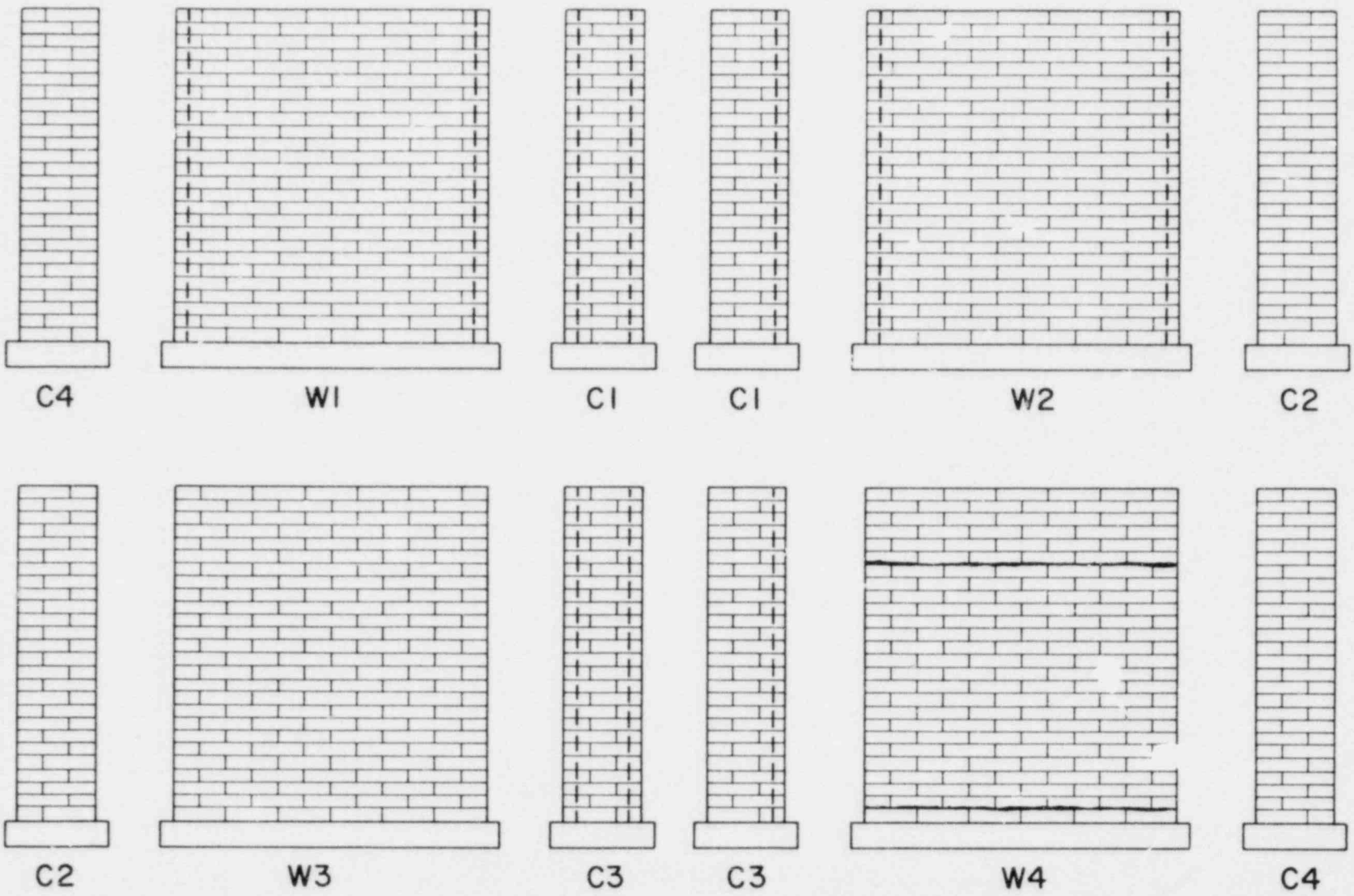

FIGURE 5.1(f) DISTRIBUTION OF CRACKS IN THE MASONRY COMPONENTS: HOUSE -, AFTER TEST 20 (EL CENTRO - 0.21 g)

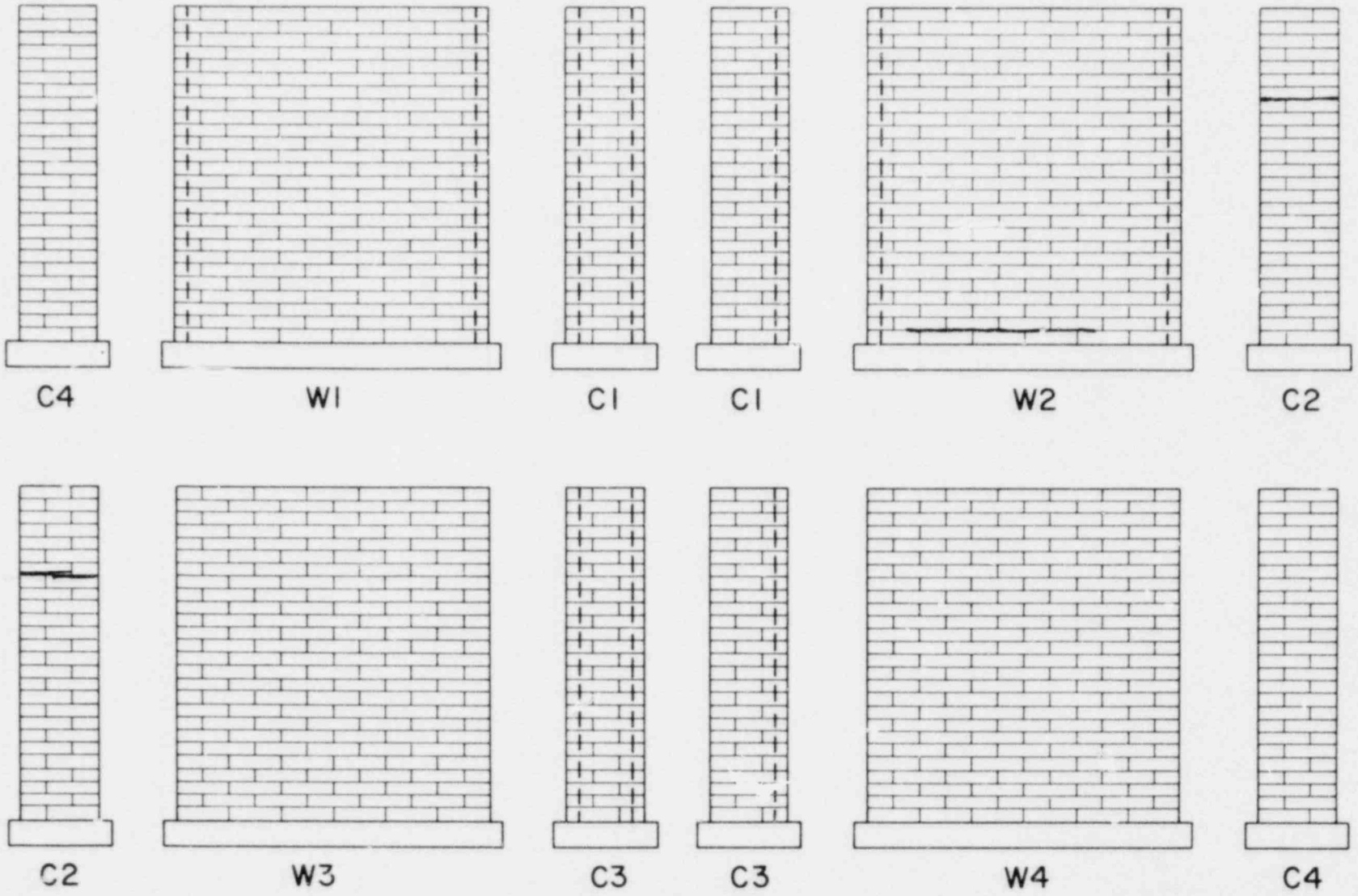

FIGURE 5.1(g) DISTRIBUTION OF CRACKS IN THE MASONRY COMPONENTS: HOUSE 1, AFTER TEST 24 (EL CENTRO - 0.46 g)

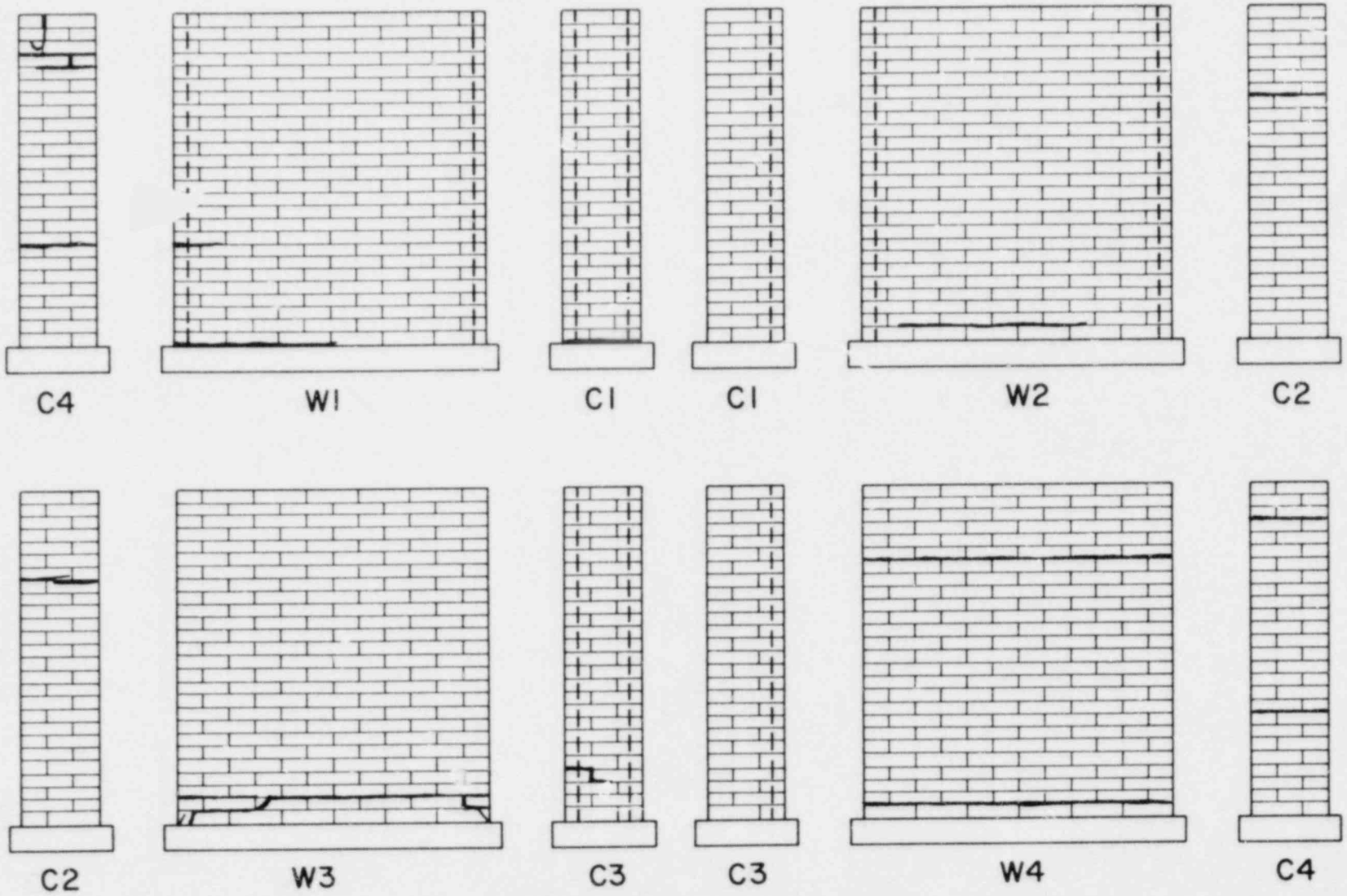

FIGURE 5.1(h) DISTRIBUTION OF CRACKS IN THE MASONRY COMPONENTS: HOUSE 1, AFTER TEST 28 (PACOIMA - 0.63 g)

FIGURE 5.2 PREVENTION OF SLIPPING IN WALL W3 BY PRESTRESSING

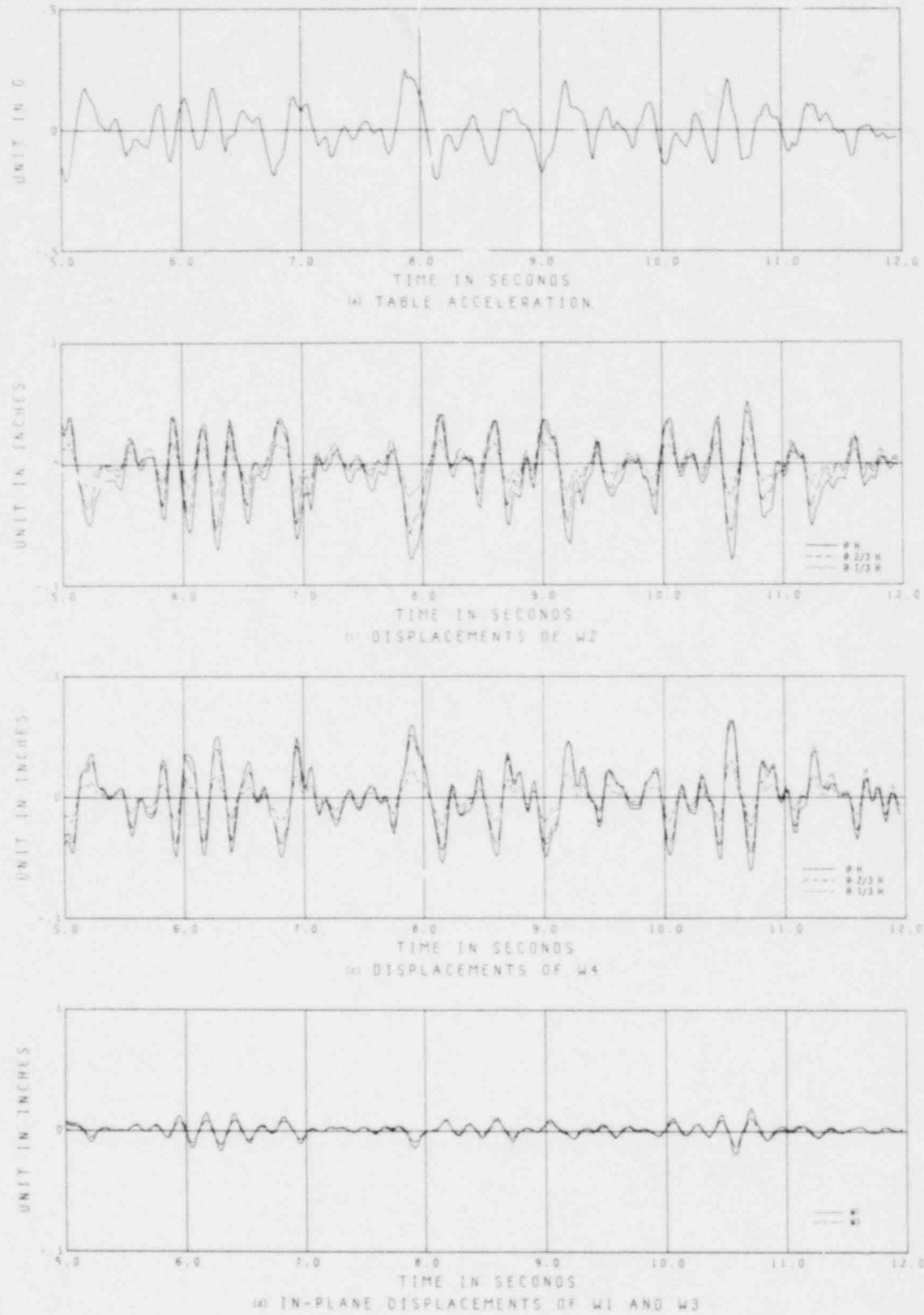

FIGURE 5.3 MEASURED RESPONSE: HOUSE 1, TEST 19 (TAFT - 0.25 g)

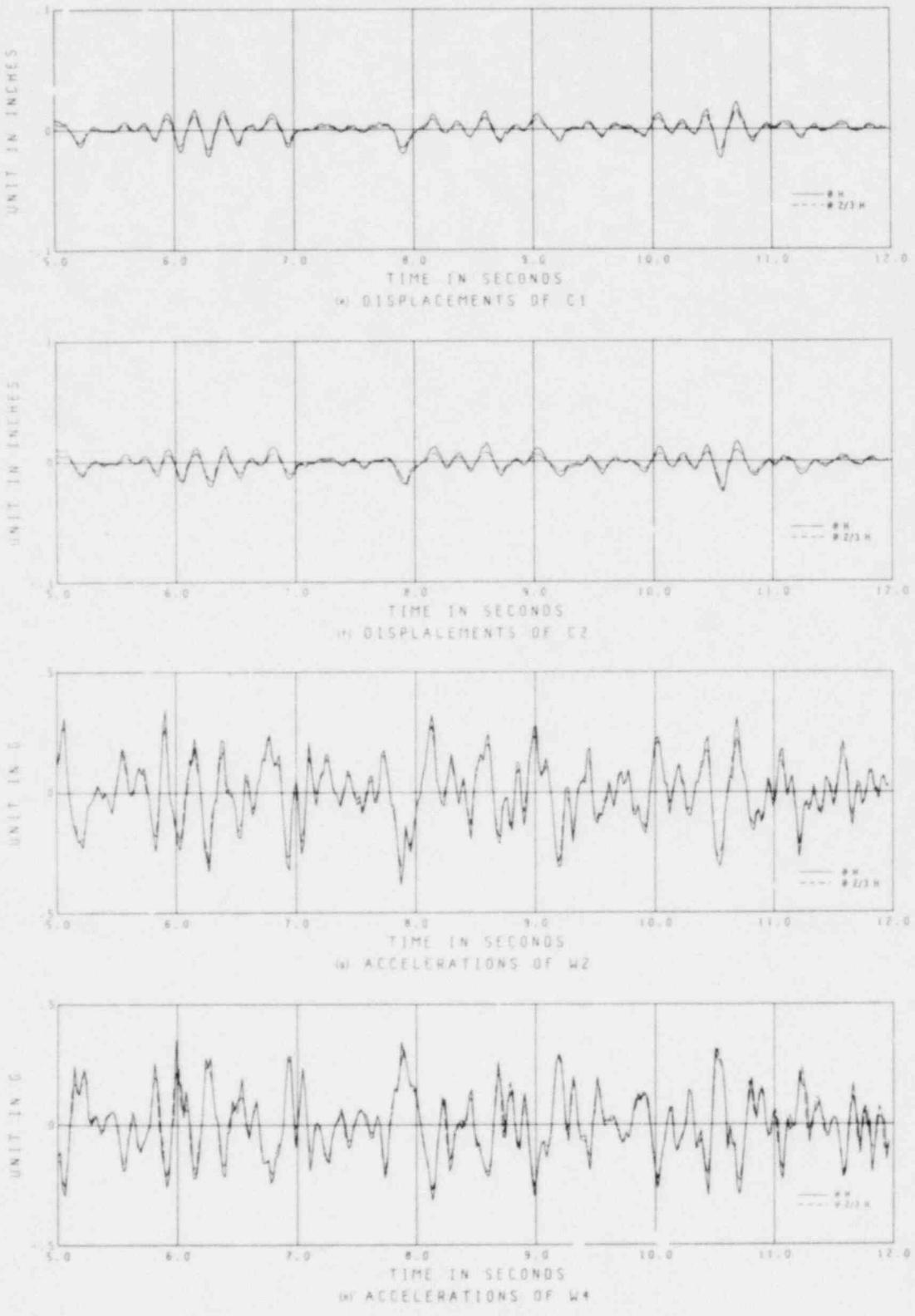

FIGURE 5.3(CONT.) MEASURED RESPONSE: HOUSE 1, TEST 19 (TAFT - 0.25 g)

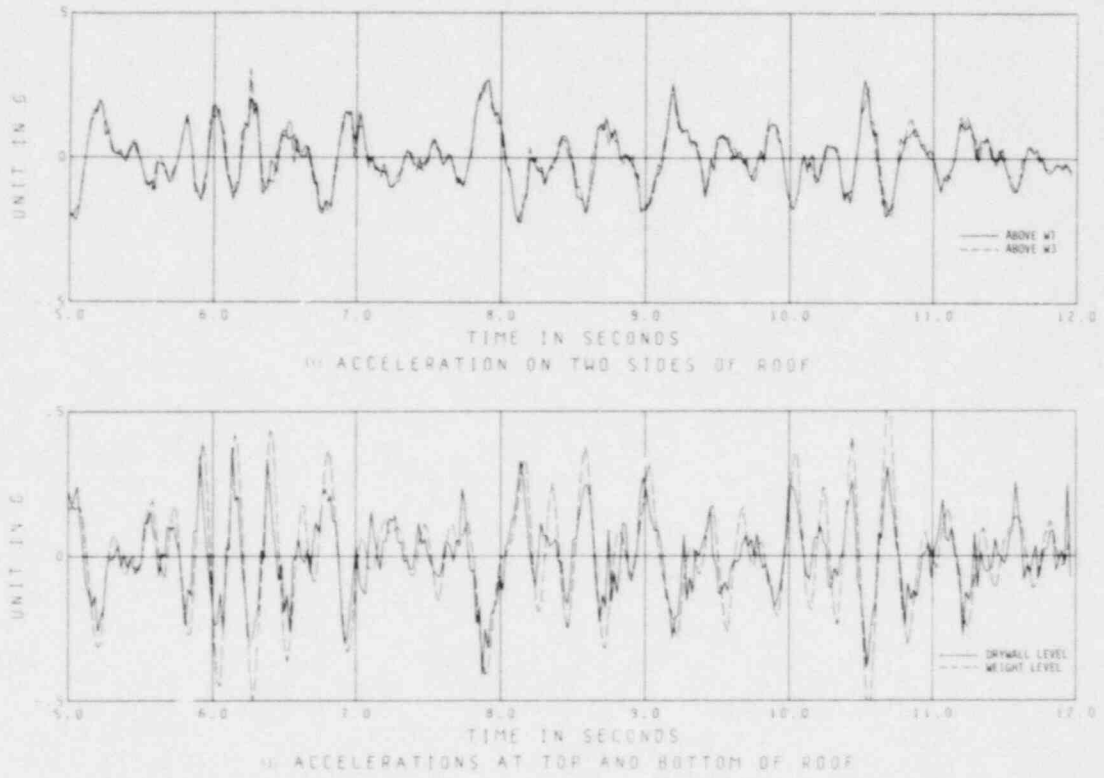

FIGURE 5.3 (CONT.) MEASURED RESPONSE: HOUSE 1, TEST 19 (TAFT - 0.25 g)

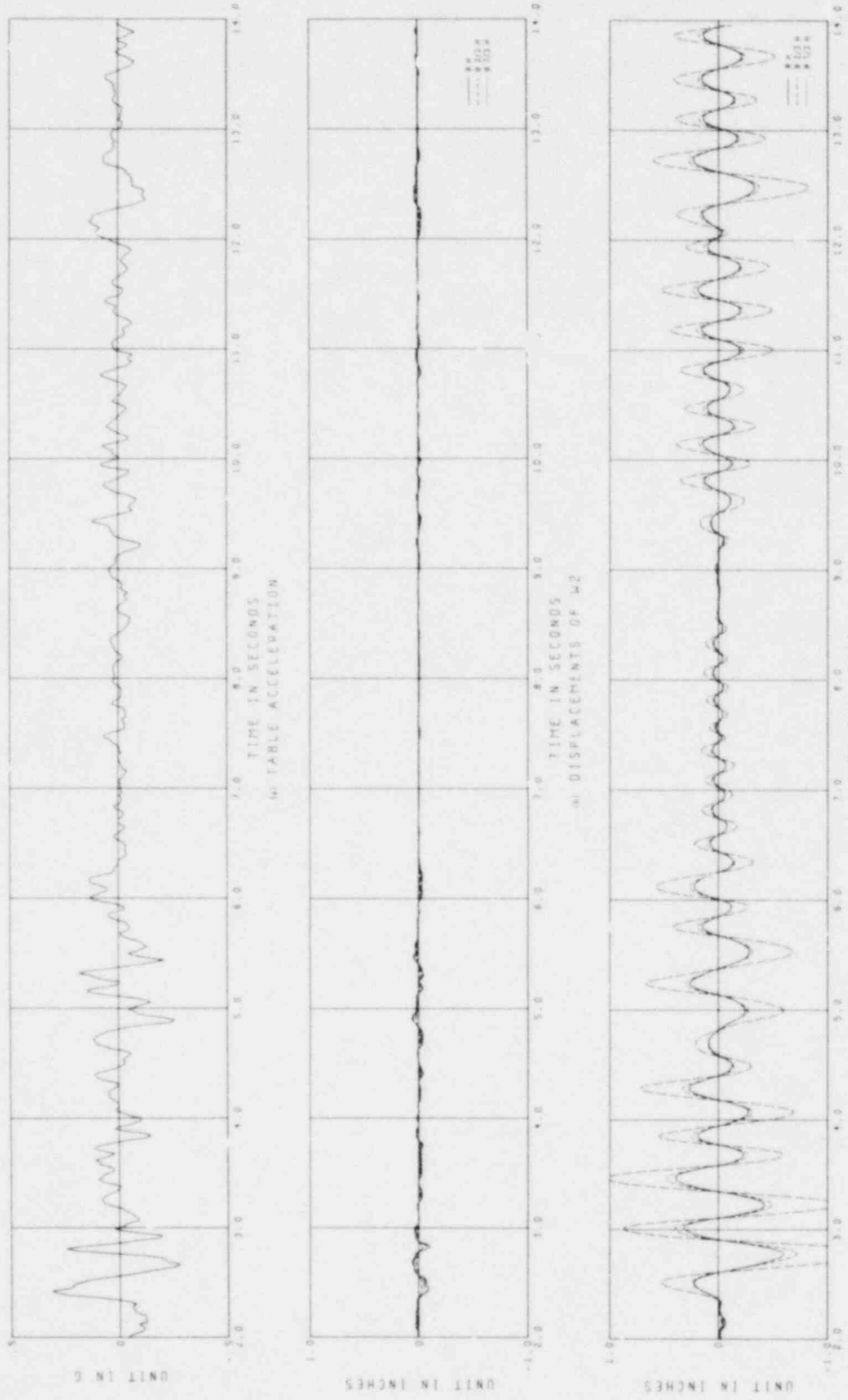

FIGURE 5.4 MEASURED RESPONSE: HOUSE 1, TEST 21 (EL CENTRO - 0.31 g)

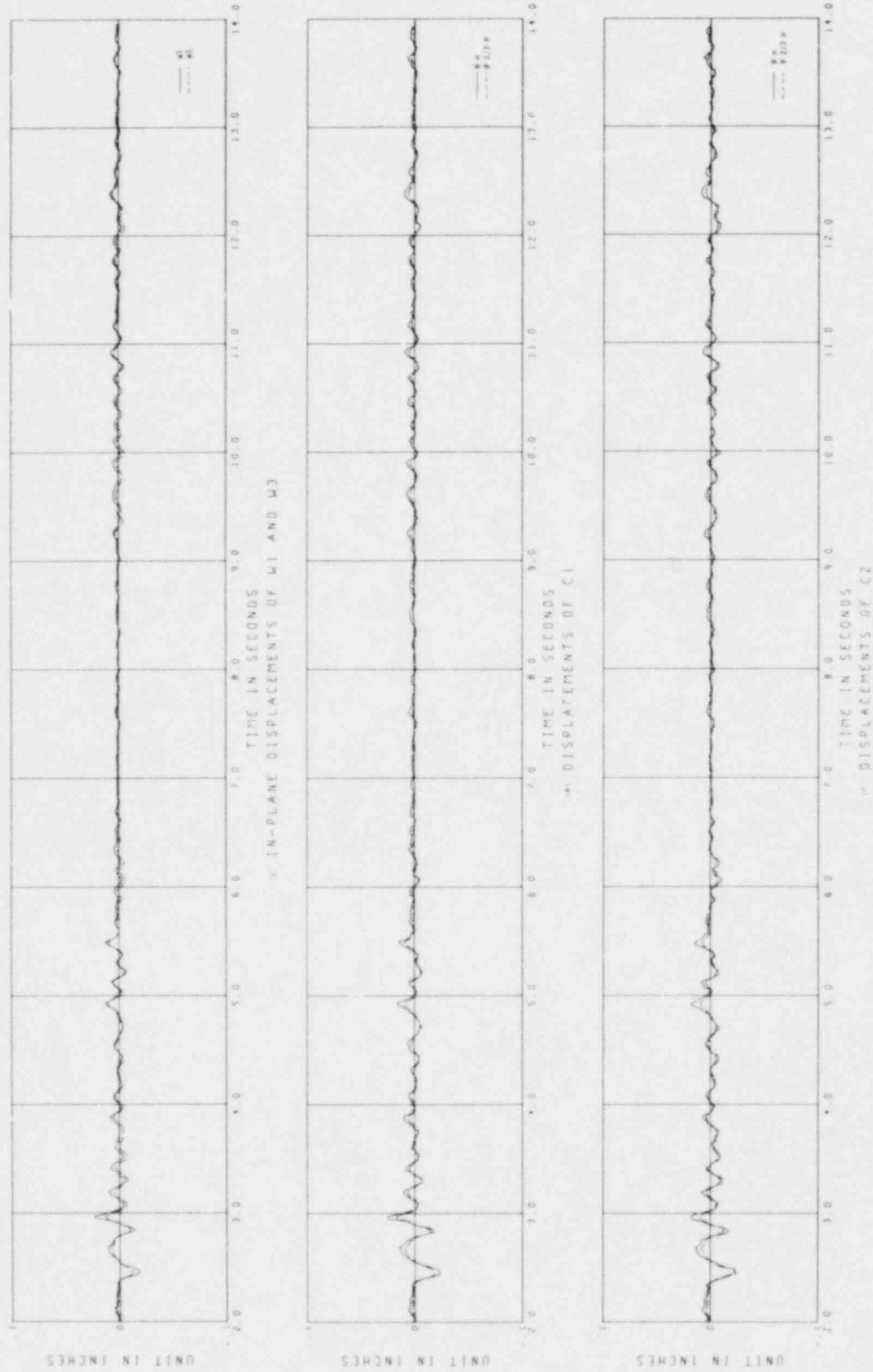

FIGURE 5.4 (CONT.) MEASURED RESPONSE: HOUSE 1, TEST 21 (EL CENTRO - 0.31 g)

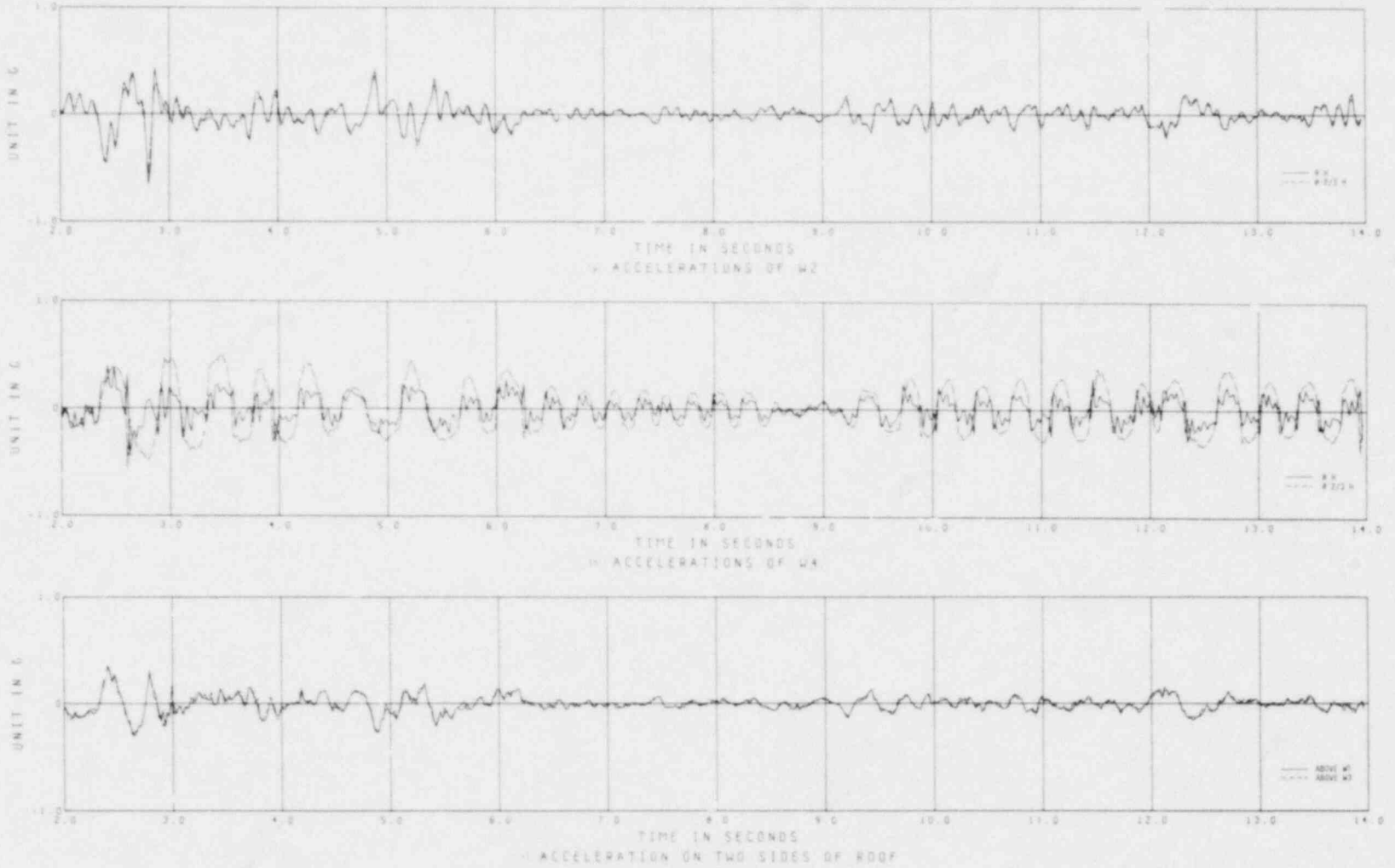

FIGURE 5.4 (CONT.) MEASURED RESPONSE: HOUSE 1, TEST 21 (EL CENTRO - 0.31 g)

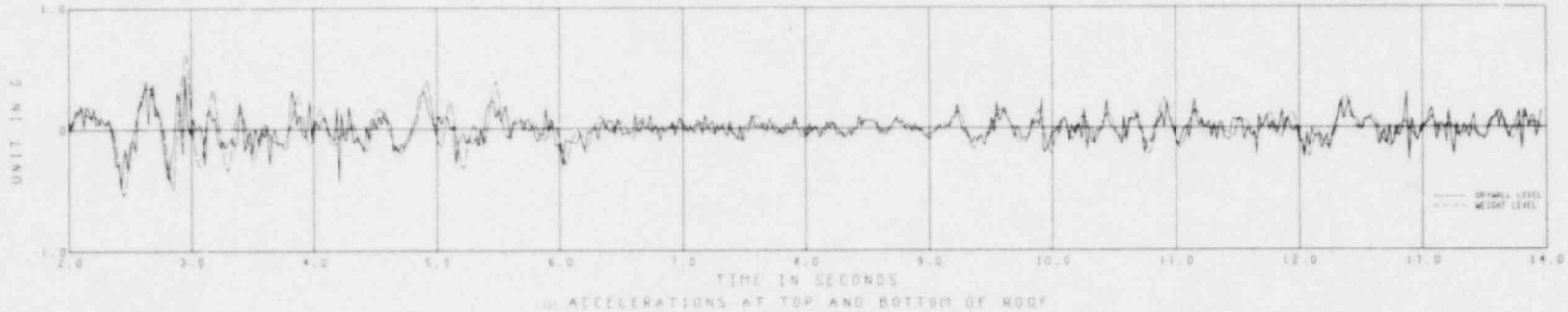

FIGURE 5.4 (CONT.) MEASURED RESPONSE: HOUSE 1, TEST 21 (EL CENTRO - 0.31 g)

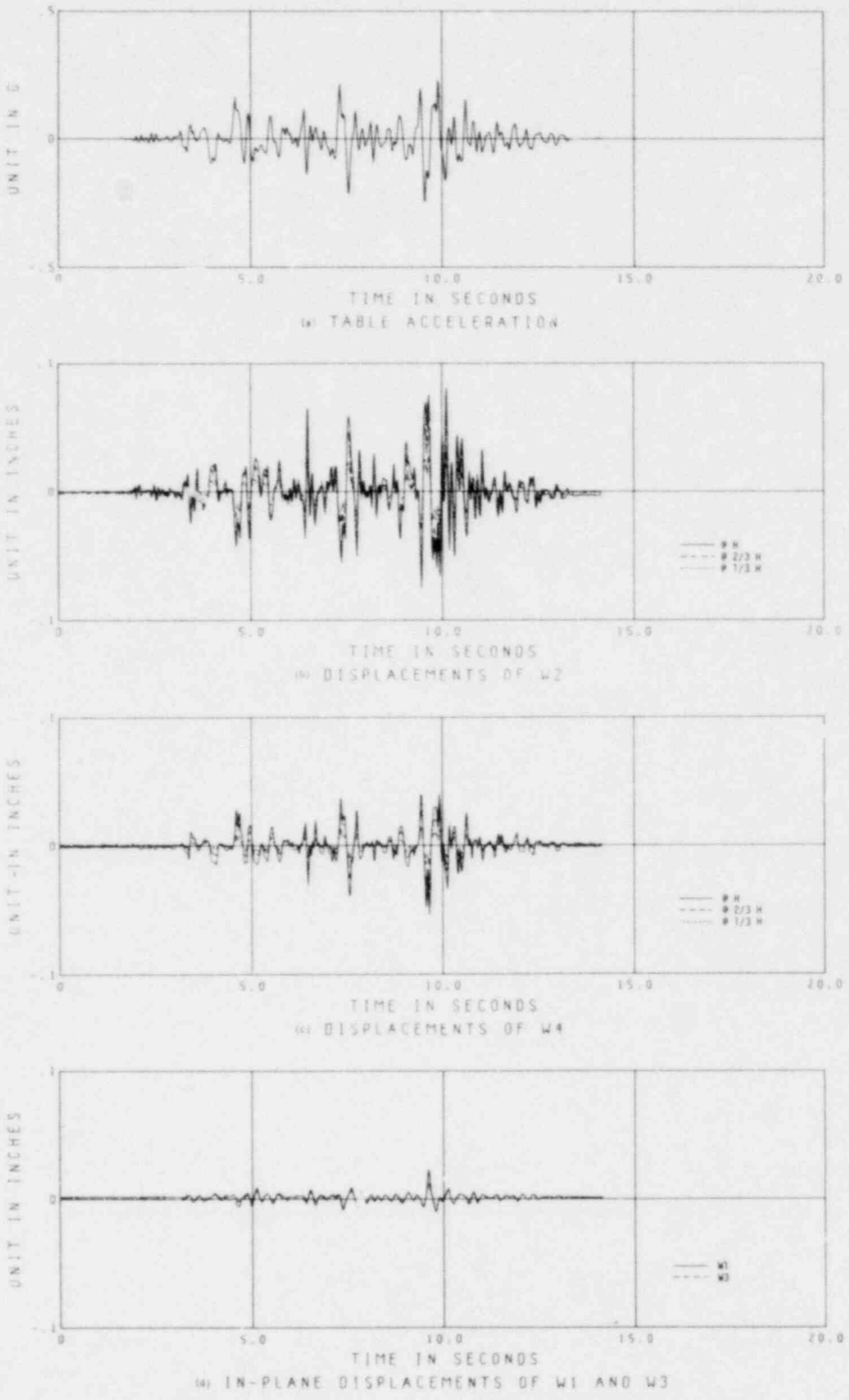

FIGURE 5.5 MEASURED RESPONSE: HOUSE 1, TEST 25 (PACOIMA - 0.25 g)

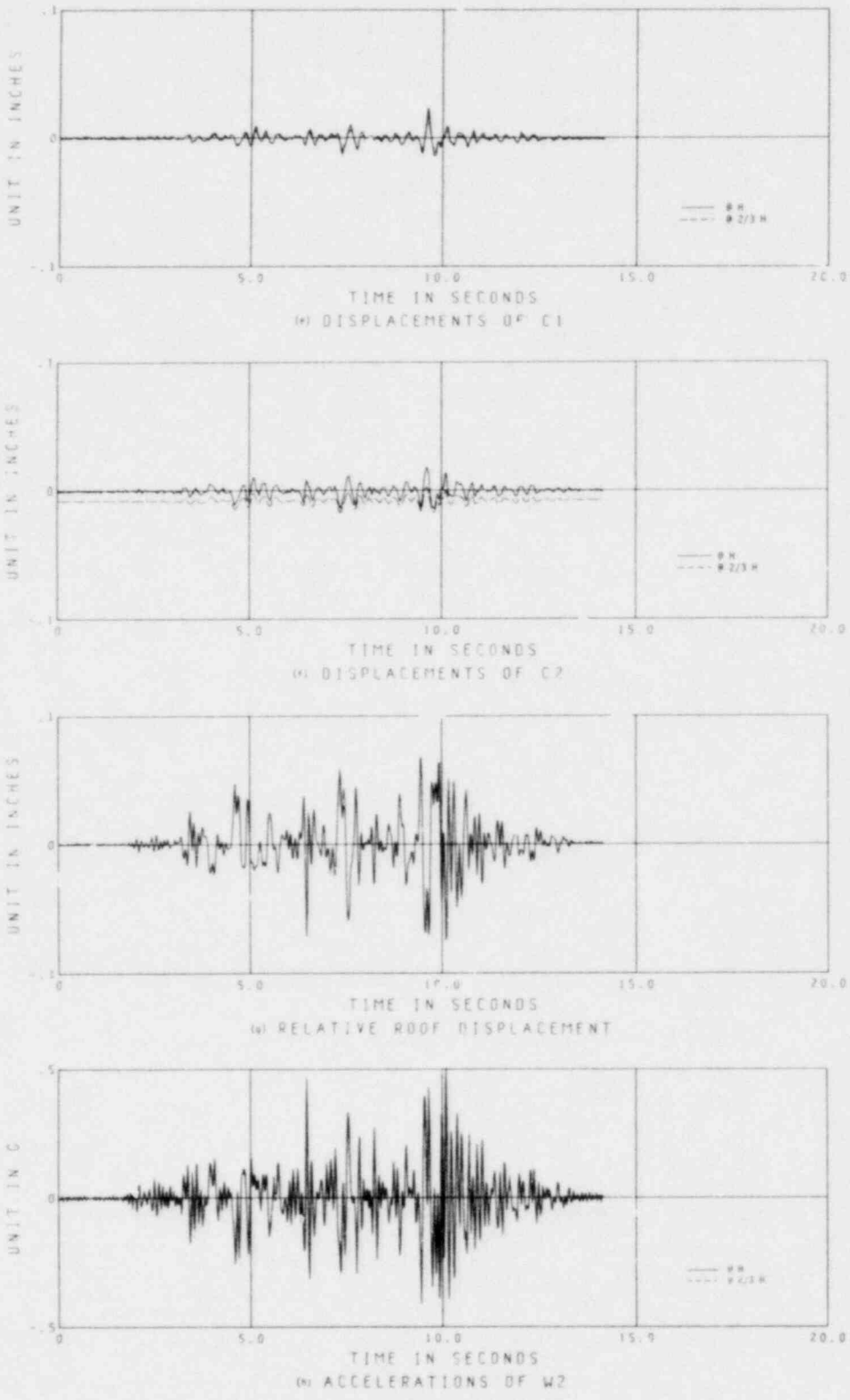

FIGURE 5.5 (CONT.) MEASURED RESPONSE: HOUSE 1, TEST 25 (PACOIMA - 0.25 g)

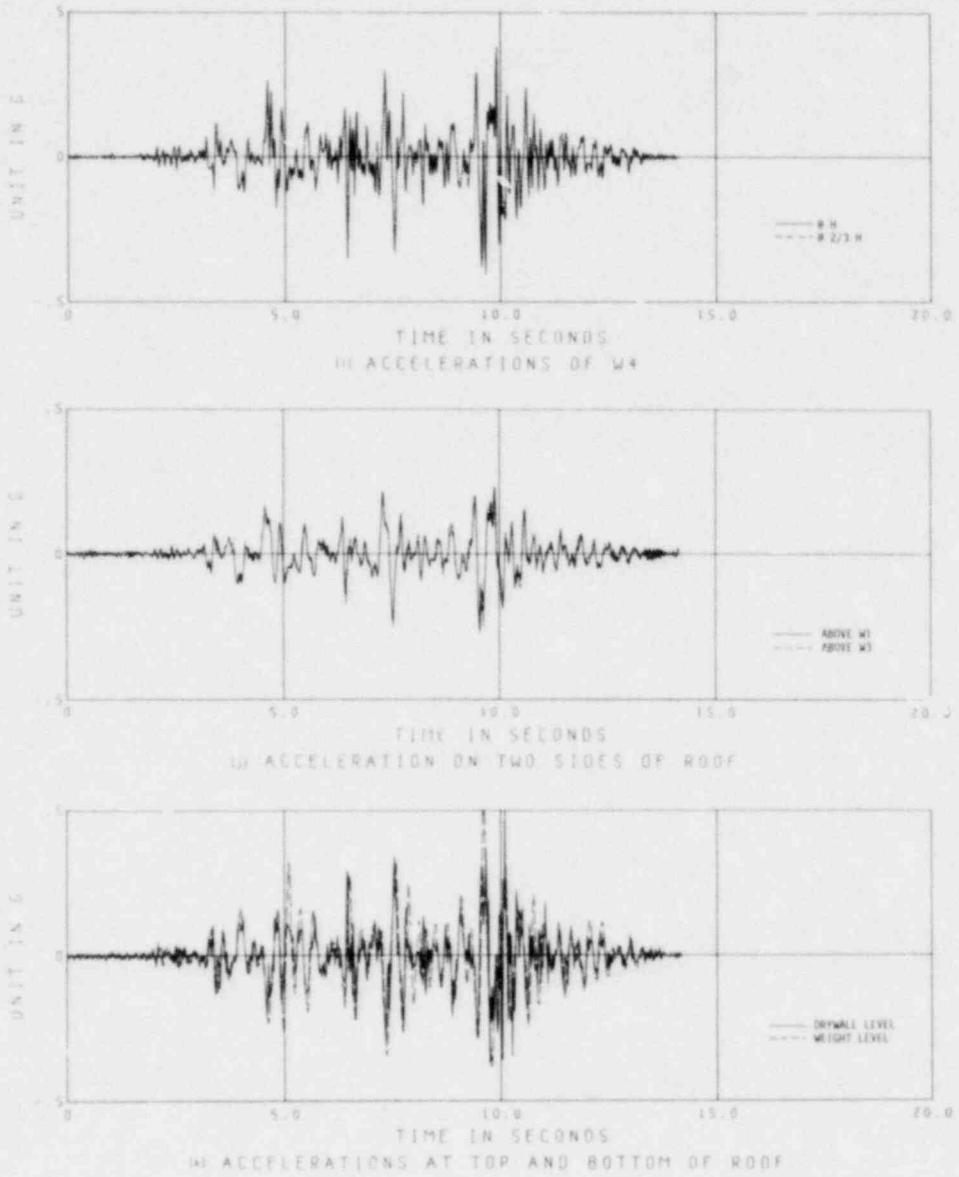

FIGURE 5.5 (CONT.) MEASURED RESPONSE: HOUSE 1, TEST 25 (PACOIMA - 0.25 g)

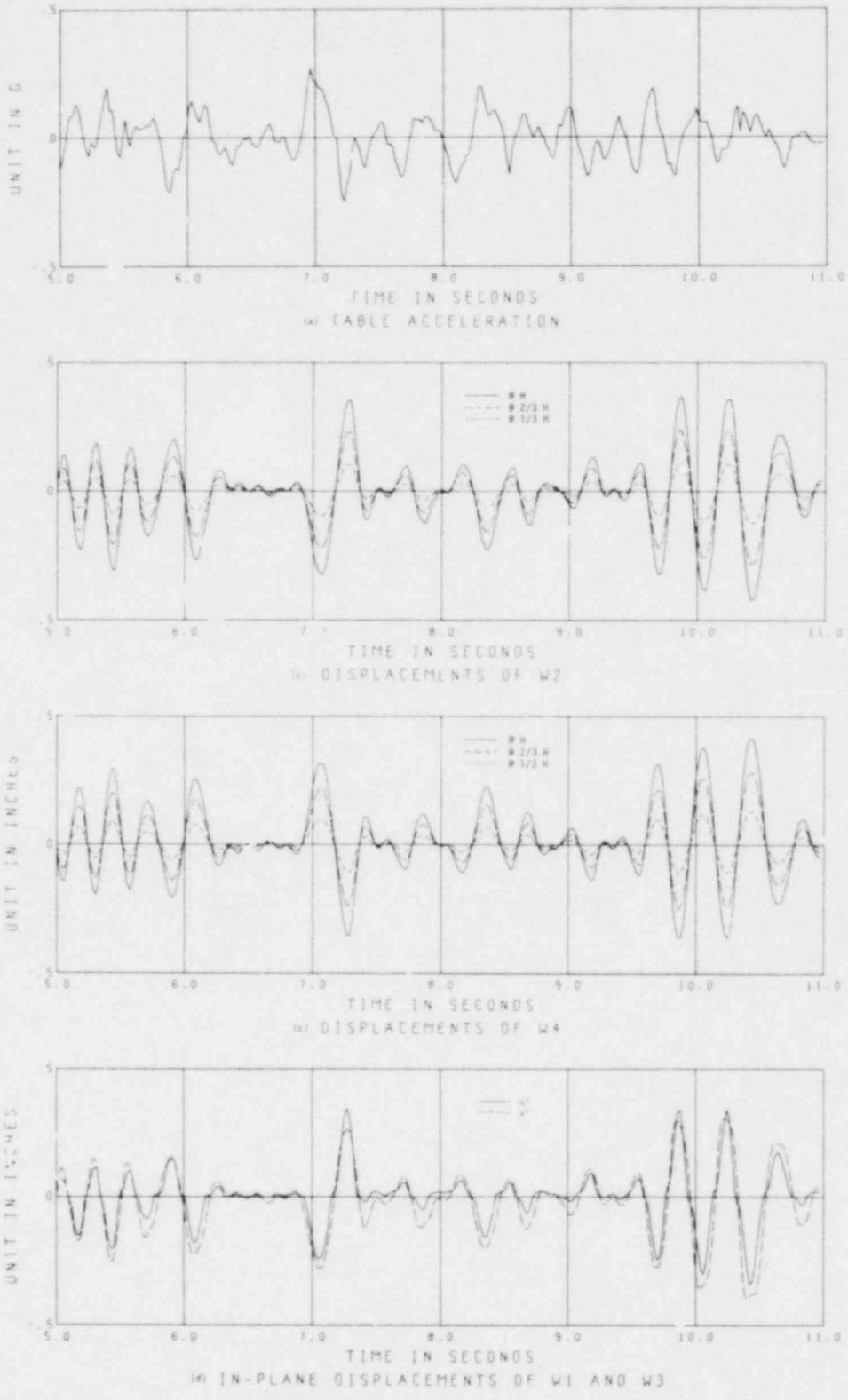

FIGURE 5.6 MEASURED RESPONSE: HOUSE 1, TEST 10 (TAFT - 0.27 g)

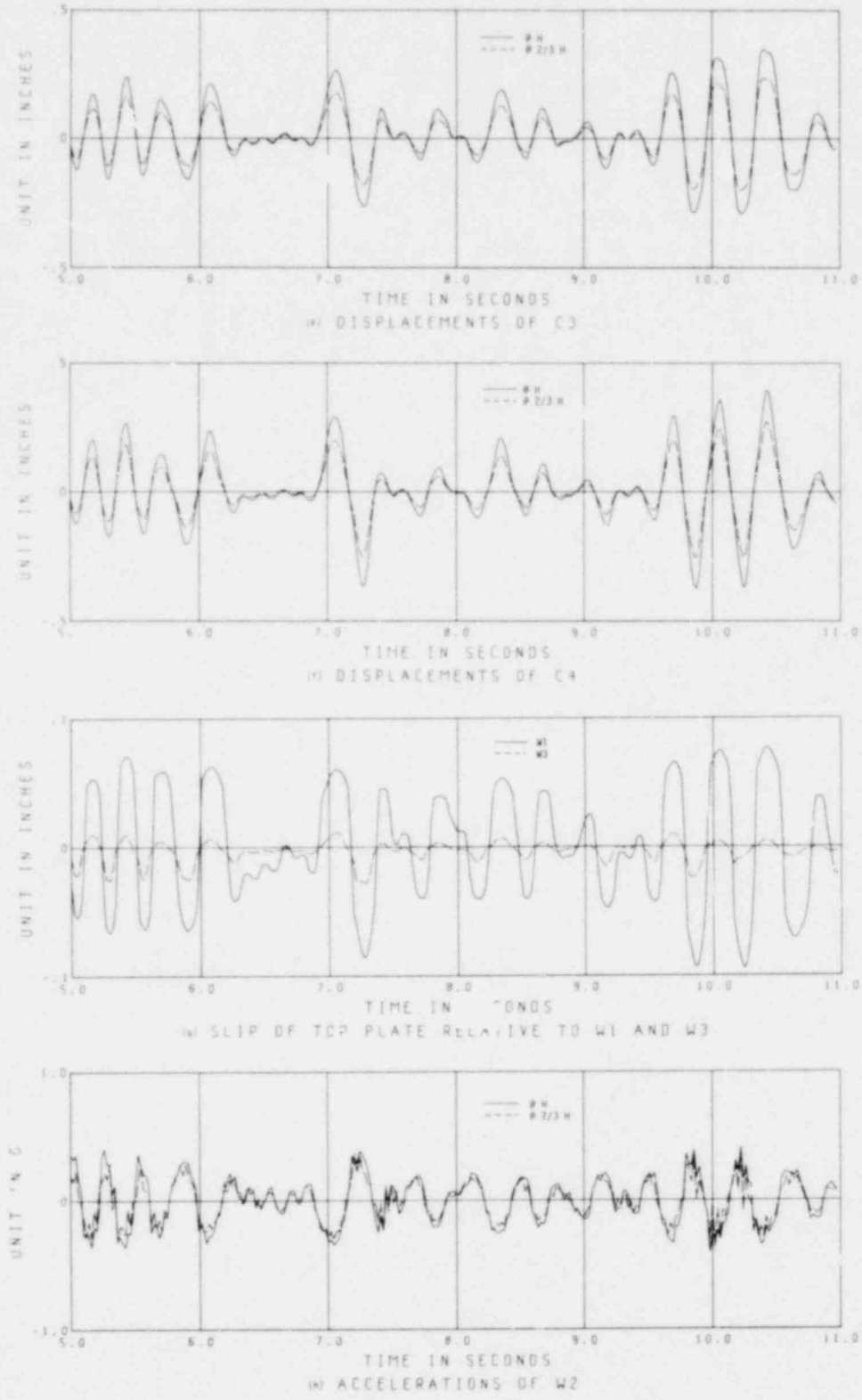

FIGURE 5.6 (CONT.) MEASURED RESPONSE: HOUSE 1, TEST 10 (TAFT - 0.27 g)

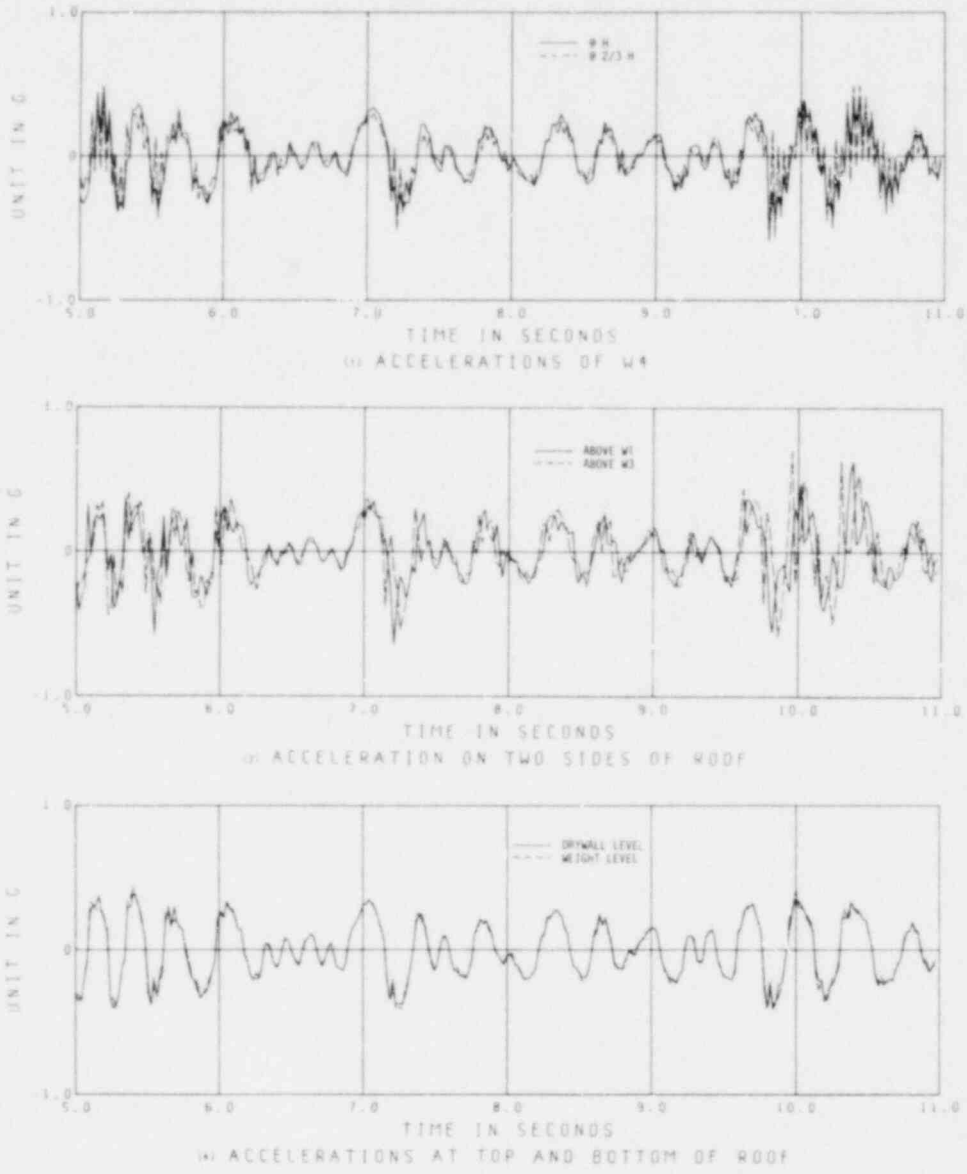

FIGURE 5.6 (CONT.) MEASURED RESPONSE: HOUSE 1, TEST 10 (TAFT - 0.27 g)

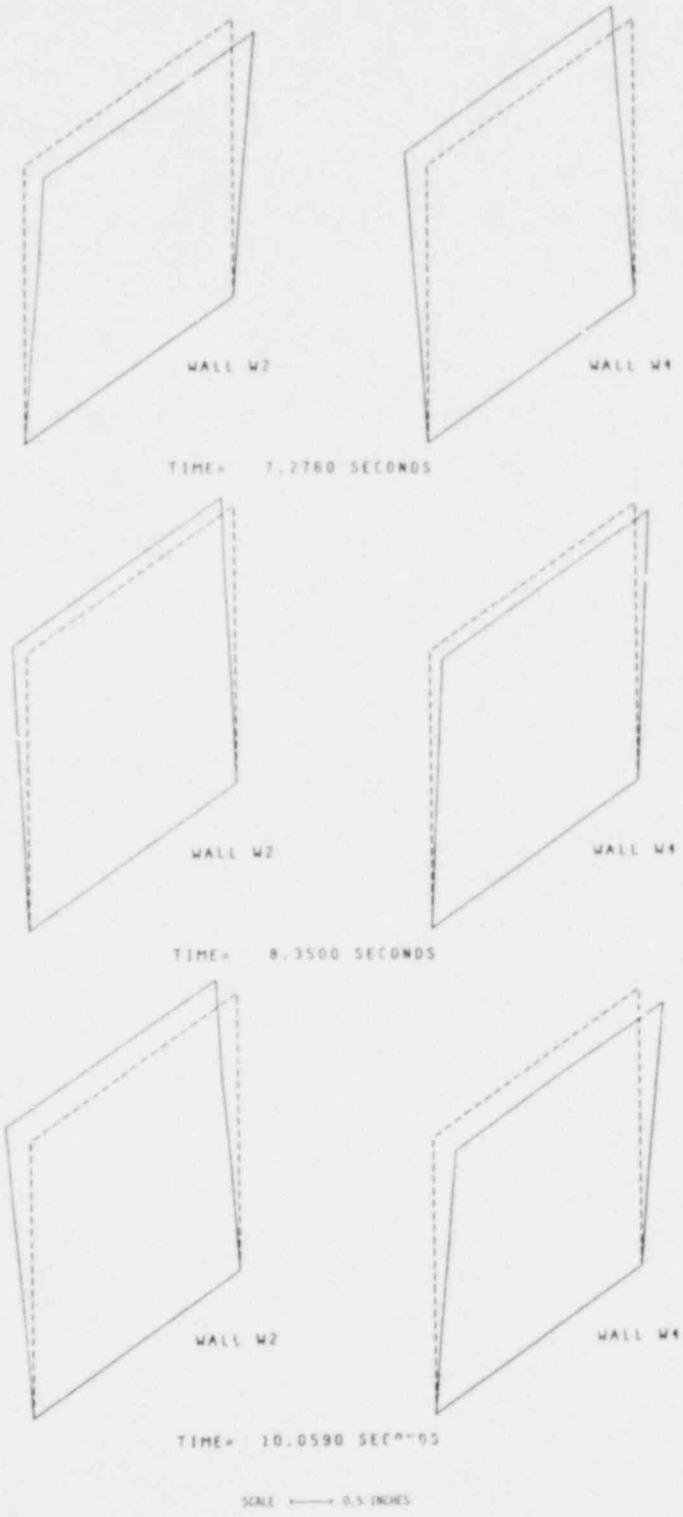

FIGURE 5.7 DEFLECTED SHAPES OF OUT-OF-PLANE WALLS: HOUSE 1 TEST 10 (TAFT - 0.27 g)

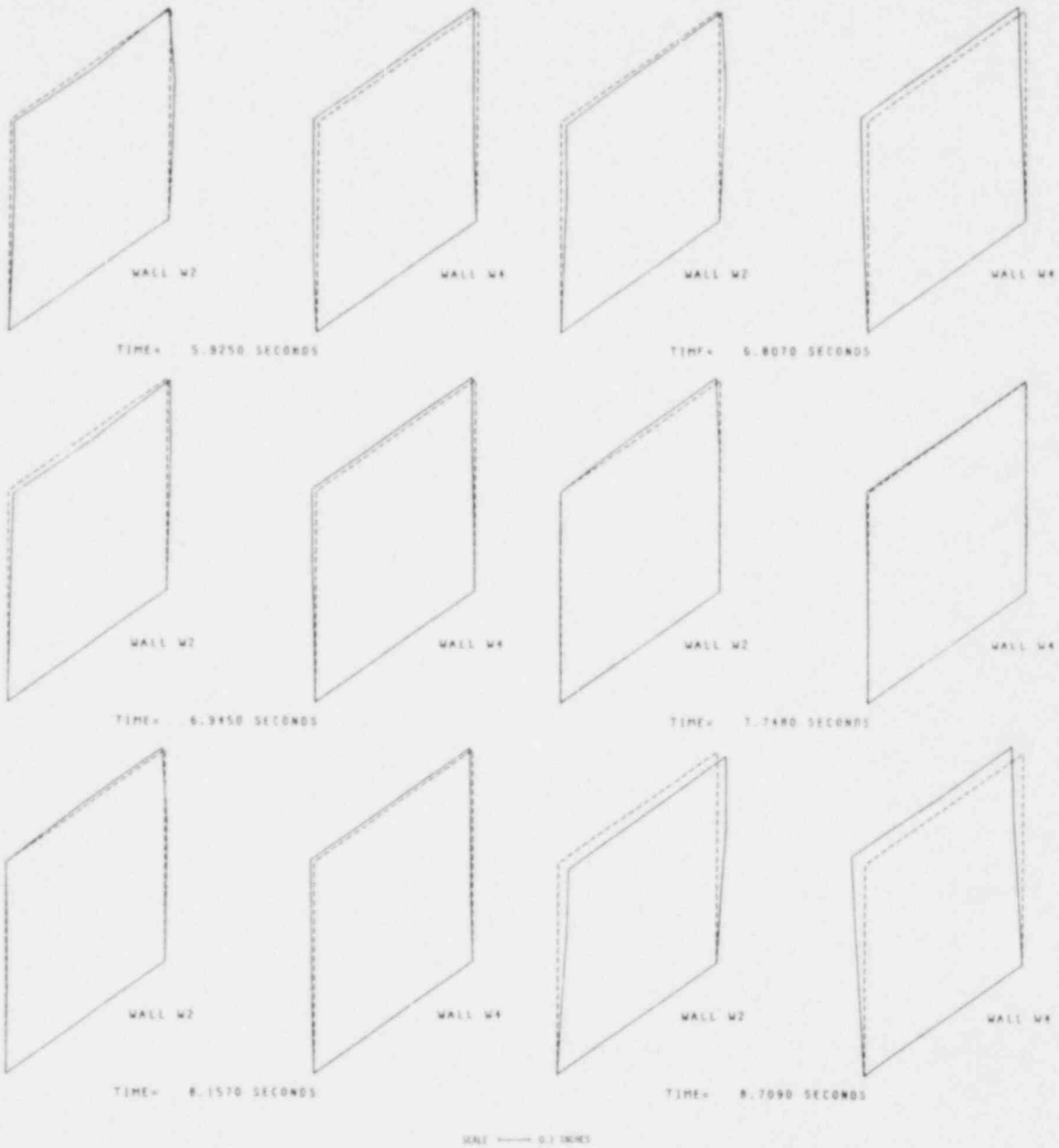

FIGURE 5.8 DEFLECTED SHAPES OF OUT-OF-PLANE WALLS: HOUSE 1
TEST 19 (TAFT - 0.25 g)

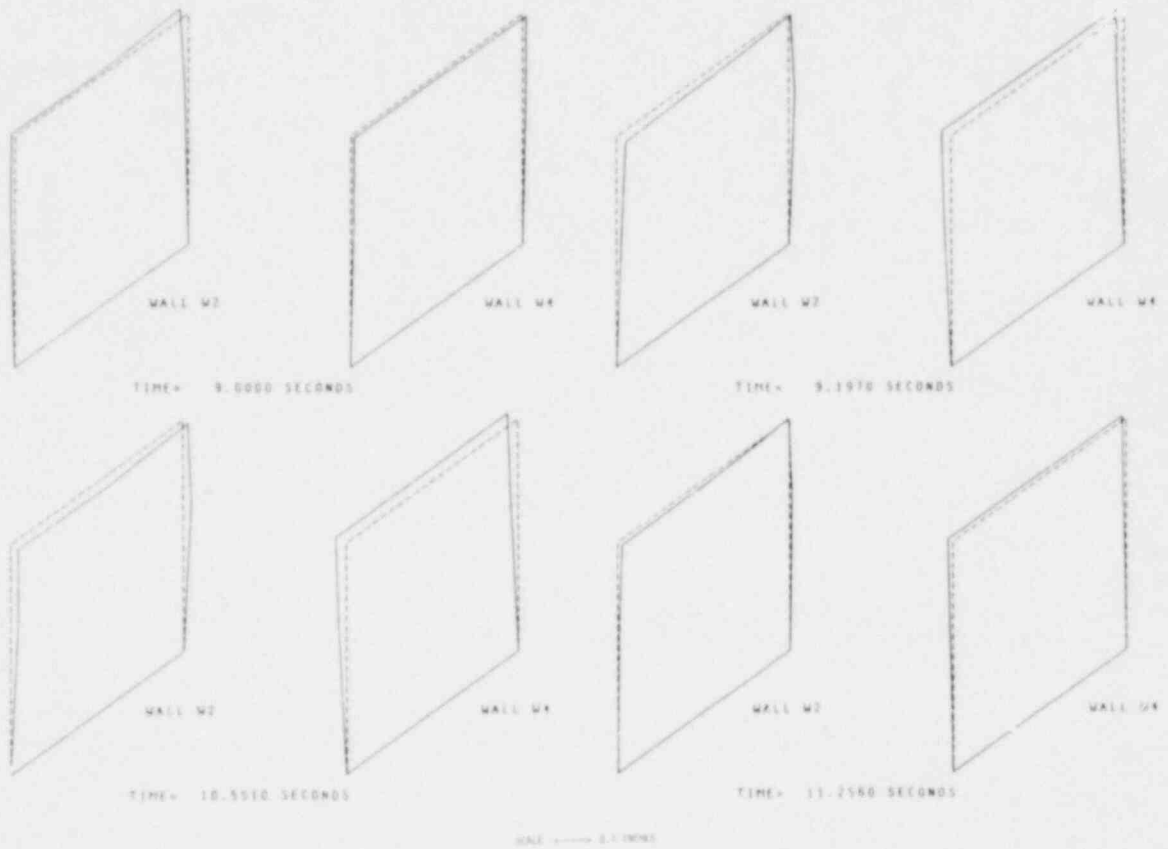

FIGURE 5.8 (CONT.) DEFLECTED SHAPES OF OUT-OF-PLANE WALLS: HOUSE 1 TEST 19 (TAFT - 0.25 g)

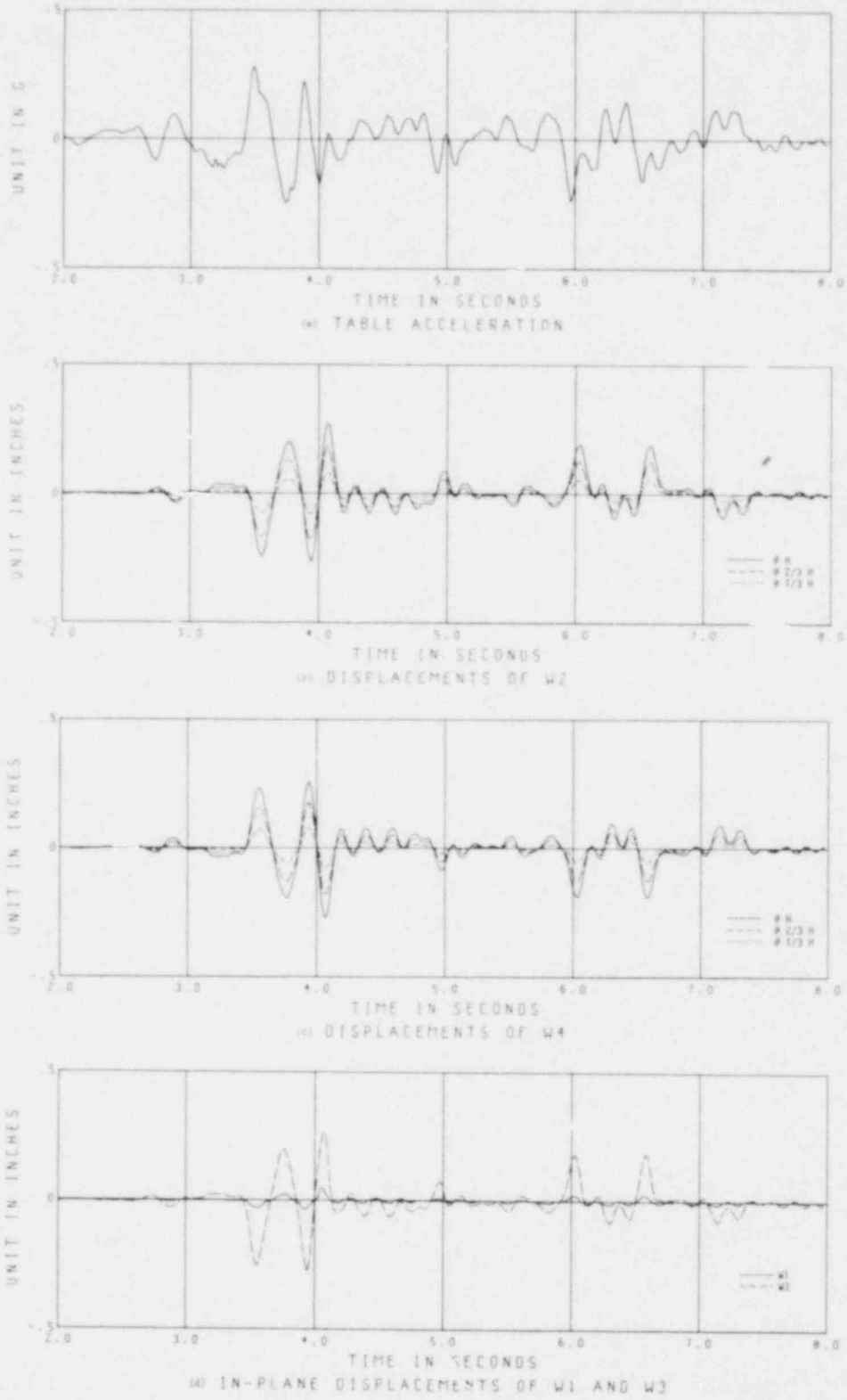

FIGURE 5.9 MEASURED RESPONSE: HOUSE 1, TEST 13 (EL CENTRO - 0.28 g)

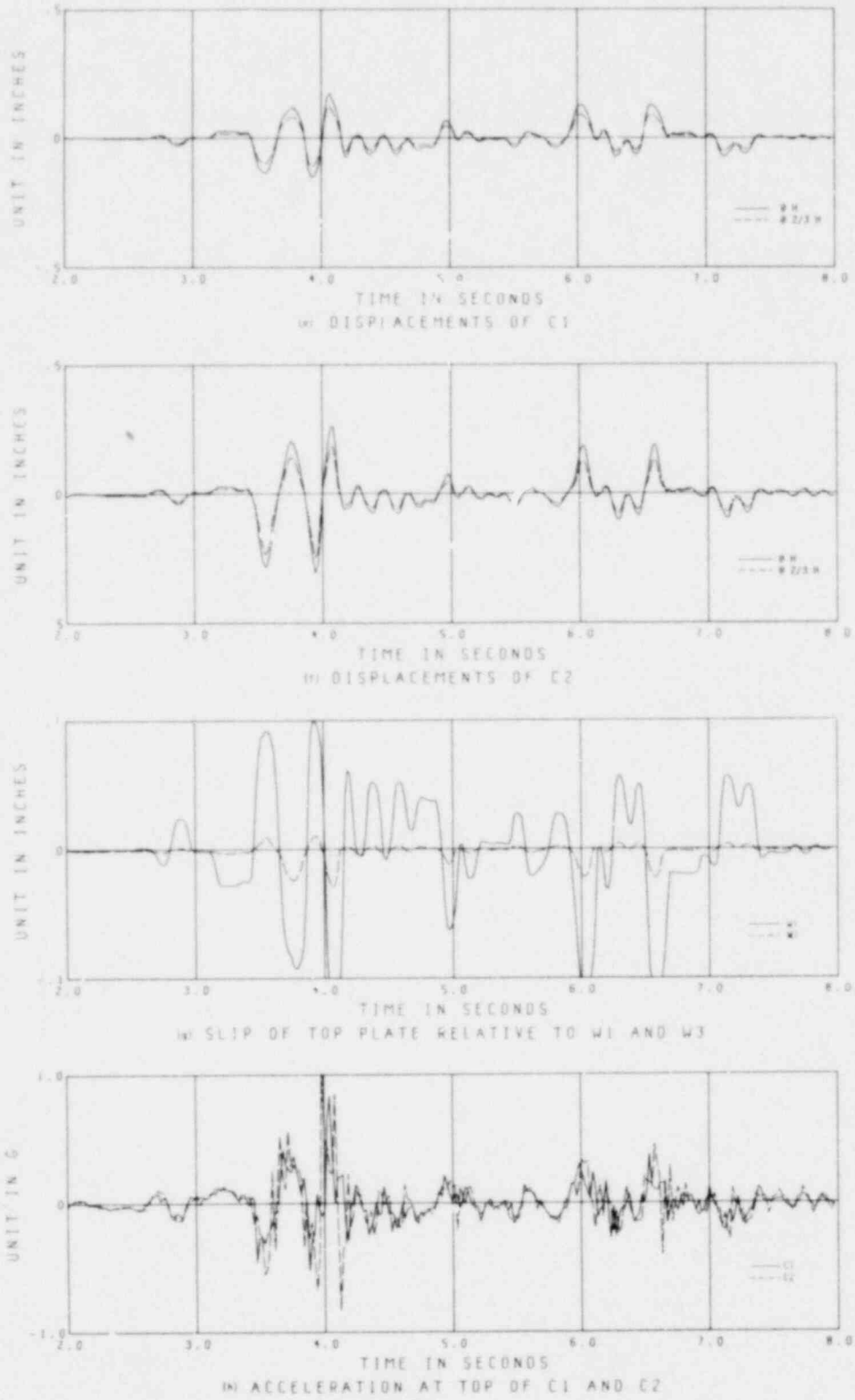

FIGURE 5.9 (CONT.) MEASURED RESPONSE: HOUSE 1, TEST 13 (EL CENTRO - 0.28 g)

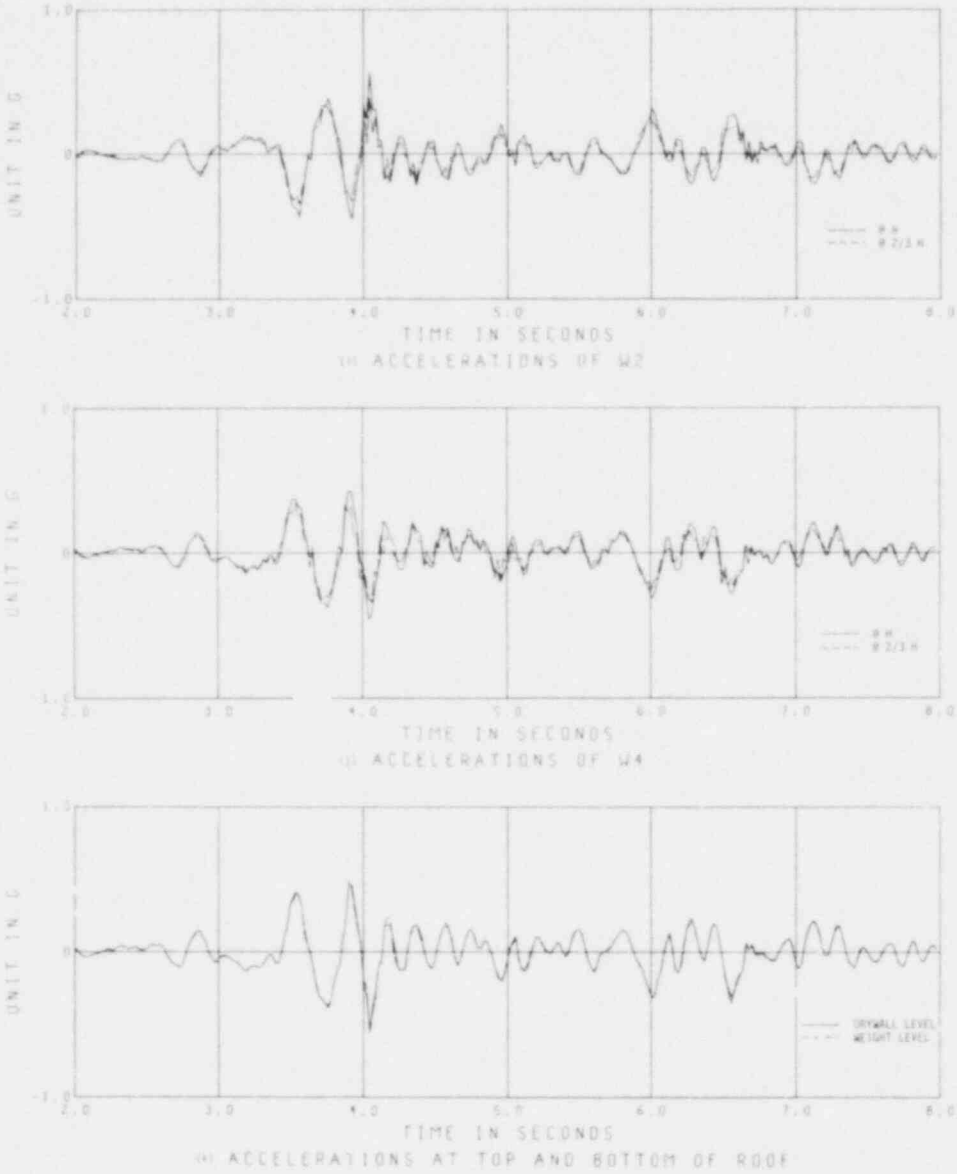

FIGURE 5.9 (CONT.) MEASURED RESPONSE: HOUSE 1, TEST 13 (EL CENTRO - 0.28 g)

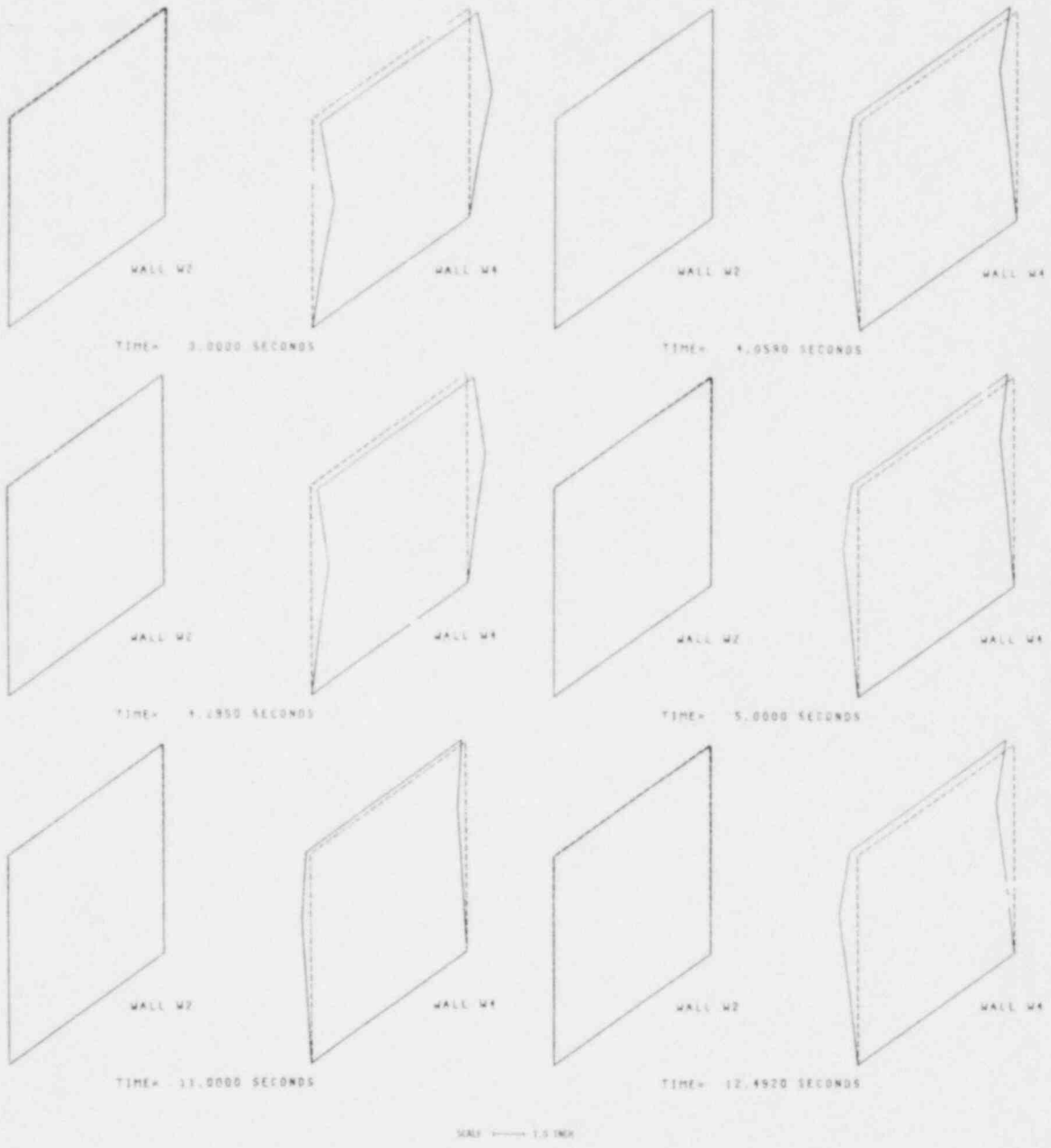

FIGURE 5.10 DEFLECTED SHAPES OF OUT-OF-PLANE WALLS: HOUSE 1 TEST 21 (EL CENTRO - 0.31 g)

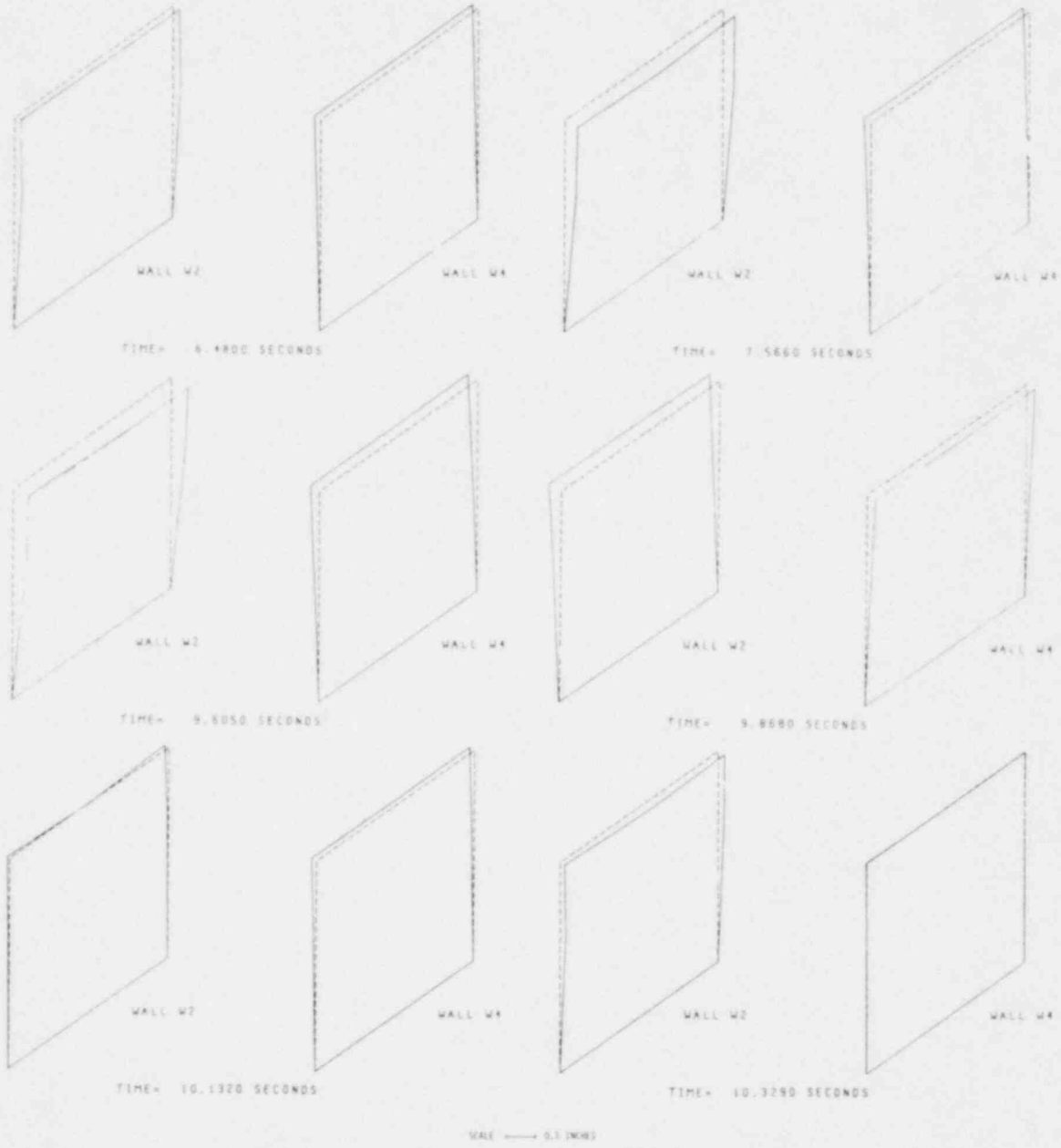

FIGURE 5.11 DEFLECTED SHAPES OF OUT-OF-PLANE WALLS: HOUSE 1 TEST 25 (PACOIMA - 0.25 g)

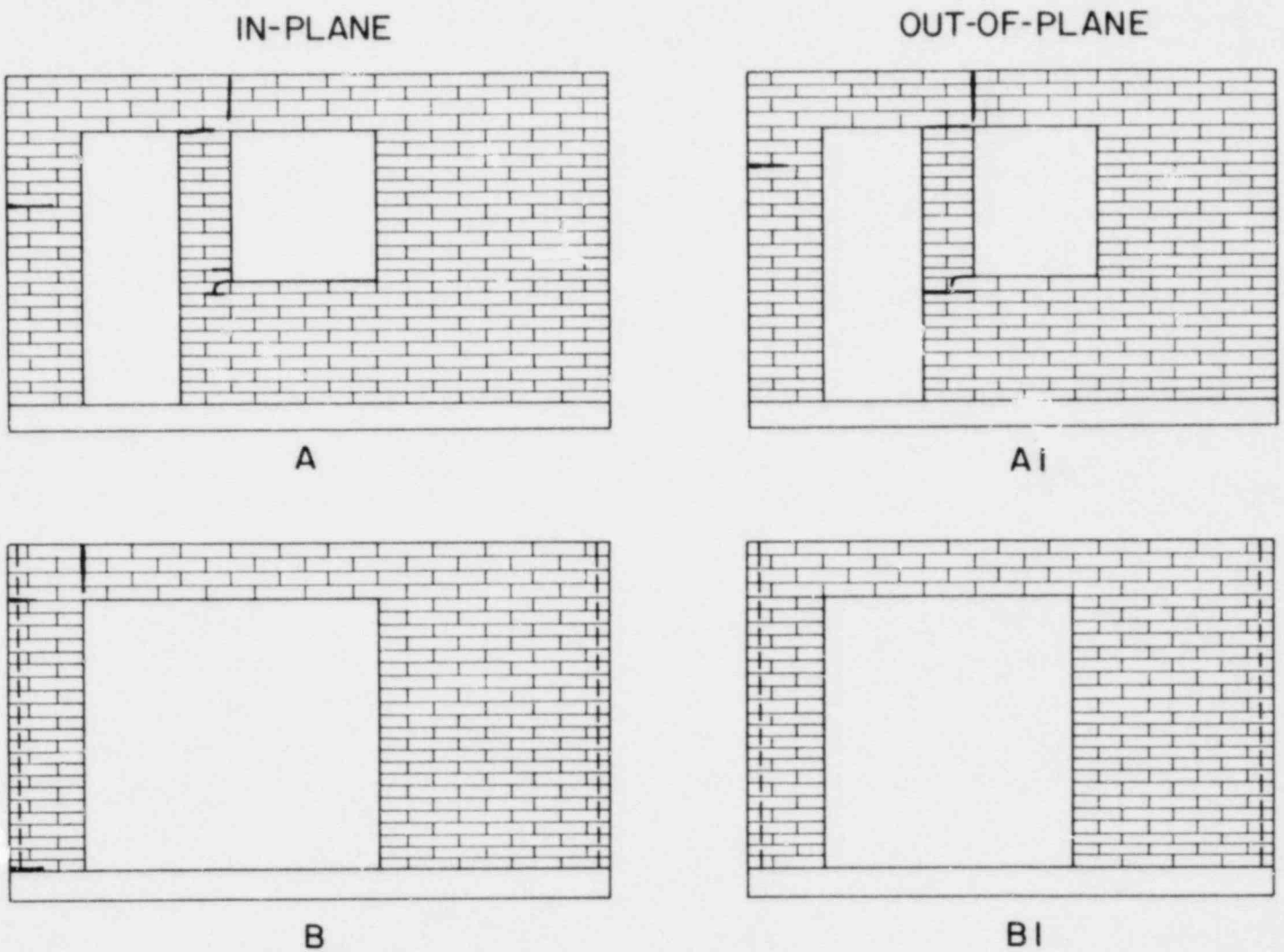

FIGURE 5.12(a) DISTRIBUTION OF CRACKS IN THE MASONRY COMPONENTS: HOUSE 2, BEFORE TESTING

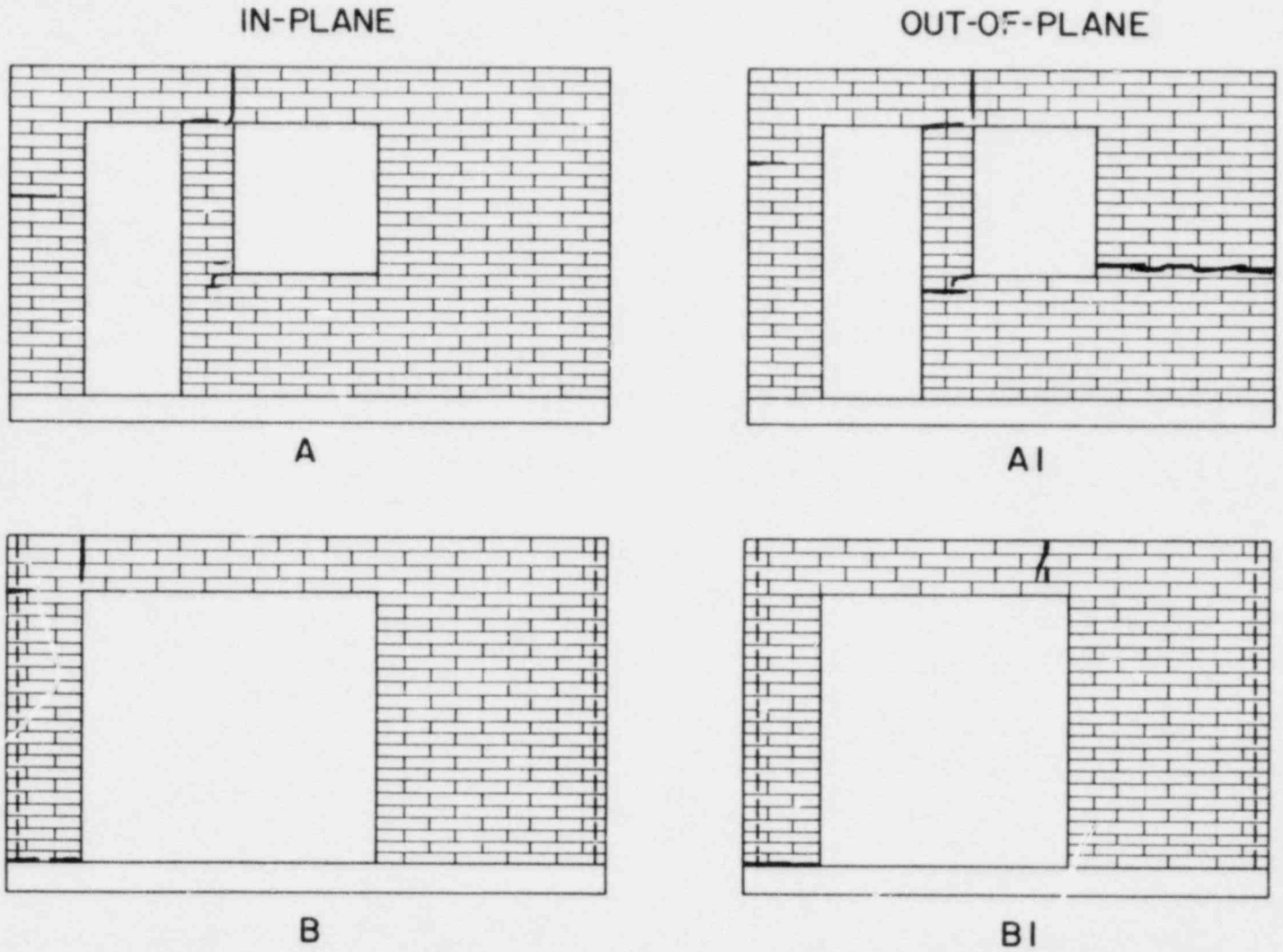

FIGURE 5.12(b) DISTRIBUTION OF CRACKS IN THE MASONRY COMPONENTS: HOUSE 2, AFTER TEST 14 (EL CENTRO - 0.33 g)

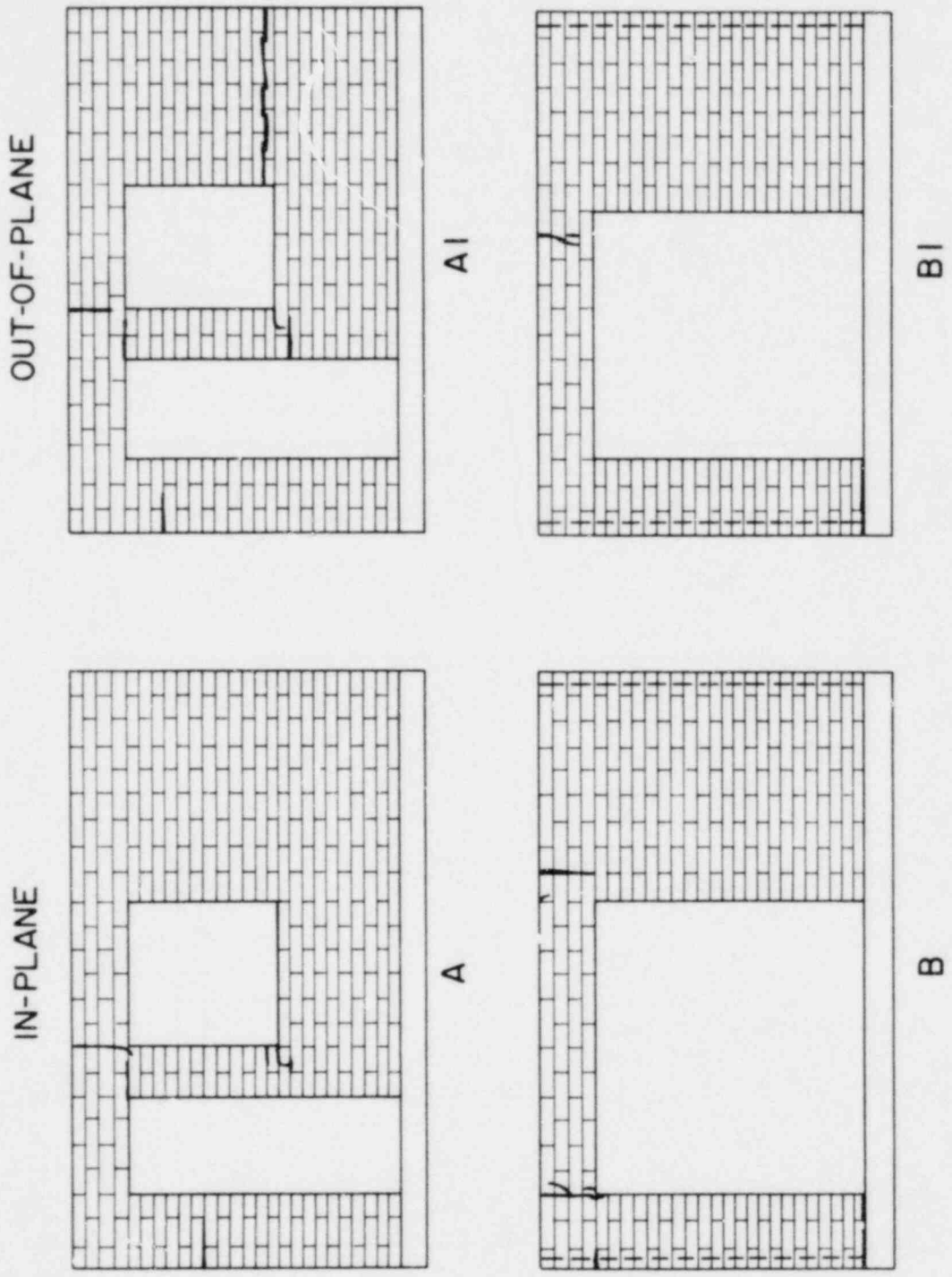

FIGURE 5.12(c) DISTRIBUTION OF CRACKS IN THE MASONRY COMPONENTS: HOUSE 2, AFTER TEST 15 (EL CENTRO - 0.45 g)

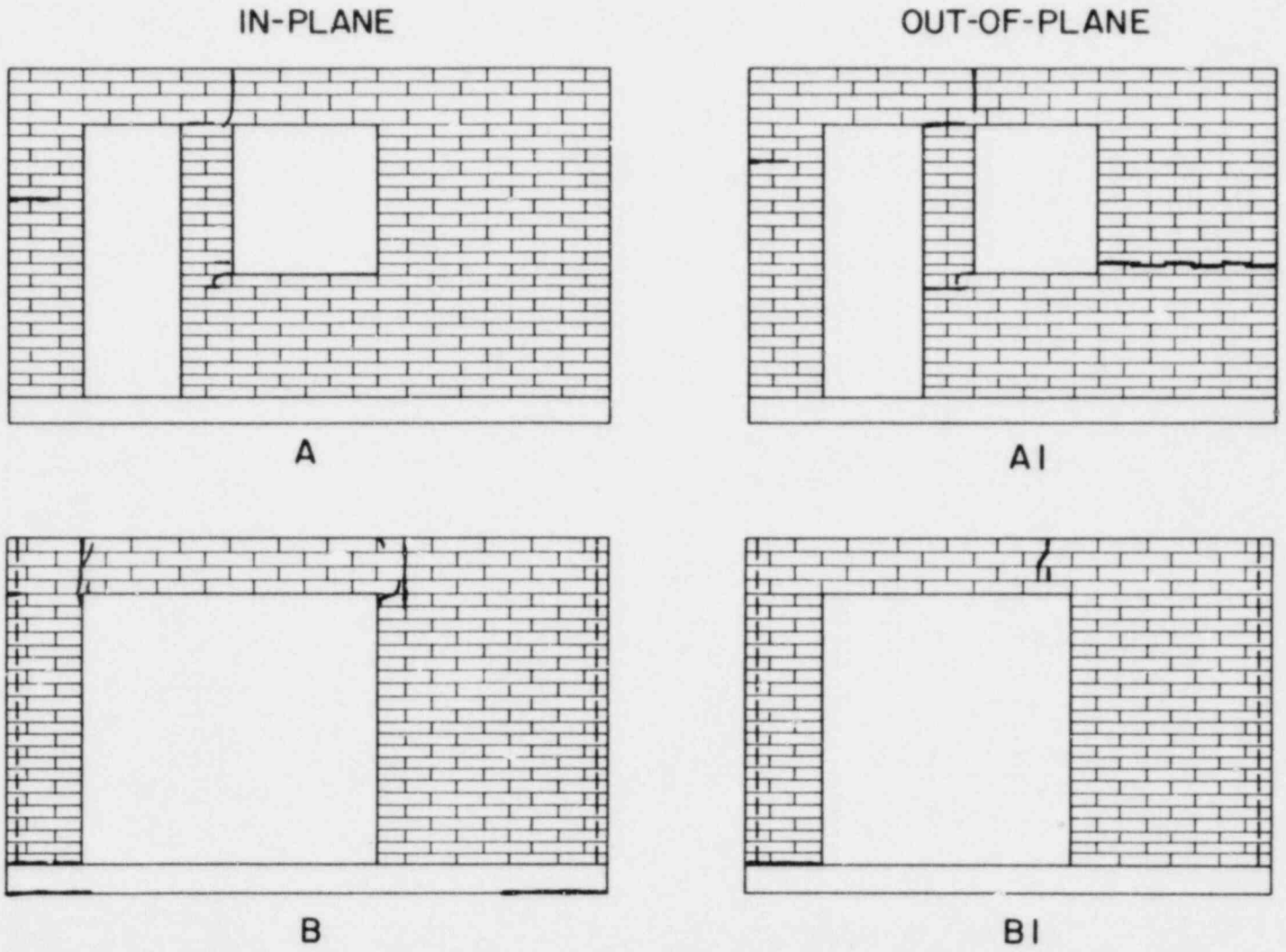

FIGURE 5.12(d) DISTRIBUTION OF CRACKS IN THE MASONRY COMPONENTS: HOUSE 2, AFTER TEST 16 (TAFT - 0.40 g)

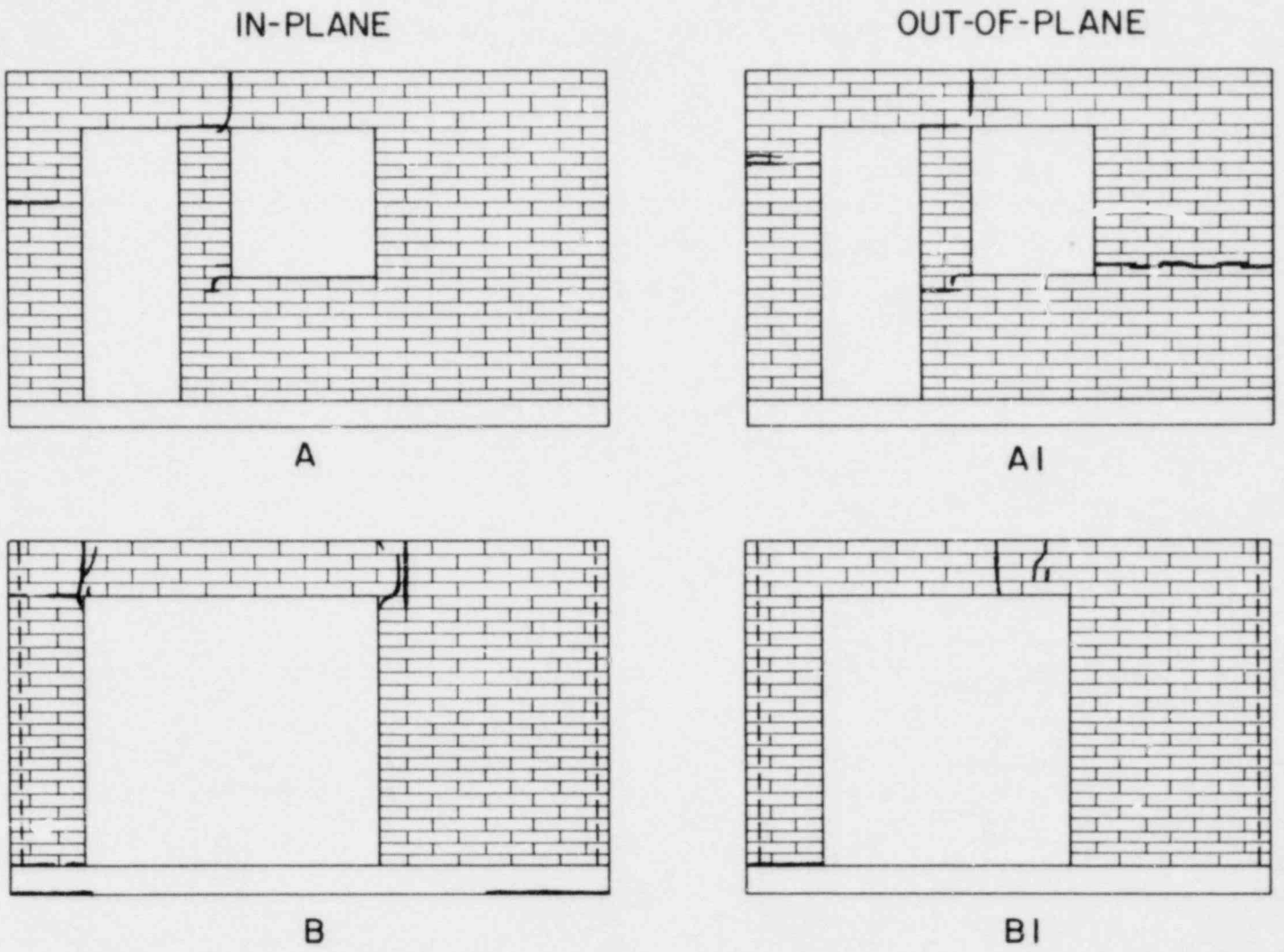

FIGURE 5.12(e) DISTRIBUTION OF CRACKS IN THE MASONRY COMPONENTS: HOUSE 2, AFTER TEST 19 (PACOIMA - 0.51 g)

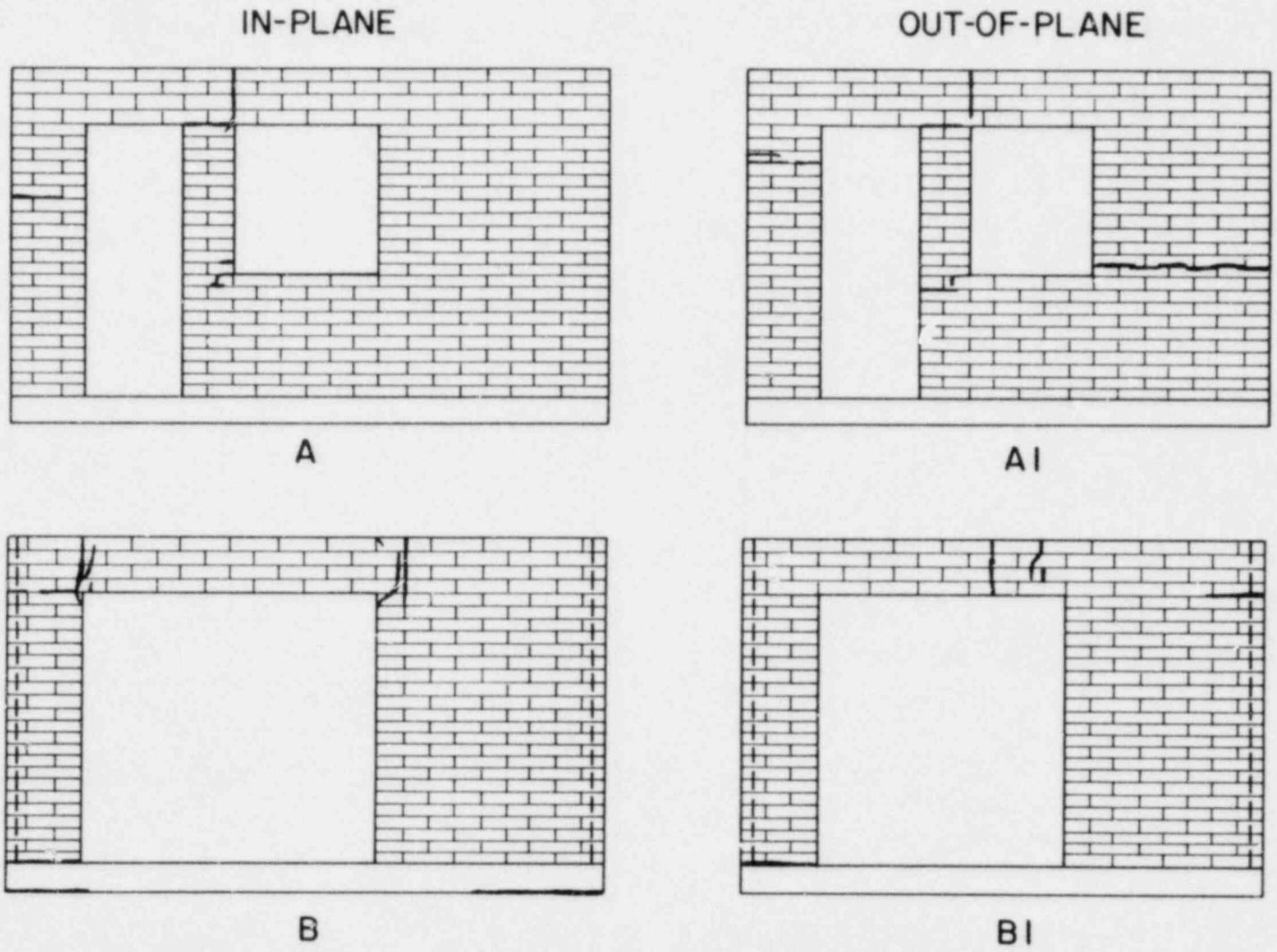

FIGURE 5.12(f) DISTRIBUTION OF CRACKS IN THE MASONRY COMPONENTS: HOUSE 2, AFTER TEST 21 (TAFT - 0.08 g)

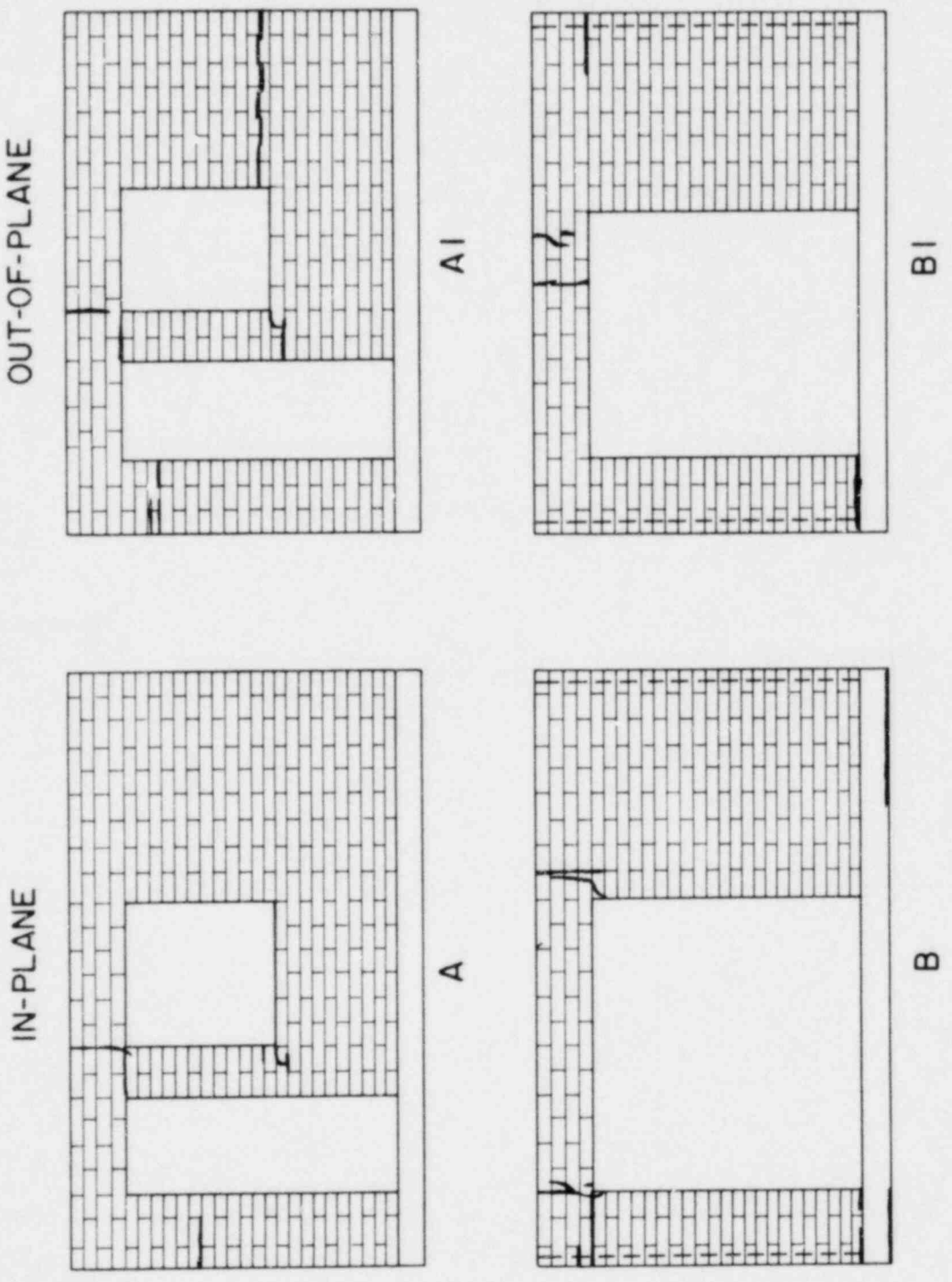

FIGURE 5.12(g) DISTRIBUTION OF CRACKS IN THE MASONRY COMPONENTS: HOUSE 2, AFTER TEST 26 (TAF, - 0.26 g)

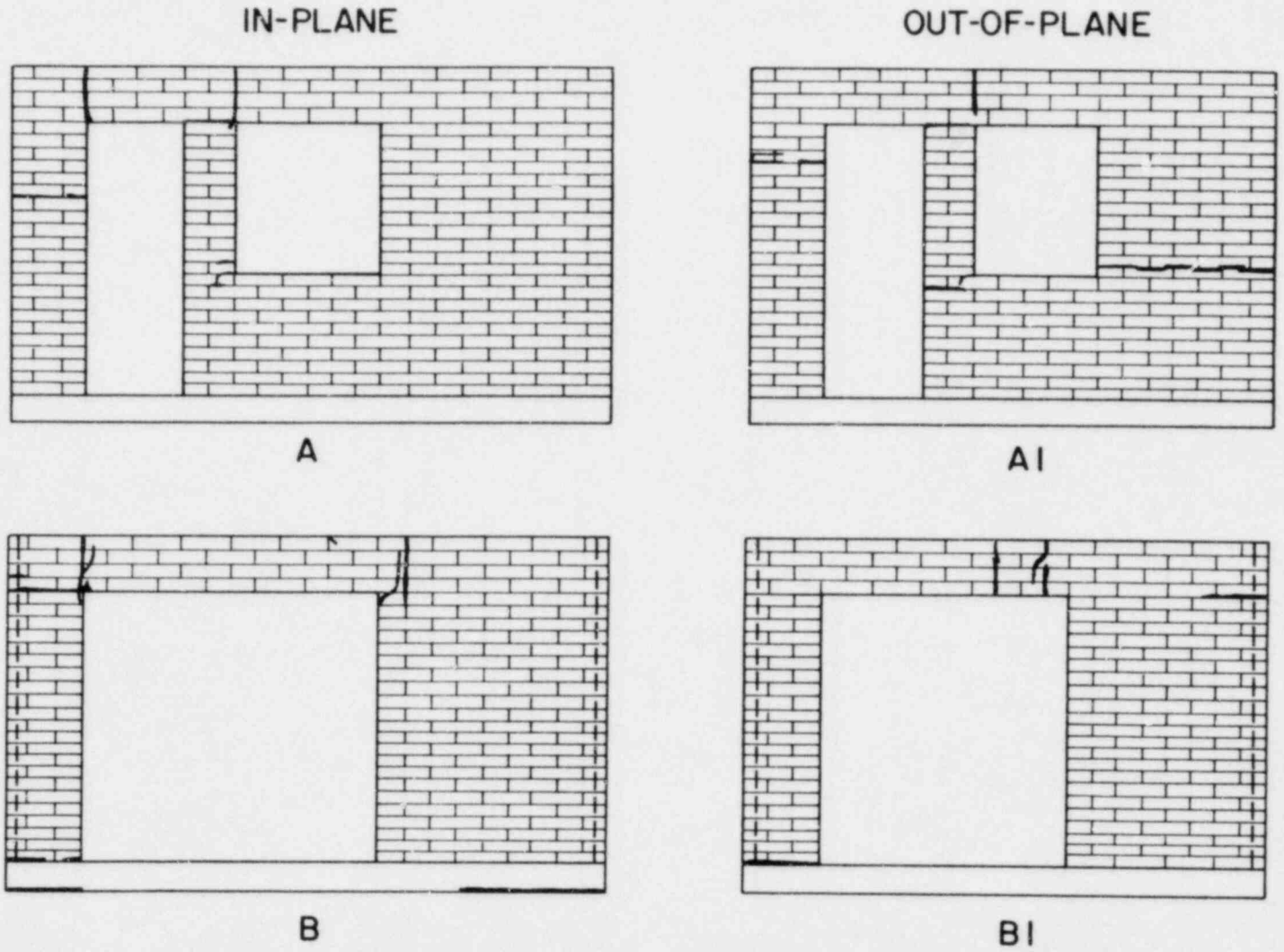

FIGURE 5.12(h) DISTRIBUTION OF CRACKS IN THE MASONRY COMPONENTS: HOUSE 2, AFTER TEST 30 (EL CENTRO - 0.37 g)

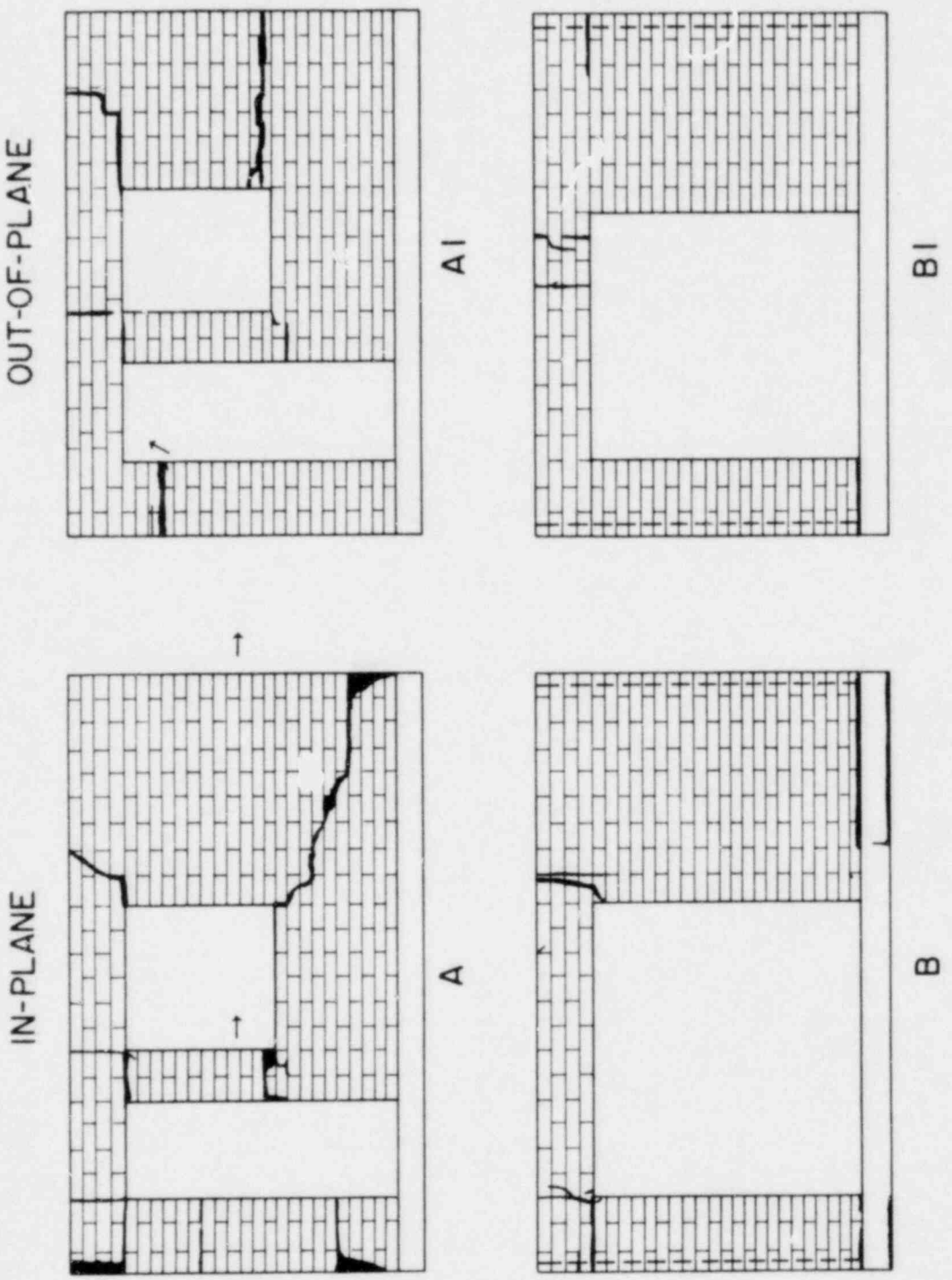

FIGURE 5.12(i) DISTRIBUTION OF CRACKS IN THE MASONRY COMPONENTS: HOUSE 2, AFTER TEST 32 (PACOIMA - 0.52 g)

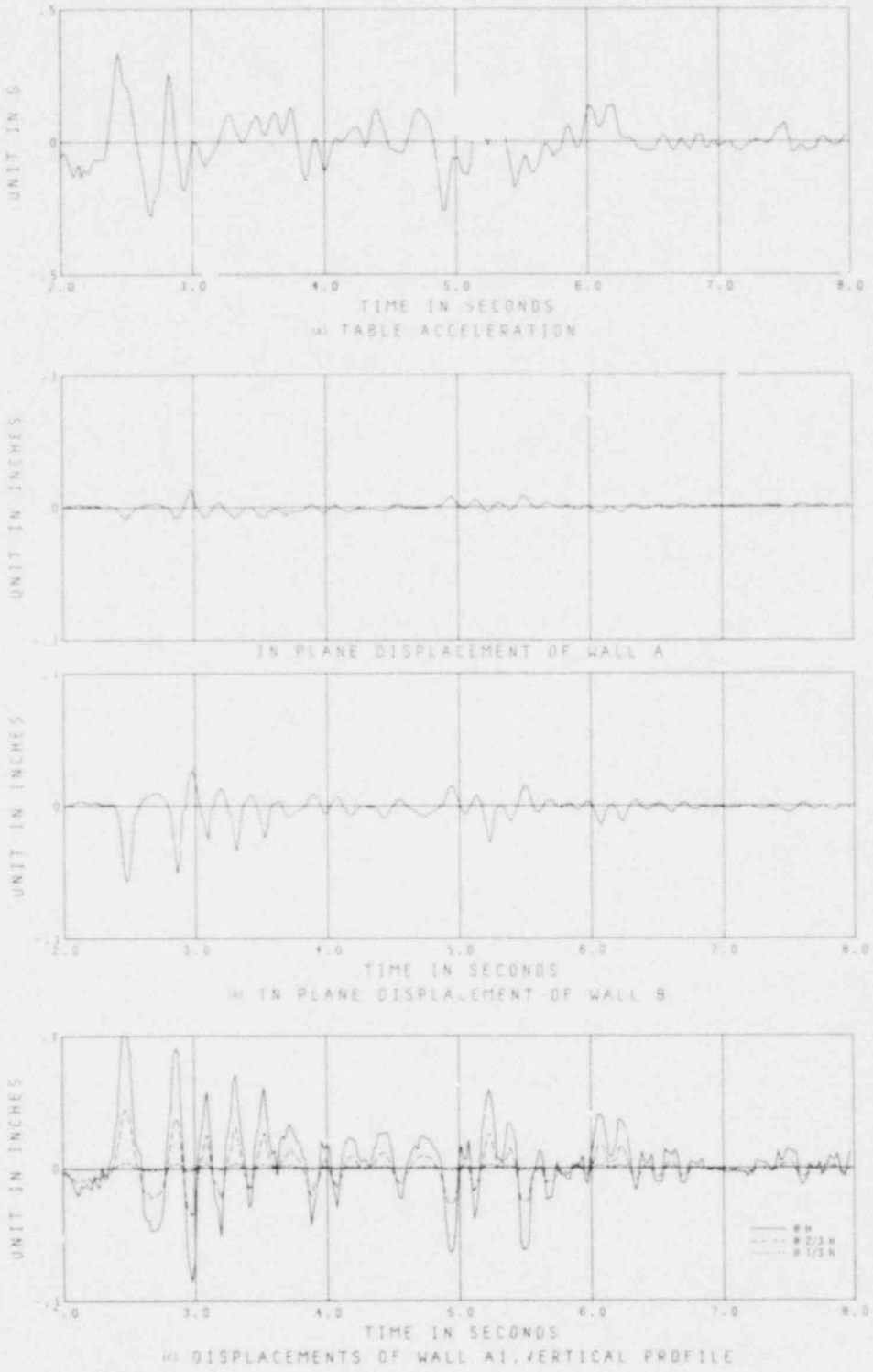

FIGURE 5.13 MEASURED RESPONSE: HOUSE 2, TEST 14 (EL CENTRO - 0.33 g)

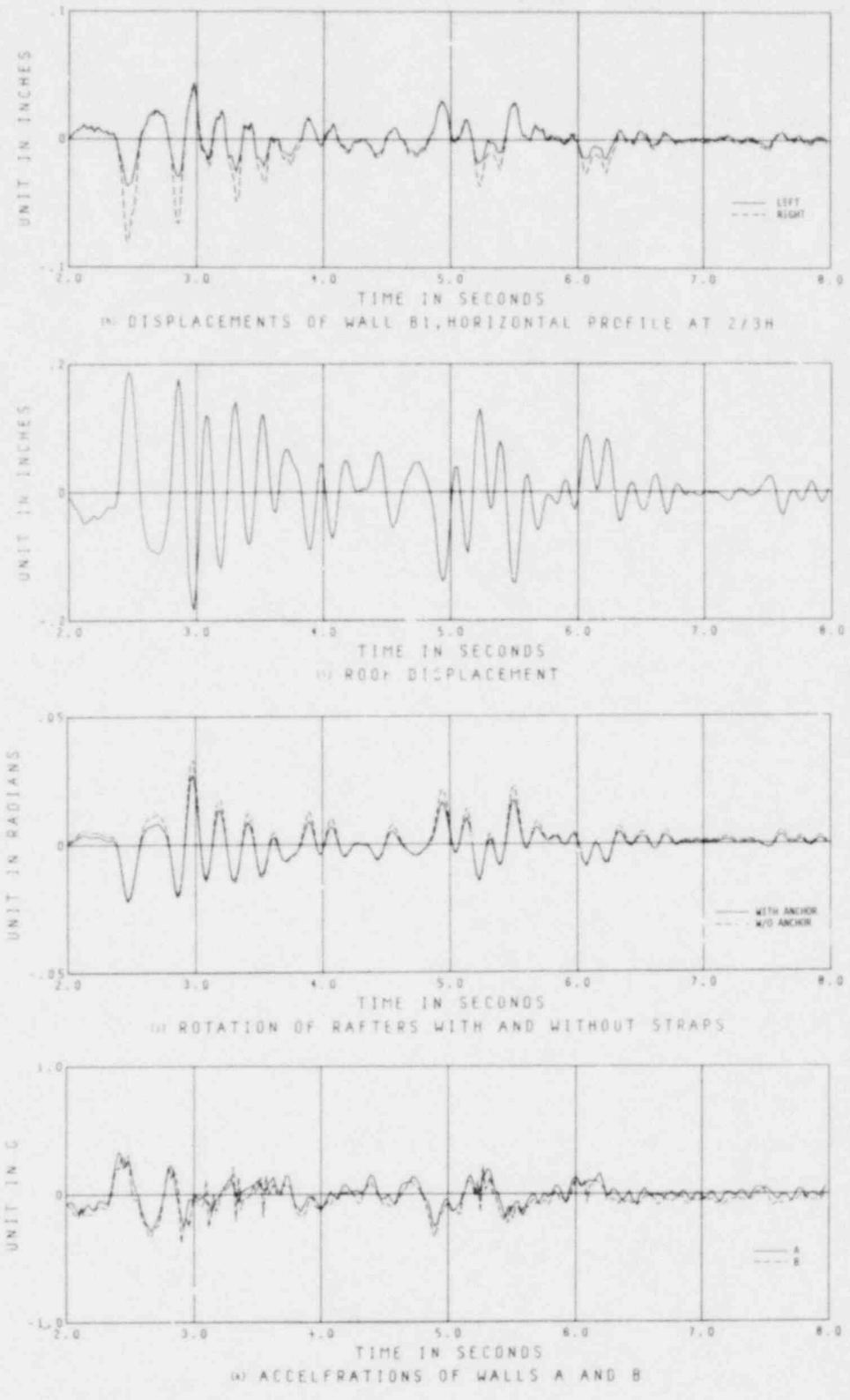

FIGURE 5.13 (CONT.) MEASURED RESPONSE: HOUSE 2, TEST 14 (EL CENTRO - 0.33 g)

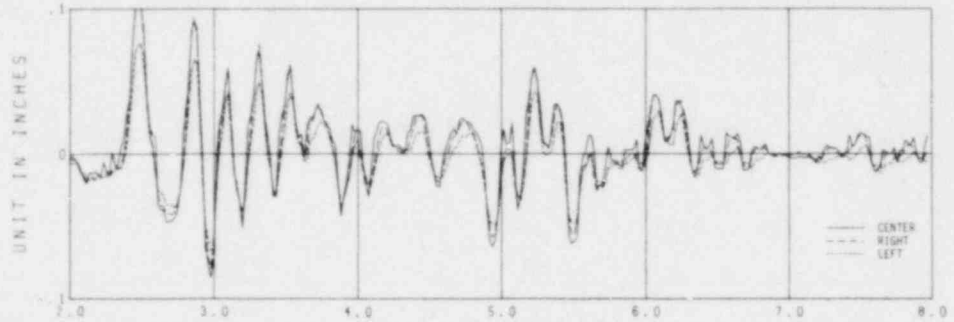

(a) DISPLACEMENTS OF WALL A1, HORIZONTAL PROFILE AT TOP

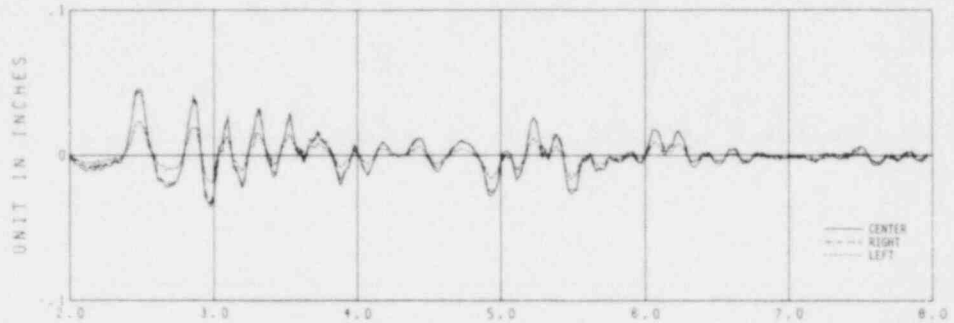

(b) DISPLACEMENTS OF WALL A1, HORIZONTAL PROFILE AT 2/3H

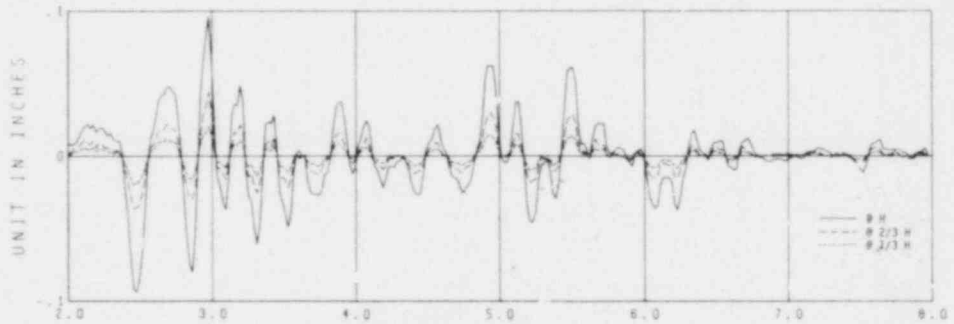

(c) DISPLACEMENTS OF WALL B1, VERTICAL PROFILE

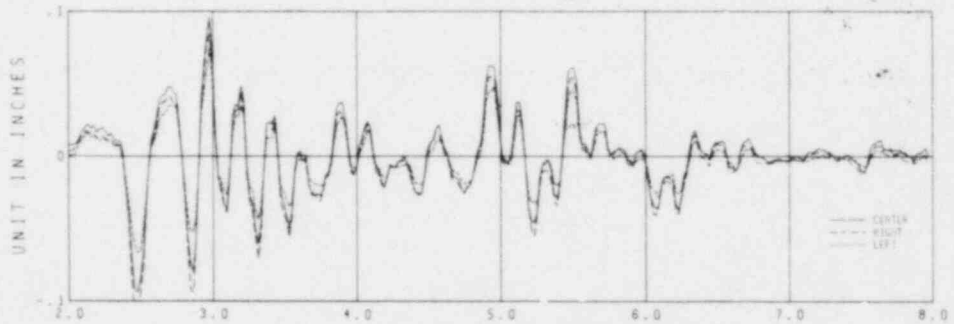

(d) DISPLACEMENTS OF WALL B1, HORIZONTAL PROFILE AT TOP

FIGURE 5.13 (CONT.) MEASURED RESPONSE: HOUSE 2, TEST 14 (EL CENTRO - 0.33 g)

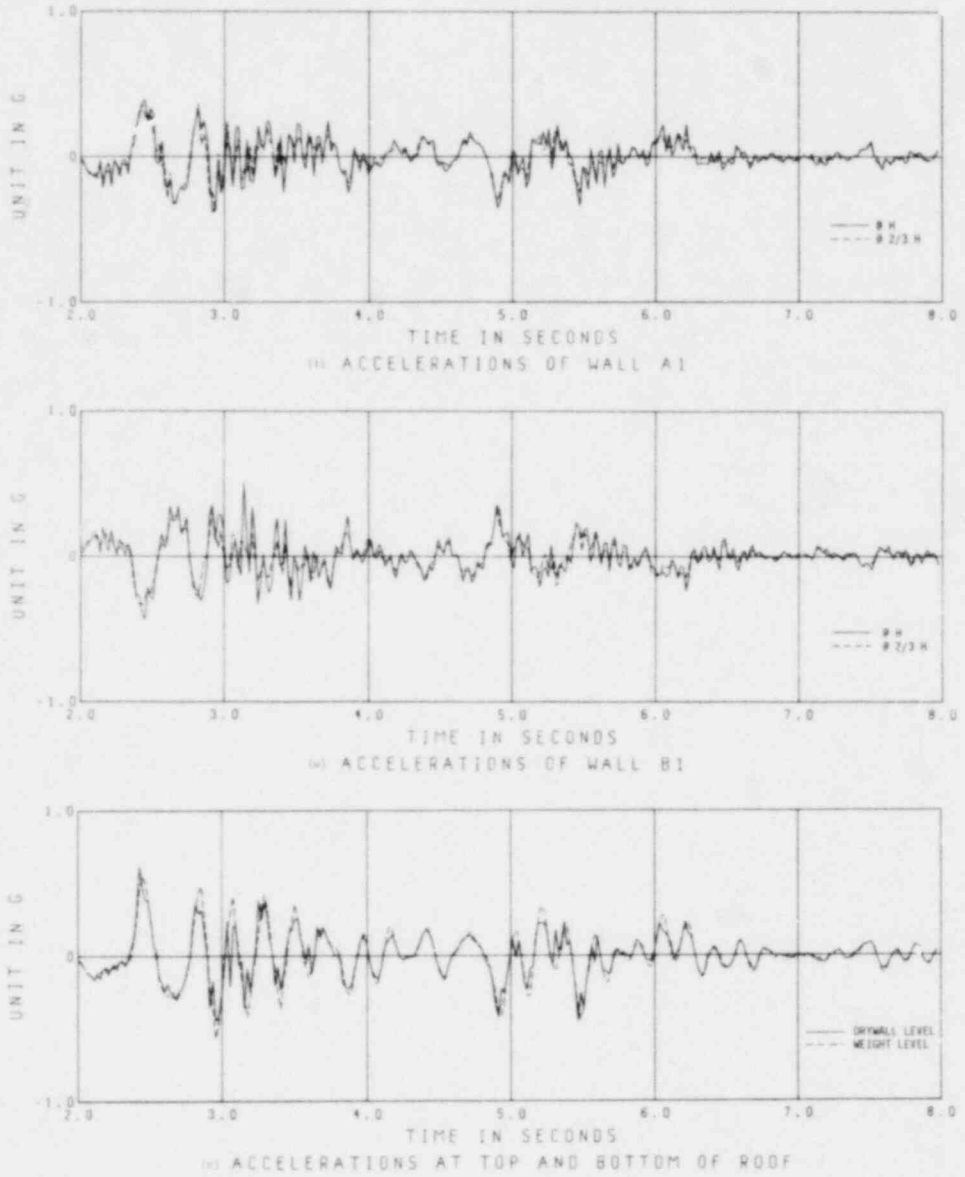

FIGURE 5.13 (CONT.) MEASURED RESPONSE: HOUSE 2, TEST 14 (EL CENTRO - 0.33 g)

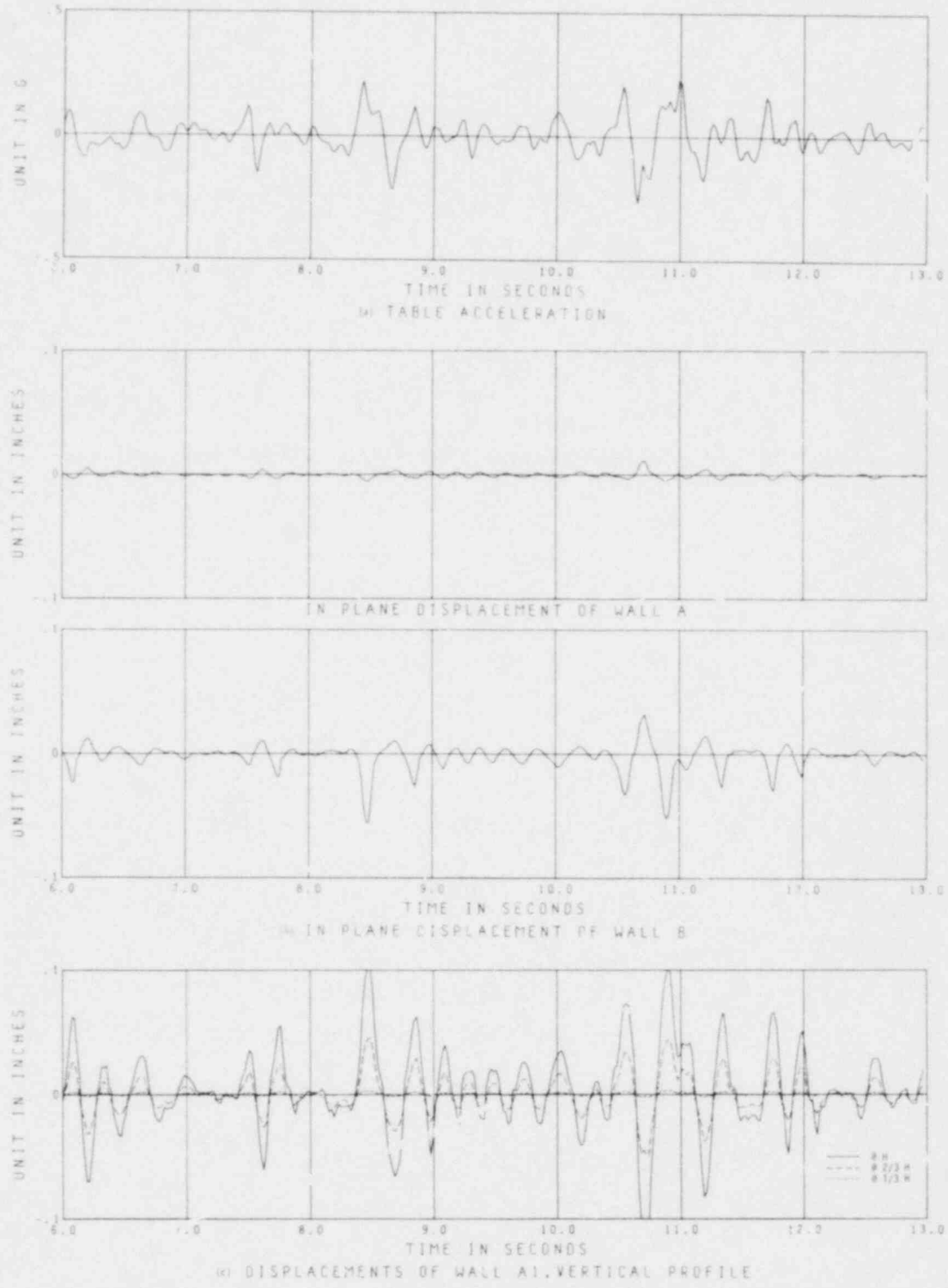

FIGURE 5.14 MEASURED RESPONSE: HOUSE 2, TEST 17 (PACOIMA - 0.27 g)

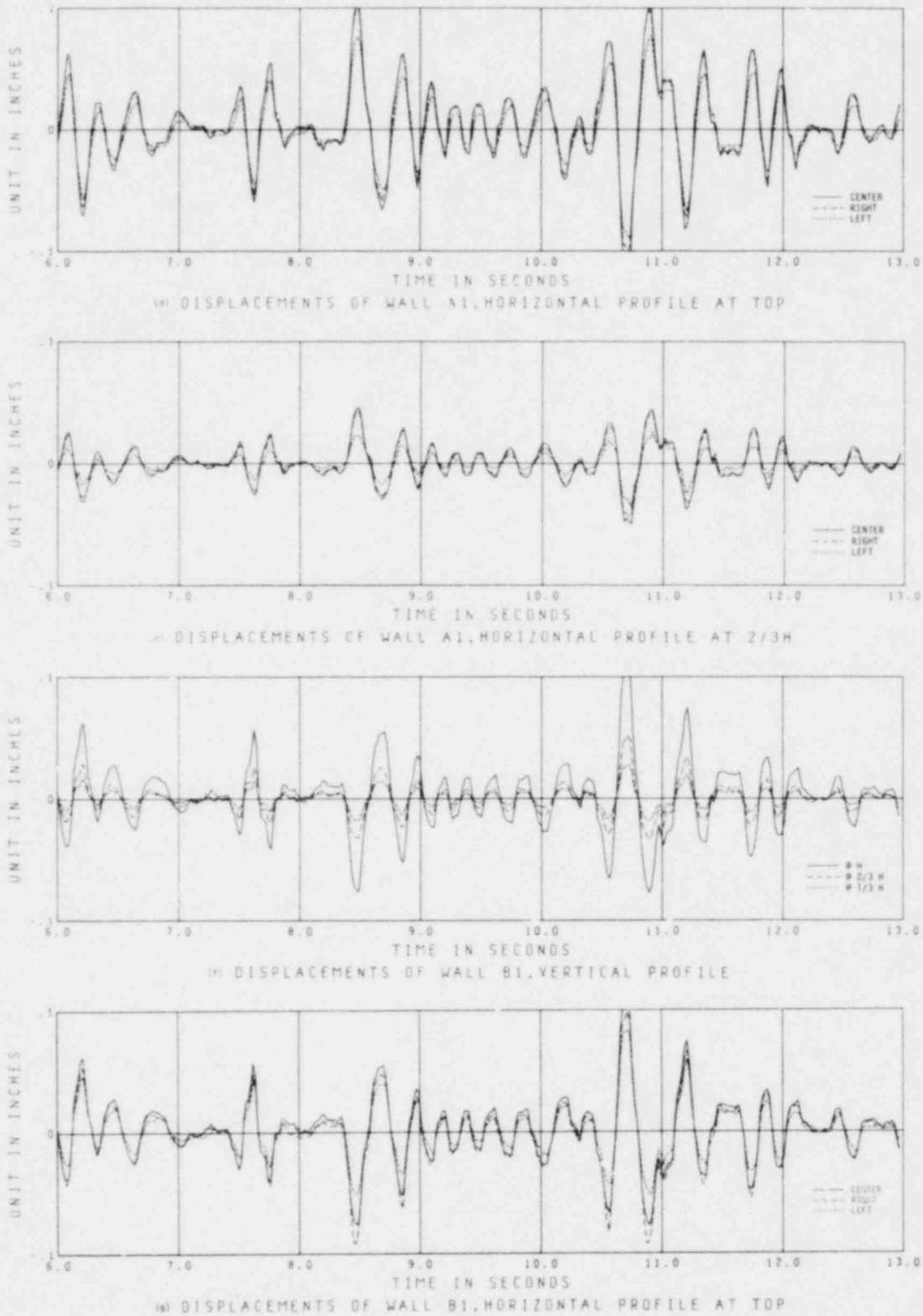

FIGURE 5.14 (CONT.) MEASURED RESPONSE: HOUSE 2, TEST 17 (PACOIMA - 0.27 g)

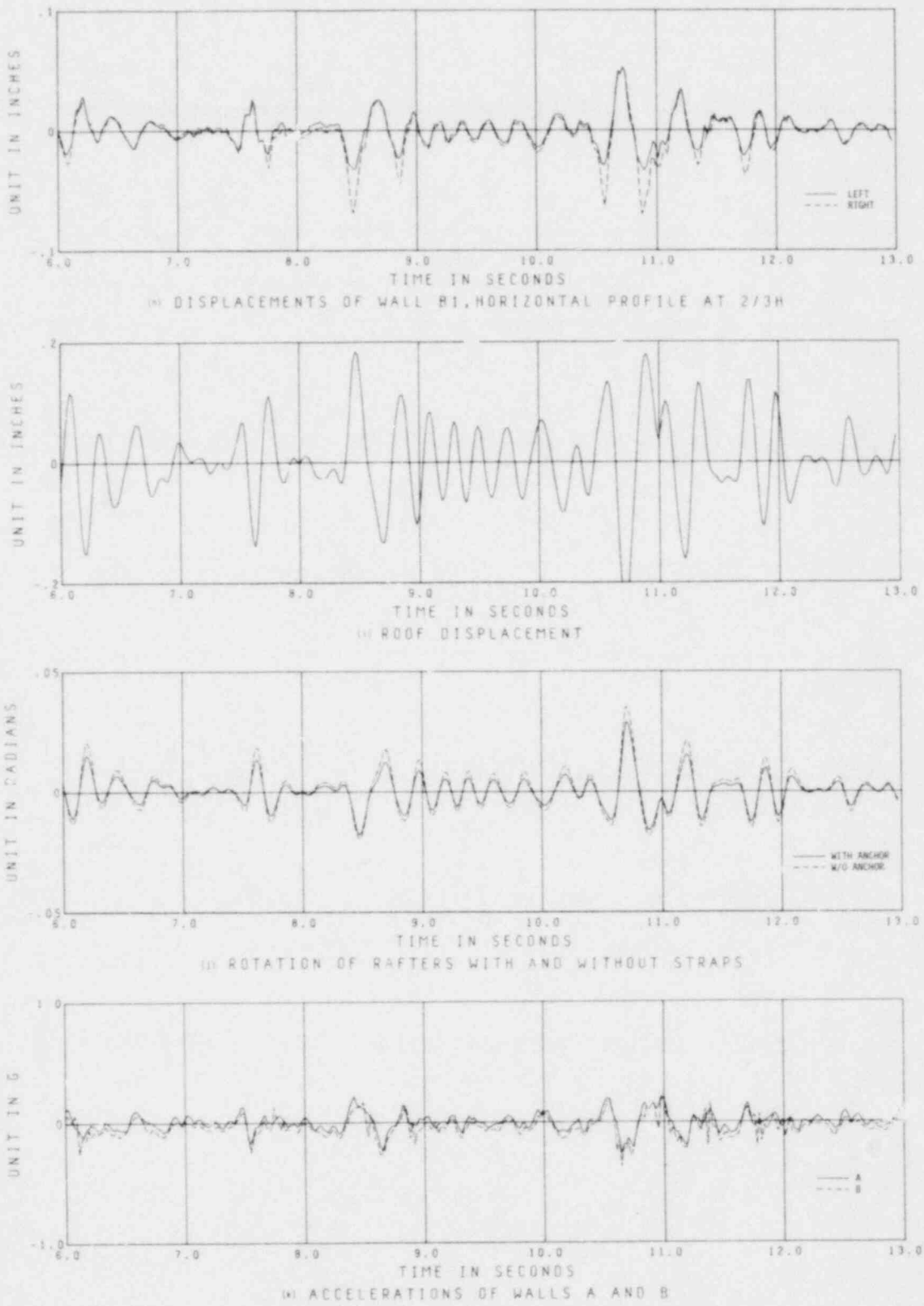

FIGURE 5.14 (CONT.) MEASURED RESPONSE: HOUSE 2, TEST 17 (PACOIMA - 0.27 g)

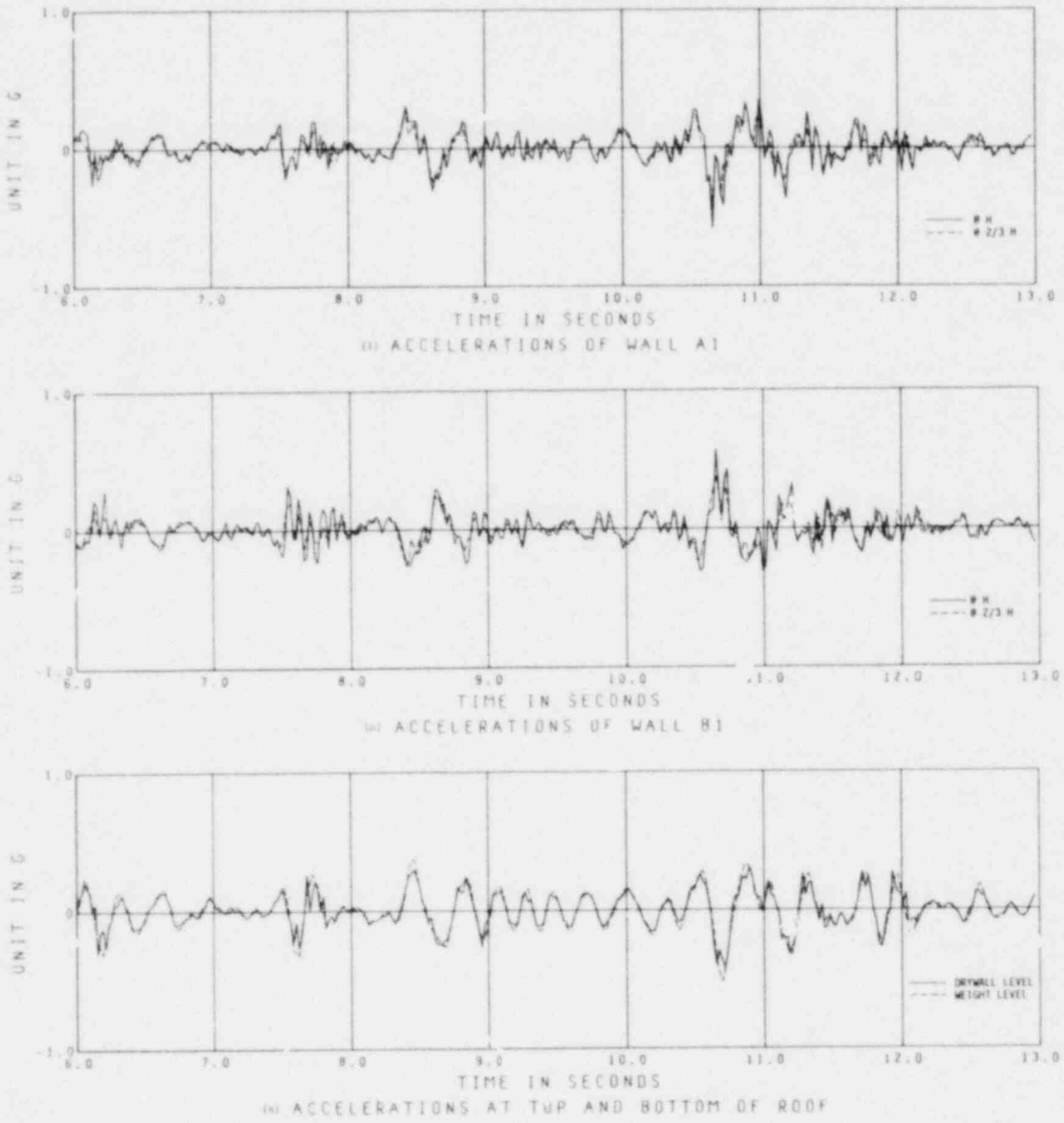

FIGURE 5.14 (CONT.) MEASURED RESPONSE: HOUSE 2, TEST 17 (PACOIMA - 0.27 g)

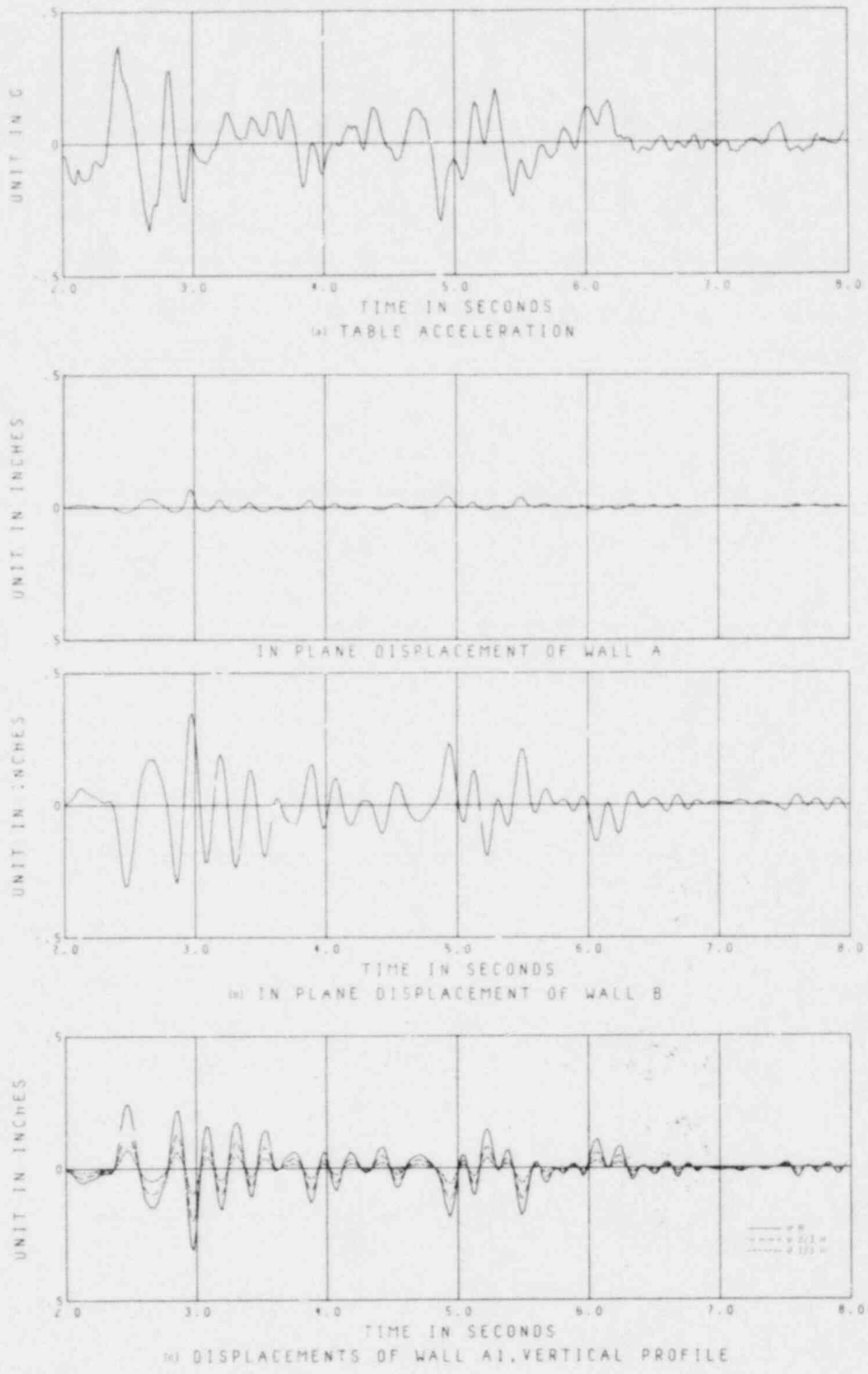

FIGURE 5.15 MEASURED RESPONSE: HOUSE 2, TEST 30 (EL CENTRO - 0.37 g)

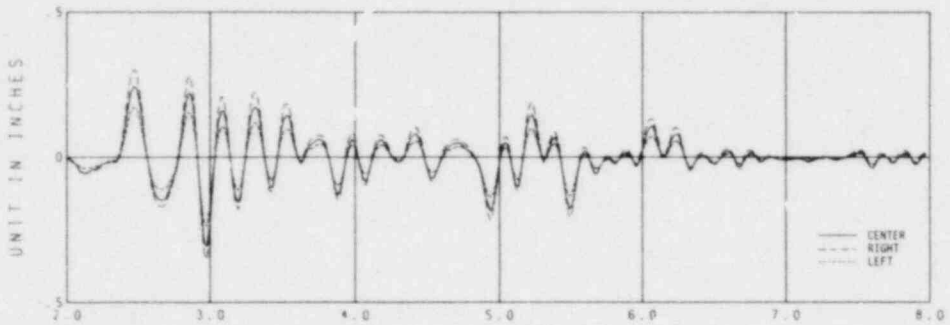

(e) DISPLACEMENTS OF WALL A1, HORIZONTAL PROFILE AT TOP

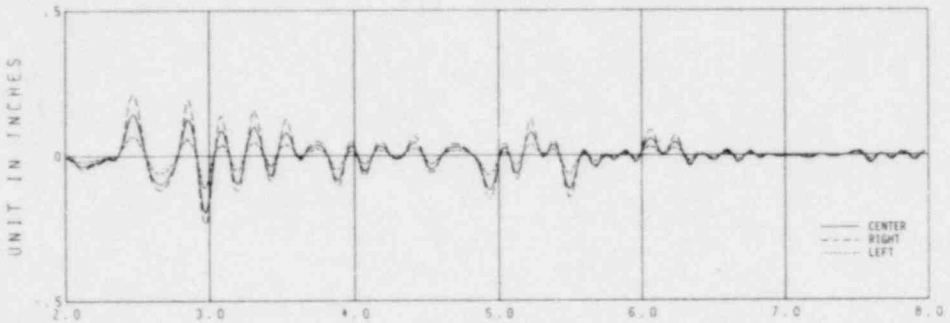

(f) DISPLACEMENTS OF WALL A1, HORIZONTAL PROFILE AT 2/3H

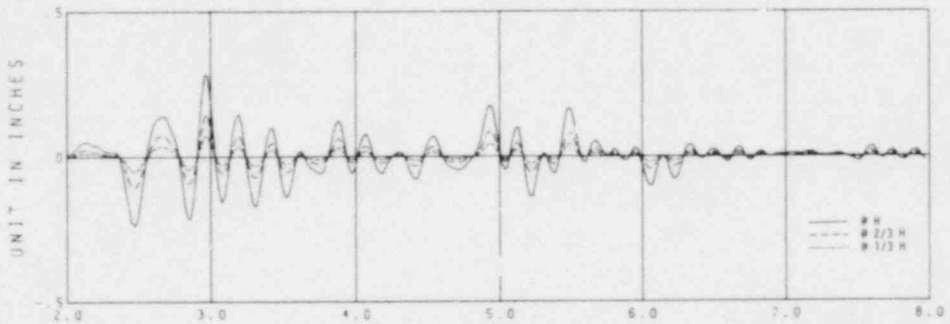

(f) DISPLACEMENTS OF WALL B1, VERTICAL PROFILE

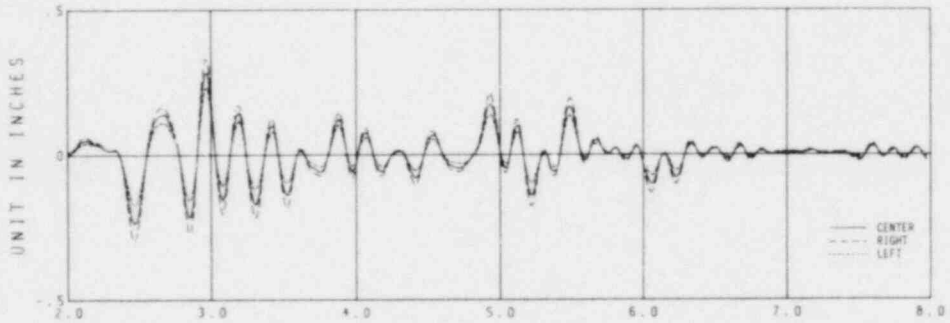

(g) DISPLACEMENTS OF WALL B1, HORIZONTAL PROFILE AT TOP

FIGURE 5.15 (CONT.) MEASURED RESPONSE: HOUSE 2, TEST 30 (EL CENTRO - 0.37 g)

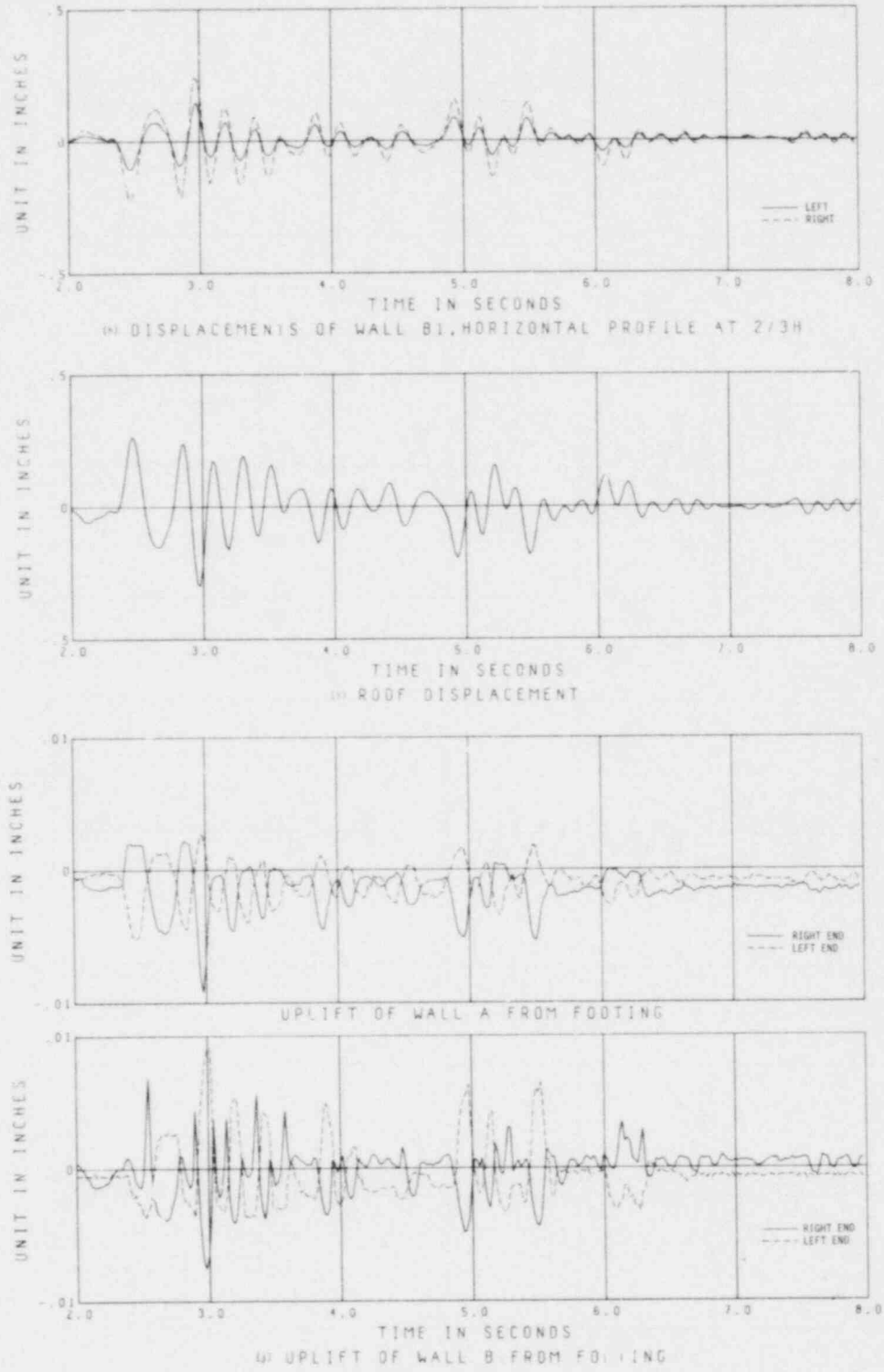

FIGURE 5.15 (CONT.) MEASURED RESPONSE: HOUSE 2, TEST 30 (EL CENTRO - 0.37 g)

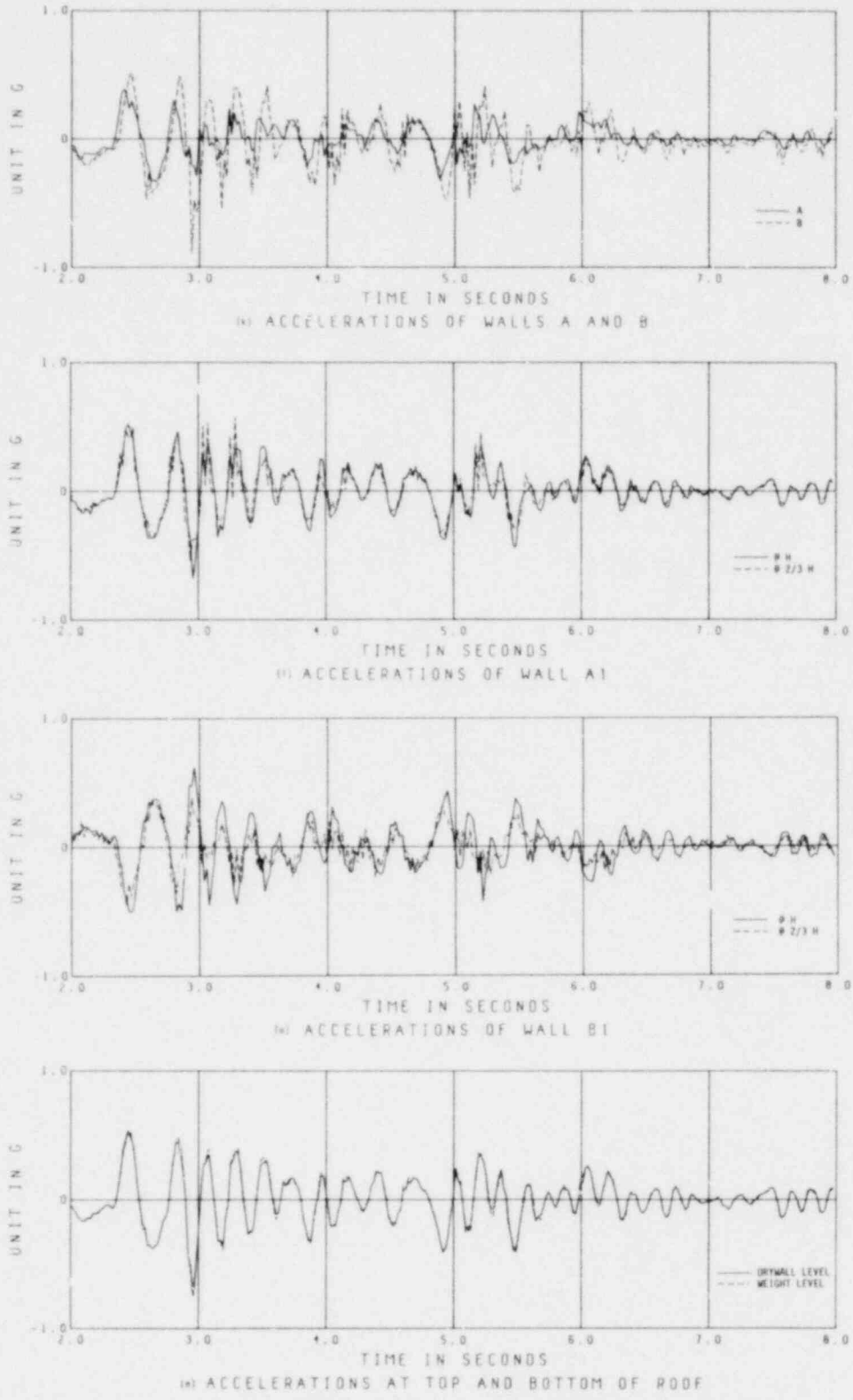

FIGURE 5.15 (CONT.) MEASURED RESPONSE: HOUSE 2, TEST 30 (EL CENTRO - 0.37 g)

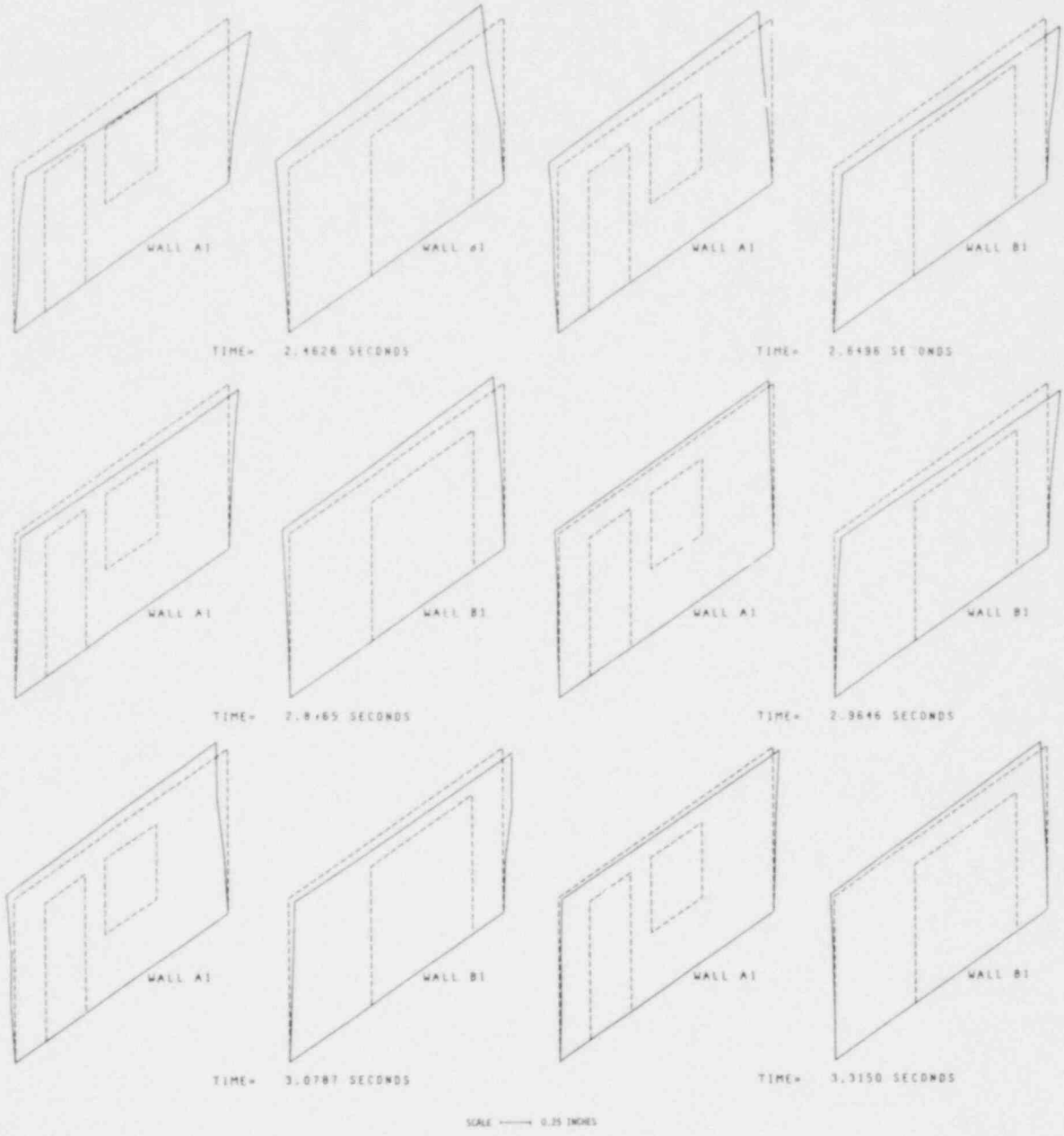

FIGURE 5.16 DEFLECTED SHAPES OF OUT-OF-PLANE WALLS: HOUSE 2 TEST 30 (EL CENTRO - 0.37 g)

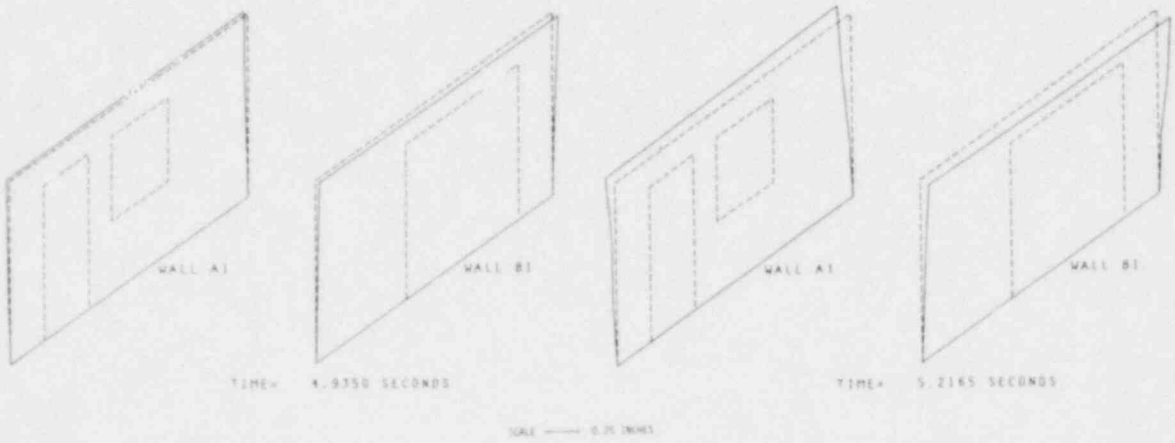

FIGURE 5.16 (CONT.) DEFLECTED SHAPES OF OUT-OF-PLANE WALLS: HOUSE 2 TEST 30 (EL CENTRO - 0.3/ g)

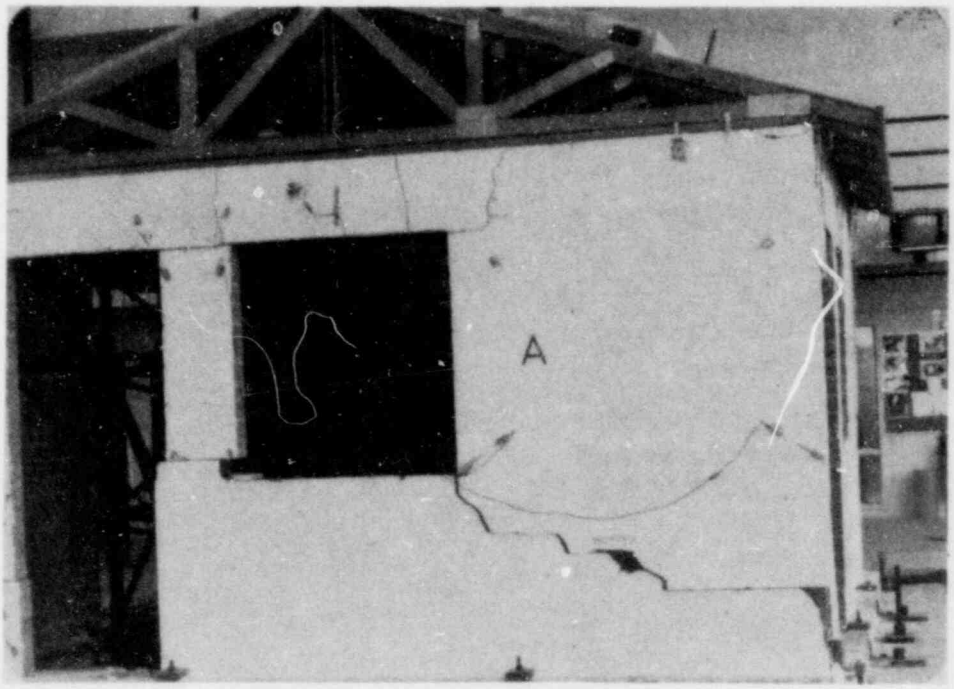

(a)

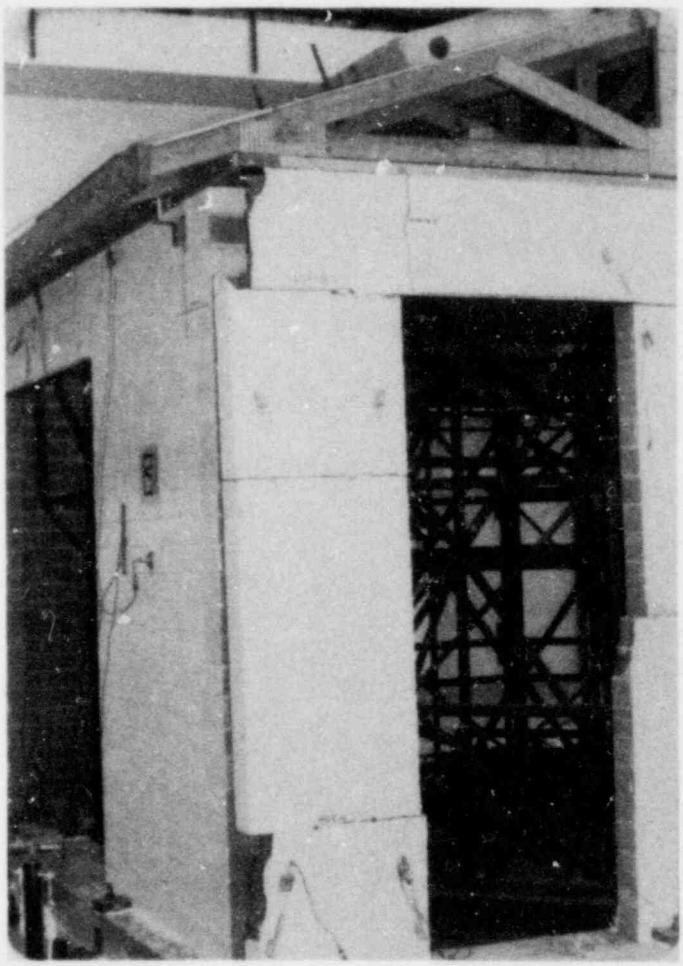

(b)

FIGURE 5.17 FAILURE OF HOUSE 2

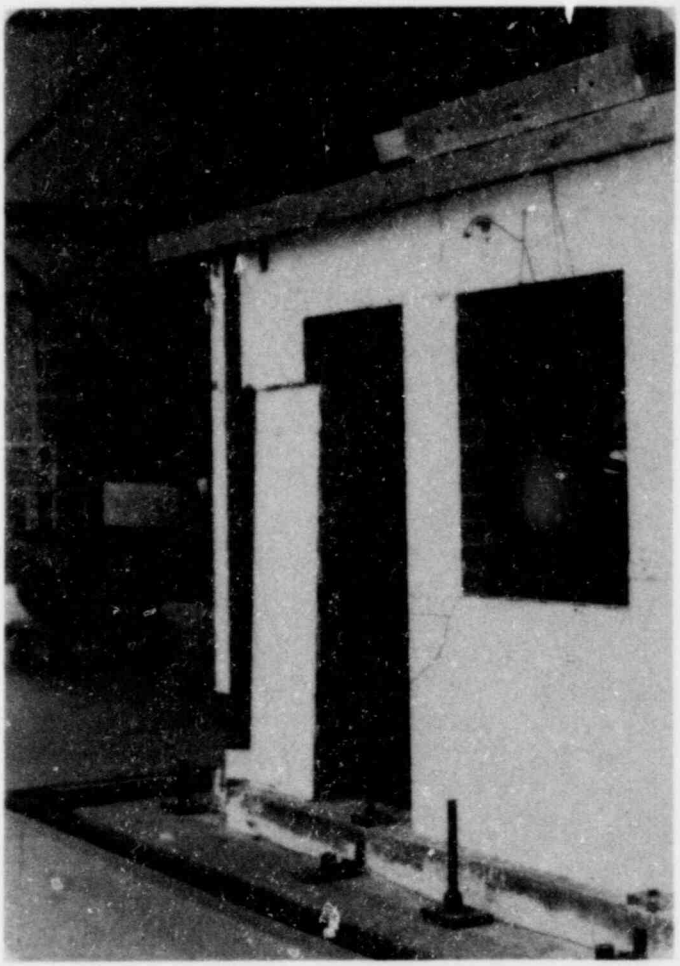

(c)

FIGURE 5.17 (CONT.) FAILURE OF HOUSE 2

6. ANALYSIS OF TEST RESULTS

6.1 Introduction

In Chapter 5, the most important experimental results obtained during the tests of Houses 1 and 2 have been presented in various graphical forms, and the significant response mechanisms observed in the wall components of these houses have been described. The purpose of this chapter is to provide an evaluation of the observed behavior, including comparisons of the strength levels determined during the tests with code provisions and results of other tests.

For convenience, a brief summary is first presented of factors influencing the strength of masonry components, based on other research findings. Section 6.2 is concerned with strength of walls subjected to out-of-plane loads while Section 6.3 summarizes behavior in response to in-plane loads. Then the results obtained in the present test program from Houses 1 and 2 are discussed in detail. Section 6.4 considers the maximum force levels developed in the various components, Section 6.5 describes the post-cracking behavior of the unreinforced walls, Section 6.6 deals with the performance of the partially reinforced walls, and Section 6.7 summarizes the amplification of base accelerations observed at various locations in the test structures.

6.2 Out-Of-Plane Strength

A study was made of the present state of knowledge concerning the out-of-plane strength of masonry walls as a part of the EERC masonry research effort, and the findings of that study have been summarized in reference (5); only the most important of the conclusions will be restated here. Three major factors influence the out-of-plane strength of masonry walls:

(1) Amount of vertical load. For loads less than the "cracking" level, increased vertical load increases the out-of-plane capacity of a masonry wall. However, for the amount of dead load supported by the walls of a single story house, this factor is not important.

(2) Reinforcement. Either vertical or horizontal reinforcement can be effective in increasing the flexural capacity of masonry walls; the reinforcement is more effective, of course, in the direction of the shorter span between supports.

(3) Mortar tensile strength. The tensile strength of the mortar bonding the masonry units together has an important effect on the out-of-plane strength of the wall. The tensile strength varies with many factors, and it is difficult to establish general conclusions concerning this factor.

6.2.1 Moment Capacity of Unreinforced Walls

As is noted above, the out-of-plane strength of masonry is dependent on the mortar tensile strength and on the amount of in-plane axial compressive load. For the values of axial load expected in masonry houses, the critical combinations of axial force and moment can be derived by the principles of mechanics, assuming a linear stress-strain relationship and that plane sections remains plane. The derivations of these relationships for solid sections and for symmetric hollow sections is presented in Appendix B. Secondary factors such as nonuniform axial load resulting from self-weight, the influence of arching, and rotational constraints at top and bottom

tend to increase the capacity above the value given by this predictive model, but for reasons of simplicity and conservatism these factors probably would be neglected in design.

For the present study, the flexural tensile strength of the masonry was determined from the diagonal compression test results summarized in Table 2.4, assuming a factor of 2.6 between the nominal shear stress at failure in the diagonal compression test and the flexural tensile strength f'_t. On this basis, average f'_t values of 53.2 and 147.2 psi were found for Houses 1 and 2, respectively. Using this flexural strength and the compressive strength obtained from prism tests, interaction curves were derived for 1 ft wide unreinforced sections of the walls of Houses 1 and 2; the results are shown in Figs. 6.1(a) and 6.2(a). Inasmuch as the axial bearing loads on the walls were only about 480 lb/ft, the curves have been plotted only for values of P less than P_k. The second expression in Eq. B.19 gives the curve labeled "cracking line"; this defines the moment capacity for the low values of axial load involved in these tests. The most important observation to be derived from this analysis is that out-of-plane flexural strength of the unreinforced walls depends essentially on the tensile strength provided by the mortar.

6.2.2 Moment Capacity of Reinforced Walls

The moment capacity of the reinforced masonry sections may be derived by standard procedures developed for reinforced concrete, assuming a rectangular compressive stress block and that plane sections remain plane[28]. Tests have shown that the reinforcement is fully effective in walls laid with running bond where the bar spacing is 8 ft[29], so this procedure is applicable to the partially reinforced walls employed in these tests.

Using the measured material strengths and standard reinforced concrete procedures, the failure envelopes for moment and axial force were derived for 1 ft sections of the walls of Houses 1 and 2. Results are presented in Figs. 6.1(b) and 6.2(b). In the former figure, the amount of steel corresponds to two #4 bars in the 8 ft section; the two curves in the second figure represent the single bar in the wide and the narrow piers.

It is interesting to note that the flexural capacity of the unreinforced section for House 2 (shown in Fig. 6.2(a)) is greater than that for the reinforced section shown in Fig. 6.2(b). This apparent contradiction is due to the high tensile strength considered in the unreinforced masonry compared with the very small steel area included in the reinforced sections; the bases of the calculations are entirely different.

6.2.3 Review of Allowable Flexural Tensile Stresses

Because the moment capacity of the unreinforced masonry walls is governed by the flexural tensile strength of the mortar bed joints, it is of interest to compare the allowable tensile stresses specified in various codes with the test results. Table 6.1 presents a list of allowable flexural tensile stresses for unreinforced brick masonry specified in several current codes. It appears that the UBC and the 1970 Canada Code permit considerably higher tensile stresses than are considered normal in Europe. The Swiss code is the most conservative, although it allows for the beneficial effect of dead load stress, with a maximum allowable stress of 56 psi. All codes except the British and Australian (which is based on the British) allow for different mortar strengths.

A plot of mortar compressive strength versus modulus of rupture, compiled from various investigations and reported in reference (5), is given in Fig. 6.3. Also included in the figure are the UBC allowable flexural tensile stresses normal to the bed joint for inspected brick masonry and unit masonry construction. The figure indicates that a factor of 2 separates the code allowable values and the lowest test results.

6.3 Shear Strength

Because of the growing use of masonry in seismic areas, and the fact that its poor reputation for seismic resistance stems largely from inadequate understanding of its fundamental behavior and improper detailing or construction practices, the shear strength of both unreinforced and reinforced masonry has been receiving increasing attention in the research community. In references (2) and (3), the state-of-the-art with regard to shear strength of both plain and reinforced masonry is reviewed in detail. The following information regarding the theoretical strength of masonry walls loaded in-plane is excerpted from reference (3).

A major observation derived from recent studies is that masonry walls exhibit two distinct modes of in-plane failure. In what is generally recognized as the flexural mode of failure, prediction of strength depends on the assumption that plane sections remain plane, and on the stress-strain relationship of steel. Because the kinematic assumptions are reasonable and the material properties can be established through tests, the ultimate strength of a reinforced wall in flexure can be determined with reasonable accuracy. On the other hand, shear failure (diagonal cracking) predictions are based on the

solution of a two-dimensional elasticity problem for a non-homogenous, inelastic material with given loads and boundary conditions. This result must be integrated with information on a biaxial failure mechanism valid for all ranges of stress[30]. Since neither basis is well-defined for masonry, the methods for estimating the ultimate strength in the shear mode of failure can only be considered as approximate. The following subsections are concerned with the shear strength of unreinforced panels and the in-plane flexural strength of vertically reinforced walls.

6.3.1 Diagonal Compression Strength

One of the earliest methods used for determining the shear strength of masonry walls is shown in Fig. 6.4. The external hold-down force P_v is applied to resist the overturning moment of the panel. This method was used by several investigators[31,32,33] and formed the basis of the standard racking test described in ASTM E72[34]. This method provides only a relative measure of the shearing or diagonal tension strength of a panel and is useful only for comparison with other panels tested in the same manner. The extent to which the assumed state of stress is violated is a matter of speculation. A subsequent variant of this test method involves the use of an internal hold down as shown in Fig. 6.5. In this arrangement, overturning resistance is derived from the development of adequate bond between the tie-down steel and the grout.

Probably the most commonly used technique to determine the relative shear strength of walls is shown in Fig. 6.6. Other investigators have used a similar diagonal compression test but added a compressive load to two opposite edges so as to provide a nominal compressive stress σ_c[35].

The following expressions give the state of stress at the center of the square panel loaded as shown in Fig. 6.6:

$$\sigma_1 = - 0.823\ \bar{\tau} + \frac{\sigma_c}{2} + \sqrt{(1.556\ \bar{\tau})^2 + \frac{\sigma_c^2}{4}} \qquad (6.1)$$

$$\sigma_3 = - 0.823\ \bar{\tau} + \frac{\sigma_c}{2} - \sqrt{(1.556\ \bar{\tau})^2 + \frac{\sigma_c^2}{4}} \qquad (6.2)$$

$$\alpha = \frac{1}{2} \cot^{-1} \frac{\sigma_c}{3.112\ \bar{\tau}} \quad . \qquad (6.3)$$

In these expressions σ_c is negative for compressive edge stress, and

$$\bar{\tau} = 0.707\ \frac{P}{A}$$

is always positive. Equation (6.1) is synonymous with Eq. (2.1).

Hypotheses for the failure of masonry panels can be examined on the basis of Eqs. (6.1) and (6.2). If one accepts the premise that failure will occur when the principal tensile stress given by Eq. (6.1) reaches a critical value or when the principal compressive stress expressed by Eq. (6.2) exceeds the compressive strength, f'_m, of the material then a critical combination of normal and shear stresses may be obtained to define the failure surface. Although it is more likely that failure in masonry occurs because of a critical combination of normal principal stresses (as in concrete), the above theory is adequate for most practical purposes. In the absence of appreciable compressive stress, and a state of "pure" shear, it then follows that failure will occur when

$$\sigma_1 = \sigma_{tcr} = 0.73 \bar{\tau} \ . \qquad (6.4)$$

Entries in Table 2.4 have been made on the basis of Eq. (6.4)

A critical note may be made on the general applicability of Eq. (6.4). This equation not only does not recognize the complex state of stress resulting from the non-homogeneity of masonry, it is more applicable to the types of failure observed in diagonal compression tests, than to pier tests[36].

6.3.2 Flexural Strength

The lateral force at which flexural failure of a vertically reinforced masonry pier will occur can be established through methods common to reinforced concrete. Assuming an ultimate crushing strain for masonry of 0.003, the flexural yield load P_y for the reinforced pier in Fig. 6.7 can be obtained as follows:

$$P_y = \frac{\Sigma A_{si} d_i}{H} f_y \qquad (6.5)$$

where the variables d_i and H are defined in Fig. 6.7, A_{si} is the area of the vertical reinforcement at location i, and f_y is the yield strength of the steel. Of course, for a flexural type failure to occur, premature failure must not have occurred due to shear or bond.

6.4 Experimental Force Levels

This and following sections provide an analysis of the results presented in Chapter 5. Given the measured table motion characteristics and the measured structural response, an approximation of the force levels acting on the resisting elements and connections can be determined. From these force levels the stresses at critical locations both at and

before cracking can be obtained from the theory presented in Sections 6.1 and 6.3. Once cracking of an unreinforced element has occurred, this method of analysis is no longer valid. Section 6.5 examines the the post-cracking performance of the cracked unreinforced piers and panels.

In order to approximate the force levels and stresses on the various elements of the test structures, the following assumptions were used.

(1) According to established practice, plywood roof systems are considered as flexible diaphragms and lateral roof loads are distributed to the resisting elements on a tributary area basis. Hence, each in-plane shear wall was assumed to resist half of the inertia force generated by the roof structure. In addition to the inertia force of the roof structure, each in-plane wall was assumed to resist half the reaction force at the roof level generated by the vibration of the out-of-plane walls.

(2) The maximum inertia force generated by the roof structure was determined by multiplying the weight of the roof by the maximum acceleration recorded by the accelerometer located at the level of the concrete weights (see Figs. 3.5 and 3.6) This is a reasonable estimate of the inertia force when the trusses are parallel to the table motion and is an upper bound when they are perpendicular.

(3) The moment which a given out-of-plane wall must resist arises from self-generated inertia forces. These were obtained from the maximum accelerations measured at the

top, two-thirds wall height and the base of the wall, assuming that the maximum value at each accelerometer occurred simultaneously. A study of the time history plots of Chapter 5 shows that while this is not strictly true it is reasonably accurate, and the moments determined from these readings are within a few percent of the maximum value obtained from simultaneously occurring accelerations.

(4) Bounds on the moments that an out-of-plane wall had to resist were obtained by assuming that the top of the walls had no rotational fixity and that the base had one of two fixity conditions. In the first case, full fixity was assumed at the footing level ($k_{\theta_2} = \infty$, see Fig. 6.8(a)), and in the second case rotational fixity was neglected ($k_{\theta_2} = 0$).

(5) To determine the stresses both at and before cracking, the seismic forces described above were applied as static loads and the stresses determined at crack locations. Cracking in most cases was determined from visual inspection after each test. In some instances and especially at the wall-footing connection cracking may have occurred before it was visually evident and marked on the sequential crack patterns of Figs. 5.1 and 5.12.

6.4.1 House 1

Significant developments recorded during the testing of House 1 are summarized in Table 5.1, and the crack occurrence is shown in Fig. 5.1. These data provide a means of visualizing the response mechanism from which an assessment of the forces is derived.

To aid in the determination of the experimental force levels, Tables 6.2 to 6.4 contain summaries of maximum displacements and accelerations recorded for each test. The location at which each measurement was recorded can be determined from the channel locations shown in Fig. 3.5. Table 6.2 lists the maximum accelerations and displacements measured at the top of the in-plane walls; Table 6.3 contains the maximum accelerations at the concrete weight and drywall ceiling levels; in addition each is expressed as a ratio to the peak base acceleration. Table 6.4 contains the maximum accelerations of the out-of-plane walls measured at the top and at two-thirds of wall height. Tables 6.15 and 6.17 provide a summary of the tensile stresses corresponding to the formation of visually noted cracks.

(A) Out-of-Plane Walls W2 and W4

The maximum moments on W2 and W4 were calculated at 50, 60 and 70 percent of the wall height for each test and are given in Table 6.5. The moments were calculated for a 1 ft width of wall from the accelerations given in Table 6.4 and the unit weight given in Table 2.1. The two fixity conditions previously described were used to get upper and lower bounds. The reaction forces imposed on the connections at the roof level are also given in Table 6.5.

The moments given in Table 6.5 were based on the assumption that the wall was uncracked and, therefore, are not valid for a wall with a horizontal joint that is cracked along its length. In this case the wall vibrates in a manner similar to a three-hinged beam as discussed in Section 6.5 and requires a greater number of accelerometer readings over the height to determine moments and connection forces.

The tensile stresses at the crack locations were calculated from the moments corresponding to the pinned-pinned assumption ($k_{\theta_2} = 0$ of Fig. 6.8(a)) since these give an upper bound to the tensile stresses.

The lower axial load regions of the interaction diagrams for the unreinforced wall W4 and the reinforced wall W2 discussed in Section 6.2 are given in Figs. 6.1(a) and (b), respectively, During the first phase of testing (up to Test 13) W2 and W4 were load bearing and the roof load per unit length of wall was of the order of 480 lb/ft. During the second phase of testing W2 and W4 were non-load bearing. Because of the small dead load in comparison to the pure axial capacity, the flexural capacity of the out-of-plane walls in both phases of testing can be considered to equal the intercept on the horizontal axis of Figs. 6.1(a) and (b). It should be noted that for the unreinforced walls the intercept is directly proportional to the tensile stress normal to the bed joints. For House 1 this was determined indirectly (Table 2.4) from the diagonal compression test to be 53.2 psi, leading to a flexural capacity of 3070 lb-in. for a 1 ft width of wall.

During the first twenty tests the maximum moment (Table 6.5) on a 1 ft wide section was of the order of 1000 lb-in. so that W4 should not have cracked. However a horizontal crack occurred at the sixth course from the top and was visually noted after Test 20; during Test 21 (E-0.31 g) its effect was visibly demonstrated as Fig. 5.4(c) indicates. The tensile stress normal to the bed joint at the crack location corresponding to the experimentally determined moments of Test 19 (T-0.25 g) was approximately 11 psi. The maximum moment resisted by W4 before cracking was during Test 13 (E-0.28 g) when it was load bearing. The tensile stresses corresponding to the moments of Test 13 are approximately 21 psi at the mid-height of the wall and

13 psi at the joint that cracked during Test 19. These values can be compared with the 53.2 psi determined indirectly from the diagonal compressive test and to the UBC allowable values for unreinforced unit masonry with Type M or S mortar of 6 psi and 12 psi for uninspected and inspected masonry, respectively.

After W4 was repaired (entire wall covered on both sides with fiberglass based plaster) the theoretical capacity of the wall could not be determined since strength characteristics were not determined for the surface bonding plaster. Cracking reoccurred at the same location in W4 during Test 27 (P-0.49 g). The moment on the walls at this stage was of the order of 2000 lb-in. or almost double that when the wall first cracked.

The flexural out-of-plane capacity per unit length of the reinforced wall W2 was computed to be 7240 lb-in. (Fig. 6.1(b)) for no axial load. This capacity is based on the assumption of a cracked reinforced section and is therefore independent of the tensile strength normal to the bed joint. It is interesting to note from the visual crack patterns of Fig. 5.1 that the only visual crack in W2 was at the first joint from the footing. The maximum moment on W2 occurred during Test 28 (P-0.63 g) and was of the order of 3700 lb-in. This is half the computed reinforced capacity, but exceeds the computed unreinforced capacity at which visual cracking would be expected to occur.

(B) In-Plane Walls W1 and W3

The model in Fig. 6.8(b) was used for the analysis of both sides of the structure of Fig. 3.1. The proportion of horizontal force that each element would resist was determined from basic principles with stiffness properties based on overall dimensions. The results, based

on the assumption that all piers were either free to rotate at the top ($k_\theta = 0$) or fixed ($k_\theta = \infty$), are summarized in Table 6.6. As would be expected, W1 and W3 resisted a far greater part of the total force than the two corners. In the opinion of the authors, the top fixity conditions were closer to being free ($k_\theta = 0$) than fixed, so the proportion of the total horizontal load resisted by the central wall when it was uncracked was put at 90 percent. After Test 14 when W3 was repaired and C2 and C3 were left in their cracked state this proportion was probably closer to 100 percent. The distribution of load when W3 was cracked is difficult to assess because the cracked response is nonlinear, as is discussed in Section 6.5.

First significant cracking for W3 occurred during Test 9 (T-0.21 g) along a horizontal joint 2 ft 8 in. above the footing, (Sec. A of Fig. 6.9). Assuming that W3 responded as a cantilever element, the flexural tensile stress at Section A determined from the overturning moment generated by the maximum lateral load of Test 9, was 42 psi. The maximum stress at this location prior to visual cracking was 29 psi during Test 8 (T-0.19 g). It should be noted that a hairline crack was noticed at this joint before testing commenced. Test 10 (T-0.27 g) was performed with W3 in this cracked condition.

After Test 10, the joint was mechanically blocked to prevent sliding, and during Test 11 (T-0.28 g) a new crack formed along the second course above the footing (Sec. A' of Fig. 6.9). The tensile stress associated with cracking at this location was 64 psi, whereas the maximum tensile stress prior to visual cracking was 42 psi during Test 8. To calculate the tensile stresses, the mortared area of the units was used, (i.e. the center web of a full unit was not considered).

After Test 13, W3 was fully plastered on both sides of the wall with a fiberglass based plaster and further cracking did not occur until Test 27 (P-0.49 g). The theoretical strength of the repaired wall could not be determined (see Section 6.4.1(A)).

The shear stresses based on net area when flexural cracks occurred in W3 were very low, of the order of 9 to 11 psi. For the repaired wall the net shear stress was approximately 23 psi when flexural cracks developed.

The shear force associated with yielding of the vertical reinforcement in the reinforced wall W1 was 9400 lb with no dead load and 11,600 lb with a dead load of 480 lb/ft. The maximum forces imposed on W1 were 2700 lb during Test 13 (E-0.29 g) when it was non-load bearing and 10,100 lb during Test 28 (P-0.63 g) when it was load bearing. The net shear stresses corresponding to these forces are 11 and 29 psi, respectively.

6.4.2 House 2

Significant developments recorded during the testing of House 2 are summarized in Table 5.3 and the crack occurrence is shown in Fig. 5.12. Tables 6.7 to 6.9 contain summaries of maximum displacements and accelerations recorded for each test. The location at which each measurement was recorded can be determined from the channel locations shown in Fig. 3.6. Table 6.7 lists the maximum accelerations and displacements measured at the top of the in-plane walls; Table 6.8 contains the maximum accelerations at the concrete weight and drywall ceiling levels as well as the ratio of these values to the peak base accelerations. Table 6.9 contains the maximum accelerations of the out-of-plane walls measured at the top and two-thirds wall height.

Tables 6.16 and 6.18 provide a summary of the tensile stresses corresponding to the formation of visually noted cracks.

(A) Out-of-Plane Walls A1 and B1

The maximum moments on the out-of-plane walls A1 and B1 were calculated at 50, 60 and 70 percent of the wall height for each test and are given in Table 6.10. The moments were calculated for a 1 ft width of wall from the accelerations given in Table 6.4 and the unit weight in Table 2.1. This assumes that lateral forces are the same at all points along a horizontal plane. In view of the deformed shapes given in Fig. 5.16, this assumption can only be regarded as approximate. Two fixity conditions previously described were used to get upper and lower bounds on the moments. The reaction forces imposed on the connections at the roof level are also given in Table 6.10.

The moments given in Table 6.10 are based on the assumption that the wall is uncracked and, therefore, are not valid for a wall with a horizontal joint cracked along its length. In that case the wall would vibrate in a manner similar to a three-hinged beam as discussed in Section 6.5. The tensile stresses at the crack locations are calculated from the moments corresponding to the pinned-pinned assumption ($k_{\theta_2} = 0$ in Fig. 6.8(a)).

During the first phase of testing (up to Test 19) A1 and B1 were non-load bearing. During the second phase of testing, A1 and B1 were load bearing and the roof load per unit length of wall was of the order of 480 lb/ft. The interaction diagrams for the unreinforced wall A1 and the reinforced wall B1 are given in Figs. 6.2(a) and (b), respectively. Because of the small dead load in comparison to the pure axial capacity, the flexural capacity of the walls in both phases of testing

is given by the intercept of the curves on the horizontal axis. It should be noted that for the unreinforced walls the intercept is directly proportional to the tensile stress normal to the bed joints. For House 2 the intercept was determined indirectly (Table 2.4) from the diagonal compression test to be 147.2 psi, with a resulting flexural capacity of 8110 lb-in.

A1 was noted to have cracked along the eleventh course from the footing (at the base of the window opening) in the larger pier during Test 14 (E-0.33 g). The maximum moment on the wall during the test was of the order of 1100 lb-in. corresponding to a tensile strength of 20 psi normal to the bed joint. The maximum moment occurring at this joint before cracking was of the order of 970 lb-in. during Test 13 (E-0.29 g) with a corresponding tensile strength of 18 psi. Subsequent tests when the wall was either non-load bearing or load bearing did not display the gross out-of-plane wall deformations and hinging action across this crack that were recorded for W4 of House 1. The tensile strengths corresponding to the cracking condition may be compared with the UBC allowable strengths for unreinforced unit masonry (with Type M or S mortar) of 6 psi and 12 psi for uninspected and inspected masonry, respectively.

The computed out-of-plane flexural capacity per unit length of the small and large pier of the reinforced wall B1 are 15,760 lb-in. and 6115 lb-in., respectively, for no axial load. This capacity is based on the assumption of a cracked reinforced section and is therefore independent of the masonry tensile strength normal to the bed joint. It is interesting to note from the visual crack patterns of Fig. 5.12 that only minor cracking was evident. The maximum measured

moment on B1 occurred during Test 19 (P-0.51 g) and Test 32 (P-0.52 g) and was of the order of 2150 lb-in.

(B) In-Plane Walls A and B

For wall A it can be quickly established that pier D shown in Fig. 6.10 is the subelement which would resist the bulk of the shear force. If spandrel beam A is assumed to provide full fixity at the upper ends of piers B, C, and D then these piers would resist 3.4, 5.7, and 90.8 percent of the total lateral load. At the other extreme, when piers B, C, and D are assumed to behave as cantilevers, these ratios become 1.5, 2.6, and 95.9 percent, respectively. The true value of the rotational fixity at the top of pier D can only be estimated in this study.

Assuming the piers to be fixed at both ends, axial loads and shears at the middle of piers B, C, and D can be determined as shown in Fig. 6.10 for a lateral force of 100 lb acting to the left. The capacity of spandrel beam A to impose fixed end conditions on the middle piers depends on whether piers B, C, and D can develop the axial forces depicted in Fig. 6.10 for both orientations of the force P, and whether spandrel beam A can provide the moment restraint required at the tops of the piers. For a force directed to the right in Fig. 6.10, piers B and C would be in tension and D in compression; whereas for a force to the left, piers B and C are in compression and D is in tension. Given the formation of horizontal cracks in piers B and C (Fig. 5.12(b)), it is the opinion of the authors that pier D tended toward a cantilever response in resisting a force acting acting to the right and toward rotational fixity for a force acting to the left. Consequently the tensile stresses that existed for Tests 19 (P-0.51 g) and 32 (P-0.52 g)

are calculated assuming in Case 1, that pier D is a cantilever, and in Case 2 that it has rotational fixity at both its top and bottom sections. These two cases will obviously provide upper and lower limits on the tensile stresses normal to the bed joint at and before cracking.

A summary of the peaks of roof acceleration at the level of concrete weights is provided in Table 6.8. It is interesting to note that the greatest roof load in either truss orientation was recorded during a simulation of the Pacoima motion: with the roof structure spanning between the in-plane walls, a peak of 1.078 g was recorded during Test 19 (P-0.51 g); after the out-of-plane walls became load bearing the same motion caused a peak of 0.878 g during Test 32 (P-0.52 g), when failure of wall A took place. In confirmation of the observation made for House 1, the more flexible orientation of the roof structure (which corresponded to Test 19) represents a more favorable condition for in-plane walls on two accounts. First, the presence of a compressive stress on the wall decreases the magnitude of the tensile stress and causes an apparent increase of strength. Secondly, the greater dissipation of kinetic energy at the truss support interface reduces the requirement for transforming part of this energy into strain energy through the deformation of in-plane walls. In the other orientation of the roof trusses both factors are absent: the in-plane walls are no longer load bearing and the much greater stiffness of the roof structure in the direction of motion coupled with a lesser amount of energy dissipation in the truss implies greater forces being transmitted into these walls for a given roof acceleration.

The shear force to be resisted by each in-plane wall consists of the inertia force generated by the roof structure and the reaction at the roof level from the vibration of the out-of-plane walls. For Test 19,

this force was 9120 lb and for Test 32 it was 7465 lb. Assigning 95 percent of these forces to pier D of wall A results in a uniform shear stress based on net area of 40 psi and 33 psi for Tests 19 and 32, respectively. The tensile stresses normal to the bed joint at the end of the reentrant corner of pier D for Test 19 were 220 psi if pier D was assumed as a cantilever and 65 psi if it was assumed to be fixed against rotation at both its top and bottom sections. The corresponding values for Test 32 were 195 psi and 69 psi, respectively.

These bounds on the tensile stress for Test 32 when major cracking was initiated at the reentrant corner of pier D may be compared with the tensile stress of 147.2 psi measured indirectly from the diagonal compressive test and the 6 psi and 12 psi values of allowable stresses from the UBC for uninspected and inspected reinforced unit masonry, respectively. It should be noted that the indirectly measured tensile strength for this house was substantially greater than that for House 1.

For wall B it is clear that the large pier resisted the major part of the shear force. During Test 15 (Fig. 5.12(c)) vertical cracking at each side of the spandrel beam was completed and further testing progressively diminished the fixity on either side of the beam to the point where the spandrel was no longer capable of providing rotational constraint. As a result, subsequent analyses of the piers assume that they responded as cantilever elements. Based on this assumption, the distribution of shear between the two piers was 96 percent for the large pier and 4 percent for the small pier.

Because wall B contained vertical rebars only at its extreme left and right ends, the theoretical capacity of both the large and small piers was dependent on the direction of the applied shear force. For a

force to the right as shown in Fig. 6.11(a) the large pier responded as an unreinforced element, whereas the small pier was a reinforced element. For a force in the opposite direction, as in Fig. 6.12(b), the large pier was effectively reinforced and the small pier was not. For the unreinforced elements the resistance mechanism and theoretical capacity depended on the state of cracking along the bottom joints. When the wall was uncracked the theoretical capacity of the element was dependent upon the tensile bond strength normal to the bed joints.

When the unreinforced elements were fully or substantially cracked along a bed joint the mechanism of response to the applied force was that of a rocking element which has a non-linear response mechanism. As the pier begins to rock it has to uplift the roof structure thereby increasing the compressive load on the wall. Shear resistance in this mode of response was mobilized both by friction across the compressive zone of the wall and by dowel action of the reinforcing bar.

The theoretical capacity for the small and large piers is given in Table 6.11 for both the bearing and non-load bearing conditions. The theoretical capacities for the unreinforced case were based on an uncracked section with a tensile capacity normal to the bed joint of 147.2 psi which was determined indirectly from the diagonal compression test. The theoretical capacities for the reinforced case are based on Eq. 6.5.

Because cracking at the wall-footing connection was difficult to identify in this test, it is not marked in Fig. 5.12. Consequently, the tensile stresses corresponding to the before and after cracked states cannot be determined. The force levels in B, previously determined for Tests 19 (P-0.51 g) and 32 (P-0.52 g) were 9120 and 7465 lb, respectively. Because the value for Test 19 is almost triple the

capacity of the uncracked unreinforced large pier, it is almost certain that cracking occurred at the unreinforced end of the pier. It is also clear from Table 6.12 that during the larger base motion tests the reinforcement was transferring significant forces to the footings since the associated uplift of the footing significantly increased as the force level increased, and reached 0.86 in. and 0.40 in. at the right and left ends of the panel, respectively, during Test 32 (P-0.52 g).

6.4.3 Connection Forces

The maximum forces transmitted through the connections of House 1 and 2 are given in Table 6.19. They are expressed in terms of the total force, the force/unit length, the force/bolt and the force/truss because with different types of connections any one of these parameters may be critical. The magnitudes of the forces from the shaking table tests are compared with those obtained from the connection test program in Volume 3 of this series of reports.

The forces acting on the out-of-plane connections are presented in Tables 6.5 and 6.10. These correspond to the assumption that the out-of-plane walls are hinged at the top and bottom, and therefore are upper bound values. The forces on the in-plane connections are obtained from the inertia forces generated in the roof, plus the forces transmitted from the top of the out-of-plane walls. These are also upper bound values since the maximums of both sets of forces are assumed to occur simultaneously. Additional conservatism is included from points (2) and (3) discussed at the beginning of Section 6.4.

6.5 Performance of Cracked Unreinforced Walls

From the previous section it is clear that considerable variation was observed in cracking of the unreinforced walls due to significant

variations in the tensile strength normal to the bed joints. However, it is also clear that the cracked, unreinforced walls were capable of resisting the unidirectional motions induced by later tests. In the cracked condition the unreinforced cantilever type in-plane walls tended to rock on the cracked section, whereas the unreinforced cracked out-of-plane walls tended to hinge at the cracked section. The in-plane wall with a window and door opening was not tested after it cracked.

The question therefore must be addressed as to what constitutes the limit of satisfactory performance of an unreinforced house. This section presents a summary of the response of the cracked unreinforced in-plane and out-of-plane walls for both Houses 1 and 2. A limitation of the following discussion is that the walls of the test houses were subjected to only unidirectional base motions. An assessment of the effect of two horizontal components of motion must be made when these results are extrapolated to field conditions.

6.5.1 Out-of-Plane Walls W4 and A1

To aid in the evaluation of the performance of the cracked unreinforced out-of-plane walls, listings of the maximum displacements are provided for each test for Houses 1 and 2 in Tables 6.13 and 6.14, respectively. Table 6.13 summarizes the maximum displacements recorded at the center of W4 at the top, 2/3 and 1/3 wall height. The exact locations at which the displacements were measured can be seen from the channel numbers of Fig. 3.5. Table 6.14 summarizes the equivalent displacements recorded for House 2; seven locations are given for A1 and the exact locations at which the displacements were measured can be seen from channel numbers of Fig. 3.6.

Tables 6.15 and 6.16 provide a complete summary of the post-cracked performance of the unreinforced out-of-plane walls for Houses 1 and 2, including the tensile stresses corresponding to maximum moments existing at and before cracking, as discussed in Section 6.4.

(A) House 1

For House 1 when W4 was load bearing the only crack that occurred was at the first joint above the footing during Test 11 (T-0.29 g). This did not change the primary cantilever response mechanism of the wall in any subsequent test. When W4 was non-load bearing (after Test 13) it cracked at the 6th course from the top during Test 19 (T-0.25 g) although this crack was not visually evident until after Test 20. During Test 20 (T-0.21 g) minor hinging of the wall occurred at the crack level; however, the deflection at the 2/3 height was only 0.25 in. During Test 21 (E-0.31 g) significant hinging occurred at the cracked joint and the displacement at 2/3 wall height was 2 in. The wall was repaired with the fiberglass based surface bonding plaster after this test, but cracking reoccurred at the same joint during Test 27 (P-0.49 g). During the next test (P-0.63 g) no hinging occurred at the crack location. This is attributed to the residual strength of the repair material after a crack is visible. During the next and last test, Test 29 (E-0.59 g), the wall hinged although the displacement was not as large as that, which occurred during Test 21 (1 in. compared with 2 in.).

It should be noted that the displacements at the top of the out-of-plane walls are a function primarily of the displacements of the in-plane walls. However, in the non-load bearing configuration deformation occurred along the length of the top of the out-of-plane walls due to the flexibility of the gable end connection. In the tests on House 1

the fixity conditions of the footings were changed after Test 13, and this had a resultant effect on the displacements at the top of both the in-plane and out-of-plane walls. When comparing the displacements at the top of the out-of-plane walls it should also be noted that the displacement during Test 21 (E-0.31 g) was as great as that of Test 29 (E-0.56 g) and was of the order of 0.70 in. During Test 21 (E-0.31 g) more significant hinging occurred in the cracked wall and this probably caused the greater displacement recorded at the top of the wall.

(B) House 2

For House 2 the unreinforced out-of-plane wall A1 had a different configuration from that of W4 of House 1. Cracking was first noted after Test 14 (E-0.33 g) when this wall was non-load bearing, in the 4 ft 8 in. pier at the joint continuous with the bottom of the window. As can be seen from Table 6.16, no subsequent test (in either the non-load or load bearing configuration) produced the hinging effect that was evident in W4 of House 1. During Test 32 no hinging was evident although large displacements occurred as a result of the failure of the in-plane wall A. It is not clear why the hinging effect did not occur in House 2 although it is postulated that the location of the crack at the bottom of the window level was a significant factor. The panel below the window must have provided a restraining effect because the small pier on its left side was not cracked at this level.

As seen from Table 6.14, the displacements at the top of the out-of-plane walls never exceeded 0.5 in. except for Test 32; for all tests with a peak acceleration less than 0.4 g they were less than 0.33 in. Displacements at the top of the out-of-plane walls, when the in-plane walls were load bearing were approximately half those that occurred for

comparable tests when the in-plane walls were non-load bearing. This is attributed to the difference in the response mechanisms of the in-plane walls rather than to the response mechanisms of the out-of-plane walls.

(C) Summary

An important aspect of the response mechanism of the out-of-plane walls resulting from hinging at the crack location can be seen in the displacement time history plots of House 1 shown in Figs. 5.3(c) and 5.4(c) for Tests 19 and 21, respectively. These plots give the displacement history at the top and 2/3 wall height locations for W4 of House 1. In the uncracked condition the response of the wall is substantially in phase with the applied base motion, indicating a rigid type response. During Test 21, however, when the cracked wall was hinging significantly, the period of the wall increased and this increase appears to be related to the amplitude of response. The period varied between 0.3 and 0.5 sec and the wall was subjected to 15 half cycles of the longer period response with an amplitude greater than 0.5 in. at the 2/3 wall height. Three of the half cycles had an amplitude greater than 1.0 in. near the crack location. It can be seen from the response spectra of Fig. 4.3 for House 1, Test 21 (E-0.31 g) that the period range of the cracked wall lies within the higher ordinates of the response spectrum.

An assessment of the hinging effect is important if unreinforced walls are to be used in any seismic zone. The response mechanism is non-linear in that it appears to be amplitude dependent, the amplitude of response, therefore, is dependent on the magnitude and frequency content of the base motion in the period range of the cracked wall.

On the other hand, the cracked unreinforced wall A1 of House 2 did not hinge at all and as the displacement time history plots of Figs. 5.13(c) to 5.15(c) and Table 6.14 indicate, the displacement at 2/3 wall height was essentially in phase with the applied base motion and always less than the top displacement.

6.5.2 In-Plane Walls W3 and A

To aid in the evaluation of the performance of the cracked unreinforced in-plane walls, the results of tests in the cracked state for Houses 1 and 2 are summarized in Tables 6.17 and 6.18, respectively. The displacement information for these tables was obtained from Tables 6.2 and 6.7.

(A) House 1

For House 1 the first 13 tests were performed with the in-plane walls non-load bearing and with the footings of the in-plane walls free to uplift. After Test 13 the footings were restrained from uplifting. W3 first cracked during Test 9 (T-0.21 g) along a joint 2 ft 8 in. above the footing when the maximum shear stress on the wall was 9 psi. Test 10 (T-0.27 g) was performed with the wall in the cracked condition. Visible rocking occurred at the crack location and slight crushing developed at each end of the wall; however, no permanent slip occurred along the joint. The maximum net shear stress on the wall during this test was 9 psi.

The wall was mechanically prevented from slipping at the cracked joint after this test, as shown in Fig. 5.2. During Test 11 (T-0.29 g) a new crack developed along the first joint above the footing when the maximum net shear stress was 11 psi. Two additional tests were performed in this cracked state: Test 12 (E-0.14 g) and Test 13 (E-0.28 g). Again

the wall visibly rocked along the cracked joint and no permanent slip occurred. The maximum net shear stresses on the wall during these two tests were 5 and 11 psi, respectively. Additional cracks shown in Fig. 5.1 developed at the 5th and 6th joints above the footing during Test 13; the cause of these cracks is not clear in view of the fact that the wall rocked on the lower joint. The wall was repaired with the fiberglass based plaster after Test 13 and the roof was rotated so the walls became load bearing.

In the repaired and load bearing state, W3 cracked again at the second joint above the footing during Test 27 (P-0.49 g). Two subsequent tests were performed in this cracked state: Test 28 (P-0.63 g) and Test 29 (E-0.59 g). Although the wall rocked and crushing was evident at the ends of the crack, it did not permanently slip. The maximum net shear stresses on the wall during these two tests were 29 and 25 psi, respectively.

The maximum displacements at the top of the wall during tests when the wall was cracked were 0.40 in. for Test 10 and 0.28 in. for Test 13 when the wall was non-load bearing and the footings were free to uplift. Uplift of the footings was not observed, however, and the displacements are attributed to the rocking mode of response. When the wall was cracked and load bearing, the displacements at the top were 0.70 in. for Test 28 and 0.37 in. for Test 29.

(B) House 2

For House 2 the large pier of B acted as an unreinforced element for a force acting to the right in Fig. 6.11(a) and as a reinforced element for a force acting to the left in Fig. 6.11(b). The displacements in the right and left directions (as shown in Fig. 6.11) for all

tests are presented in Table 6.7 and a summary of the performance is given in Table 6.18. In assessing these results it should be noted that the footing of B was bolted to the shaking table with bolts spaced 6 ft apart and located 5 ft from either end of the footing. As a result the dowelled reinforcement at each end of the panel caused the footing to uplift and the magnitude of uplift is given in Table 6.12.

In the load bearing configuration the displacements to the right for the large pier of B when it responded as an unreinforced element were 0.04 in., 0.07 in. and 0.28 in. for the E-0.45 g, T-0.40 g and P-0.51 g sequence of base motions, respectively. The corresponding net shear stresses on the large pier were 26, 26 and 35 psi, respectively. When the same panel was non-load bearing the displacements increased significantly for corresponding base motions. The displacements for the T-0.26 g, E-0.37 g and P-0.52 g base motions were 0.16 in., 0.35 in. and 1.07 in., respectively. The corresponding net shear stresses on the large pier were 16, 24 and 29 psi, respectively.

A comparison of the displacements given in Table 6.7, of the large pier responding as an unreinforced element (forces to the right) and as a reinforced element (forces to the left), shows that the displacements in the former case were almost always less than or equal to those in the latter case. This is a direct result of the uplift of the footing and should not be attributed to the effect of reinforcement.

During Test 32, wall A of House 2 failed dramatically with the formation of a diagonal crack from the reentrant corner of the window propagating toward the footing, (Fig. 5.12(i). This failure mechanism was associated with a permanent displacement of approximately 1 in. and the performance was considered unacceptable. Initial cracking at the reentrant corner of the window is attributed to a concentration of tensile

stresses. Since it also occurred in Houses 3 and 4, this is postulated to be a typical mode of failure for walls with the geometric configuration of wall A. Unfortunately no base motion tests were performed in the range 0.15 to 0.30 g with wall A cracked, so its performance in the cracked condition could not be determined.

(C) Summary

Unlike the out-of-plane walls which hinged at the crack locations the rocking mode of response of the cracked unreinforced in-plane walls was essentially a rigid body motion. The displacement time histories at the tops of the walls, in Figs. 5.6(d) and 5.9(d) for Tests 10 and 13 of House 1 and in Figs. 5.13(b), 5.14(b) and 5.15(b) for Tests 14, 17 and 30 of House 2, were essentially in phase with the applied base motion.

The mechanism of rocking is such that as the wall tends to rock it uplifts the roof structure, thereby increasing the compressive load on the wall. No permanent slip occurred along the cracked joint for net shear stresses on the pier of up to 30 psi for House 1 and 35 psi for House 2, although it should be noted that in House 2 one end of the wall was reinforced. The amplitudes of rocking displacements at the top of the walls depended on whether the walls were load bearing or non-load bearing. For base motions with peak accelerations of the order of 0.30 g, the displacements at the top of non-load bearing walls were 0.3 to 0.4 in. The displacements for load-bearing walls in corresponding tests were 0.04 to 0.08 in. For base motions with peak accelerations between 0.50 g and 0.65 g the displacements at the top of the non-load bearing walls were 0.7 to 1.0 in. For load bearing walls the corresponding displacements were 0.3 to 0.7 in.

For the base motion at which A failed, (P-0.52 g), the performance was considered unacceptable because of the 1 in. permanent displacement that occurred. Obviously the base motion at which this mode of failure will occur depends on the tensile strength of the material in the vicinity of the reentrant corner.

6.6 Performance of Partially Reinforced Walls

From Section 6.4 it is clear that the performance of partially reinforced walls is superior to unreinforced walls; for all the tests performed on Houses 1 and 2 satisfactory performance was obtained for all partially reinforced walls. This section presents a summary of the response of the partially reinforced in-plane and out-of-plane walls for both Houses 1 and 2.

6.6.1 Out-of-Plane Walls W2 and B1

To aid in the evaluation of the performance of the partially reinforced walls, listings of the maximum displacements are provided for each test for Houses 1 and 2 in Tables 6.13 and 6.14, respectively. Table 6.13 summarizes the maximum displacements recorded at the center of W2 at the top, 2/3 and 1/3 wall height. The exact locations at which the displacements were measured can be seen from the channel numbers of Fig. 3.5. Table 6.14 summarizes the equivalent displacements recorded for House 2; five locations are given for B1 and the exact locations at which the displacements were measured can be seen from channel numbers of Fig. 3.6.

(A) House 1

For House 1, W2 was load bearing for the first 13 tests and non-load bearing for the remainder. As can be seen from Table 6.13, W2

responded to all base motions in a "cantilever mode" response mechanism. The displacement at the 2/3 wall height never exceeded the top displacement and the only visible crack that occurred in the wall was at the first course above the footing (see Fig. 5.1).

It should be noted that the displacements at the top of the out-of-plane walls are a function primarily of the displacements of the in-plane walls although in the non-load bearing configuration there was deformation along the length of the top of the out-of-plane walls due to the flexibility of the gable end connection. In the tests on House 1 the fixity conditions of the footings changed during the sequence of tests with a resultant effect on the displacements at the top of both the in-plane and out-of-plane walls. After Test 13 the footings of both in-plane walls were restrained from uplifting, whereas prior to this they were free to uplift.

A comparison of the responses of the unreinforced and reinforced out-of-plane walls from Table 6.13 shows that when the unreinforced wall was uncracked the responses were almost identical. When the unreinforced wall was repaired and still uncracked (Tests 22 to 27), the out-of-plane displacements of the repaired wall were 30 to 50 percent less than those of the reinforced wall. This reduction is attributed to the additional stiffness provided by the repair material.

(B) House 2

For House 2, B1 was non-load bearing for the first 19 tests and load bearing for the remainder. As can be seen from Table 6.13 and Fig. 5.16, B1 was subjected to some twisting along its length in addition to out-of-plane displacements as a result of the difference in displacements of the in-plane walls. With this mode of response, the displacement

at the 2/3 wall height never exceeded the top displacement and along the length of the wall the vertical displacement profile was essentially a straight line. The very large displacements that occurred during Test 32 are attributed to the failure of the in-plane wall A.

Only minor cracking was observed in B1, as shown in Fig. 5.12. This occurred at the bottom of the small pier, at the right end of the beam connecting the two piers and toward the top right side of the large pier. These cracks were all visible prior to Test 32, and the 3 in. displacement recorded at the top of the out-of-plane walls during Test 32 did not produce any additional cracks.

(C) Summary

The performance of the partially reinforced out-of-plane walls in Houses 1 and 2 was very satisfactory. The displacements at the top of the walls in House 1 reached a maximum of 0.42 in. when they were non-load bearing and 0.72 in. when they were load bearing and the associated cracking was insignificant. For House 2, again only minor cracking occurred even though differential out-of-plane displacements (twisting) occurred along the top of the wall; the maximum relative displacement was 0.08 in. when the walls were non-load bearing and 0.27 in. when they were load bearing. The maximum total out-of-plane displacements were 0.41 in. when the walls were non-load bearing and 3.05 in. when they were load bearing. Both partially reinforced walls responded essentially as rigid body elements in that the displacement time histories of the walls were essentially in phase with the base motion as shown in Figs. 5.6(c) and 5.9(c) for Tests 10 and 13 of House 1 and Figs. 5.13(f), 5.14(f) and 5.15(f) for Tests 16, 17 and 30 of House 2.

6.6.2 In-Plane Walls W1 and B

The performance of the partially reinforced in-plane walls is discussed in terms of the displacements at the top of the walls listed in Tables 6.2 and 6.7, and the crack pattern diagrams shown in Figs. 5.1 and 5.12.

(A) House 1

For House 1, W1 was non-load bearing up to and including Test 13, and was load bearing for the remainder of the tests. Also, up to and including Test 11 the footing of W1 was free to uplift. After Test 11 it was bolted to the shaking table.

The displacements of both the reinforced and unreinforced walls up to Test 11 were approximately the same and that of W1 reached a maximum of 0.36 in. during Test 11 (T-0.29 g) when footings of both walls were free to uplift. After the footing of W1 was bolted to the shaking table the displacements at the top of the wall decreased dramatically, almost by an order of magnitude. During Test 13 (E-0.28 g) the displacement was 0.05 in.

When W1 was load bearing with its footing bolted to the shaking table the maximum displacement recorded was 0.09 in. during Test 28 (P-0.63 g). Minor visible cracking occurred at the wall footing connection and a small crack occurred at about the 1/3 height on the left side of the wall.

The horizontal force which would induce yielding of the vertical reinforcement was 9410 lb when the wall was not carrying dead load and 11,580 lb when subjected to the 480 lb/ft dead load. The maximum forces transmitted to W1 were 3695 lb during Test 13 when it was non-load bearing and 10,060 lb during Test 28 when it was load bearing, and

therefore yielding of the vertical reinforcement probably did not occur. The net shear stresses on the wall sections associated with these forces were 11 psi and 29 psi, respectively.

(B) House 2

For House 2 the large pier of B acted as a reinforced element for a force acting to the left in Fig. 6.11(b); a detailed discussion of its response and a comparison with the performance in the opposite direction is given in Section 6.5.2 (B). In summary the displacements recorded in the reinforced direction were greater than in the unreinforced direction as a result of the uplift of the footing. (The results obtained subsequently for House 3, in which the footing was more firmly anchored, indicate that the displacements in the reinforced direction were less than in the unreinforced direction.)

In the load bearing configuration, the displacements to the left for the large pier of B (when it was responding and uplifting the footing as a reinforced element) were 0.13 in., 0.21 in. and 0.40 in. for the E-0.45 g, T-0.40 g and P-0.51 g base motions, respectively. The corresponding net shear stresses in the pier were 26, 26 and 35 psi, respectively. When the wall was non-load bearing the displacements increased significantly for corresponding base motions; for the T-0.26 g, E-0.37 g and P-0.52 g base motions the displacements were 0.25 in., 0.31 in. and 1.06 in., respectively. The corresponding net shear stresses were 16, 24 and 29 psi, respectively.

The horizontal force inducing yielding of the vertical reinforcement would be 7740 lb with no dead load and 8715 lb with the dead load of 480 lb/ft. The maximum forces transmitted to the wall were 7465 lb during Test 32 when it was non-load bearing, and 9120 lb during Test 19

when it was load bearing; therefore the vertical reinforcement probably yielded during one or two cycles of load.

The small pier of wall B responded as a reinforced element for forces acting to the right in Fig. 6.11(a). Significant forces were transmitted through the dowel for forces in this direction as attested by the uplift of the footing,given in Table 6.12, at this end of the wall. The actual distribution of forces between the small and large piers in this direction is difficult to assess because of the rocking response of the large pier.

(C) Summary

The performance of the partially reinforced in-plane walls in Houses 1 and 2 was very satisfactory. Both W1 in House 1 and B in House 2 responded as cantilever type elements; the deflections at the top of the walls were dependent on the fixity of the footing to which they were dowelled, the intensity of the base motion and the presence of dead load. The displacements of both walls increased significantly when they were non-load bearing and when the footings were permitted to uplift.

Both partially reinforced walls responded essentially as rigid body elements in that the displacement time histories at the top of the walls were essentially in phase with the base motions, as shown in Figs. 5.6(d) and 5.9(d) for Tests 10 and 13, respectively, of House 1 and Figs. 5.13(b), 5.14(b) and 5.15(b) for Tests 16, 17 and 30, respectively, of House 2.

No permanent displacements of the walls occurred and cracking was minor during all tests. The maximum net shear stresses developed in the walls were 11 psi for W1 of House 1 when it was non-load bearing, and

29 psi when it was load bearing. The corresponding values for B of House 2 where 29 and 35 psi, respectively. The vertical reinforcement may have yielded for one or two cycles of load during Test 19 of House 2; however, no yielding of the vertical reinforcement occurred in any other test.

6.7 Amplification of Peak Base Acceleration

During all tests on Houses 1 and 2 accelerations were measured at the ceiling and concrete weight levels of the roof, at the top of the in-plane walls, and at the top and 2/3 wall height of the out-of-plane walls. Peak values of the accelerations measured at the ceiling and concrete weight levels are given in Tables 6.3 and 6.8 for Houses 1 and 2, respectively. Figures 6.12 and 6.13 are plots of these maximum values expressed as ratios to the peak table accelerations for Houses 1 and 2, respectively. For each figure two plots,(a) and (b), are given; (a) summarizes the tests when the roof trusses were parallel to the table motion, and (b) refers to tests when they were perpendicular to the table motion.

Peak values of the accelerations measured at the top of the in-plane walls are given in Tables 6.2 and 6.7 for Houses 1 and 2, respectively. Figures 6.14 and 6.15 are plots of these maximum values expressed as ratios to the peak table accelerations for Houses 1 and 2, respectively. As with the roof accelerations, separate plots are presented for the two different orientations of the roof trusses.

Peak values of the accelerations measured at the top and 2/3 wall height of the out-of-plane walls are given in Tables 6.4 and 6.9 for Houses 1 and 2, respectively. Figures 6.16 and 6.17 are plots of these maximum values expressed as ratios to the peak table accelerations for

Houses 1 and 2, respectively. Each figure contains four plots; for the two locations at which the accelerations were measured a plot is provided for each orientation of the roof trusses.

The influence of short pulses of accelerations associated with impact after uplift is included to some extent in Figs. 6.12 and 6.17. Where possible, such uncharacteristically high peaks were omitted from the figures by inspection of the time history plots; however these plots were not available for all tests so not all the uncharacteristically high values could be removed.

6.7.1 Peak Roof Accelerations

Figures 6.12 and 6.13 provide an overview of the structural response, whereas Figs. 6.14 to 6.17 provide information on the response of individual elements. The following observations are presented with respect to the overall structural response:

(1) The amplification factor measured at the roof level appears to be independent of both the type of base motion and the peak table acceleration.

(2) The amplification factor at the concrete weight level generally was greater than at the ceiling level; this difference was increased when the roof trusses were oriented transverse to the table motion.

(3) The variations in the amplification factors at the top of the in-plane walls were not directly related to those obtained at the center of the roof level.

(4) For both Houses 1 and 2, the range of the amplification factors at the roof level was greater when the roof trusses

were oriented transverse to the table motion (in-plane walls load bearing). This was due to the greater flexibility of the roof system with this orientation of the roof trusses. The range of the roof amplification factors for the transverse roof orientation, considering both the ceiling and concrete weight levels was 1.3 to 2.4 for House 1, and 1.2 to 2.5 for House 2. For the roof orientation parallel to the table motion the corresponding ranges of amplification factors were 1.1 to 2.0 for House 1 and 1.3 to 2.3 for House 2.

6.7.2 In-Plane Wall Accelerations

Plots of the peak accelerations for the in-plane walls, expressed as ratios to the peak table accelerations, are presented in Figs. 6.14 and 6.15 for Houses 1 and 2, respectively. These plots graphically illustrate the response observed for the in-plane walls and discussed in Sections 6.4, 6.5 and 6.6.

For House 1 when the in-plane walls were non-load bearing, the footings were free to uplift and W3 was cracked for 5 of the first 13 tests. Under these conditions significant variations were obtained in the amplification factors as shown in Fig. 6.14(a). When the unreinforced wall W3 was repaired and the in-plane walls became load bearing there was virtually no amplification at the top of either in-plane wall. The maximum amplification factor recorded was approximately 1.3 with a range of 0.9 to 1.3.

For House 2 when the in-plane walls were non-load bearing the acceleration amplification factors reflected the larger displacement response of B. The range of the amplification factor for B was 1.3

to 3.5, whereas for the more rigid wall A it was 0.9 to 1.3. When the in-plane walls were load bearing the difference in the amplification factors for the two walls decreased, and for most tests the amplification was between 1.0 and 1.5, a range similar to that observed in House 1.

6.7.3 Out-of-Plane Wall Accelerations

Plots of the peak accelerations for the out-of-plane walls, expressed as ratios to the peak base accelerations, are presented in Figs. 6.16 and 6.17 for Houses 1 and 2, respectively. These plots provide another means of understanding the response of the structure, in particular the response of the out-of-plane walls. In evaluating these figures it should be noted that the displacements at the top of the out-of-plane walls are governed by the response of the in-plane walls. Also, if the out-of-plane walls are non-load bearing a small amount of additional flexibility arises from the support of the gable end trusses at the top of the walls.

For House 1 with the out-of-plane walls load bearing the amplification factors at both the top and 2/3 wall height generally showed the same trends observed for the in-plane walls (see Fig. 6.14(a)). The amplification factor at the 2/3 wall height was generally less than that at the top of the wall although in a few tests it was not. When the out-of-plane walls were non-load bearing the amplification factors at both the top and 2/3 wall height were greater than those obtained for the in-plane walls (see Fig. 6.14(b)), and this is attributed to the flexibility of the out-of-plane gable end roof truss attached at the top of the walls. The range of amplification factors except for the last two tests was 1.3 to 2.3 at the top of the wall and 1.1 to 2.1 at 2/3

wall height. The corresponding range for the in-plane walls was 0.9 to 1.3.

Trends in the results for House 2 are not as clear as those for House 1, because they were affected by the locations at which the accelerations were recorded. For A1 the acceleration at the top of the wall was recorded at the center of the wall (Channel 80 of Fig. 3.6) and the acceleration at 2/3 wall height was measured at the center of the 4 ft 8 in. pier (Channel 79 of Fig. 3.6). For B1 the acceleration at the top of the wall was measured at the center of the spandrel beam (Channel 82 of Fig. 3.6) and the acceleration at the 2/3 wall height was measured at the center of the larger pier (Channel 81 of Fig. 3.6). Thus the accelerations at the top of the walls were measured close to the center of the walls, whereas at the 2/3 wall height the measurements for A1 were made closer to the more flexible in-plane wall B, while for B1 they were made closer to the more rigid in-plane wall A. The difference associated with the different measurement locations was more pronounced when the in-plane walls were non-load bearing. With this as background the observations for House 2 are as follows.

With the trusses transverse to the motion (in-plane walls load bearing, out-of-plane walls non-load bearing), the amplification factors at the top of the out-of-plane walls followed the same trends obtained for the in-plane walls (see Fig. 6.15(a)), although the values, and also the range, were slightly greater because of the additional flexibility of the gable end connection. The amplification factors at the 2/3 wall height were similar but slightly lower than those at the top of the wall. The range of the amplification factors at the top of the walls for most of the tests was 1.2 to 2.5, whereas for the 2/3 wall height the range for most of the tests was 1.0 to 2.0.

When the trusses were parallel to the motion considerable variation was observed in the amplification factors measured both at the top and at 2/3 wall height. The range of values was considerably greater than was observed for the in-plane walls, although the trends were similar. The range of amplification factors at the top of the walls was 1.0 to 4.0, and at the 2/3 wall height it was 1.0 to 3.0. The range of values for both the in-plane walls was 0.9 to 2.5.

TABLE 6.1

ALLOWABLE FLEXURAL TENSILE STRESSES IN NATIONAL CODES
(UNREINFORCED BRICK MASONRY)

Code	Mortar Type, Mortar Mix (C:L:S) or Strength	Allowable Stress in Tension Flexure psi	
		Parallel to bed joints	Normal to bed joints
1976 USA Uniform Building Code	M or S N	72* (36)** 56* (28)**	36* (18)** 28* (14)**
1970 Canada National Building Code	M or S N	72 56	36 28
Britain (and Australia)	1:1:6 or better	20 (to be used with caution)	10
Germany	1:0:4	28	Only exceptionally permitted
Switzerland	1:2:8 1:0:3.2-3.7	14 5.95-12.4***	Not permitted
Japan	1:0:3 or 1:2:5	32 or less than $\frac{f'_m}{53}$	

* Special inspection required

** No special inspection required

*** At mid-height of a story height panel

From Reference (5)

TABLE 6.2

MAXIMUM ACCELERATIONS AND DISPLACEMENTS AT THE TOP OF IN-PLANE WALLS OF HOUSE 1

Test No.	Base Accel. g	W1 Accel.(97) g	W3 Accel.(88) g	Ratio W1/Base	Ratio W3/Base	W1 Displ.(63) in	W3 Displ(62) in
1	T-0.002	0.000	-0.013	——	——	0.000	0.000
2	T-0.026	0.000	0.038	——	1.462	0.000	0.000
3	T-0.050	0.000	0.067	——	1.340	0.000	0.000
4	T-0.066	-0.071	-0.074	1.076	1.121	0.003	-0.006
5	T-0.089	-0.108	0.118	1.213	1.326	-0.005	-0.012
6	T-0.122	-0.159	0.164	1.303	1.344	-0.009	-0.022
7	T-0.147	-0.183	0.236	1.245	1.605	-0.019	-0.041
8	T-0.190	-0.241	0.256	1.268	1.347	-0.040	-0.058
9	T-0.214	-0.391	-0.398	1.827	1.860	-0.135	-0.143
10	T-0.269	0.704	-0.640	2.617	2.379	0.344	-0.397
11	T-0.285	-0.732	0.892	2.568	3.130	0.361	0.303
12	E-0.140	-0.381	-0.279	2.721	1.993	0.007	0.072
13	E-0.282	-0.619	0.758	2.195	2.688	0.047	-0.277
14	T-0.051	0.055	0.051	1.078	1.000	0.001	-0.001
15	T-0.062	0.081	0.077	1.306	1.242	-0.001	0.001
16	T-0.092	0.103	0.094	1.120	1.022	0.002	-0.003
17	T-0.119	0.135	0.142	1.134	1.193	0.003	-0.004
18	T-0.193	0.244	0.199	1.264	1.031	-0.011	-0.008
19	T-0.248	0.306	0.271	1.234	1.093	-0.019	-0.014
20	E-0.209	0.198	0.223	0.947	1.067	0.014	0.009
21	E-0.311	0.336	0.362	1.080	1.164	0.022	-0.013
22	E-0.214	0.216	0.239	1.009	1.117	0.013	0.009
23	E-0.323	0.396	0.343	1.226	1.062	0.023	-0.013
24	E-0.455	-0.434	0.417	0.954	0.916	0.029	-0.019
25	P-0.247	-0.279	-0.251	1.130	1.016	0.021	0.011
26	P-0.386	-0.422	-0.422	1.093	1.093	0.038	0.020
27	P-0.492	-0.544	-0.599	1.106	1.217	0.051	-0.112
28	P-0.627	-0.799	0.780	1.274	1.244	0.084	-0.700
29	E-0.592	0.637		1.075		0.036	-0.369

Note: The numbers in brackets associated with the designation of each wall measurement correspond to the channel numbers located in Fig. 3.5.

TABLE 6.3

MAXIMUM ROOF ACCELERATIONS AT THE CONCRETE WEIGHT AND DRYWALL LEVELS FOR HOUSE 1

Test No.	Base Accel. g	Weight Level Accel.(90) g	Drywall Level Accel.(86) g	Ratio Weight / Base	Ratio Drywall / Base
1	T-0.002	0.000	0.011	—	—
2	T-0.026	0.002	-0.045	—	1.731
3	T-0.050	0.001	0.073	—	1.460
4	T-0.066	0.080	-0.080	1.212	1.212
5	T-0.089	-0.117	0.118	1.315	1.326
6	T-0.122	-0.157	0.159	1.287	1.303
7	T-0.147	-0.214	0.208	1.456	1.415
8	T-0.190	-0.269	-0.259	1.416	1.363
9	T-0.214	0.397	-0.412	1.855	1.925
10	T-0.269	-0.432	-0.403	1.606	1.498
11	T-0.285	0.449	-0.456	1.575	1.600
12	E-0.140	0.245	-0.248	1.750	1.771
13	E-0.282	0.556	-0.538	1.972	1.908
14	T-0.051	-0.080	-0.083	1.569	1.627
15	T-0.062	0.097	0.113	1.565	1.823
16	T-0.092	-0.143	-0.161	1.554	1.750
17	T-0.119	-0.211	-0.209	1.773	1.756
18	T-0.193	-0.373	-0.304	1.933	1.575
19	T-0.248	-0.562		2.266	
20	E-0.209	0.431		2.062	
21	E-0.311	0.622	0.480	2.000	1.543
22	E-0.214	0.415	-0.285	1.939	1.332
23	E-0.323	0.601	-0.654	1.861	2.025
24	E-0.455	0.727	-0.849	1.598	1.866
25	P-0.247	0.564	0.503	2.283	2.036
26	P-0.386	0.834	0.677	2.161	1.754
27	P-0.492	0.914	0.931	1.858	1.892
28	P-0.627	1.162	1.836	1.853	2.928
29	E-0.592	0.994		1.679	

Note: The number in brackets associated with the designation of each wall measurement corresponds to the channel number located in Fig. 3.5

TABLE 6.4

MAXIMUM ACCELERATIONS AT TOP AND TWO THIRDS WALL HEIGHT OF OUT-OF-PLANE WALLS FOR HOUSE 1

Test No.	Base Accel. g	W2 Top Accel.(81) g	W2 2/3 H-Accel.(83) g	W4 Top Accel.(84) g	W4 2/3 H-Accel.(85) g
2	T-0.026	0.042	0.038	0.038	0.030
3	T-0.050	0.074	0.077	0.072	0.066
4	T-0.066	0.083	0.069	0.083	0.069
5	T-0.081	0.017	0.114	0.118	0.103
6	T-0.122	0.158	0.138	0.151	0.145
7	T-0.147	0.206	0.176	0.207	0.175
8	T-0.190	0.244	0.220	0.251	0.364
9	T-0.214	0.405	0.357	0.392	0.357
10	T-0.267	0.382	0.370	0.395	0.375
11	T-0.285	0.420	0.432	0.456	0.661
12	E-0.140	0.256	0.218	0.233	0.190
13	E-0.282	0.563	0.390	0.459	0.469
14	T-0.051	0.088	0.076	0.091	0.080
15	T-0.062	0.093	0.082	0.101	0.085
16	T-0.092	0.144	0.130	0.129	0.127
17	T-0.119	0.202	0.180	0.189	0.162
18	T-0.193	0.289	0.263	0.254	0.224
19	T-0.248	0.384	0.309	0.345	0.312
20	E-0.209	0.422	0.355	0.463	0.314
21	E-0.311	0.658	0.563	0.521	0.617
22	E-0.214	0.397	0.296	0.299	0.261
23	E-0.323	0.601	0.493	0.427	0.360
24	E-0.455	0.822	0.698	0.687	0.532
25	P-0.247	0.514	0.442	0.406	0.334
26	P-0.386	0.788	0.539	0.697	0.533
27	P-0.492	0.824	0.683	0.774	0.667
28	P-0.627	1.784	1.416	1.987	1.456
29	E-0.592	1.184	1.525	1.907	1.130

Note: The numbers in brackets associated with the designation of each wall measurement correspond to the channel numbers located in Fig. 3.5.

TABLE 6.5

MAXIMUM OUT-OF-PLANE WALL MOMENTS AND CONNECTION FORCES: HOUSE 1

Test No.	WALL W2							WALL W4							
	$k_{\theta_2} = 0$				$k_{\theta_2} = \infty$			$k_{\theta_2} = 0$				$k_{\theta_2} = \infty$			
	Roof Connection Force lb/ft (2)	Max. Moment,(1) lb-in./ft x/H			Roof Connection Force lb/ft	Max. Moment, lb-in./ft x/H			Roof Connection Force lb/ft	Max. Moment, lb-in./ft x/H			Roof Connection Force lb/ft	Max. Moment, lb-in./ft x/H		
		= 0.5	= 0.6	= 0.7		= 0.5	= 0.6	= 0.7		= 0.5	= 0.6	= 0.7		= 0.5	= 0.6	= 0.7
10	43	1,058	1,031	915	35	538	616	603	44	1,071	1,045	928	33	545	624	612
11	46	1,115	1,084	960	35	564	643	630	47	1,169	1,155	1,083	—	—	—	—
13	50	1,080	1,072	971	40	557	654	657	51	1,215	1,201	1,076	40	629	733	725
19	39	936	910	808	30	473	540	530	38	933	905	801	29	471	536	524
21	67	1,568	1,541	1,380	52	804	930	921	67	1,528	1,520	1,430	—	—	—	—
23	59	1,356	1,338	1,202	47	697	811	806	44	1,048	1,023	911	34	533	611	602
24	83	1,906	1,880	1,688	65	981	1,140	1,133	67	1,540	1,511	1,352	52	785	907	899
26	61	1,474	1,434	1,273	47	745	851	836	68	1,584	1,548	1,382	53	804	924	913
27	84	2,011	1,963	1,746	65	1,021	1,170	1,151	73	1,786	1,734	1,536	63	998	1,141	1,120
28	163	3,474	3,501	3,202	132	1,830	2,186	2,216	173	3,702	3,639	3,339	141	1,897	2,275	2,317
29	147	3,660	3,627	3,240	114	1,916	2,232	2,194	153	3,167	3,162	2,888	124	1,635	1,937	1,969

Notes: (1) These moments are based on the assumption that the wall was uncracked. For panels with a full horizontal joint crack the moments could not be calculated because insufficient acceleration readings were measured over the height of the wall.

(2) Roof connection forces are given per foot length of the connection.

TABLE 6.6

PERCENTAGE OF LATERAL LOAD RESISTED BY MASONRY ELEMENTS: HOUSE 1

C2 or C4		W1 or W3		C1 or C3	
$k_\theta = 0$	$k_\theta = \infty$	$k_\theta = 0$	$k_\theta = \infty$	$k_\theta = 0$	$k_\theta = \infty$
4.1	7.2	91.7	85.6	4.1	7.2

Note: Total lateral force in Fig. 6.8(b) is P = 100 lb

TABLE 6.7

MAXIMUM ACCELERATIONS AND DISPLACEMENTS AT THE TOP OF IN-PLANE WALLS FOR HOUSE 2

Test No.	Base Accel. g	A Accel.(83) g	B Accel.(84) g	Ratio A/Base	Ratio B/Base	A Displ.(42) in.	B(1) Right Displ.(48) in.	B(1) Left Displ.(48) in.
2	T-0.030	-0.045	-0.038	1.500	1.267	0.000	+0.001	-0.001
3	T-0.059	-0.061	0.072	1.034	1.220	0.001	+0.001	-0.002
4	T-0.117	-0.146	0.143	1.248	1.222	-0.002	+0.004	-0.005
5	T-0.160	0.156	0.177	0.975	1.106	-0.003	+0.005	-0.006
6	T-0.178	0.186	0.221	1.045	1.242	-0.003	+0.007	-0.010
7	T-0.232	0.249	0.250	1.073	1.078	0.005	+0.009	-0.014
8	T-0.241	0.264	0.316	1.095	1.311	0.007	+0.012	-0.029
9	T-0.280	0.276	0.451	0.986	1.611	0.009	+0.018	-0.064
10	E-0.132	0.133	0.137	1.008	1.038	0.004	+0.009	-0.009
11	E-0.168	0.171	-0.164	1.018	0.976	0.005	+0.013	-0.016
12	E-0.207	0.236	-0.264	1.140	1.275	0.007	+0.017	-0.023
13	E-0.285	0.315	-0.559	1.105	1.961	0.011	+0.024	-0.042
14	E-0.331	0.334	0.354	1.009	1.069	0.013	+0.028	-0.056
15	E-0.452	-0.456	-1.288	1.009	2.850	0.016	+0.042	-0.131
16	T-0.400	0.383	-1.224	0.958	3.060	0.021	+0.066	-0.214
17	P-0.268	-0.269	-0.331	1.004	1.235	0.012	+0.033	-0.054
18	P-0.385	-0.400	-0.620	1.039	1.610	0.025	+0.105	-0.158
19	P-0.505	-0.533	-1.773	1.055	3.511	0.049	+0.284	-0.400
20	T-0.059	0.051	0.084	0.864	1.373	0.002	+0.007	-0.006
21	T-0.076	0.068	0.125	0.895	1.645	0.003	+0.011	-0.018
22	T-0.119	0.106	0.174	0.891	1.462	0.005	+0.019	-0.037
23	T-0.156	0.193	-0.245	1.237	1.571	0.008	+0.030	-0.062
24	T-0.188	0.169	0.315	0.899	1.676	0.011	+0.049	-0.079
25	T-0.227	0.201	0.390	0.885	1.718	0.017	+0.079	-0.125
26	T-0.262	0.248	-0.559	0.947	2.134	0.035	+0.162	-0.248
27	E-0.140	0.156	-0.342	1.114	2.443	0.016	+0.082	-0.076
28	E-0.212	0.256	-0.495	1.208	2.335	0.031	+0.153	-0.147
29	E-0.304	0.297	-0.599	0.977	1.970	0.044	+0.235	-0.209
30	E-0.370	0.390	-0.861	1.054	2.327	0.070	+0.350	-0.308
31	P-0.258	-0.279	-0.605	1.081	2.345	0.040	+0.261	-0.188
32	P-0.519	-2.506	-1.077	4.829	2.075	1.115	+1.067	-1.061

Notes: (1) The right and left deflections for the displacements of Panel B refer to the directions looking at the outside face of Panel B.

(2) The number in brackets associated with the designation of each wall measurement corresponds to the channel number located in Fig. 3.6.

TABLE 6.8

MAXIMUM ROOF ACCELERATIONS AT THE CONCRETE WEIGHT AND DRYWALL LEVELS FOR HOUSE 2

Test No.	Base Accel. g	Weight Level Accel.(87) g	Drywall Level Accel.(88) g	Ratio Weight / Base	Ratio Drywall / Base
2	T-0.030	0.055	0.047	1.833	1.567
3	T-0.059	0.079	-0.079	1.339	1.339
4	T-0.117	-0.182	0.160	1.556	1.368
5	T-0.160	-0.237	0.230	1.481	1.438
6	T-0.178	-0.294	0.268	1.652	1.506
7	T-0.232	-0.371	0.317	1.599	1.366
8	T-0.241	-0.480	0.476	1.992	1.975
9	T-0.280	-0.604	-0.574	2.157	2.050
10	E-0.132	0.270	-0.250	2.045	1.894
11	E-0.168	0.394	-0.385	2.345	2.292
12	E-0.207	0.42	-0.410	2.043	1.981
13	E-0.285	0.572	-0.579	2.007	2.032
14	E-0.331	0.565	0.622	1.707	1.879
15	E-0.452	0.808	0.746	1.788	1.650
16	T-0.400	-0.821	-1.098	2.053	2.745
17	P-0.268	0.525	-0.428	1.959	1.597
18	P-0.385	0.920	-0.932	2.390	2.421
19	P-0.505	1.078	-2.170	2.135	4.297
20	T-0.059	0.081	-0.080	1.373	1.356
21	T-0.076	-0.113	0.117	1.487	1.539
22	T-0.119	-0.172	0.167	1.445	1.403
23	T-0.156	-0.225	0.224	1.442	1.436
24	T-0.188	-0.272	0.284	1.447	1.511
25	T-0.227	0.368	-0.360	1.621	1.586
26	T-0.262	0.517	-0.492	1.973	1.878
27	E-0.140	0.310	-0.292	2.214	2.086
28	E-0.212	0.483	-0.479	2.278	2.259
29	E-0.304	0.575	-0.569	1.891	1.872
30	E-0.370	0.759	-0.735	2.051	1.986
31	P-0.258	0.498	-0.468	1.930	1.814
32	P-0.519	0.878	-0.817	1.692	1.574

Note: The number in brackets associated with the designation of each wall measurement corresponds to the channel number located in Fig. 3.6

TABLE 6.9

MAXIMUM ACCELERATIONS AT TOP AND TWO THIRDS WALL HEIGHT OF OUT-OF-PLANE WALLS FOR HOUSE 2

Test No.	Base Accel. g	A1 Top Accel.(80) g	A1 2/3 H-Accel.(79) g	B1 Top Accel.(82) g	B1 2/3 H-Accel.(81) g
2	T-0.030	0.057	0.041	0.061	0.039
3	T-0.059	0.093	0.064	0.078	0.070
4	T-0.117	0.165	0.150	0.160	0.138
5	T-0.160	0.230	0.210	0.214	0.170
6	T-0.178	0.243	0.219	0.231	0.229
7	T-0.232	0.298	0.280	0.275	0.263
8	T-0.241	0.521	0.443	0.420	0.296
9	T-0.280	0.496	0.414	0.492	0.322
10	E-0.132	0.191	0.159	0.168	0.150
11	E-0.169	0.248	0.186	0.241	0.208
12	E-0.207	0.2[illegible]	0.239	0.237	0.226
13	E-0.285	0.3[illegible]	0.342	0.430	0.362
14	E-0.331	0.393	0.366	0.437	0.345
15	E-[illegible].452	0.583	0.592	0.625	0.513
16	T-0.400	0.553	0.450	0.487	0.461
17	P-0.268	0.587	0.448	0.570	0.378
18	P-0.385	0.863	0.703	0.944	0.557
19	P-0.505	1.450	1.144	1.145	0.697
20	T-0.059	[illegible]	0.076	0.074	0.068
21	T-0.076		0.115	0.120	0.091
22	T-0.119	0.[illegible]3	0.152	0.157	0.135
23	T-0.156	0.236	0.206	0.231	0.185
24	T-0.188	0.236	0.224	0.244	0.225
25	T-0.227	0.290	0.298	0.362	0.352
26	T-0.262	0.355	0.378	0.411	0.312
27	T-0.140	0.286	0.194	0.217	0.178
28	E-0.212	0.458	0.367	0.471	0.275
29	E-0.304	0.600	0.422	0.626	0.336
30	E-0.370	0.687	0.538	0.621	0.445
31	P-0.258	0.451	0.366	0.391	0.322
32	P-0.519	1.006	1.110	0.844	0.938

Note: The number in brackets associated with the designation of each wall measurement corresponds to the channel number located in Fig. 3.6.

TABLE 6.10

MAXIMUM OUT-OF-PLANE WALL MOMENTS AND CONNECTION FORCES: HOUSE 2

Test No.	WALL A1								WALL B1							
	$k_{\theta_2} = 0$				$k_{\theta_2} = \infty$				$k_{\theta_2} = 0$				$k_{\theta_2} = \infty$			
	Roof Connection Force lb/ft (2)	Max. Moment,(1) lb-in./ft x/H			Roof Connection Force lb/ft	Max. Moment, lb-in./ft x/H			Roof Connection Force lb/ft	Max. Moment, lb-in./ft x/H			Roof Connection Force lb/ft	Max. Moment, lb-in./ft x/H		
		= 0.5	= 0.6	= 0.7		= 0.5	= 0.6	= 0.7		= 0.5	= 0.6	= 0.7		= 0.5	= 0.6	= 0.7
8	32	830	804	708	25	421	477	463	38	869	849	759	28	414	484	482
12	29	730	705	621	22	367	415	403	28	700	675	594	21	352	396	384
13	38	974	939	825	29	489	552	535	41	981	949	841	31	492	559	548
14	45	1,132	1,093	961	34	569	642	624	44	1,074	1,037	916	34	538	608	594
15	69	1,744	1,691	1,492	52	882	1,002	975	64	1,540	1,500	1,332	50	780	891	876
16	58	1,402	1,358	1,201	44	715	801	783	56	1,407	1,360	1,198	42	708	801	778
17	56	1,286	1,265	1,135	44	657	762	758	51	1,140	1,119	1,006	40	580	671	669
18	86	1,973	1,942	1,741	67	1,012	1,173	1,165	79	1,697	1,672	1,510	63	863	1,005	1,010
19	139	3,111	3,083	2,781	110	1,606	1,879	1,879	98	2,136	2,099	1,891	77	1,084	1,258	1,260
24	27	679	657	579	21	342	388	377	27	681	659	582	21	343	389	379
26	42	1,080	1,049	925	31	499	574	563	39	954	925	818	30	450	519	515
	53	1,121	1,121	1,022	42	583	691	699	48	953	956	878	39	493	588	602
	65	1,448	1,438	1,300	52	749	879	880	55	1,353	1,312	1,159	42	683	775	757
32	107	2,405	2,387	2,248	—	—	—	—	99	2,149	2,125	1,993	—	—	—	—

Notes: (1) These moments are based on the assumption that the wall was uncracked. For panels with a full horizontal joint crack the moments could not be calculated because insufficient acceleration readings were measured over the height of the wall.

(2) Roof connection forces are given per foot length of the connection.

TABLE 6.11

THEORETICAL CAPACITIES OF PIERS IN WALL B FOR HOUSE 2

	Unreinforced-Uncracked		Reinforced	
	With DL[1]	Without DL	With DL	Without DL
Large Pier	3770 lb	3230 lb	8715 lb	7740 lb
Small Pier	465 lb	355 lb	2380 lb	2275 lb

(1) Dead Load

TABLE 6.12

MAXIMUM UPLIFT OF FOOTING UNDER WALL B FROM TABLE: HOUSE 2

Test Sequence	Uplift at Right End, in.	Uplift at Left End, in.
27	0.048	0.001
28	0.099	0.018
29	0.146	0.038
30	0.215	0.066
31	0.121	0.031
32	0.859	0.399

Note: Left and right ends refer to the directions looking at the outside face of Panel B.

TABLE 6.13

VERTICAL DISPLACEMENT PROFILES FOR OUT-OF-PLANE WALLS OF HOUSE 1

		WALL W4			WALL W2		
Channel No.		40	46	61	37	52	58
Test No.	Max. Horiz. Acc. g	Disp.-TC in.	Disp.-MC in.	Disp.-BC in.	Disp.-TC in.	Disp.-MC in.	Disp.-BC in.
1	T-0.002	0.002	0.001	0.002	0.002	0.001	0.000
2	T-0.026	0.003	0.001	0.002	0.003	0.003	0.000
3	T-0.050	0.003	0.001	0.002	0.003	0.003	0.001
4	T-0.066	0.009	0.004	0.003	0.010	0.008	0.002
5	T-0.089	0.016	0.009	0.004	0.017	0.011	0.004
6	T-0.122	0.026	0.01[illegible]	0.006	0.027	0.020	0.007
7	T-0.147	0.043	0.030	0.011	0.052	0.033	0.013
8	T-0.190	0.072	0.047	0.021	0.071	0.051	0.020
9	T-0.214	0.184	0.125	0.055	0.186	0.128	0.054
10	T-0.269	0.427	0.282	0.129	0.423	0.280	0.124
11	T-0.285	0.395	0.264	0.123	0.403	0.253	0.117
12	E-0.140	0.081	0.051	0.020	0.080	0.054	0.022
13	E-0.282	0.275	0.180	0.079	0.282	0.185	0.082
14	T-0.051	0.011	0.009	0.006	0.017	0.009	0.004
15	T-0.062	0.013	0.010	0.006	0.012	0.010	0.005
16	T-0.092	0.018	0.014	0.009	0.021	0.016	0.008
17	T-0.119	0.026	0.020	0.011	0.031	0.025	0.012
18	T-0.193	0.046	0.035	0.019	0.050	0.043	0.021
19	T-0.248	0.067	0.065	0.031	0.078	0.057	0.028
20	E-0.209	0.129	0.253	0.118	0.055	0.054	0.027
21	E-0.311	0.698	1.961	0.866	0.118	0.080	0.038
22	E-0.214	0.032	0.018	0.009	0.065	0.057	0.028
23	E-0.323	0.059	0.037	0.016	0.108	0.091	0.044
24	E-0.455	0.093	0.062	0.028	0.154	0.125	0.061
25	P-0.247	0.056	0.035	0.016	0.079	0.063	0.030
26	P-0.386	0.093	0.061	0.025	0.134	0.094	0.046
27	P-0.492	0.172	0.113	0.052	0.225	0.160	0.076
28	P-0.627	0.751	0.513	0.239	0.721	0.487	0.229
29	E-0.592	0.659	1.095	0.493	0.434	0.379	0.192

Note: 1) The channel numbers and locations are shown in Fig. 3.5

2) TC, MC, and BC refer to the top, middle and lower center of the wall.

TABLE 6.14

VERTICAL DISPLACEMENT PROFILES FOR OUT-OF-PLANE WALLS OF HOUSE 2

Channel Nos.		WALL A1							WALL B1				
		53	58	52	57	51	56	50	76	64	66	78	75
Test No.	Max.Horiz.Acc. g	Disp.-BC in.	Disp.-TL in	Disp.-ML in.	Disp.-TC in.	Disp.-MC in.	Disp.-TR in.	Disp.-MR in.	Disp.-TL in.	Disp.-ML in.	Disp.-BL in.	Disp.-TR in.	Disp.-MR in.
1	T-0.004	0.000	0.001	0.001	0.001	0.001	0.001	0.001	0.001	0.001	0.000	0.001	0.001
2	T-0.030	0.000	0.003	0.001	0.003	0.002	0.002	0.001	0.005	0.001	0.000	0.004	0.002
3	T-0.059	0.000	0.004	0.002	0.006	0.003	0.005	0.002	0.005	0.001	0.001	0.005	0.003
4	T-0.117	0.001	0.011	0.005	0.015	0.008	0.017	0.007	0.014	0.002	0.003	0.014	0.008
5	T-0.160	0.002	0.018	0.006	0.024	0.011	0.021	0.010	0.018	0.001	0.004	0.021	0.010
6	T-0.178	0.003	0.025	0.009	0.033	0.017	0.030	0.015	0.022	0.001	0.006	0.028	0.017
7	T-0.232	0.004	0.033	0.010	0.044	0.021	0.043	0.020	0.029	0.001	0.009	0.046	0.032
8	T-0.241	0.008	0.058	0.018	0.078	0.037	0.078	0.040	0.048	0.002	0.014	0.079	0.060
9	T-0.280	0.008	0.084	0.025	0.109	0.049	0.111	0.053	0.066	0.001	0.021	0.116	0.083
10	E-0.132	0.001	0.024	0.007	0.030	0.014	0.029	0.012	0.026	0.001	0.007	0.028	0.016
11	E-0.168	0.002	0.035	0.010	0.046	0.021	0.042	0.019	0.035	0.001	0.010	0.042	0.027
12	E-0.207	0.002	0.047	0.013	0.059	0.025	0.054	0.025	0.046	0.002	0.012	0.054	0.041
13	E-0.285	0.003	0.062	0.017	0.081	0.036	0.085	0.038	0.072	0.040	0.019	0.089	0.065
14	E-0.331	0.004	0.076	0.023	0.102	0.044	0.103	0.047	0.074	0.044	0.020	0.112	0.079
15	E-0.452	0.005	0.131	0.045	0.173	0.074	0.183	0.084	0.111	0.061	0.032	0.170	0.124
16	T-0.400	0.005	0.180	0.058	0.243	0.102	0.260	0.119	0.150	0.090	0.047	0.233	0.174
17	P-0.268	0.002	0.090	0.037	0.112	0.049	0.105	0.044	0.084	0.053	0.027	0.098	0.070
18	P-0.385	0.004	0.176	0.074	0.218	0.096	0.208	0.091	0.181	0.112	0.058	0.214	0.138
19	P-0.505	0.010	0.313	0.090	0.438	0.182	0.446	0.197	0.335	0.212	0.108	0.414	0. 79
20	T-0.059	0.000	0.009	0.004	0.010	0.005	0.010	0.004	0.010	0.001	0.002	0.009	0.007
21	T-0.076	0.001	0.012	0.006	0.017	0.008	0.020	0.010	0.012	0.001	0.003	0.020	0.016
22	T-0.119	0.002	0.023	0.011	0.046	0.015	0.037	0.020	0.021	0.001	0.006	0.040	0.030
23	T-0.156	0.004	0.037	0.014	0.048	0.023	0.061	0.031	0.034	0.000	0.011	0.065	0.049
24	T-0.188	0.005	0.047	0.019	0.067	0.031	0.079	0.041	0.050	0.001	0.014	0.082	0.061
25	T-0.227	0.009	0.072	0.028	0.106	0.047	0.124	0.063	0.071	0.001	0.021	0.127	0.095
26	T-0.262	0.054	0.139	0.063	0.196	0.111	0.242	0.163	0.143	0.001	0.043	0.244	0.179
27	E-0.140	0.024	0.058	0.029	0.077	0.050	0.084	0.059	0.052	0.001	0.015	0.082	0.059
28	E-0.212	0.044	0.115	0.056	0.133	0.092	0.153	0.109	0.105	0.003	0.030	0.151	0.110
29	E-0.304	0.062	0.161	0.077	0.208	0.136	0.239	0.162	0.162	0.100	0.049	0.228	0.163
30	E-0.370	0.097	0.238	0.110	0.309	0.197	0.350	0.239	0.232	0.147	0.071	0.331	0.241
31	P-0.258	0.062	0.146	0.069	0.194	0.125	0.229	0.158	0.146	0.089	0.044	0.219	0.167
32	P-0.519	0.893	3.072	3.019	3.026	2.912	2.794	1.903	3.043	2.048	0.840	2.772	1.621

Notes: 1) The channel numbers and locations are shown on Fig. 3.6

2) TC, MC and BC refer to the top, middle and lower center of the wall.

TABLE 6.15

PERFORMANCE OF UNREINFORCED OUT-OF-PLANE WALLS OF HOUSE 1

House and Tensile Stress of Subassemblage	Panel and/or Pier	State of Cracking	Test No.	Test Input	Deflection at Top of Cracked Wall in.	Deflection at 2/3 Height of Cracked Wall in.	Tensile Stress at Crack Location psi	Description of Crack	Comments
House 1 53 psi from diagonal compression test	W4 8' Wide Load Bearing	Before Cracking	11	T-0.29 g	0.40	0.26	20 at mid-height	At first joint above footing.	This crack is of no structural significance but is consistent with the assumption that the out-of-plane walls are hinged at their bases.
		At Cracking	13	E-0.28 g	0.28	0.18	25 at mid-height		
	W4 8' Wide Non-Load Bearing	At Cracking	19	T-0.25 g	0.07	0.07	11	At 6th course, 24" from the top.	The maximum tensile stress prior to cracking was 13 psi in Test 13. W4 was repaired over the full height of the wall after Test 21. The top deflections are less in this series of tests as the footings were bolted after Test 13.
		After Cracking	20 21	T-0.21 g E-0.31 g	0.13 0.70	0.25 1.96	N/A		
	W4 8' Wide Non-Load Bearing Repaired	Before Cracking	24	E-0.46 g	0.09	0.06	N/A	At 6th course, 24" from the top.	Because the strength properties of the repair material were not determined stresses corresponding are not applicable.
		At Cracking	27	P-0.49 g	0.17	0.11	N/A		
		After Cracking	28 29	P-0.63 g E-0.59 g	0.75 0.66	0.51 1.10	N/A		

Note: T, E and P in column five refer to the Taft, El Centro and Pacoima earthquake motions, respectively.

TABLE 6.16

PERFORMANCE OF UNREINFORCED OUT-OF-PLANE WALLS OF HOUSE 2

House and Tensile Stress of Subassemblage	Panel and/or Pier	State of Cracking	Test No.	Test Input	Deflection at Top of Cracked Wall in.	Deflection at 2/3 Height of Cracked Wall in.	Tensile Stress at Crack Location psi	Description of Crack	Comments
House 2 147 psi from diagonal compression test	4'-8" Pier of A1 Non-Load Bearing	Before Cracking	13	E-0.29 g	0.09	0.04	18	At 11th course from footing at the level of the bottom of the window	There were pre-existing cracks at the top of the small pier on the left of the window. The displacements of this pier were similar to those measured for the 4'-8" pier. Crack was not repaired.
		At Cracking	14	E-0.33 g	0.10	0.05	20		
		After Cracking	15	E-0.45 g	0.18	0.08			
			16	T-0.40 g	0.26	0.12	N/A		
			19	P-0.51 g	0.45	0.20			
	4'-8" Pier of A1 Load Bearing	After Cracking as original was not repaired	26	T-0.26 g	0.24	0.16		At 11th course from footing	The large deflections that occurred during Test 32 are attributed to the in-plane failure of wall A.
			30	E-0.37 g	0.35	0.24	N/A		
			32	P-0.52 g	2.80	1.90			

Note: T, E and P in column five refer to the Taft, El Centro and Pacoima earthquake motions, respectively.

TABLE 6.17

PERFORMANCE OF UNREINFORCED IN-PLANE WALLS OF HOUSE 1

House and Tensile Stress of Subassemblage	Panel and/or Pier	State of Cracking	Test No.	Test Input	Deflection at Top of Wall in.	Net Shear Stress on Panel psi	Tensile Stress at Crack Location psi	Description of Crack	Comments
House 1 53 psi from diagonal compression test	W3 Non-Load Bearing	Before Cracking	8	T-0.19 g	0.06	6	29 2'-8" from footing 42 at the footing	Along joint 2'-8" above the footing	During Test 10 slight crushing occurred at the ends of the cracked joint but no permanent displacement occurred. Slip along this joint was mechanically prevented after Test 10
		At Cracking	9	T-0.21 g	0.14	9	42		
		After Cracking	10	T-0.27 g	0.40	9	N/A		
	W3 Non-Load Bearing (Slip prevented at cracked joint)	At Cracking	11	T-0.29 g	0.30	11	64	Along joint 8" above the footing	No significant permanent displacement occurred during Tests 12 and 13. Additional cracks formed at the 5th and 6th joints from the footing during Test 13. The wall was repaired and the roof rotated after Test 13.
		After Cracking	12	E-0.14 g	0.07	5	N/A		
			13	E-0.28 g	0.28	11	N/A		
	W3 Load Bearing and Repaired	At Cracking	27	P-0.49 g	0.11	22	N/A	Along joint 8" above the footing	No permanent displacement occurred during Tests 28 and 29 although crushing was evident at the ends of the walls. Strength properties were not available for the repair material.
		After Cracking	28	P-0.63 g	0.70	29	N/A		
			29	E-0.59 g	0.37	25	N/A		

Note: T, E and P in column five refer to the Taft, El Centro and Pacoima earthquake motions, respectively.

TABLE 6.18

PERFORMANCE OF UNREINFORCED IN-PLANE WALLS OF HOUSE 2

House and Tensile Stress of Subassemblage	Panel and/or Pier	State of Cracking	Test No.	Test Input	Deflection at Top of Wall in.	Net Shear Stress on Panel psi	Tensile Stress at Crack Location psi	Description of Crack	Comments
House 2 147 psi from diagonal compression test	6' Pier of Panel A Load Bearing	Before Cracking	19	P-0.51 g	0.05	35	220 Cant. 65 F.E.	No crack formed	Roof was rotated after this test.
	6' Pier of Panel A Non-Load Bearing	Before Cracking	30	E-0.37 g	0.07	29	Max. Stress as for Test 19	Diagonal from reentrant corner	There was a one inch permanent displacement in panel after Test 32 and no further tests were performed
		At Cracking	32	P-0.52 g	1.12	29	195 Cant. 69 F.E.		
	6' Pier of Panel B Load Bearing	At and After Cracking	15 16 19	E-0.45 g T-0.40 g P-0.51 g	R=0.04 L=0.13 R=0.07 L=0.21 R=0.28 L=0.40	26 26 35	N/A	None identified	No cracks were identified but were assumed to exist. No permanent displacements occurred for the tests given.
	6' Pier of Panel B Non-Load Bearing		26 30 32	T-0.26 g E-0.37 g P-0.52 g	R=0.16 L=0.25 R=0.35 L=0.31 R=1.07 L=1.06	16 24 29	N/A	None identified	No permanent displacements occurred for the test results given.

Notes: (1) R in column six refers to the deflection to the right in Panel B looking at the exterior face of the panel

(2) L refers to the deflection to the left

(3) Cant. is the tensile stress calculated on the assumption that the pier is a cantilever, whereas F.E. refers to the condition of rotational fixity at the top and bottom of the pier.

(4) T, E and P in column five refer to the Taft, El Centro and Pacoima earthquake motions, respectively.

TABLE 6.19

FORCES ON CONNECTIONS IN HOUSES 1 AND 2

Connection Type	House	Test No. Test Input	Total Force lb	Force per Unit Length[1] lb/ft	Force per Bolt[2] lb	Force per Truss[3] lb
In-Plane Load Bearing	1	Test 28 E-0.59 g	9930	620	1985	1105
	2	Test 19 P-0.51 g	9125	570	1825	1015
In-Plane Non-Load Bearing	1	Test 13 E-0.28 g	4575	285	915	N/A
	2	Test 32 P-0.52 g	7580	475	1515	N/A
Out-Of-Plane Load Bearing	1	Test 13 E-0.28 g	410	25	80	35
	2	Test 32 P-0.52 g	1035	65	205	115
Out-Of-Plane Non-Load Bearing	1	Test 28 E-0.59 g	1305	80	260	N/A
	2	Test 19 P-0.51 g	1345	85	270	N/A

Notes: (1) The length of the connections was 16 ft

(2) The number of bolts was 5

(3) The number of trusses was 9

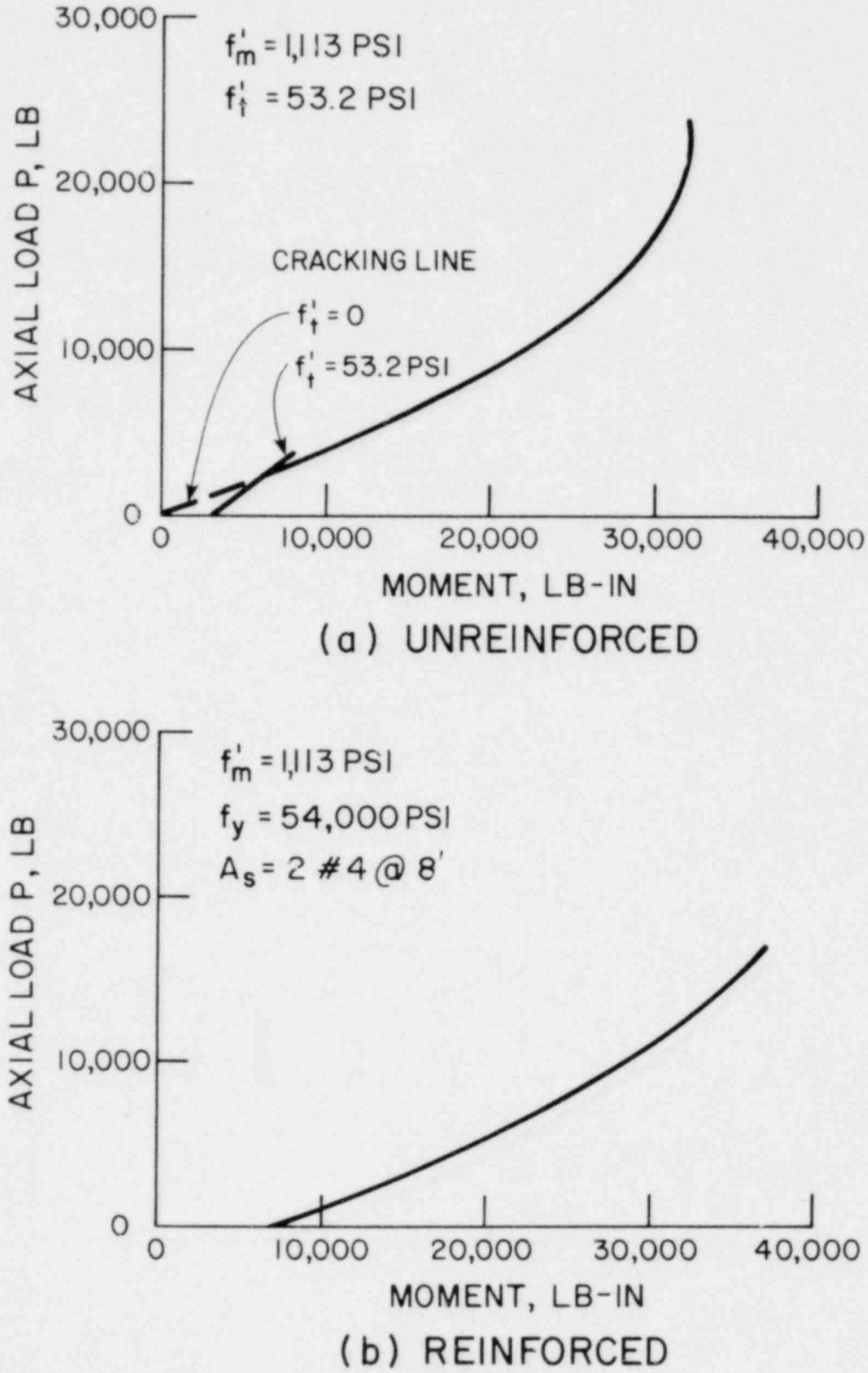

FIGURE 6.1 INTERACTION DIAGRAMS FOR OUT-OF-PLANE WALLS OF HOUSE 1

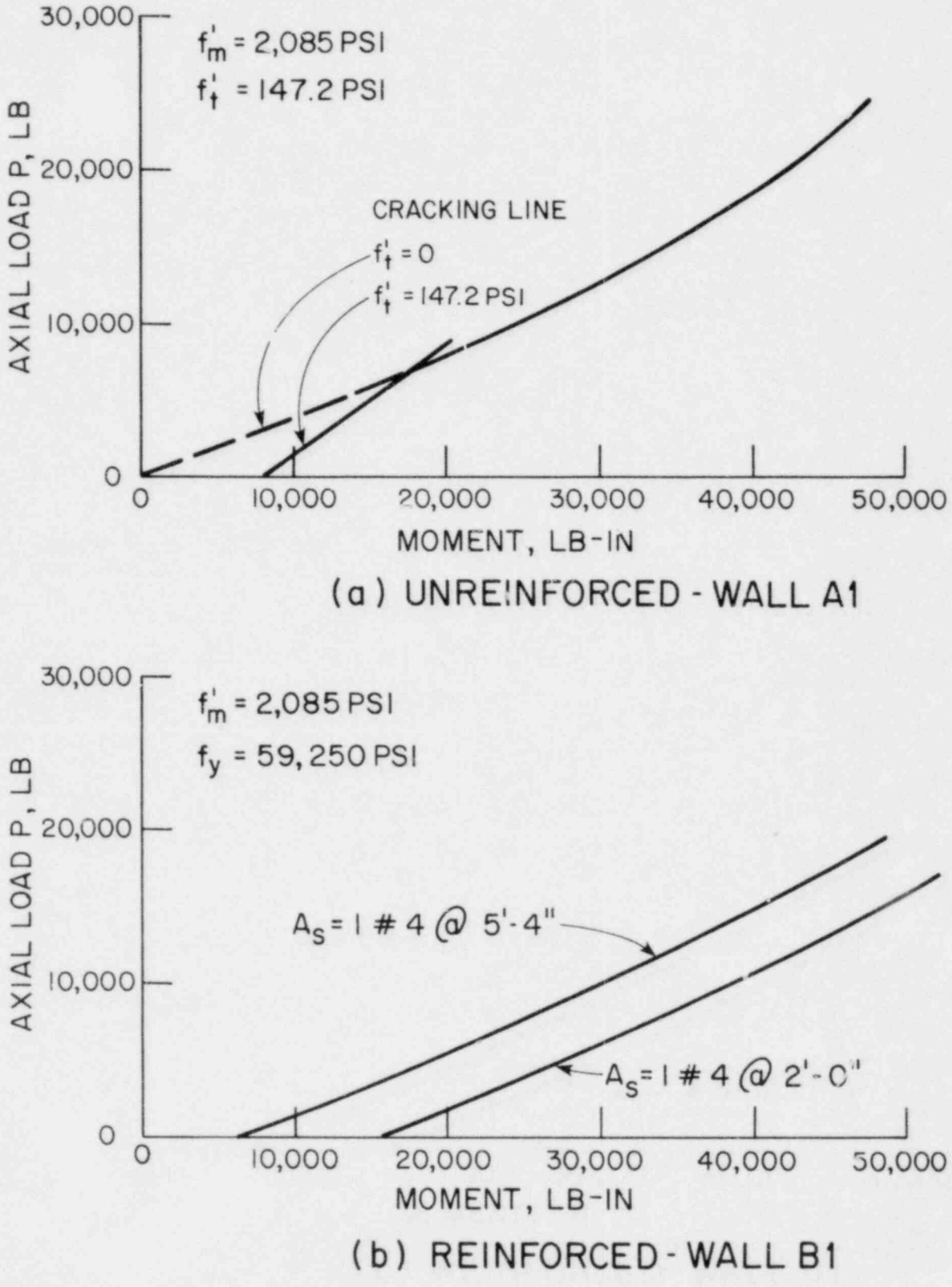

FIGURE 6.2 INTERACTION DIAGRAMS FOR OUT-OF-PLANE WALLS OF HOUSE 2

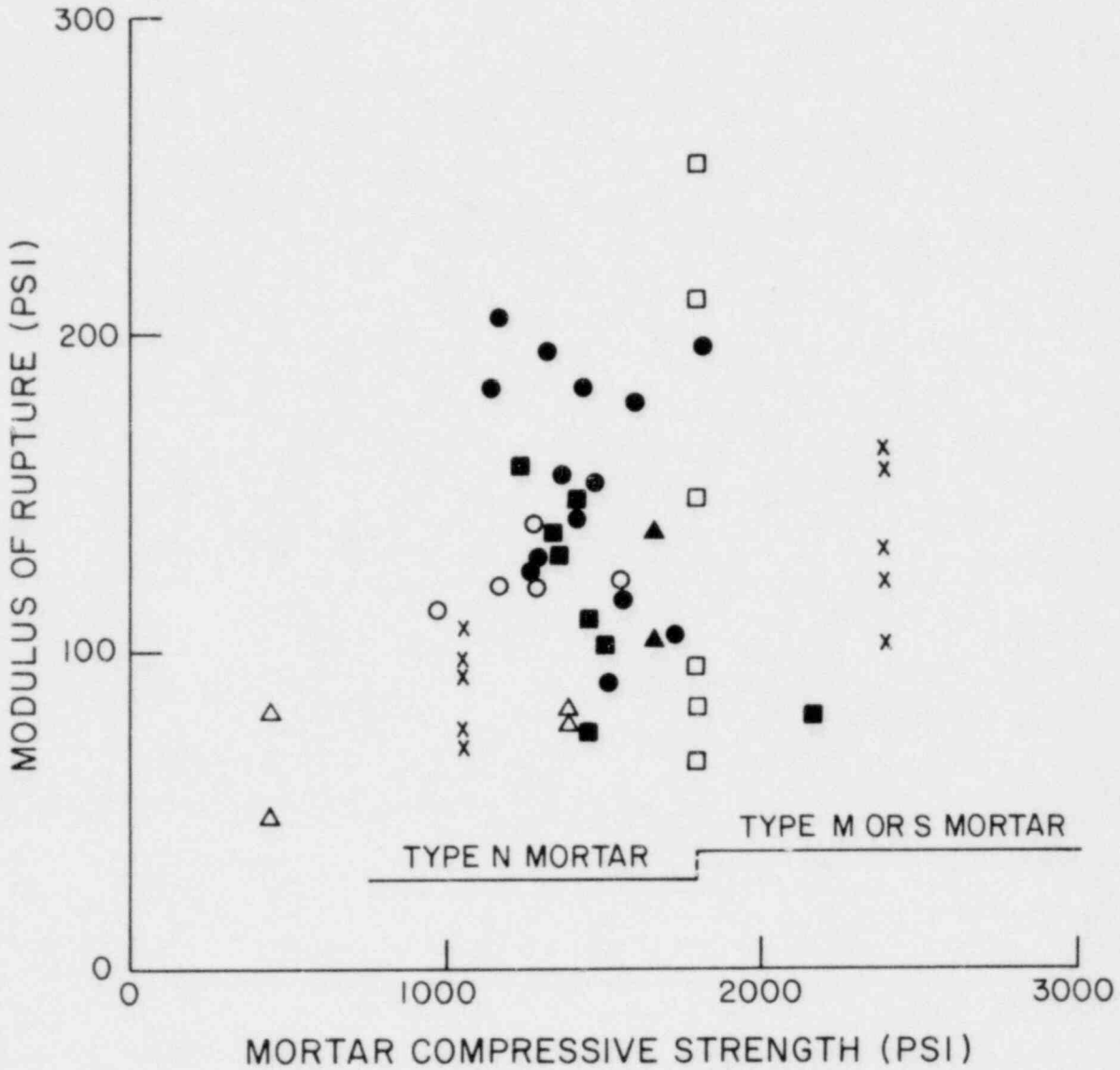

FIGURE 6.3 COMPARISON OF EXPERIMENTAL AND CODE MODULUS OF RUPTURE VALUES FOR CLAY BRICK

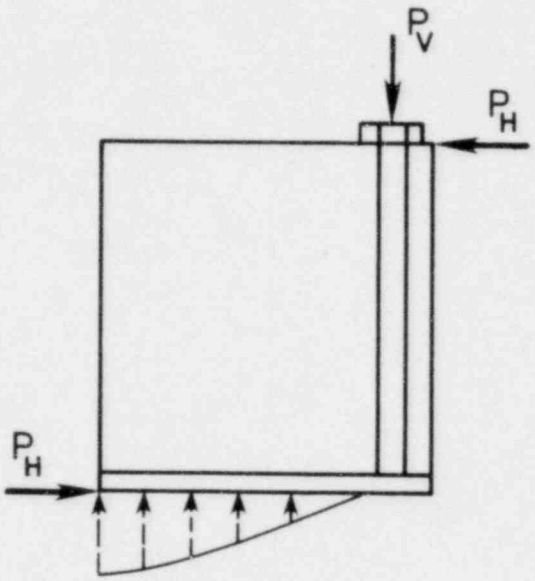

EXTERNAL HOLD DOWN

FIGURE 6.4

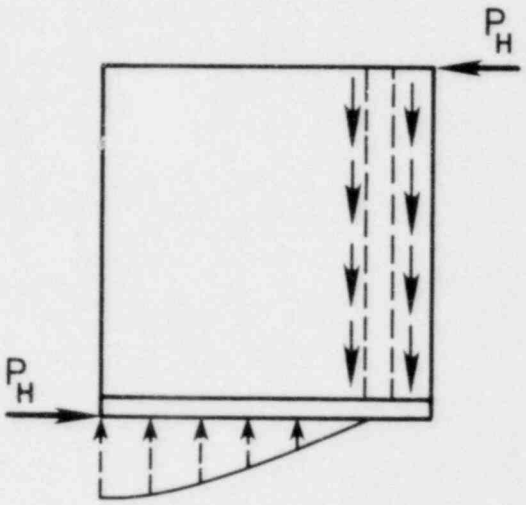

INTERNAL HOLD DOWN

FIGURE 6.5

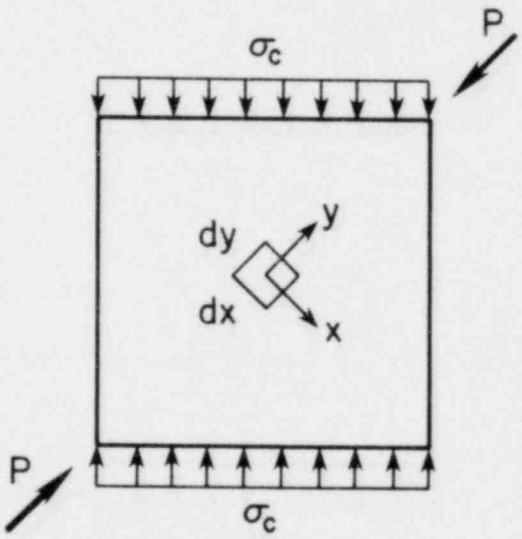

RACKING PANEL WITH EDGE LOAD

FIGURE 6.6

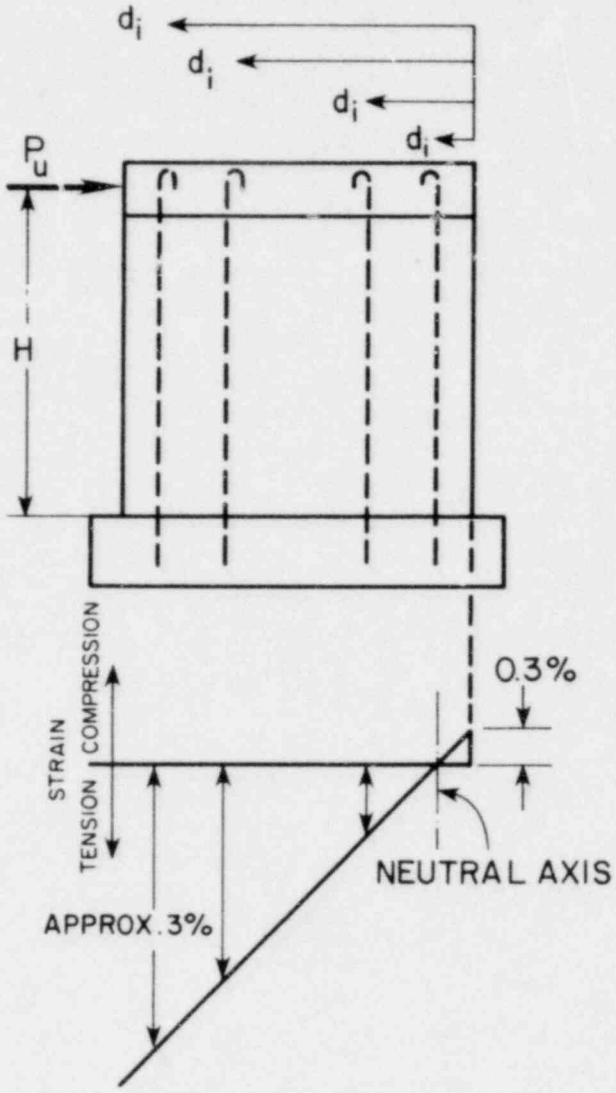

FIGURE 6.7 ASSUMED STRAIN DISTRIBUTION
FOR REINFORCED IN-PLANE WALLS

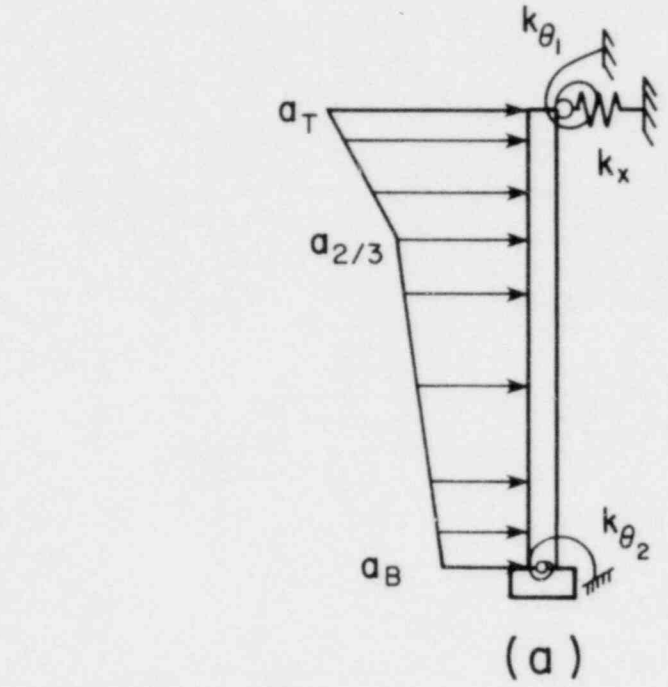

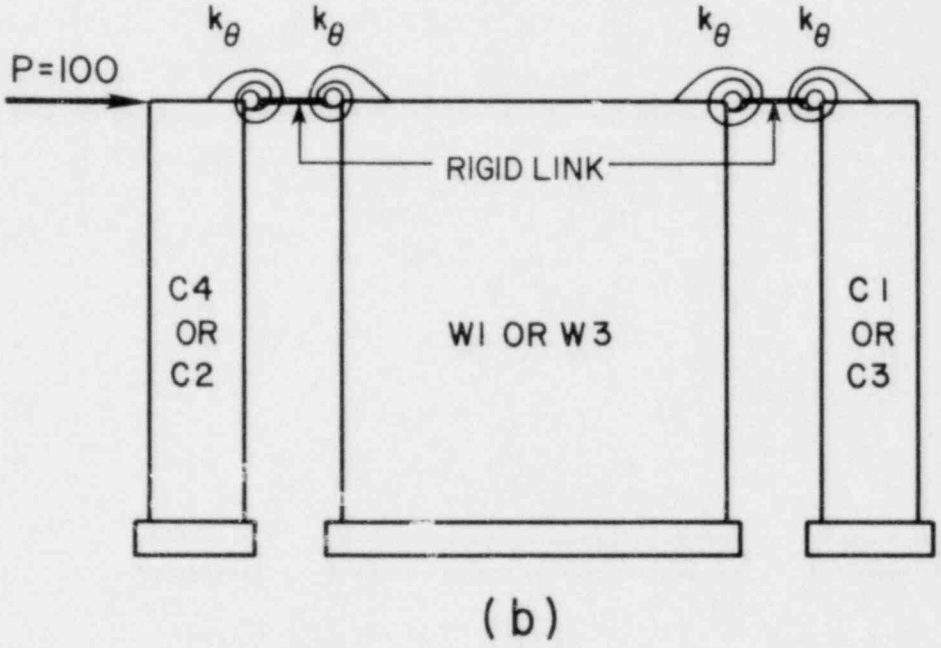

FIGURE 6.8 ANALYTICAL WALL MODELS FOR HOUSE 1

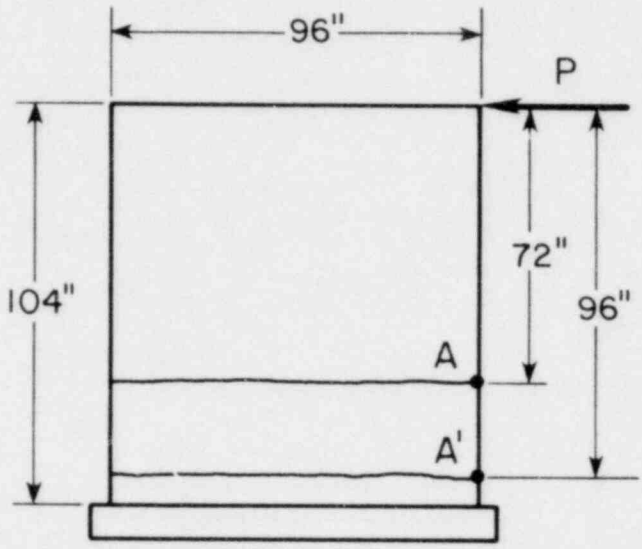

FIGURE 6.9 CRACK LOCATIONS IN WALL W3 OF HOUSE 1

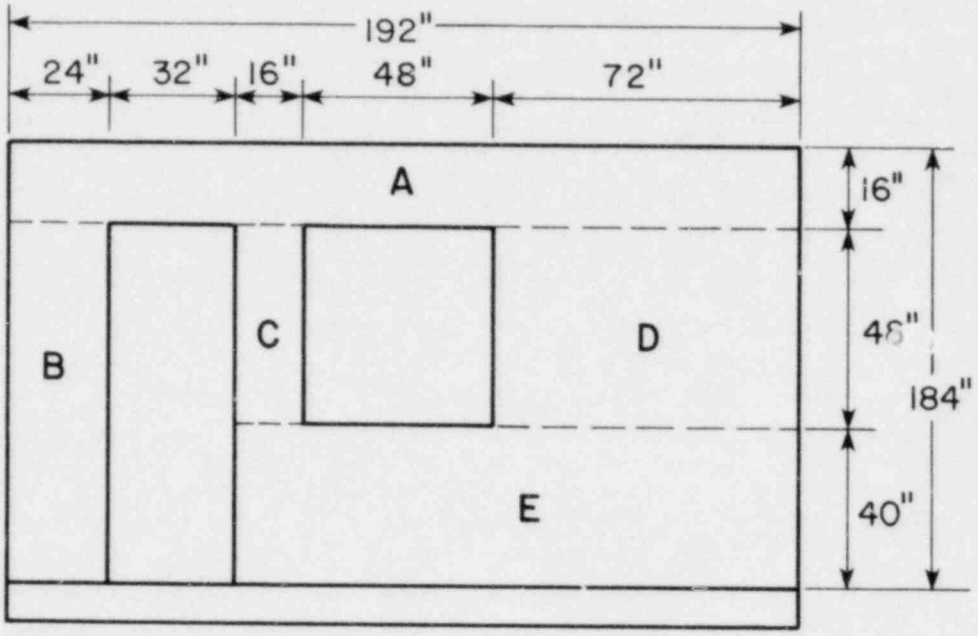

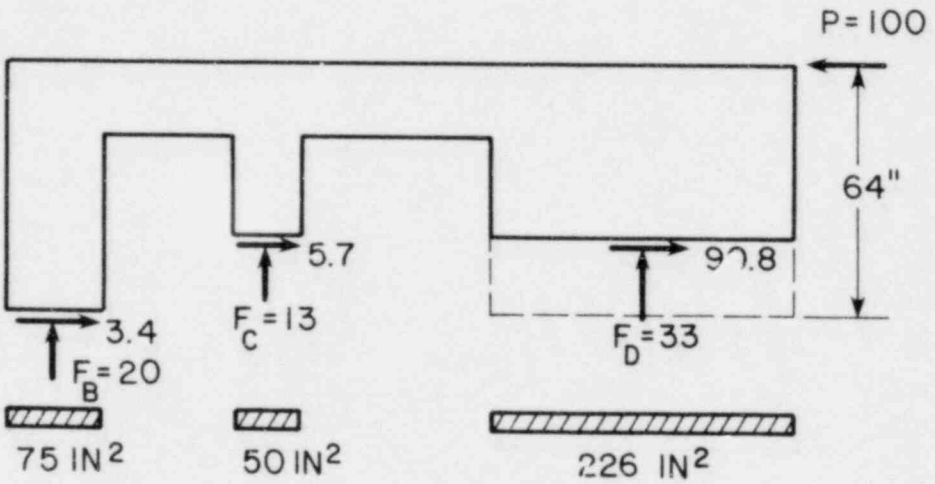

FIGURE 6.10 FORCE DISTRIBUTION IN WALL A OF HOUSE 2

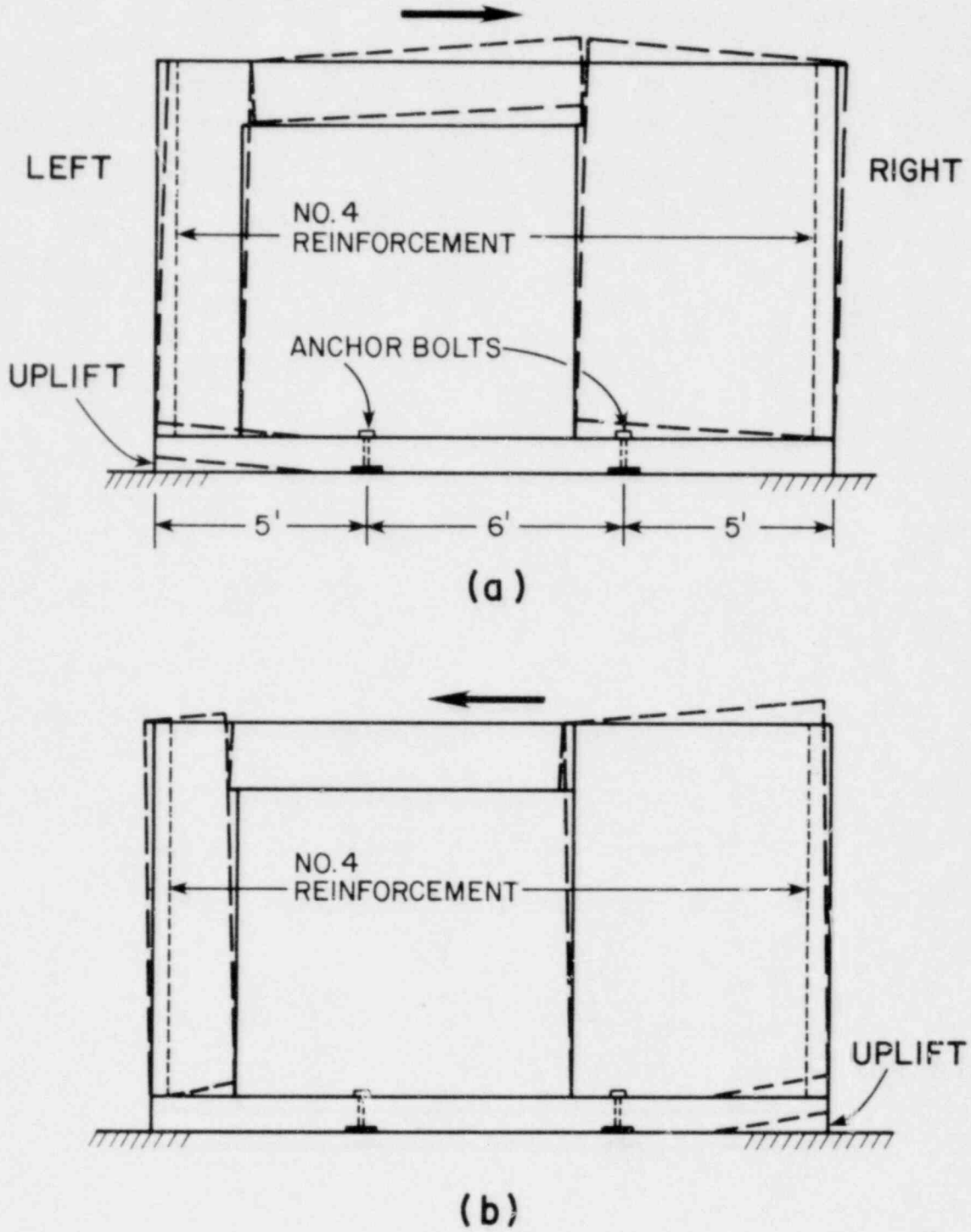

FIGURE 6.11 DEFORMED SHAPE OF WALL B FOR HOUSE 2

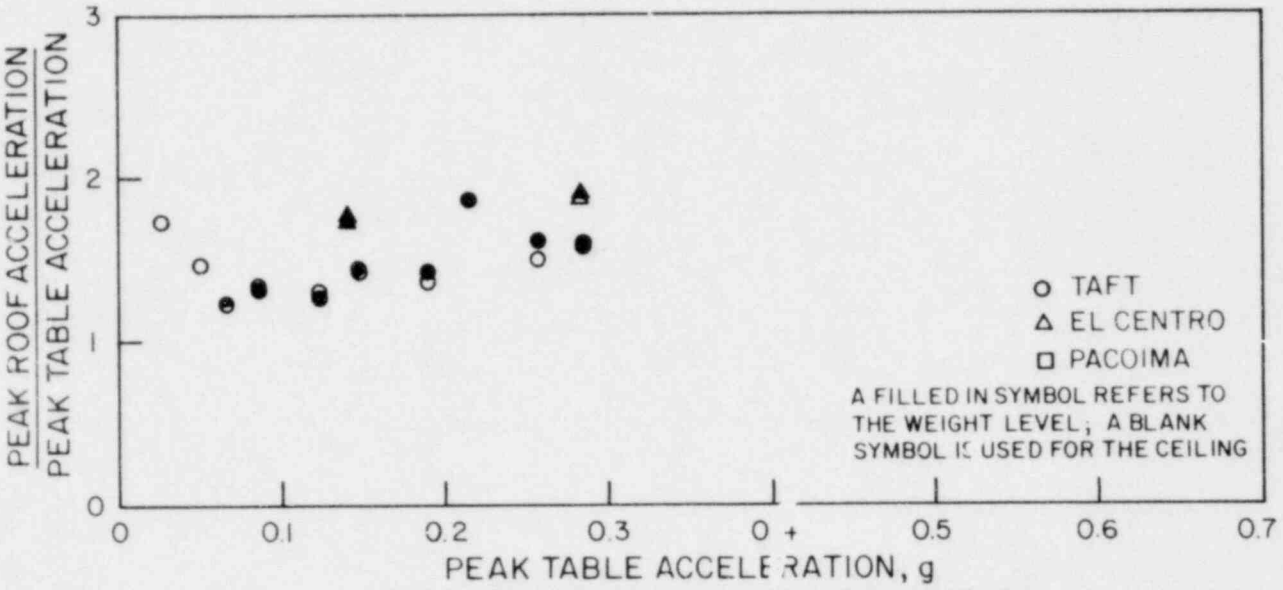

(a) TRUSSES PARALLEL TO MOTION

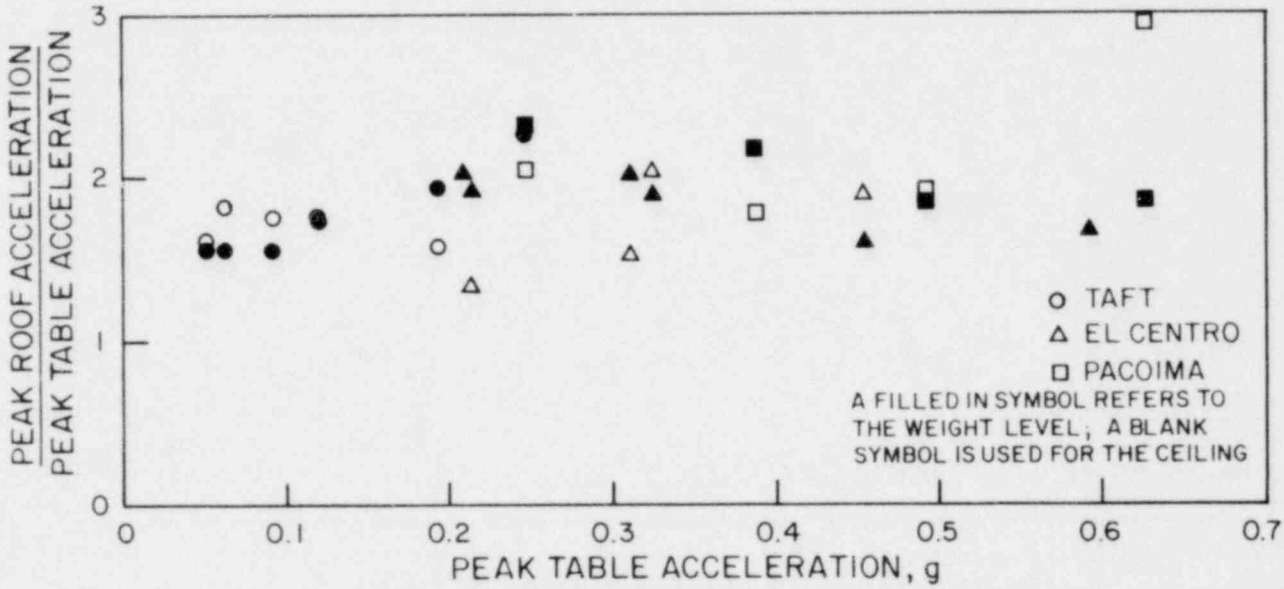

(b) TRUSSES TRANSVERSE TO MOTION

FIGURE 6.12 ROOF AMPLIFICATION FACTORS FOR HOUSE 1

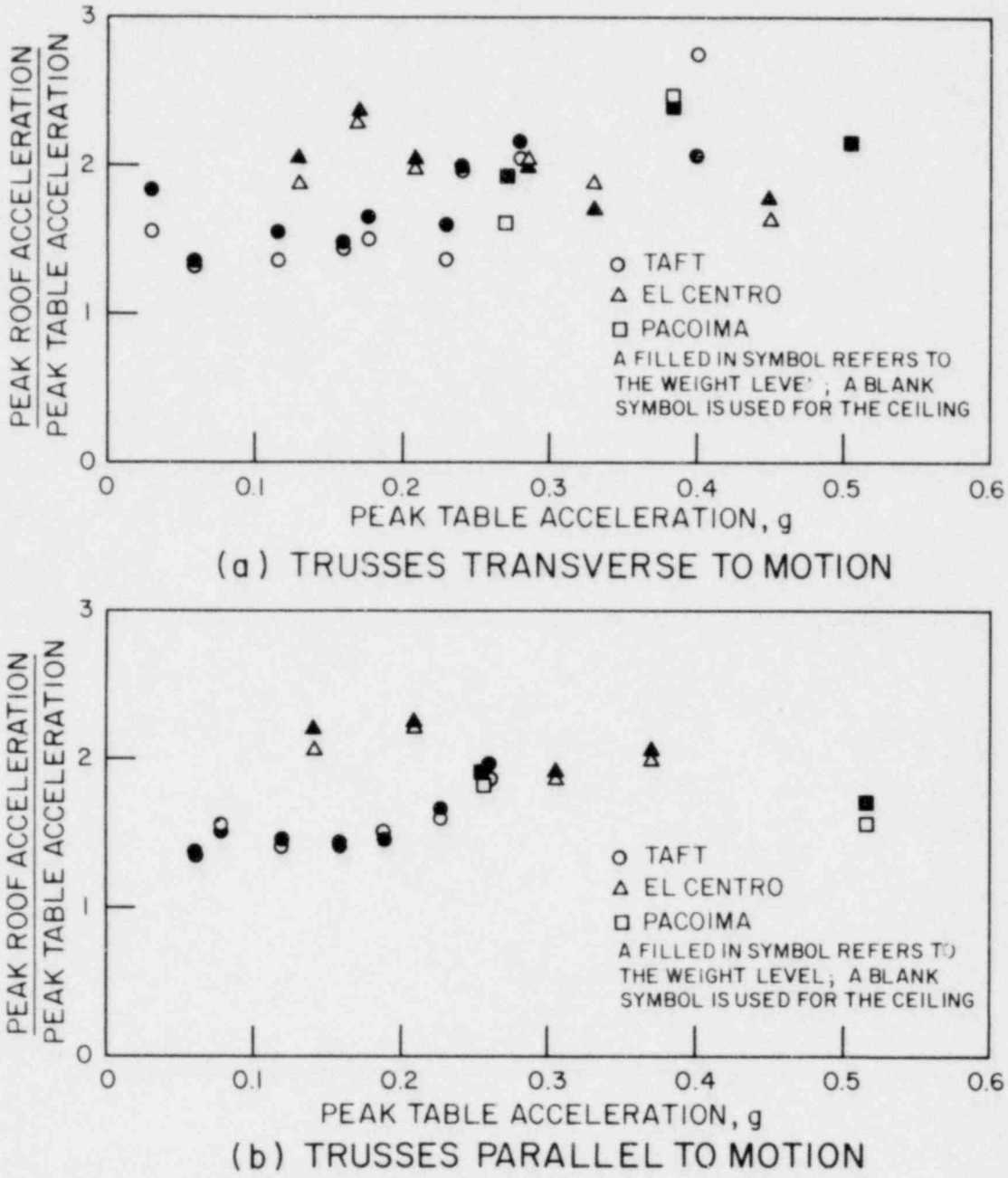

FIGURE 6.13 ROOF AMPLIFICATION FACTORS FOR HOUSE 2

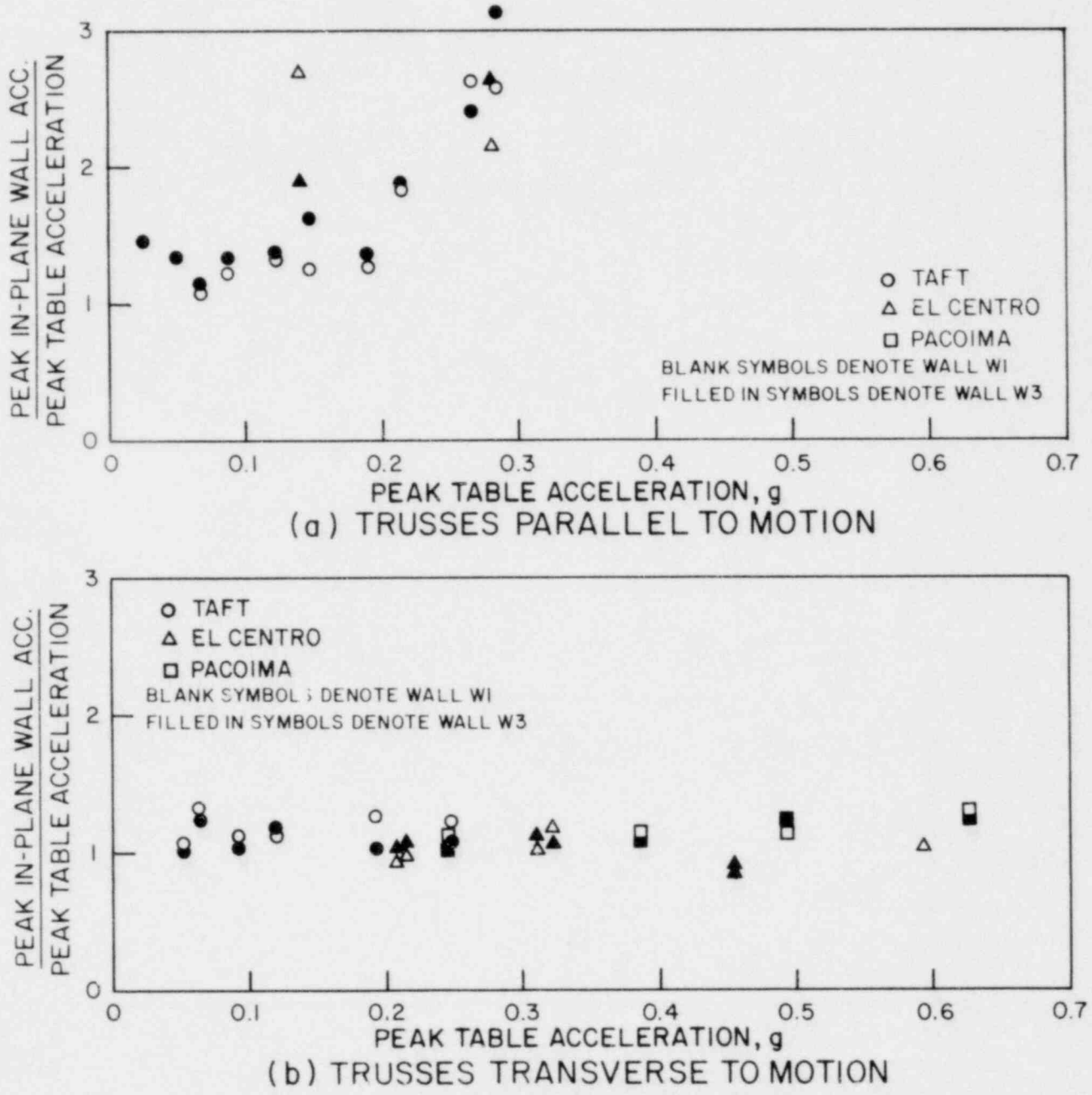

FIGURE 6.14 IN-PLANE WALL AMPLIFICATION FACTORS FOR HOUSE 1

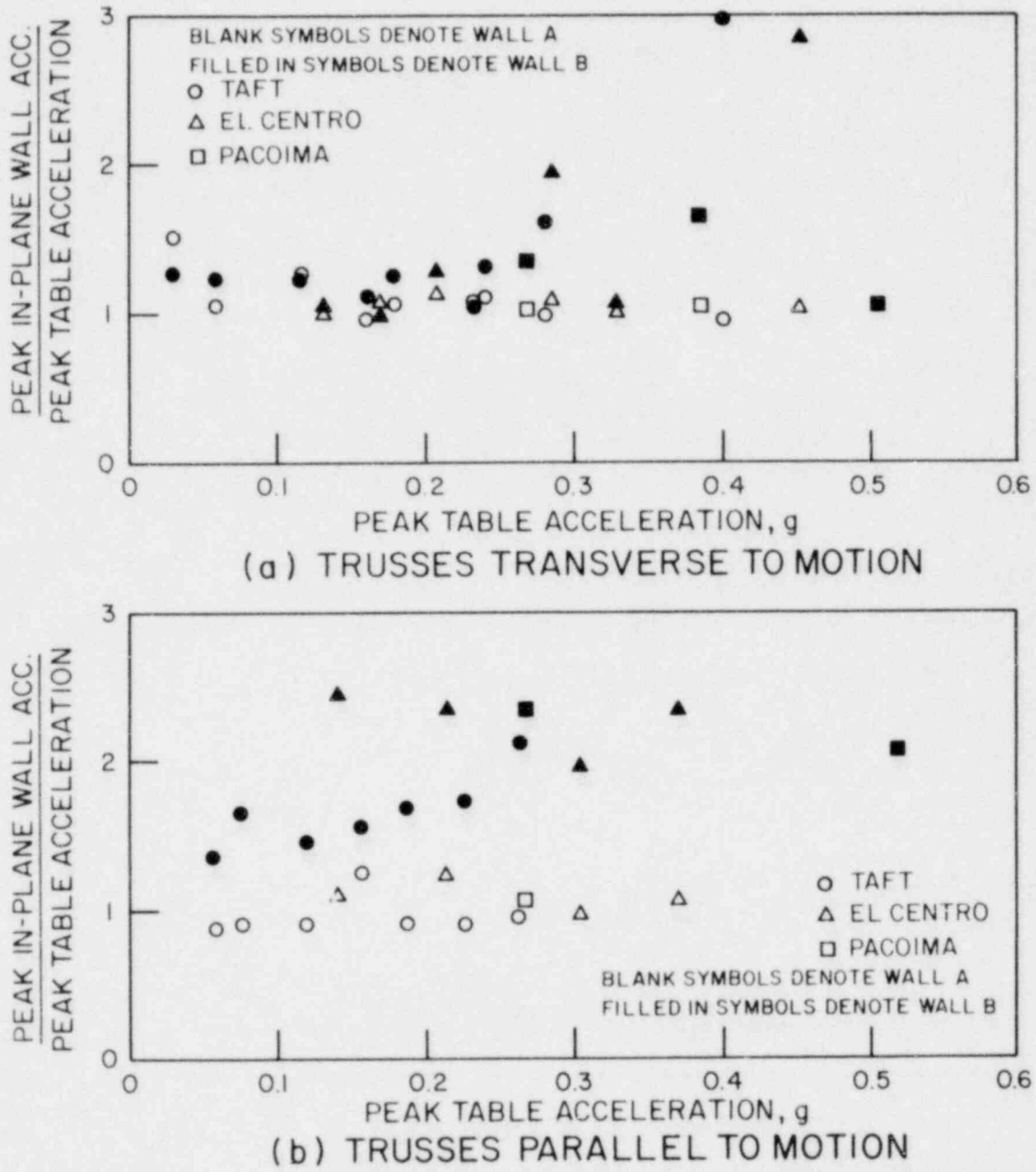

FIGURE 6.15 IN-PLANE WALL AMPLIFICATION FACTORS FOR HOUSE 2

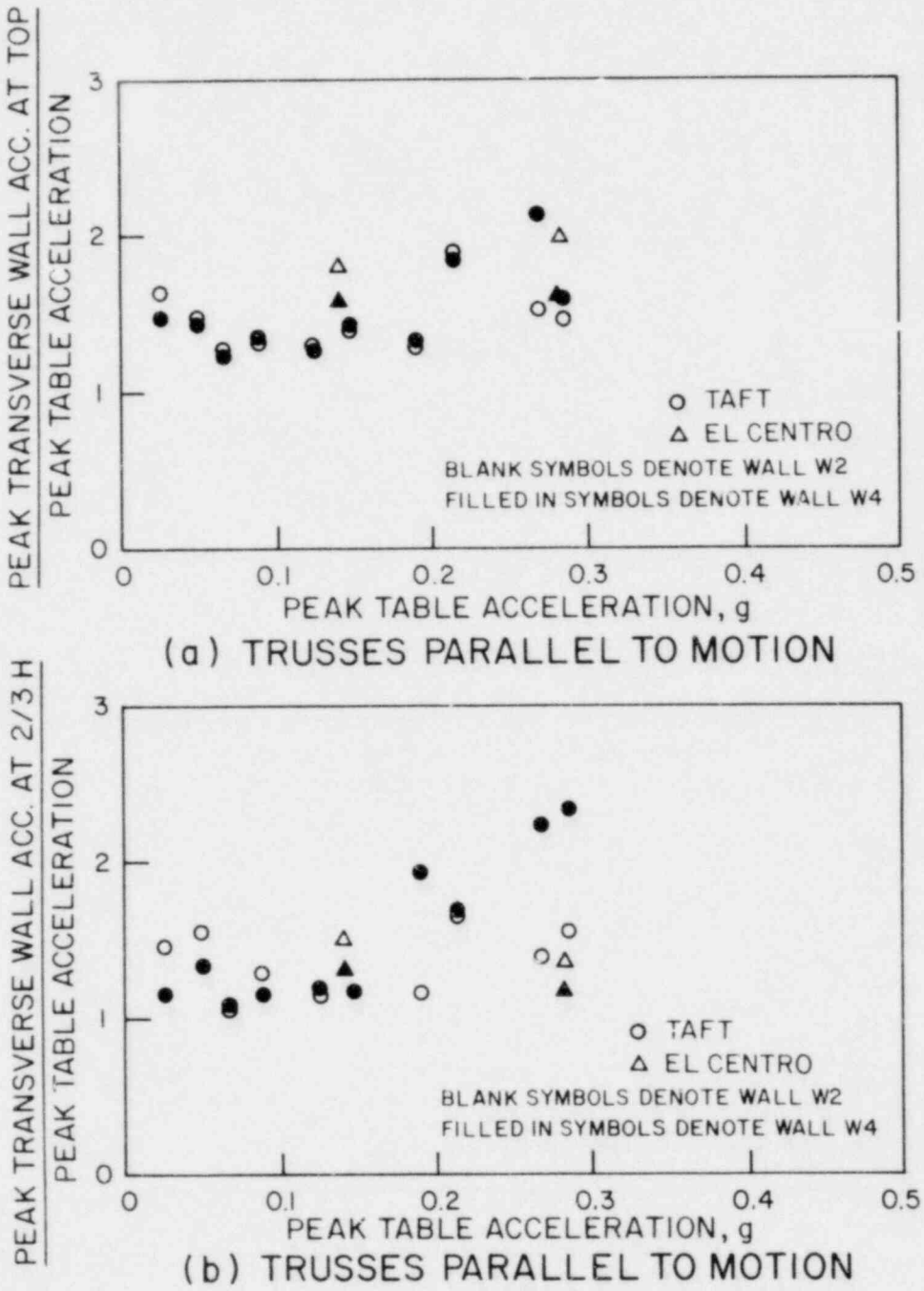

FIGURE 6.16 OUT-OF-PLANE WALL AMPLIFICATION FACTORS FOR HOUSE 1

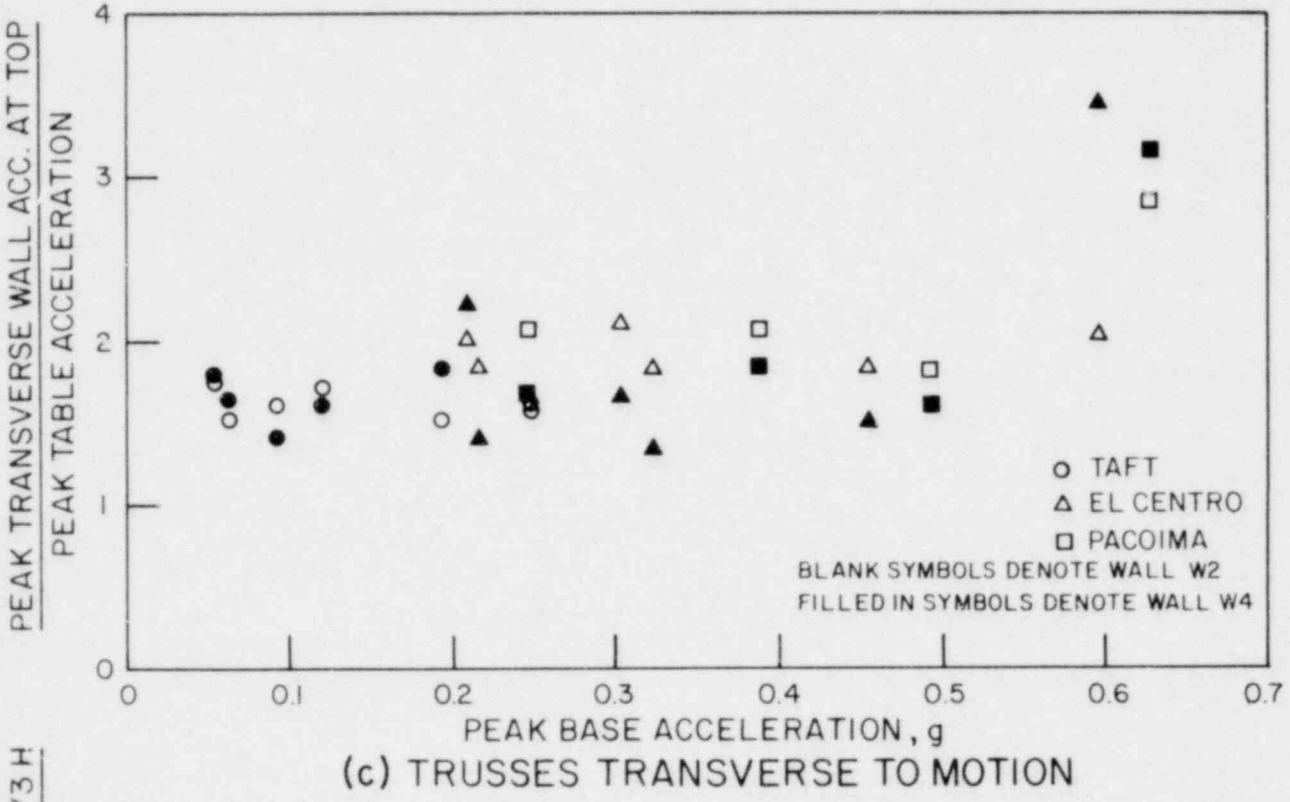

(c) TRUSSES TRANSVERSE TO MOTION

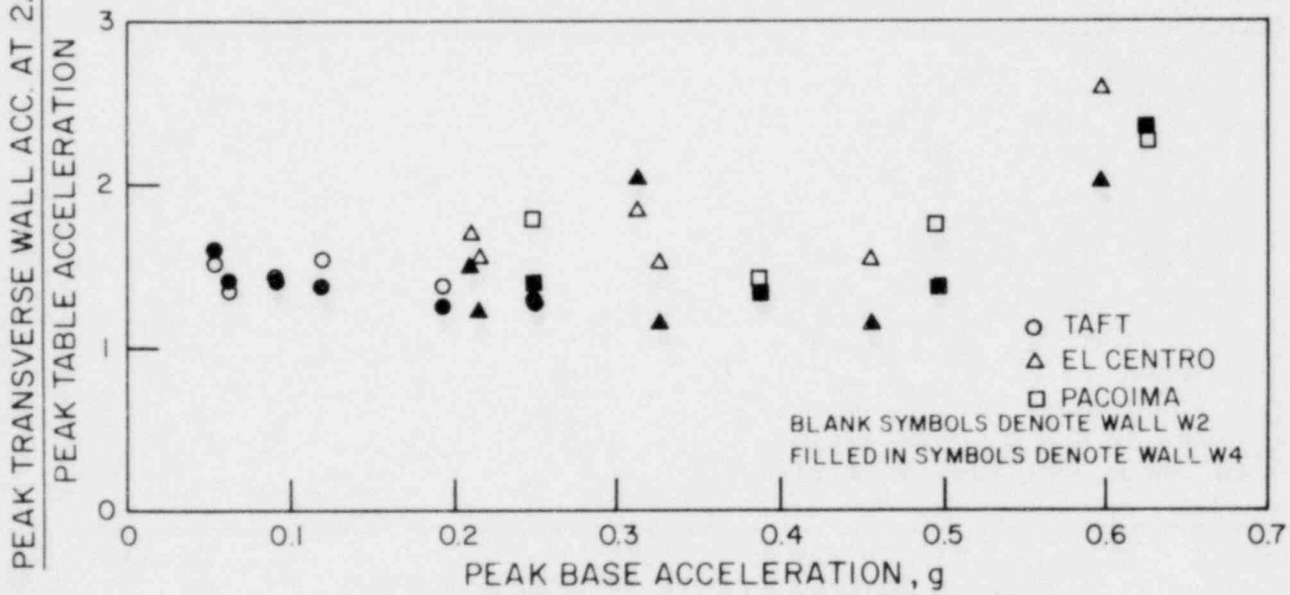

(d) TRUSSES TRANSVERSE TO MOTION

FIGURE 6.16 (CONT.) OUT-OF-PLANE WALL AMPLIFICATION FACTORS FOR HOUSE 1

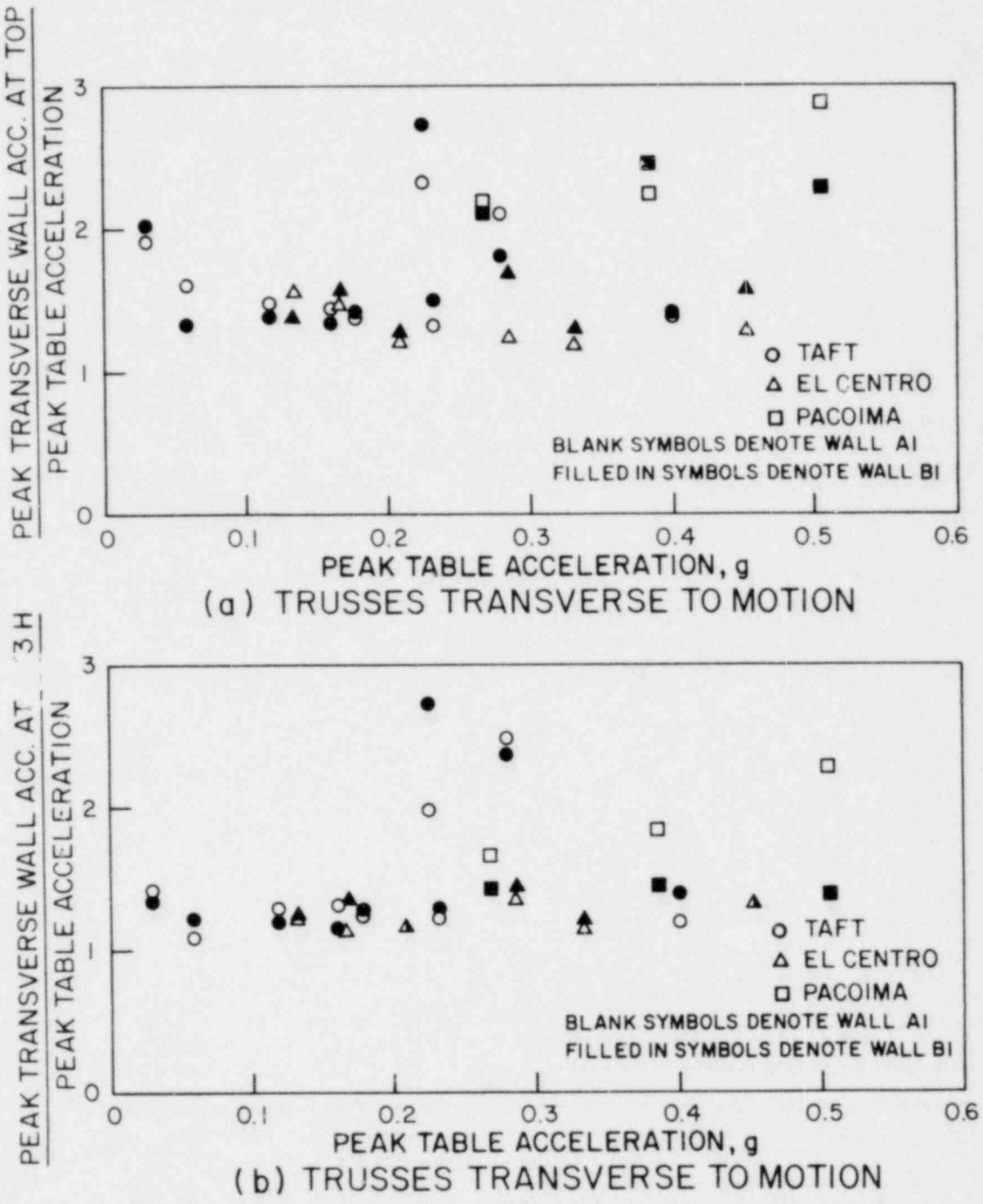

FIGURE 6.17 OUT-OF-PLANE WALL AMPLIFICATION FACTORS FOR HOUSE 2

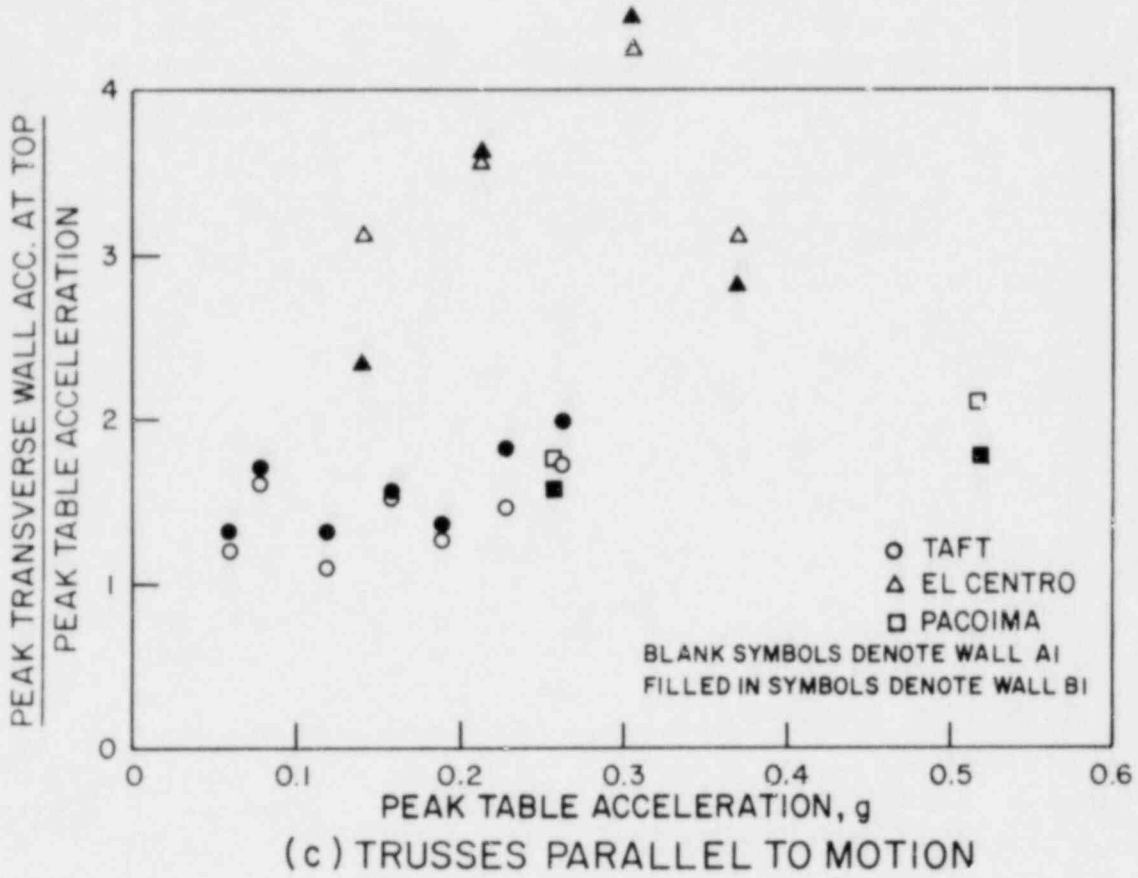

(c) TRUSSES PARALLEL TO MOTION

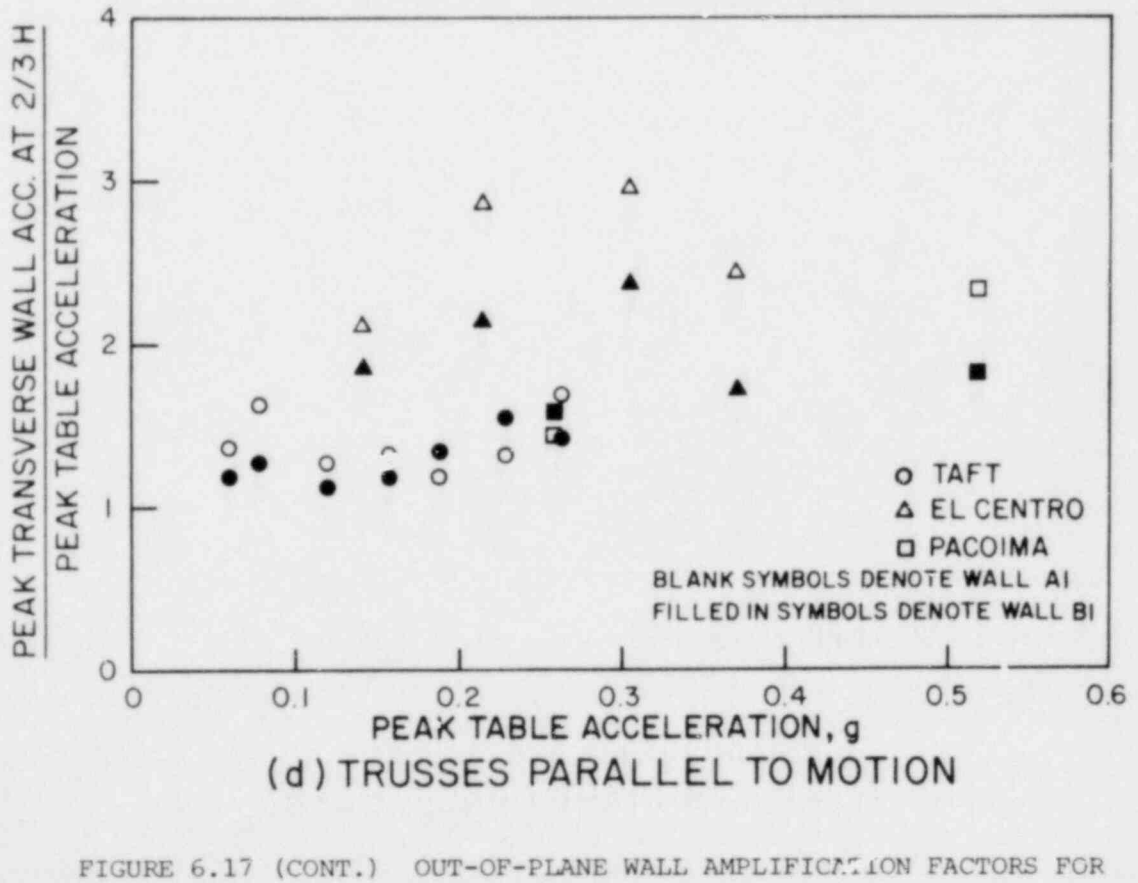

(d) TRUSSES PARALLEL TO MOTION

FIGURE 6.17 (CONT.) OUT-OF-PLANE WALL AMPLIFICATION FACTORS FOR HOUSE 2

7. SUMMARY AND CONCLUSIONS

The ultimate objective of this investigation is the establishment of minimum reinforcement requirements for single-story masonry dwellings for Seismic Zone 2 conditions. The experimental program was planned to make the test conditions as close to field conditions as possible: full-scale components of masonry structures were constructed from commercially available masonry units and were tied together using a small but typical roofing system. The addition of concrete slabs to the roof structure provided a reasonable approximation of both the dead load per foot of load bearing wall and the inertia load transferred to the in-plane shear walls. Because of the limited size of the shaking table, plan dimensions were scaled down by a factor of approximately 3; however to maintain realistic response conditions the height of walls was kept as 8 ft 8 in.

This report presents a detailed description of the experiments conducted on Houses 1 and 2 of the program as well as a detailed analysis of the test results. Similar treatment of the test results for Houses 3 and 4 and a summary of the program and the recommendations will be given in subsequent volumes. The experimental program and the most significant observations presented in this volume are summarized in the following paragraphs:

(1) Houses 1 and 2 were both constructed with 6 in. wide concrete masonry units and were 16 ft square in plan (Figs. 3.1 and 3.3). House 1 consisted of four 8 ft wide wall segments and four L-shaped corner units. None of these panels had openings in them. The four wall panels which formed House 2

were provided with openings simulating windows or doors. In each house walls with similar reinforcement (partial or unreinforced) were placed at right angles to each other so that under the action of a single horizontal component of simulated earthquake motion both out-of-plane and in-plane behavior would be recorded simultaneously. For both houses, the partially reinforced wall panels had one #4 bar grouted at each end of the panel.

(2) The response of the structures to the applied base motions was complex, and was affected by the direction in which the roof trusses were oriented, by base fixity conditions, by the geometry of the in-plane walls, and by pre-existing cracks and reinforcement.

(3) Three different earthquake motions were utilized in the test program (see Fig. 4.3), but the type of base motion applied to the structure appeared to have little effect on the response. Measurements indicated a strong correlation between the peak base accelerations and the recorded structure displacements.

(4) When the timber roof structure was oriented so that the in-plane walls were non-load bearing (trusses parallel to the motion) the displacements of the in-plane walls were consistently larger than when they were load bearing. These displacements were also significantly affected by the fixity of the footings; when the footings were free to uplift the displacements increased considerably.

(5) The surface bonding method of repair used in House 1 was quite effective: a repaired panel had to be subjected to significantly greater intensity base motions before cracking reoccurred.

(6) The roof-wall connection details used in the test specimens were adequate and no connection failures were observed in either house.

(7) Tensile stresses normal to the bed joint were calculated at critical locations, both before and at cracking,for both the in-plane and out-of-plane unreinforced walls. The variation in the calculated values was considerable but it was generally less when the tensile stresses were calculated at cracking in the out-of-plane walls.

(8) The observed cracking in both the unreinforced and partially reinforced in-plane walls of Houses 1 and 2 was caused by overturning moments. The net shear stresses on the piers reached a maximum value of 30 psi in House 1 and 35 psi in House 2; diagonal cracking associated with the shear mode of failure never occurred in the piers.

(9) The performance of the partially reinforced walls was clearly superior to that of the unreinforced walls; very satisfactory performance was obtained for both in-plane and out-of-plane partially reinforced walls even though several tests with peak accelerations above 0.5 g were included.

(10) Unreinforced walls generally were capable of resisting the unidirectional base motions in the cracked condition. The

unreinforced "cantilever type" in-plane walls tended to rock at the cracked section, whereas the unreinforced out-of-plane walls of House 1 tended to hinge at the crack location. The unreinforced in-plane wall of House 2 with the window and door opening was not tested after it cracked; the unreinforced out-of-plane wall of House 2 did not hinge after it cracked. This was attributed to the location of the crack.

(11) The roof level amplification factor, expressed in terms of the peak recorded acceleration divided by the peak base acceleration, appears to be independent of both the type and the intensity of the base motion. The acceleration measured at the concrete weight level was generally greater than that at the ceiling level and this difference generally increased when the roof trusses were oriented transverse to the table motion. Moreover, the amplification factors measured at the top of the in-plane walls were not identical to those obtained at the center of the roof level.

(12) For both Houses 1 and 2 the range of the amplification factors measured at the center of the roof was greater for the roof trusses oriented transverse to the table motion (in-plane walls load bearing); this is a reflection of the greater flexibility of the roof system with this orientation. The range of the roof amplification factors including both the ceiling and concrete weight levels was 1.3 to 2.4 for the transverse roof orientation of House 1 and 1.2 to 2.5 for House 2. For the roof orientation parallel to the table

motion the corresponding ranges of the amplification factors were 1.1 to 2.0 for House 1 and 1.3 to 2.3 for House 2.

(13) The amplification factor determined for the top of the in-plane walls was dependent on the fixity of the footings, on the in-plane flexibility of the walls, and on whether the walls were load or non-load bearing. The range of the amplification factors for all load bearing walls in Houses 1 and 2 was 0.9 to 1.5. For all non-load bearing walls in Houses 1 and 2 the range was 1 to 3.

(14) The amplification factors for the top and 2/3 wall height of the out-of-plane walls were related to the amplification factors for the top of the in-plane walls in corresponding tests, and also were influenced by the flexibility of the connection at the top of the out-of-plane walls. The amplification factor at the 2/3 wall height was generally slightly less than that at the top of the walls. At the top of the walls the range of the amplification factor for all non-load bearing out-of-plane walls was 1.2 to 3.5 and for all load bearing out-of-plane walls the range was 1 to 4.

(15) The out-of-plane unreinforced wall W4 in House 1 cracked at the 6th course from the top during Test 19 (T-0.25 g) when it was non-load bearing. During Test 21 (E-0.31 g) significant hinging occurred at the cracked joint and the displacement at 2/3 wall height was 2 in. During this test, the period of the cracked wall varied between 0.3 sec. and 0.5 sec. After the wall was repaired it cracked again at the same location during Test 27 (P-0.49 g) and significant

hinging occurred during Test 29 (E-0.59 g) although the maximum displacement was only 1 in.

(16) The out-of-plane unreinforced wall A1 of House 2 cracked in the 4 ft 8 in. pier at the mortar joint level with the bottom of the window, during Test 14 (E-0.33 g) when it was non-load bearing. No hinging effect was observed at the crack location during eighteen additional tests (both load bearing and non-load bearing). This lack of hinging is attributed to the crack location.

(17) For both houses the time history response of the unreinforced out-of-plane walls when it was uncracked was essentially a rigid body type response with the displacement time history essentially in phase with the base motion. When wall A1 of House 2 cracked no hinging was evident and the response was similar to the uncracked state. In the cracked state the period of vibration of wall W4 of House 1 varied between 0.3 sec. and 0.5 sec.; the wall was subjected to 15 half cycles of the longer period response with amplitude greater than 0.5 in. at the 2/3 wall height. The amplitude for three of these half cycles was greater than 1 in. An assessment of this hinging effect is obviously important; for House 1 the period of vibration of the cracked wall corresponded to the higher ordinates of the response spectrum for the El Centro base motion of Test 21 (see Fig. 4.3).

(18) The in-plane unreinforced wall W3 of House 1 first cracked along the mortar joint 2 ft 8 in. above the footing during

Test 9 (T-0.21 g) when it was non-load bearing. After the first crack was mechanically prevented from sliding, additional horizontal cracking occurred during Test 11 (T-0.27 g) at the first joint above the footing. When the wall had been repaired and made load bearing, it cracked at the second joint above the footing during Test 27 (P-0.49 g). The in-plane unreinforced wall A of House 2 did not crack until the final test, Test 32 (P-0.52 g). This crack started at the reentrant corner of the window opening and propagated diagonally downward toward the footing. The failure was associated with a permanent displacement of 1 in., which was considered as unacceptable performance.

(19) The large pier of wall B acted as an unreinforced element for half of each cycle of its response because it was vertically reinforced only at one end. Cracking occurred at the wall-footing connection at the unreinforced end of the pier.

(20) After cracking, the unreinforced in-plane walls of Houses 1 and 2 responded in a rigid body rocking mode. This mode of response was quite stable for all tests conducted on Houses 1 and 2, and no permanent slip occurred along the cracked joint for net shear stresses up to 30 psi for House 1 and 35 psi for House 2. The displacements at the top of these cracked walls depended on whether the walls were load bearing or non-load bearing, and increased with increasing intensity of base motion. For base motions with peak accelerations of the order of 0.3 g, the displacements at

the top of non-load bearing walls were 0.3, in. to 0.4 in.; the corresponding displacements for load bearing walls were 0.04 in. to 0.08 in.

(21) The performance of the partially reinforced out-of-plane walls was very satisfactory for all tests performed. The walls responded in a "cantilever" mode which was essentially a rigid body type response. The displacements at the top of W2 in House 1 reached a maximum of 0.42 in. when it was load bearing and 0.72 in. when it was non-load bearing. The corresponding displacements for House 2 were 3.05 in. and 0.41 in.; in addition the wall twisted due to the differential displacements of the in-plane walls. The maximum value of the relative displacement along the top of the wall was 0.27 in. when it was load bearing. The computed flexural capacity of the out-of-plane walls was never exceeded during any test.

(22) The performance of the partially reinforced in-plane walls in Houses 1 and 2 was very satisfactory. Both responded as cantilever type elements with essentially a rigid body type response. The deflections at the top of the walls depended on the fixity of the footings to which they were dowelled, on the presence of dead load, and on the intensity of base motion. The displacements increased significantly when the walls were non-load bearing, and when the footings were permitted to uplift. The maximum net shear stresses on the walls were 11 psi for W1 of House 1 when it was non-load bearing and 29 psi when it was load bearing. The corresponding

values for wall B of House 2 were 29 and 35 psi, respectively. The flexural yield capacity of the in-plane walls was slightly exceeded during one test, but for all others the shear forces were lower than the computed capacity corresponding to yielding of the vertical reinforcement.

LIST OF REFERENCES

1. Gülkan, P., R.L. Mayes, and R.W. Clough, "Strength of Timber Roof Connections Subjected to Cyclic Loads," Earthquake Engineering Research Center Report No. 78/17, University of California, Berkeley, 1978.

2. Mayes, R.L., and R.W. Clough, "A Literature Survey-Compressive, Tensile, Bond and Shear Strength of Masonry," Earthquake Engineering Research Center Report No. 75-15, University of California, Berkeley, 1975.

3. Mayes, R.L., and R.W. Clough, "State-of-the-Art in Seismic Shear Strength of Masonry-An Evaluation and Review," Earthquake Engineering Research Center Report No. 75-21, University of California, Berkeley, 1975.

4. Hegemier, G.A., "Mechanics of Reinforced Concrete Masonry: A Literature Survey," Report No. AMES-NSF-75-5, University of California, San Diego, 1975.

5. Omote, Y., R.L. Mayes, S.W.J. Chen, and R.W. Clough, "A Literature Survey-Transverse Strength of Masonry Walls," Earthquake Engineering Research Center Report No. 77/07, University of California, Berkeley, 1977.

6. Mayes, R.L., Y. Omote, S.W. Chen, and R.W. Clough, "Expected Performance of Uniform Building Code Designed Masonry Structures," Earthquake Engineering Research Center Report No. 76-7, University of California, Berkeley, 1976.

7. Crist, R.A., and L.E. Cattaneo, editors, "Earthquake Resistant Masonry Construction: National Workshop," NBS Building Science Series 106, National Bureau of Standards, Washington, D.C., 1977.

8. Recommended Building Code Requirements for Engineered Brick Masonry, Structural Clay Products Institute (Brick Institute of America), McLean, Virginia, 1966.

9. Tentative Provisions for the Development of Seismic Regulations for Buildings, prepared by the Applied Technology Council, publication No. ATC 3-06, National Bureau of Standards, Washington, D.C., 1978.

10. ACI Committee 531, "Proposed ACI Standard: Building Code Requirements for Concrete Masonry Structures," Journal of the American Concrete Institute, August, 1978, pp. 384-403.

11. Williams, D.W., "Seismic Behavior of Reinforced Masonry Shear Walls," Ph.D. Thesis, University of Canterbury, Christchurch, New Zealand, 1971.

12. Meli, R., "Behavior of Masonry Walls under Lateral Loads," Proceedings of the Fifth World Conference on Earthquake Engineering, Rome, 1973.

13. Priestley, M.J.N., and D.O. Bridgeman, "Seismic Resistance of Brick Masonry Walls," Bulletin of the New Zealand Society for Earthquake Engineering, Vol. 7, No. 4, December, 1974.

14. Mayes, R.L., Y. Omote, and R.W. Clough, "Cyclic Shear Tests of Masonry Piers: Volume 1 - Test Results," Earthquake Engineering Research Center Report No. 76-8, University of California, Berkeley, 1976.

15. Mayes, R.L., R.W. Clough, P. Hidalgo, and H.D. McNiven, "Seismic Research on Multistory Masonry Buildings," Proceedings of the North American Masonry Conference, J.L. Noland and J.E. Amrhein, editors, University of Colorado, Boulder, 1978.

16. Yokel, F.Y., R.G. Mathey, and R.D. Dikkers, "Strength of Masonry Walls under Compressive and Transverse Loads," National Bureau of Standards,Building Science Series 34, 1971.

17. Fattal, S.G., and L.E. Cattaneo, "Structural Performance of Masonry Walls under Compression and Flexure," National Bureau of Standards, Building Science Series 73, 1976.

18. Standard Specifications for Mortar for Unit Masonry, ASTM C 270-73, 1973.

19. Standard Specifications for Portland Cement, ASTM C 150-76, 1976.

20. Standard Specifications for Hydrated Lime for Masonry Purposes, ASTM C 207-76, 1976.

21. Standard Methods of Test for Compressive Strength of Masonry Prisms, ASTM E 447-74, 1974.

22. Uniform Building Code, International Conference of Building Officials, Whittier, California, 1976.

23. Blume, J.A., and J. Proulx, "Shear in Grouted Brick Masonry Wall Elements," report to Western States Clay Products Association, San Francisco, California, 1968.

24. Rea, D., and J. Penzien, "Dynamic Response of a 20'x20' Shaking Table," Proceedings of the Fifth World Conference on Earthquake Engineering, Rome, 1973.

25. Rogers, F.J., "Experiments with a Shaking Machine," Report to the State Earthquake Investigation Commission, California Earthquake of 18 April 1906, Vol. 1, Part II, State of California, Sacramento, 1908.

26. Earthquake Environment Simulation, Final Report and Proceedings of a Workshop on Simulation of Earthquake Effects on Structures, held in San Francisco, 7-9 September, 1973, published by National Academy of Engineering, Washington, D.C., 1974.

27 Sozen, M.A., "Earthquake Simulation in the Laboratory," Proceedings of a Workshop on Earthquake Resistant Reinforced Concrete Building Construction, edited by V.V. Bertero, University of California, Berkeley, 1978.

28. Scrivener, J.C., "Reinforced Masonry-Seismic Behavior and Design," Bulletin of the New Zealand Society for Earthquake Engineering, Vol. 5, No. 4, December, 1974.

29. Dickey, W.L., and A. Mackintosh, "Results of Variation of "b" or Effective Width in Flexure in Concrete Block Panels," Masonry Institute of America reprint, Los Angeles, California, 1971.

30. Yokel, F.Y., and S.G. Fattal, "A Failure Hypothesis for Masonry Shear-walls," Center for Building Technology, National Bureau of Standards, Washington, D.C., May, 1975.

31. Schneider, R.R., "Tests of Reinforced Grouted Brick Masonry Shear Panels," Report issued by California State Division of Architecture, Los Angeles, California, 1956.

32. Scrivener, J.C., "Static Racking Tests on Masonry Walls," Designing, Engineering and Constructing with Masonry Products, edited by F.B. Johnston, Gulf Publishing Co., Houston, Texas, 1969.

33. Structural Clay Products Research Foundation, "Compressive Transverse and Racking Tests of 4" Brick Walls," SCPRF Research Report No. 9, 1965.

34. Strength Tests of Panels for Building Construction, ASTM E 72-77, 1977.

35. Borchelt, J.G., "Analysis of Brick Walls Subject to Axial Compression and In-Plane Shear," Proceedings of the Second International Brick Masonry Conference, Stoke-on-Trent, England, April, 1970.

36. Hidalgo, P.A., and H.D. McNiven, "Seismic Behavior of Masonry Piers," Proceedings of the Second U.S. National Conference on Earthquake Engineering, Stanford University, Stanford, California, 1979.

APPENDIX A

List of Data Channels

HOUSE 1 (See Fig. 3.5)

Channel #	Channel ID	Type	Calibration		Description
0	T/R Acc-1		0.984	V/V	
1	T/R Acc-2		0.992	"	
2	CMD H Disp	DCDT	0.950	V/in.	Table horizontal displacement input
3	CMD V Disp	"	3.894	"	Table vertical displacement input
4	AV H T Disp	"	0.998	"	Average horizontal table displacement
5	AV V T Disp	"	3.945	"	Average vertical table displacement
6	AV H T Acc	Acc	4.899	V/g	Average horizontal table acceleration
7	AV V T Acc	"	4.903	"	Average vertical table acceleration
8	Pitch	"	0.981	$V/Rad/S^2$	Rotational acceleration in pitching mode
9	Roll	"	0.996	"	Rotational acceleration in rolling mode
10	Twist	"	1.187	"	Rotational acceleration in twisting mode
11	Force H1	Load cell	0.078	V/kip	Horizontal actuator force
12	Force H2	"	0.077	"	"
13	Force H3	"	0.076	"	"
14	Acc H1	Acc	4.888	V/g	Individual horizontal table acceleration
15	Acc H2	"	4.918	"	"
16	Acc V1	"	4.847	"	Individual vertical table acceleration
17	Acc V2	"	4.904	"	"
18	Acc V3	"	4.842	"	"
19	Acc V4	"	4.921	"	"
20	Force V1	Load cell	0.206	V/kip	Vertical actuator force
21	Force V2	"	0.205	"	"
22	Force V3	"	0.208	"	"
23	Force V4	"	0.206	"	"
24	Disp V1	DCDT	3.871	V/in.	Individual vertical table displacement
25	Disp V2	"	4.075	"	"
26	Disp V3	"	3.929	"	"
27	Disp V4	"	3.490	"	"
28	Disp H1	"	0.997	"	Individual horizontal table displacement
29	Disp H2	"	1.006	"	"
30	Disp H3	"	1.000	"	"

31	Blank				
32	PS-Force-1	Load cell	0.072	V/kip	Vertical stabilizer force
33	PS-Force-2	"	0.072	"	"
34	PS-Force-3	"	0.071	"	"
35	PS-Force-4	"	0.072	"	"
36	W2-Disp-TL	Pot.	1.500	V/in.	Out-of-plane displacement of W2, top left
37	W2-Disp-TC	"	1.501	"	" , top center
38	W2-Disp-TR	"	1.492	"	" , top right
39	C3-Disp-TO	"	1.501	"	Out-of-plane displacement of C3, top
40	W4-Disp-TC	"	1.498	"	Out-of-plane displacement of W4, top center
41	C4-Disp-TO	"	1.497	"	Out-of-plane displacement of C4, top
42	C2-Disp-TO	"	2.970	"	" C2, "
43	C1-Disp-TC	"	2.996	"	" C1, "
44*	W4-Disp-TL	"	3.054	"	" W4, top left
45*	W4-Disp-TR	"	7.930	"	" , top right
46	W4-Disp-MC	DCDT	3.086	"	" , at center 2/3 height
47*	Roof Gable	Pot.	0.771	"	Absolute displacement of roof at ridge line
48	C2-Disp-TL	DCDT	2.662	"	Out-of-plane displacement of C2, top
49	C1-Disp-TL	"	2.742	"	" C1, "
50	C3-Disp-TL	"	2.714	"	" C3, "
51	C4-Disp-TL	"	2.761	"	" C4, "
52	W2-Disp-MC	"	2.672	"	Out-of-plane displacement of W2, at center 2/3 height
53	R-Disp-C	"	2.738	"	Roof displacement at drywall level
54	W3-Crack	"	101.726	"	Change in crack width on W3
55	C2-Crack	"	93.159	"	" C2
56	C2-Disp-ML	"	9.172	"	Out-of-plane displacement of C2, at 2/3 wall height
57	C1-Disp-ML	"	9.618	"	" C1, "
58	W2-Disp-BL	"	9.421	"	" W2, at 1/3 wall height
59	C3-Disp-ML	"	9.078	"	" C3, at 2/3 wall height
60	C4-Disp-ML	"	8.657	"	" C4, "
61	W4-Disp-BC	"	7.082	"	" W4, at 1/3 wall height
62	W3-Disp-TI	"	12.001	"	In-plane displacement at top of W3
63	W1-Disp-TI	"	11.703	"	" W1
64	TP/C2/R	"	10.739	"	Slip of top plane relative to C2
65	TP/W2/R	"	11.859	"	" W2
66	TP/C1/R	"	12.024	"	" C1
67	TP/C3/R	"	11.443	"	" C3

68	TP/W4/R	DCDT	12.468	V/in.	Slip of top plane relative to W4
69	TP/C4/R	"	12.781	"	" C4
70	TP/W3/R	"	12.854	"	" W3
71	TP/W1/R	"	12.107	"	" W1
72*	J/TP/W-W2	"	11.687	"	Slip of truss rafter with framing anchor rel. to top plate
73*	J/TP/W0-W2	"	10.630	"	" without "
74*	J/TP/W-W4	"	11.171	"	" with "
75*	J/TP/W0-W4	"	11.137	"	" without "
76	ROT-W2-1	"	10.583	"	Rotation of footing under W2, instrument 1
77	ROT-W2-2	"	10.790	"	" " 2
78	ROT-W4-1	"	10.640	"	" W4, " 1
79	ROT-W4-2	"	10.802	"	" " 2
80	C2-Acc-TC	Acc.	3.903	g/V	Out-of-plane acceleration of C2, top
81	W2-Acc-TC	"	4.399	"	" W2, "
82	C1-Acc-TC	"	3.981	"	" C1, "
83	W2-Acc-MC	"	4.306	"	" W2, at 2/3 wall height
84	W4-Acc-TC	"	4.251	"	" W4, top
85	W4-Acc-MC	"	4.389	"	" W4, at 2/3 wall height
86	Roof-Acc-C	"	3.959	"	Roof acceleration at drywall level
87	Blank				
88*	Roof-Acc-2	"	3.991	"	Roof acceleration at top plate level, instrument 1
89	Blank				
90*	Roof-Acc-3	"	4.017	"	Roof acceleration at weight level
97*	Roof-Acc-1	"	4.010	"	Roof acceleration at top plate level, instrument 2

*Due to the rotation of the roof, the location of these instruments was changed relative to Fig. 3.5, however their function remained the same.

HOUSE 2 (See Fig. 3.6)

Channel #	Channel ID	Type	Calibration		Description
0	Blank				
1	"				
2	"				
3	"				
4	AV H T Disp	DCDT	0.998	V/in.	Average horizontal table displacement
5	AV V T Disp	"	3.945	"	Average vertical table displacement
6	AV H T Acc	Acc.	4.899	V/g	Average horizontal table acceleration
7	AV V T Acc	"	4.903	"	Average vertical table acceleration
8	Pitch	"	0.981	$V/Rad/S^2$	Rotational acceleration in pitching mode
9	Roll	"	0.996	"	Rotational acceleration in rolling mode
10	Twist	"	1.187	"	Rotational acceleration in twisting mode
11	Force H1	Load cell	0.078	V/kip	Horizontal actuator force
12	Force H2	"	0.077	"	"
13	Force H3	"	0.076	"	"
14	Acc H1	Acc.	4.888	V/g	Individual horizontal table acceleration
15	Acc H2	"	4.918	"	"
16	Blank				
17	"				
18	"				
19	"				
20	Force V1	Load cell	0.206	V/kip	Vertical actuator force
21	Force V2	"	0.205	"	"
22	Force V3	"	0.208	"	"
23	Force V4	"	0.206	"	"
24	Disp V1	DCDT	3.871	V/in	Individual vertical table displacement
25	Disp V2	"	4.075	"	"
26	Disp V3	"	3.929	"	"
27	Disp V4	"	3.490	"	"
28	Disp H1	"	0.997	"	Individual horizontal table displacement
29	Disp H2	"	1.006	"	"
30	Disp H3	"	1.000	"	"
31	Blank				
32	PS-Force-1	Load cell	0.072	V/kip	Vertical stabilizer force

33	PS-Force-2	Load cell	0.072	V/kip	Vertical stabilizer force
34	PS-Force-3	"	0.071	"	"
35	PS-Force-4	"	0.072	"	"
36	A-MPS-1	DCDT	12.663	V/in.	Shear deformation main pier of wall A
37	A-MPS-2	"	12.861	"	"
38	A-WPS-1	"	12.432	"	Shear deformation window pier of wall A
39	A-WPS-2	"	12.289	"	"
40	A-DPS-1	"	12.678	"	Shear deformation door pier of wall A
41	A-DPS-2	"	12.418	"	"
42	A-IPD-TL	"	9.109	"	In-plane displacement of wall A
43	A-WP-IP	"	46.319	"	Slip of top plate relative to wall A
44	B-MPS-1	"	12.324	"	Shear deformation main pier of wall B
45	B-MPS-2	"	12.437	"	"
46	B-DPS-1	"	12.319	"	Shear deformation door pier of wall B
47	B-DPS-2	"	12.893	"	"
48	B-IPD-TR	"	9.396	"	In-plane displacement of wall B
49	B-WP-IP	"	55.290	"	Slip of top plate relative to wall B
50	A1-Disp-MR	"	2.816	"	Out-of-plane displacement of A1 at 2/3 wall height
51	A1-Disp-MC	"	2.728	"	"
52	A1-Disp-ML	"	2.731	"	"
53	A1-Disp-BC	"	9.293	"	Out-of-plane displacement of A1 at 1/3 wall height
54	A1-ROT-I	"	12.295	"	Rotation of footing under A1, interior instrument
55	A1-ROT-E	"	12.023	"	" exterior "
56	A1-Disp-TR	Pot.	3.052	"	Out-of-plane displacement of A1, top right
57	A1-Disp-TC	"	3.028	"	Out-of-plane displacement of A1, top center
58	A1-Disp-TL	"	3.159	"	Out-of-plane displacement of A1, top left
59*	Roof Gable	"	1.225	"	Absolute displacement of roof at ridge line
60	A1-WP-OPL	DCDT	50.983	"	Slip of top plate relative to wall A1
61	A1-WP-OPR	"	56.810	"	"
62	B1-WP-OPL	"	49.488	"	Slip of top plate relative to wall B1
63	B1-WP-OPR	"	46.110	"	"
64	B1-Disp-ML	"	2.822	"	Out-of-plane displacement of B1 at 2/3 wall height
65	B1-Disp-MR	"	2.695	"	"
66	B1-Disp-BL	"	9.298	"	Out-of-plane displacement of B1 at 1/3 wall height
67	Blank				
68	B1-ROT-I	"	10.464	"	Rotation of footing under B1, interior instrument
69	B1-ROT-E	"	9.815	"	Rotation of footing under B1, exterior instrument

70	R-Disp-C	DCDT	2.15[illegible]	V/in.	Roof displacement at drywall level
71	Blank				
72*	A-JP-NS	"	11.471	"	Slip of truss rafter with no framing anchor relative to top plate
73*	B-JP-NS	"	10.909	"	"
74*	A-JP-S	"	11.264	"	Slip of truss rafter with framing anchor relative to top plate
75*	B-JP-S	"	11.645	"	"
76	B1-Disp-TL	Pot.	3.065	"	Out-of-plane displacement of B1, top left
77	B1-Disp-TC	"	3.050	"	Out-of-plane displacement of B1, top center
78	B1-Disp-TR	"	3.137	"	Out-of-plane displacement of B1, top right
79	A1-Acc-MR	Acc.	3.962	V/g	Out-of-plane acceleration of A1, at 2/3 wall height
80	A1-Acc-TC	"	2.232	"	Out-of-plane acceleration of A1, at top of wall
81	B1-Acc-ML	"	6.327	"	Out-of-plane acceleration of B1, at 2/3 wall height
82	B1-Acc-TC	"	2.222	"	Out-of-plane acceleration of B1, at top of wall
83	A-Acc-TC	"	4.010	"	In-plane acceleration of A, at top of wall
84	B-Acc-TR	"	3.991	"	In-plane acceleration of B, at top of wall
85	Blank				
86	R-Acc-A	Acc.	3.944	V/g	Roof acceleration above wall A
87	R-Acc-TOP	"	3.997	"	Roof acceleration at ridge line
88	R-Acc-CEN	"	2.150	"	Roof acceleration at drywall level

During the conduct of the tests, modifications and revisions were made in the above list. Rather than reassigning the same numbers to the new instruments, these were renumbered in Fig. 3.6 as follows.

89	B-UL-L	DCDT	10.464	V/in.	Total uplift of top of wall B from footing, left side
90	B-UL-R	"	9.815	"	Total uplift of top of wall B from footing, right side
91	A-UL-L	"	12.295	"	Total uplift of top of wall A from footing, left side
92	A-UL-R	"	12.023	"	Total uplift of top of wall A from footing, right side
93	B-FTUL-L	"	11.386	"	Uplift of footing under B from table, left side
94	B-FTUL-R	"	11.188	"	Uplift of footing under B from table, right side
95	A-FTUL-L	"	10.327	"	Uplift of footing under A from table, left side
96	A-FTUL-R	"	11.737	"	Uplift of footing under A from table, right side
97	B-WP-IP	"	55.290	"	Slip of top plate relative to wall B
98	A-WP-IP	"	46.319	"	Slip of top plate relative to wall A

*These instruments continued to serve the same function after the rotation of the roof, but their locations were rotated by 90 degrees.

APPENDIX B

Transverse Strength of Unreinforced Masonry Walls

Appendix B

The theory for the transverse strength of an unreinforced masonry cross section can be established with reference to Fig. B.1(a) which shows a solid prismatic section of thickness t and width b, which is acted upon by a vertical load P at an eccentricity e. With the axial load at the centroid of the cross section, Fig. B.1(b), the axial load capacity may be determined as

$$P_o = f'_m \, b \, t = f'_m \, A_n \, , \tag{B.1}$$

where

f'_m = compression strength of masonry

A_n = net cross sectional area.

Stress distribution at flexural failure when no resultant force acts at the cross section is shown in Fig. B.1(c). The moment capacity for this stress distribution is given by

$$M_t = \frac{f'_t I}{c} \, . \tag{B.2}$$

Denoting

$$s = \frac{f'_t}{f'_m} \, ,$$

where

f'_t = tensile strength of masonry determined from a modulus of rupture test

Equation (B.2) may be written as

$$M_t = s\, f_m' \frac{bt^2}{6}$$

$$= s \frac{P_o t}{6} . \qquad \text{(B.2a)}$$

When the tensile stress at the extreme fiber exceeds the tensile capacity, the section will crack. This does not necessarily lead to structural failure since the ultimate moment capacity of a cracked section at any particular axial load may be greater than the cracking moment expressed in Eq. (B.2a). In Fig. (B.1d) the stress distribution on a cracked section at maximum compressive and tensile stress is shown. Length u is the uncracked width of the section, and P is the corresponding compressive force acting on the section. The following expression may be developed for P:

$$P = (f_m' + f_t') \frac{bu}{2} - f_t' b u$$

$$= \frac{bu}{2} (f_m' - f_t') \qquad \text{(B.3)}$$

$$= \frac{bu}{2} f_m' (1 - s) .$$

The resultant moment M_e acting at the section, corresponding to this ultimate condition may be expressed as

$$M_e = \frac{bu}{2} (f_m' + f_t')(\frac{t}{2} - \frac{u}{3}) - f_t' b u (\frac{t}{2} - \frac{u}{2})$$

$$= \frac{bu}{2} (f_m' + f_t')(\frac{t}{2} - \frac{u}{3}) - \frac{bu}{2} 2 f_t' (\frac{t}{2} - \frac{u}{3}) \qquad \text{(B.4)}$$

$$+ \frac{bu}{2} 2 f_t' \frac{u}{6} .$$

Substituting Eq. (B.3) into Eq. (B.4) yields

$$M_e = P\left(\frac{t}{2} - \frac{u}{3}\right) + b\,u\,f'_t\,\frac{u}{6}\,. \tag{B.4a}$$

From Eq. (B.3)

$$b\,u = \frac{2P}{f'_m(1 - s)}\,.$$

Given

$$f'_m = \frac{P_o}{bt}\,,$$

then

$$b\,u = \frac{2Pbt}{P_o(1 - s)} \tag{B.5}$$

so that

$$u = \frac{2Pt}{P_o(1 - s)} \tag{B.5a}$$

$$P\,\frac{u}{3} = \frac{P}{3}\,\frac{P}{P_o}\,\frac{2t}{1 - s}\,,$$

and

$$b\,u\,f'_t\,\frac{u}{6} = \frac{1}{6}\,\frac{sP_o}{bt}\,\frac{2Pbt}{P_o(1 - s)}\,\frac{2Pt}{P_o(1 - s)}$$

$$= \frac{2}{3}\,\frac{P^2}{P_o}\,\frac{ts}{(1 - s)^2}\,. \tag{B.6}$$

Substituting Eqs. (B.5a) and (B.6) into Eq. (B.4a) yields

$$M_e = \frac{Pt}{2}\left\{1 - 1.33\,\frac{P}{P_o}\,\frac{(1 - 2s)}{(1 - s)^2}\right\}\,. \tag{B.7}$$

For masonry with negligible tensile strength ($s \approx 0$). Eq. (B.7)

luces to

$$M_e \simeq \frac{Pt}{2}\left(1 - 1.33\,\frac{P}{P_o}\right) . \qquad (B.8)$$

Figure B.1(d) illustrates the stress distribution when the section is loaded to capacity by a vertical load applied so that there is zero tensile stress at the extreme fiber. Thus, adopting the subscript "k" to denote the condition when the axial load is at the edge of the kern,

$$\frac{P_k e_k c}{I_n} = \frac{P_k}{A_n} \qquad (B.9)$$

or

$$e_k = \frac{I_n}{A_n c} = \frac{t}{6} \qquad (B.10)$$

where

e_k = distance from centroid to edge of kern

P_k = corresponding axial load capacity

c = distance from centroid to outer fiber

I_n = moment of inertia based on uncracked net section.

An noted earlier, the ultimate cracked moment is not necessarily the maximum moment that a section can resist at a given vertical load. For example, at P = o the ultimate moment capacity equals M_t given by Eq. (B.2a) whereas according to Eq. (B.7) it would vanish. This apparent discrepancy may be explained with respect to Fig. B.2 which shows two different distributions initially corresponding to the stage when cracking is imminent. In Fig. B.2(a) the vertical load is gradually decreased and always placed at an eccentricity which will cause maximum tensile stress, f_t', at the outer fiber but not cause the

section to crack. In Fig. B.2(b) the load is also decreased but is placed so that it will generate maximum compressive and tensile stresses simultaneously on the cracked section. Equation (B.7) corresponds to this second case. An expression corresponding to incipient cracking at all stages of loading can be developed with reference to Fig. B.2(c). The cracking moment is given by

$$M_c = M_2 + M_3$$

$$M_2 = s\, P_o \frac{t}{6} = M_t$$

$$M_3 = P\, e_k \,.$$

Therefore

$$M_c = \frac{t}{6}\,(s\, P_o + P). \tag{B.11}$$

At axial loads greater than P_c (applied at eccentricities less than e_c) the section will not crack. Figure B.3 shows the stress block corresponding to such a load. The vertical load P acting at the section will then be

$$P = b\, t\, (f'_m - \frac{\Delta f}{2})$$

$$= P_o - \frac{bt\Delta f}{2} \,. \tag{B.12}$$

The elastic ultimate moment will be

$$M_e = \frac{bt\Delta f}{2}\, e_k$$

$$= \frac{bt\Delta f}{2}\, \frac{t}{6} \,. \tag{B.13}$$

But from Eq. (B.12) we have

$$\frac{bt\Delta f}{2} = P_o - P \ ,$$

so

$$M_e = (P_o - P)\ \frac{t}{6} \ . \tag{B.14}$$

With only slight modification, the equations developed for solid sections can be extended to symmetrical hollow sections. The distance from the centroid to the edge of the kern may be written as

$$e_k = \frac{I_n}{A_n c} = \frac{2I_n}{A_n t} \ . \tag{B.10a}$$

The corresponding load and moment capacities are

$$P_k = \frac{P_o}{2}$$

$$M_k = P_k\ e_k = \frac{P_o I_n}{A_n t} \ . \tag{B.15}$$

An expression similar to Eq. (B.8) which is continuously applicable to hollow sections can be developed as follows:

Rewrite Eq. (B.8) as

$$M_e = P\ c\ (1 - g\ \frac{P}{P_o}) \tag{B.8a}$$

where

g = a constant depending on section geometry.

At $P = P_k$, $M_e = M_k = P_k\ e_k$

$$P_k\ e_k = P_k\ c\ (1 - g\ \frac{P_k}{P_o}) \ .$$

Hence

$$g = \frac{P_o}{P_k} \left(1 - \frac{e_k}{c}\right) . \qquad \text{(B.16)}$$

For symmetrical sections

$$\frac{P_o}{P_k} = 2$$

and

$$\frac{e_k}{c} = \frac{4I_n}{A_n t^2} ,$$

so that

$$g = 2 \left(1 - \frac{4I_n}{A_n t^2}\right) . \qquad \text{(B.16a)}$$

It should be noted that g equals 1.33 for a symmetrical solid section and asymptotically approaches zero as the net area of the section is diminished.

The expression for M_t, the ultimate moment at P = 0, can be determined from

$$M_t = f'_t \frac{I_n}{c} = s P_o e_k = 2 s P_o \frac{I_n}{A_n t} , \qquad \text{(B.17)}$$

and the equation for the cracking line is

$$M_c = \frac{2I_n}{A_n t} (s P_o + P) . \qquad \text{(B.18)}$$

Hence the approximate equation for M_c between P = 0 and P = P_k can be written as

$$M_e = P c \left(1 - g \frac{P}{P_o}\right) \qquad \text{(B.19)}$$

or

$$M_e = \frac{2I_n}{A_n t} (s P_o + P) ,$$

whichever is larger. Likewise for P greater then P_c

$$M_e = e_k (P_o - P)$$

$$= \frac{2I_n}{A_n t} (P_o - P) . \qquad (B.20)$$

Equation (B.19) is valid from P = 0 to P = P_k while Eq. (B.20) covers the range from P_c to P_o. Since the vertical load corresponding to cracking, P_c, is lower than P_k, the range between P_k and P_c is covered by both expressions. The discrepancy is due to the approximate nature of Eq. (B.19) which does not account for the tensile strength of the masonry. For nonzero values of s and very small axial loads (say 10 percent or less of P_o), Eq. (B.18) governs strength. Therefore, ultimate flexural capacity is intimately related to the tensile strength of masonry in this region.

In addition to neglecting possible strain gradient effects, no discussion related to slenderness effects is included on account of the very low axial stresses on the load bearing transverse walls of the test specimens. An overview of the effect of slenderness and related code provisions is given in reference (5).

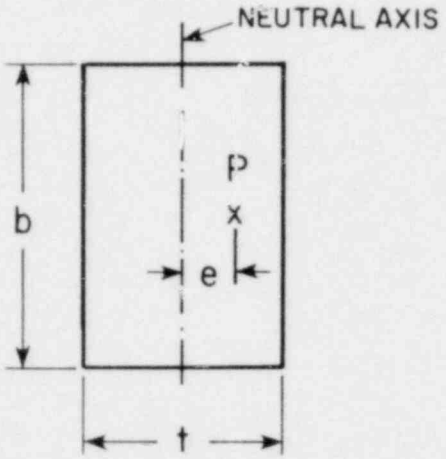

(a) CROSS SECTION

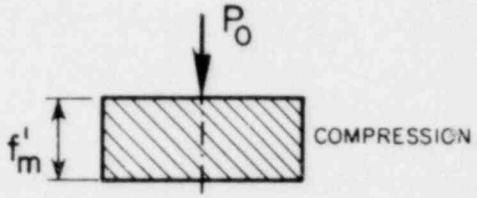

(b) AXIAL LOAD

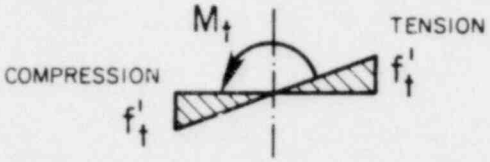

(c) PURE FLEXURE

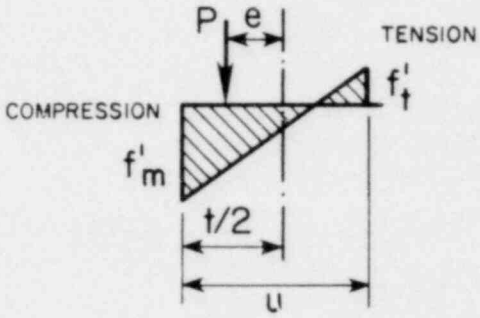

(d) CRACKED SECTION

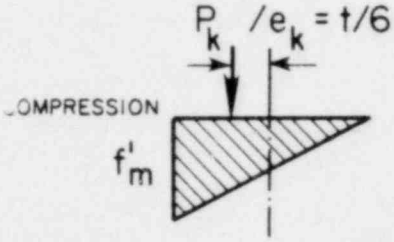

(e) LOAD AT EDGE OF KERN

FIGURE B.1 CRITICAL STRESS STATES FOR AN UNREINFORCED INTERACTION DIAGRAM

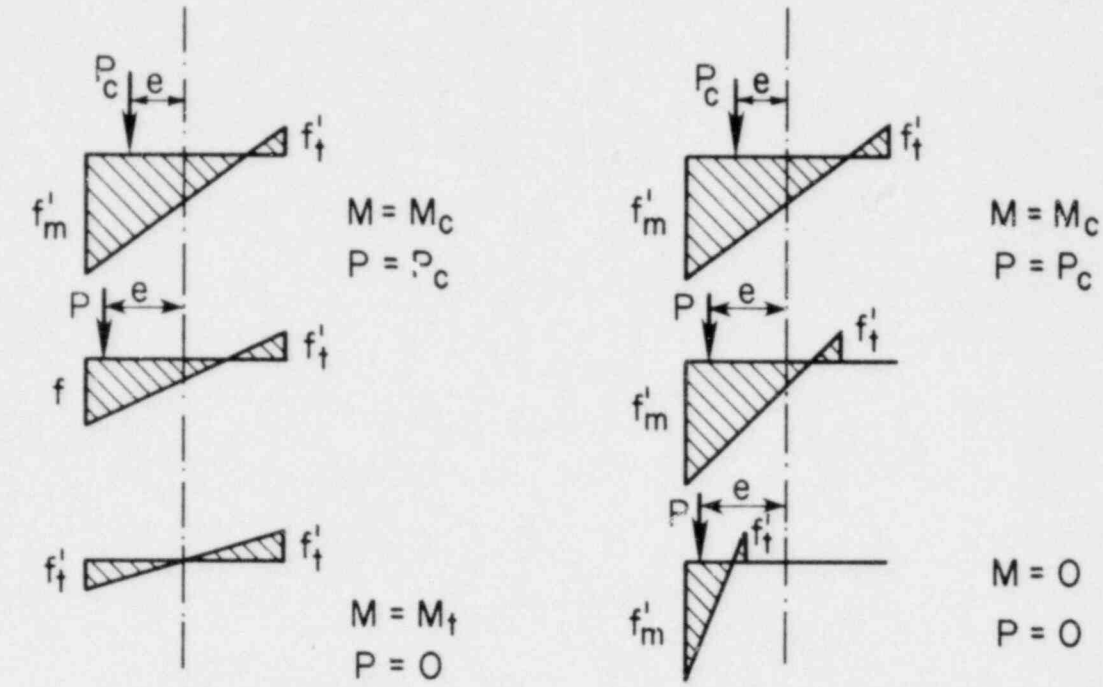

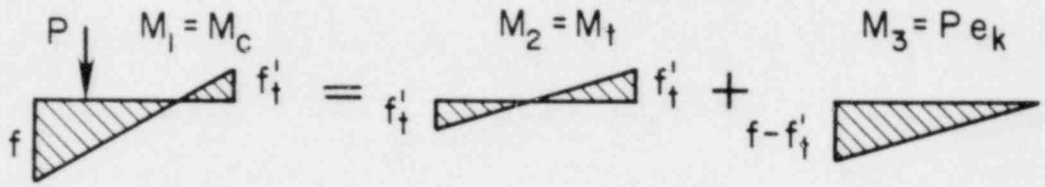

(c) CRACKING MOMENT

FIGURE B.2 CRITICAL STRESS STATES FOR AN UNREINFORCED INTERACTION DIAGRAM

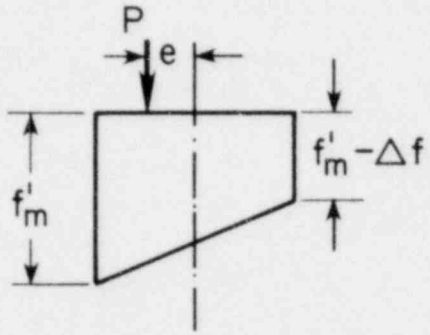

FIGURE B.3 CRITICAL STRESS STATES FOR AN UNREINFORCED INTERACTION DIAGRAM

EARTHQUAKE ENGINEERING RESEARCH CENTER REPORTS

NOTE: Numbers in parenthesis are Accession Numbers assigned by the National Technical Information Service; these are followed by a price code. Copies of the reports may be ordered from the National Technical Information Service, 5285 Port Royal Road, Springfield, Virginia, 22161. Accession Numbers should be quoted on orders for reports (PB --- ---) and remittance must accompany each order. Reports without this information were not available at time of printing. Upon request, EERC will mail inquirers this information when it becomes available.

EERC 67-1 "Feasibility Study Large-Scale Earthquake Simulator Facility," by J. Penzien, J.G. Bouwkamp, R.W. Clough and D. Rea - 1967 (PB 187 905)A07

EERC 68-1 Unassigned

EERC 68-2 "Inelastic Behavior of Beam-to-Column Subassemblages Under Repeated Loading," by V.V. Bertero - 1968 (PB 184 888)A05

EERC 68-3 "A Graphical Method for Solving the Wave Reflection-Refraction Problem," by H.D. McNiven and Y. Mengi - 1968 (PB 187 943)A03

EERC 68-4 "Dynamic Properties of McKinley School Buildings," by D. Rea, J.G. Bouwkamp and R.W. Clough - 1968 (PB 187 902)A07

EERC 68-5 "Characteristics of Rock Motions During Earthquakes," by H.B. Seed, I.M. Idriss and F.W. Kiefer - 1968 (PB 188 338)A03

EERC 69-1 "Earthquake Engineering Research at Berkeley," - 1969 (PB 187 906)A11

EERC 69-2 "Nonlinear Seismic Response of Earth Structures," by M. Dibaj and J. Penzien - 1969 (PB 187 904)A08

EERC 69-3 "Probabilistic Study of the Behavior of Structures During Earthquakes," by R. Ruiz and J. Penzien - 1969 (PB 187 886)A06

EERC 69-4 "Numerical Solution of Boundary Value Problems in Structural Mechanics by Reduction to an Initial Value Formulation," by N. Distefano and J. Schujman - 1969 (PB 187 942)A02

EERC 69-5 "Dynamic Programming and the Solution of the Biharmonic Equation," by N. Distefano - 1969 (PB 187 941)A03

EERC 69-6 "Stochastic Analysis of Offshore Tower Structures," by A.K. Malhotra and J. Penzien - 1969 (PB 187 903)A09

EERC 69-7 "Rock Motion Accelerograms for High Magnitude Earthquakes," by H.B. Seed and I.M. Idriss - 1969 (PB 187 940)A02

EERC 69-8 "Structural Dynamics Testing Facilities at the University of California, Berkeley," by R.M. Stephen, J.G. Bouwkamp, R.W. Clough and J. Penzien - 1969 (PB 189 111)A04

EERC 69-9 "Seismic Response of Soil Deposits Underlain by Sloping Rock Boundaries," by H. Dezfulian and H.B. Seed 1969 (PB 189 114)A03

EERC 69-10 "Dynamic Stress Analysis of Axisymmetric Structures Under Arbitrary Loading," by S. Ghosh and E.L. Wilson 1969 (PB 189 026)A10

EERC 69-11 "Seismic Behavior of Multistory Frames Designed by Different Philosophies," by J.C. Anderson and V. V. Bertero - 1969 (PB 190 662)A10

EERC 69-12 "Stiffness Degradation of Reinforcing Concrete Members Subjected to Cyclic Flexural Moments," by V.V. Bertero, B. Bresler and H. Ming Liao - 1969 (PB 202 942)A07

EERC 69-13 "Response of Non-Uniform Soil Deposits to Travelling Seismic Waves," by H. Dezfulian and H.B. Seed - 1969 (PB 191 023)A03

EERC 69-14 "Damping Capacity of a Model Steel Structure," by D. Rea, R.W. Clough and J.G. Bouwkamp - 1969 (PB 190 663)A06

EERC 69-15 "Influence of Local Soil Conditions on Building Damage Potential during Earthquakes," by H.B. Seed and I.M. Idriss - 1969 (PB 191 036)A03

EERC 69-16 "The Behavior of Sands Under Seismic Loading Conditions," by M.L. Silver and H.B. Seed - 1969 (AD 714 982)A07

EERC 70-1 "Earthquake Response of Gravity Dams," by A.K. Chopra - 1970 (AD 709 640)A03

EERC 70-2 "Relationships between Soil Conditions and Building Damage in the Caracas Earthquake of July 29, 1967," by H.B. Seed, I.M. Idriss and H. Dezfulian - 1970 (PB 195 762)A05

EERC 70-3 "Cyclic Loading of Full Size Steel Connections," by E.P. Popov and R.M. Stephen - 1970 (PB 213 545)A04

EERC 70-4 "Seismic Analysis of the Charaima Building, Caraballeda, Venezuela," by Subcommittee of the SEAONC Research Committee: V.V. Bertero, P.F. Fratessa, S.A. Mahin, J.H. Sexton, A.C. Scordelis, E.L. Wilson, L.A. Wyllie, H.B. Seed and J. Penzien, Chairman - 1970 (PB 201 455)A06

EERC 70-5 "A Computer Program for Earthquake Analysis of Dams," by A.K. Chopra and P. Chakrabarti - 1970 (AD 723 994)A05

EERC 70-6 "The Propagation of Love Waves Across Non-Horizontally Layered Structures," by J. Lysmer and L.A. Drake 1970 (PB 197 896)A03

EERC 70-7 "Influence of Base Rock Characteristics on Ground Response," by J. Lysmer, H.b. Seed and P.B. Schnabel 1970 (PB 197 897)A03

EERC 70-8 "Applicability of Laboratory Test Procedures for Measuring Soil Liquefaction Characteristics under Cyclic Loading," by H.B. Seed and W.H. Peacock - 1970 (PB 198 016)A03

EERC 70-9 "A Simplified Procedure for Evaluating Soil Liquefaction Potential," by H.B. Seed and I.M. Idriss - 1970 (PB 198 009)A03

EERC 70-10 "Soil Moduli and Damping Factors for Dynamic Response Analysis," by H.B. Seed and I.M. Idriss - 1970 (PB 197 869)A03

EERC 71-1 "Koyna Earthquake of December 11, 1967 and the Performance of Koyna Dam," by A.K. Chopra and P. Chakrabarti 1971 (AD 731 496)A06

EERC 71-2 "Preliminary In-Situ Measurements of Anelastic Absorption in Soils Using a Prototype Earthquake Simulator," by R.D. Borcherdt and P.W. Rodgers - 1971 (PB 201 454)A03

EERC 71-3 "Static and Dynamic Analysis of Inelastic Frame Structures," by F.L. Porter and G.H. Powell - 1971 (PB 210 135)A06

EERC 71-4 "Research Needs in Limit Design of Reinforced Concrete Structures," by V.V. Bertero - 1971 (PB 202 943)A04

EERC 71-5 "Dynamic Behavior of a High-Rise Diagonally Braced Steel Building," by D. Rea, A.A. Shah and J.G. Bouwkamp 1971 (PB 203 584)A06

EERC 71-6 "Dynamic Stress Analysis of Porous Elastic Solids Saturated with Compressible Fluids," by J. Ghaboussi and E. L. Wilson - 1971 (PB 211 396)A06

EERC 71-7 "Inelastic Behavior of Steel Beam-to-Column Subassemblages," by H. Krawinkler, V.V. Bertero and E.P. Popov 1971 (PB 211 335)A14

EERC 71-8 "Modification of Seismograph Records for Effects of Local Soil Conditions," by P. Schnabel, H.B. Seed and J. Lysmer - 1971 (PB 214 450)A03

EERC 72-1 "Static and Earthquake Analysis of Three Dimensional Frame and Shear Wall Buildings," by E.L. Wilson and H.H. Dovey - 1972 (PB 212 904)A05

EERC 72-2 "Accelerations in Rock for Earthquakes in the Western United States," by P.B. Schnabel and H.B. Seed - 1972 (PB 213 100)A03

EERC 72-3 "Elastic-Plastic Earthquake Response of Soil-Building Systems," by T. Minami - 1972 (PB 214 868)A08

EERC 72-4 "Stochastic Inelastic Response of Offshore Towers to Strong Motion Earthquakes," by M.K. Kaul - 1972 (PB 215 713)A05

EERC 72-5 "Cyclic Behavior of Three Reinforced Concrete Flexural Members with High Shear," by E.P. Popov, V.V. Bertero and H. Krawinkler - 1972 (PB 214 555)A05

EERC 72-6 "Earthquake Response of Gravity Dams Including Reservoir Interaction Effects," by P. Chakrabarti and A.K. Chopra - 1972 (AD 762 330)A08

EERC 72-7 "Dynamic Properties of Pine Flat Dam," by D. Rea, C.Y. Liaw and A.K. Chopra - 1972 (AD 763 928)A05

EERC 72-8 "Three Dimensional Analysis of Building Systems," by E.L. Wilson and H.H. Dovey - 1972 (PB 222 438)A06

EERC 72-9 "Rate of Loading Effects on Uncracked and Repaired Reinforced Concrete Members," by S. Mahin, V.V. Bertero, D. Rea and M. Atalay - 1972 (PB 224 520)A08

EERC 72-10 "Computer Program for Static and Dynamic Analysis of Linear Structural Systems," by E.L. Wilson, K.-J. Bathe, J.E. Peterson and H.H.Dovey - 1972 (PB 220 437)A04

EERC 72-11 "Literature Survey - Seismic Effects on Highway Bridges," by T. Iwasaki, J. Penzien and R.W. Clough - 1972 (PB 215 613)A19

EERC 72-12 "SHAKE-A Computer Program for Earthquake Response Analysis of Horizontally Layered Sites," by P.B. Schnabel and J. Lysmer - 1972 (PB 220 207)A06

EERC 73-1 "Optimal Seismic Design of Multistory Frames," by V.V. Bertero and H. Kamil - 1973

EERC 73-2 "Analysis of the Slides in the San Fernando Dams During the Earthquake of February 9, 1971," by H.B. Seed, K.L. Lee, I.M. Idriss and F. Makdisi - 1973 (PB 223 402)A14

EERC 73-3 "Computer Aided Ultimate Load Design of Unbraced Multistory Steel Frames," by M.B. El-Hafez and G.H. Powell 1973 (PB 248 315)A09

EERC 73-4 "Experimental Investigation into the Seismic Behavior of Critical Regions of Reinforced Concrete Components as Influenced by Moment and Shear," by M. Celebi and J. Penzien - 1973 (PB 215 884)A09

EERC 73-5 "Hysteretic Behavior of Epoxy-Repaired Reinforced Concrete Beams," by M. Celebi and J. Penzien - 1973 (PB 239 568)A03

EERC 73-6 "General Purpose Computer Program for Inelastic Dynamic Response of Plane Structures," by A. Kanaan and G.H. Powell - 1973 (PB 221 260)A08

EERC 73-7 "A Computer Program for Earthquake Analysis of Gravity Dams Including Reservoir Interaction," by P. Chakrabarti and A.K. Chopra - 1973 (AD 766 271)A04

EERC 73-8 "Behavior of Reinforced Concrete Deep Beam-Column Subassemblages Under Cyclic Loads," by O. Küstü and J.G. Bouwkamp - 1973 (PB 246 117)A12

EERC 73-9 "Earthquake Analysis of Structure-Foundation Systems," by A.K. Vaish and A.K. Chopra - 1973 (AD 766 272)A07

EERC 73-10 "Deconvolution of Seismic Response for Linear Systems," by R.B. Reimer - 1973 (PB 227 179)A08

EERC 73-11 "SAP IV: A Structural Analysis Program for Static and Dynamic Response of Linear Systems," by K.-J. Bathe, E.L. Wilson and F.E. Peterson - 1973 (PB 221 967)A09

EERC 73-12 "Analytical Investigations of the Seismic Response of Long, Multiple Span Highway Bridges," by W.S. Tseng and J. Penzien - 1973 (PB 227 816)A10

EERC 73-13 "Earthquake Analysis of Multi-Story Buildings Including Foundation Interaction," by A.K. Chopra and J.A. Gutierrez - 1973 (PB 222 970)A03

EERC 73-14 "ADAP: A Computer Program for Static and Dynamic Analysis of Arch Dams," by R.W. Clough, J.M. Raphael and S. Mojtahedi - 1973 (PB 223 763)A09

EERC 73-15 "Cyclic Plastic Analysis of Structural Steel Joints," by R.B. Pinkney and R.W. Clough - 1973 (PB 226 843)A08

EERC 73-16 "QUAD-4: A Computer Program for Evaluating the Seismic Response of Soil Structures by Variable Damping Finite Element Procedures," by I.M. Idriss, J. Lysmer, R. Hwang and H.B. Seed - 1973 (PB 229 424)A05

EERC 73-17 "Dynamic Behavior of a Multi-Story Pyramid Shaped Building," by R.M. Stephen, J.P. Hollings and J.G. Bouwkamp - 1973 (PB 240 718)A06

EERC 73-18 "Effect of Different Types of Reinforcing on Seismic Behavior of Short Concrete Columns," by V.V. Bertero, J. Hollings, O. Küstü, R.M. Stephen and J.G. Bouwkamp - 1973

EERC 73-19 "Olive View Medical Center Materials Studies, Phase I," by B. Bresler and V.V. Bertero - 1973 (PB 235 986)A06

EERC 73-20 "Linear and Nonlinear Seismic Analysis Computer Programs for Long Multiple-Span Highway Bridges," by W.S. Tseng and J. Penzien - 1973

EERC 73-21 "Constitutive Models for Cyclic Plastic Deformation of Engineering Materials," by J.M. Kelly and P.P. Gillis 1973 (PB 226 024)A03

EERC 73-22 "DRAIN - 2D User's Guide," by G.H. Powell - 1973 (PB 227 016)A05

EERC 73-23 "Earthquake Engineering at Berkeley - 1973," (PB 226 033)A11

EERC 73-24 Unassigned

EERC 73-25 "Earthquake Response of Axisymmetric Tower Structures Surrounded by Water," by C.Y. Liaw and A.K. Chopra 1973 (AD 773 052)A09

EERC 73-26 "Investigation of the Failures of the Olive View Stairtowers During the San Fernando Earthquake and Their Implications on Seismic Design," by V.V. Bertero and R.G. Collins - 1973 (PB 235 106)A13

EERC 73-27 "Further Studies on Seismic Behavior of Steel Beam-Column Subassemblages," by V.V. Bertero, H. Krawinkler and E.P. Popov - 1973 (PB 234 172)A06

EERC 74-1 "Seismic Risk Analysis," by C.S. Oliveira - 1974 (PB 235 920)A06

EERC 74-2 "Settlement and Liquefaction of Sands Under Multi-Directional Shaking," by R. Pyke, C.K. Chan and H.B. Seed 1974

EERC 74-3 "Optimum Design of Earthquake Resistant Shear Buildings," by D. Ray, K.S. Pister and A.K. Chopra - 1974 (PB 231 172)A06

EERC 74-4 "LUSH - A Computer Program for Complex Response Analysis of Soil-Structure Systems," by J. Lysmer, T. Udaka, H.B. Seed and R. Hwang - 1974 (PB 236 796)A05

EERC 74-5 "Sensitivity Analysis for Hysteretic Dynamic Systems: Applications to Earthquake Engineering," by D. Ray 1974 (Pa 233 213)A06

EERC 74-6 "Soil Structure Interaction Analyses for Evaluating Seismic Response," by H.B. Seed, J. Lysmer and R. Hwang 1974 (PB 236 519)A04

EERC 74-7 Unassigned

EERC 74-8 "Shaking Table Tests of a Steel Frame - A Progress Report," by R.W. Clough and D. Tang - 1974 (PB 240 869)A03

EERC 74-9 "Hysteretic Behavior of Reinforced Concrete Flexural Members with Special Web Reinforcement," by V.V. Bertero, E.P. Popov and T.Y. Wang - 1974 (PB 236 797)A07

EERC 74-10 "Applications of Reliability-Based, Global Cost Optimization to Design of Earthquake Resistant Structures," by E. Vitiello and K.S. Pister - 1974 (PB 237 231)A06

EERC 74-11 "Liquefaction of Gravelly Soils Under Cyclic Loading Conditions," by R.T. Wong, H.B. Seed and C.K. Chan 1974 (PB 242 042)A03

EERC 74-12 "Site-Dependent Spectra for Earthquake-Resistant Design," by H.B. Seed, C. Ugas and J. Lysmer - 1974 (PB 240 953)A03

EERC 74-13 "Earthquake Simulator Study of a Reinforced Concrete Frame," by P. Hidalgo and R.W. Clough - 1974 (PB 241 974)A13

EERC 74-14 "Nonlinear Earthquake Response of Concrete Gravity Dams," by N. Pal - 1974 (AD/A 006 583)A06

EERC 74-15 "Modeling and Identification in Nonlinear Structural Dynamics - I. One Degree of Freedom Models," by N. Distefano and A. Rath - 1974 (PB 241 548)A06

EERC 75-1 "Determination of Seismic Design Criteria for the Dumbarton Bridge Replacement Structure, Vol. I: Description, Theory and Analytical Modeling of Bridge and Parameters," by F. Baron and S.-H. Pang - 1975 (PB 259 407)A15

EERC 75-2 "Determination of Seismic Design Criteria for the Dumbarton Bridge Replacement Structure, Vol. II: Numerical Studies and Establishment of Seismic Design Criteria," by F. Baron and S.-H. Pang - 1975 (PB 259 408)A11 (For set of EERC 75-1 and 75-2 (PB 259 406))

EERC 75-3 "Seismic Risk Analysis for a Site and a Metropolitan Area," by C.S. Oliveira - 1975 (PB 248 134)A09

EERC 75-4 "Analytical Investigations of Seismic Response of Short, Single or Multiple-Span Highway Bridges," by M.-C. Chen and J. Penzien - 1975 (PB 241 454)A09

EERC 75-5 "An Evaluation of Some Methods for Predicting Seismic Behavior of Reinforced Concrete Buildings," by S.A. Mahin and V.V. Bertero - 1975 (PB 246 306)A16

EERC 75-6 "Earthquake Simulator Study of a Steel Frame Structure, Vol. I: Experimental Results," by R.W. Clough and D.T. Tang - 1975 (PB 243 981)A13

EERC 75-7 "Dynamic Properties of San Bernardino Intake Tower," by D. Rea, C.-Y. Liaw and A.K. Chopra - 1975 (AD/A008 406) A05

EERC 75-8 "Seismic Studies of the Articulation for the Dumbarton Bridge Replacement Structure, Vol. I: Description, Theory and Analytical Modeling of Bridge Components," by F. Baron and R.E. Hamati - 1975 (PB 251 539)A07

EERC 75-9 "Seismic Studies of the Articulation for the Dumbarton Bridge Replacement Structure, Vol. 2: Numerical Studies of Steel and Concrete Girder Alternates," by F. Baron and R.E. Hamati - 1975 (PB 251 540)A10

EERC 75-10 "Static and Dynamic Analysis of Nonlinear Structures," by D.P. Mondkar and G.H. Powell - 1975 (PB 242 434)A08

EERC 75-11 "Hysteretic Behavior of Steel Columns," by E.P. Popov, V.V. Bertero and S. Chandramouli - 1975 (PB 252 365)A11

EERC 75-12 "Earthquake Engineering Research Center Library Printed Catalog," - 1975 (PB 243 711)A26

EERC 75-13 "Three Dimensional Analysis of Building Systems (Extended Version)," by E.L. Wilson, J.P. Hollings and H.H. Dovey - 1975 (PB 243 989)A07

EERC 75-14 "Determination of Soil Liquefaction Characteristics by Large-Scale Laboratory Tests," by P. De Alba, C.K. Chan and H.B. Seed - 1975 (NUREG 0027)A08

EERC 75-15 "A Literature Survey - Compressive, Tensile, Bond and Shear Strength of Masonry," by R.L. Mayes and R.W. Clough - 1975 (PB 246 292)A10

EERC 75-16 "Hysteretic Behavior of Ductile Moment Resisting Reinforced Concrete Frame Components," by V.V. Bertero and E.P. Popov - 1975 (PB 246 388)A05

EERC 75-17 "Relationships Between Maximum Acceleration, Maximum Velocity, Distance from Source, Local Site Conditions for Moderately Strong Earthquakes," by H.B. Seed, R. Murarka, J. Lysmer and I.M. Idriss - 1975 (PB 248 172)A03

EERC 75-18 "The Effects of Method of Sample Preparation on the Cyclic Stress-Strain Behavior of Sands," by J. Mulilis, C.K. Chan and H.B. Seed - 1975 (Summarized in EERC 75-28)

EERC 75-19 "The Seismic Behavior of Critical Regions of Reinforced Concrete Components as Influenced by Moment, Shear and Axial Force," by M.B. Atalay and J. Penzien - 1975 (PB 258 842)A11

EERC 75-20 "Dynamic Properties of an Eleven Story Masonry Building," by R.M. Stephen, J.P. Hollings, J.G. Bouwkamp and D. Jurukovski - 1975 (PB 246 945)A04

EERC 75-21 "State-of-the-Art in Seismic Strength of Masonry - An Evaluation and Review," by R.L. Mayes and R.W. Clough 1975 (PB 249 040)A07

EERC 75-22 "Frequency Dependent Stiffness Matrices for Viscoelastic Half-Plane Foundations," by A.K. Chopra, P. Chakrabarti and G. Dasgupta - 1975 (PB 248 121)A07

EERC 75-23 "Hysteretic Behavior of Reinforced Concrete Framed Walls," by T.Y. Wong, V.V. Bertero and E.P. Popov - 1975

EERC 75-24 "Testing Facility for Subassemblages of Frame-Wall Structural Systems," by V.V. Bertero, E.P. Popov and T. Endo - 1975

EERC 75-25 "Influence of Seismic History on the Liquefaction Characteristics of Sands," by H.B. Seed, K. Mori and C.K. Chan - 1975 (Summarized in EERC 75-28)

EERC 75-26 "The Generation and Dissipation of Pore Water Pressures during Soil Liquefaction," by H.B. Seed, P.P. Martin and J. Lysmer - 1975 (PB 252 648)A03

EERC 75-27 "Identification of Research Needs for Improving Aseismic Design of Building Structures," by V.V. Bertero 1975 (PB 248 136)A05

EERC 75-28 "Evaluation of Soil Liquefaction Potential during Earthquakes," by H.B. Seed, I. Arango and C.K. Chan - 1975 (NUREG 0026)A13

EERC 75-29 "Representation of Irregular Stress Time Histories by Equivalent Uniform Stress Series in Liquefaction Analyses," by H.B. Seed, I.M. Idriss, F. Makdisi and N. Banerjee - 1975 (PB 252 635)A03

EERC 75-30 "FLUSH - A Computer Program for Approximate 3-D Analysis of Soil-Structure Interaction Problems," by J. Lysmer, T. Udaka, C.-F. Tsai and H.B. Seed - 1975 (PB 259 332)A07

EERC 75-31 "ALUSH - A Computer Program for Seismic Response Analysis of Axisymmetric Soil-Structure Systems," by E. Berger, J. Lysmer and H.B. Seed - 1975

EERC 75-32 "TRIP and TRAVEL - Computer Programs for Soil-Structure Interaction Analysis with Horizontally Travelling Waves," by T. Udaka, J. Lysmer and H.B. Seed - 1975

EERC 75-33 "Predicting the Performance of Structures in Regions of High Seismicity," by J. Penzien - 1975 (PB 248 130)A03

EERC 75-34 "Efficient Finite Element Analysis of Seismic Structure - Soil - Direction," by J. Lysmer, H.B. Seed, T. Udaka, R.N. Hwang and C.-F. Tsai - 1975 (PB 253 570)A03

EERC 75-35 "The Dynamic Behavior of a First Story Girder of a Three-Story Steel Frame Subjected to Earthquake Loading," by R.W. Clough and L.-Y. Li - 1975 (PB 248 841)A05

EERC 75-36 "Earthquake Simulator Study of a Steel Frame Structure, Volume II - Analytical Results," by D.T. Tang - 1975 (PB 252 926)A10

EERC 75-37 "ANSR-I General Purpose Computer Program for Analysis of Non-Linear Structural Response," by D.P. Mondkar and G.H Powell - 1975 (PB 252 386)A08

EERC 75-38 "Nonlinear Response Spectra for Probabilistic Seismic Design and Damage Assessment of Reinforced Concrete Structures," by M. Murakami and J. Penzien - 1975 (PB 259 530)A05

EERC 75-39 "Study of a Method of Feasible Directions for Optimal Elastic Design of Frame Structures Subjected to Earthquake Loading," by N.D. Walker and K.S. Pister - 1975 (PB 257 781)A06

EERC 75-40 "An Alternative Representation of the Elastic-Viscoelastic Analogy," by G. Dasgupta and J.L. Sackman - 1975 (PB 252 173)A03

EERC 75-41 "Effect of Multi-Directional Shaking on Liquefaction of Sands," by H.B. Seed, R. Pyke and G.R. Martin - 1975 (PB 258 781)A03

EERC 76-1 "Strength and Ductility Evaluation of Existing Low-Rise Reinforced Concrete Buildings - Screening Method," by T. Okada and B. Bresler - 1976 (PB 257 906)A11

EERC 76-2 "Experimental and Analytical Studies on the Hysteretic Behavior of Reinforced Concrete Rectangular and T-Beams," by S.-Y.M. Ma, E.P. Popov and V.V. Bertero - 1976 (PB 260 843)A12

EERC 76-3 "Dynamic Behavior of a Multistory Triangular-Shaped Building," by J. Petrovski, R.M. Stephen, E. Gartenbaum and J.G. Bouwkamp - 1976 (PB 273 279)A07

EERC 76-4 "Earthquake Induced Deformations of Earth Dams," by N. Serff, H.B. Seed, F.I. Makdisi & C.-Y. Chang - 1976 (PB 292 065)A08

EERC 76-5 "Analysis and Design of Tube-Type Tall Building Structures," by H. de Clercq and G.H. Powell - 1976 (PB 252 220) A10

EERC 76-6 "Time and Frequency Domain Analysis of Three-Dimensional Ground Motions, San Fernando Earthquake," by T. Kubo and J. Penzien (PB 260 556)A11

EERC 76-7 "Expected Performance of Uniform Building Code Design Masonry Structures," by R.L. Mayes, Y. Omote, S.W. Chen and R.W. Clough - 1976 (PB 270 098)A05

EERC 76-8 "Cyclic Shear Tests of Masonry Piers, Volume 1 - Test Results," by R.L. Mayes, Y. Omote, R.W. Clough - 1976 (PB 264 424)A06

EERC 76-9 "A Substructure Method for Earthquake Analysis of Structure - Soil Interaction," by J.A. Gutierrez and A.K. Chopra - 1976 (PB 257 783)A08

EERC 76-10 "Stabilization of Potentially Liquefiable Sand Deposits using Gravel Drain Systems," by H.B. Seed and J.R. Booker - 1976 (PB 258 820)A04

EERC 76-11 "Influence of Design and Analysis Assumptions on Computed Inelastic Response of Moderately Tall Frames," by G.H. Powell and D.G. Row - 1976 (PB 271 409)A06

EERC 76-12 "Sensitivity Analysis for Hysteretic Dynamic Systems: Theory and Applications," by D. Ray, K.S. Pister and E. Polak - 1976 (PB 262 859)A04

EERC 76-13 "Coupled Lateral Torsional Response of Buildings to Ground Shaking," by C.L. Kan and A.K. Chopra - 1976 (PB 257 907)A09

EERC 76-14 "Seismic Analyses of the Banco de America," by V.V. Bertero, S.A. Mahin and J.A. Hollings - 1976

EERC 76-15 "Reinforced Concrete Frame 2: Seismic Testing and Analytical Correlation," by R.W. Clough and J. Gidwani - 1976 (PB 261 323)A08

EERC 76-16 "Cyclic Shear Tests of Masonry Piers, Volume 2 - Analysis of Test Results," by R.L. Mayes, Y. Omote and R.W. Clough - 1976

EERC 76-17 "Structural Steel Bracing Systems: Behavior Under Cyclic Loading," by E.P. Popov, K. Takanashi and C.W. Roeder - 1976 (PB 260 715)A05

EERC 76-18 "Experimental Model Studies on Seismic Response of High Curved Overcrossings," by D. Williams and W.G. Godden - 1976 (PB 269 548)A08

EERC 76-19 "Effects of Non-Uniform Seismic Disturbances on the Dumbarton Bridge Replacement Structure," by F. Baron and R.E. Hamati - 1976 (PB 282 981)A16

EERC 76-20 "Investigation of the Inelastic Characteristics of a Single Story Steel Structure Using System Identification and Shaking Table Experiments," by V.C. Matzen and H.D. McNiven - 1976 (PB 258 453)A07

EERC 76-21 "Capacity of Columns with Splice Imperfections," by E.P. Popov, R.M. Stephen and R. Philbrick - 1976 (PB 260 378)A04

EERC 76-22 "Response of the Olive View Hospital Main Building during the San Fernando Earthquake," by S. A. Mahin, V.V. Bertero, A.K. Chopra and R. Collins - 1976 (PB 271 425)A14

EERC 76-23 "A Study on the Major Factors Influencing the Strength of Masonry Prisms," by N.M. Mostaghel, R.L. Mayes, R. W. Clough and S.W. Chen - 1976 (Not published)

EERC 76-24 "GADFLEA - A Computer Program for the Analysis of Pore Pressure Generation and Dissipation during Cyclic or Earthquake Loading," by J.R. Booker, M.S. Rahman and H.B. Seed - 1976 (PB 263 947)A04

EERC 76-25 "Seismic Safety Evaluation of a R/C School Building," by B. Bresler and J. Axley - 1976

EERC 76-26 "Correlative Investigations on Theoretical and Experimental Dynamic Behavior of a Model Bridge Structure," by K. Kawashima and J. Penzien - 1976 (PB 263 388)A11

EERC 76-27 "Earthquake Response of Coupled Shear Wall Buildings," by T. Srichatrapimuk - 1976 (PB 265 157)A07

EERC 76-28 "Tensile Capacity of Partial Penetration Welds," by E.P. Popov and R.M. Stephen - 1976 (PB 262 899)A03

EERC 76-29 "Analysis and Design of Numerical Integration Methods in Structural Dynamics," by H.M. Hilber - 1976 (PB 264 410)A06

EERC 76-30 "Contribution of a Floor System to the Dynamic Characteristics of Reinforced Concrete Buildings," by L.E. Malik and V.V. Bertero - 1976 (PB 272 247)A13

EERC 76-31 "The Effects of Seismic Disturbances on the Golden Gate Bridge," by F. Baron, M. Arikan and R.E. Hamati - 1976 (PB 272 279)A09

EERC 76-32 "Infilled Frames in Earthquake Resistant Construction," by R.E. Klingner and V.V. Bertero - 1976 (PB 265 892)A13

UCB/EERC-77/01 "PLUSH - A Computer Program for Probabilistic Finite Element Analysis of Seismic Soil-Structure Interaction," by M.P. Romo Organista, J. Lysmer and H.B. Seed - 1977

UCB/EERC-77/02 "Soil-Structure Interaction Effects at the Humboldt Bay Power Plant in the Ferndale Earthquake of June 7, 1975," by J.E. Valera, H.B. Seed, C.F. Tsai and J. Lysmer - 1977 (PB 265 795)A04

UCB/EERC-77/03 "Influence of Sample Disturbance on Sand Response to Cyclic Loading," by K. Mori, H.B. Seed and C.K. Chan - 1977 (PB 267 352)A04

UCB/EERC-77/04 "Seismological Studies of Strong Motion Records," by J. Shoja-Taheri - 1977 (PB 269 655)A10

UCB/EERC-77/05 "Testing Facility for Coupled-Shear Walls," by L. Li-Hyung, V.V. Bertero and E.P. Popov - 1977

UCB/EERC-77/06 "Developing Methodologies for Evaluating the Earthquake Safety of Existing Buildings," by No. 1 - B. Bresler; No. 2 - B. Bresler, T. Okada and D. Zisling; No. 3 - T. Okada and B. Bresler; No. 4 - V.V. Bertero and B. Bresler - 1977 (PB 267 354)A08

UCB/EERC-77/07 "A Literature Survey - Transverse Strength of Masonry Walls," by Y. Omote, R.L. Mayes, S.W. Chen and R.W. Clough - 1977 (PB 277 933)A07

UCB/EERC-77/08 "DRAIN-TABS: A Computer Program for Inelastic Earthquake Response of Three Dimensional Buildings," by R. Guendelman-Israel and G.H. Powell - 1977 (PB 270 693)A07

UCB/EERC-77/09 "SUBWALL: A Special Purpose Finite Element Computer Program for Practical Elastic Analysis and Design of Structural Walls with Substructure Option," by D.Q. Le, H. Peterson and E.P. Popov - 1977 (PB 270 567)A05

UCB/EERC-77/10 "Experimental Evaluation of Seismic Design Methods for Broad Cylindrical Tanks," by D.P. Clough (PB 272 280)A13

UCB/EERC-77/11 "Earthquake Engineering Research at Berkeley - 1976," - 1977 (PB 273 507)A03

UCB/EERC-77/12 "Automated Design of Earthquake Resistant Multistory Steel Building Frames," by N.D. Walker, Jr. - 1977 (PB 276 526)A09

UCB/EERC-77/13 "Concrete Confined by Rectangular Hoops Subjected to Axial Loads," by J. Vallenas, V.V. Bertero and E.P. Popov - 1977 (PB 275 165)A06

UCB/EERC-77/14 "Seismic Strain Induced in the Ground During Earthquakes," by Y. Sugimura - 1977 (PB 284 201)A04

UCB/EERC-77/15 "Bond Deterioration under Generalized Loading," by V.V. Bertero, E.P. Popov and S. Viwathanatepa - 1977

UCB/EERC-77/16 "Computer Aided Optimum Design of Ductile Reinforced Concrete Moment Resisting Frames," by S.W. Zagajeski and V.V. Bertero - 1977 (PB 280 137)A07

UCB/EERC-77/17 "Earthquake Simulation Testing of a Stepping Frame with Energy-Absorbing Devices," by J.M. Kelly and D.F. Tsztoo - 1977 (PB 273 506)A04

UCB/EERC-77/18 "Inelastic Behavior of Eccentrically Braced Steel Frames under Cyclic Loadings," by C.W. Roeder and E.P. Popov - 1977 (PB 275 526)A15

UCB/EERC-77/19 "A Simplified Procedure for Estimating Earthquake-Induced Deformations in Dams and Embankments," by F.I. Makdisi and H.B. Seed - 1977 (PB 276 820)A04

UCB/EERC-77/20 "The Performance of Earth Dams during Earthquakes," by H.B. Seed, F.I. Makdisi and P. de Alba - 1977 (PB 276 821)A04

UCB/EERC-77/21 "Dynamic Plastic Analysis Using Stress Resultant Finite Element Formulation," by P. Lukkunapvasit and J.M. Kelly - 1977 (PB 275 453)A04

UCB/EERC-77/22 "Preliminary Experimental Study of Seismic Uplift of a Steel Frame," by R.W. Clough and A.A. Huckelbridge 1977 (PB 278 769)A08

UCB/EERC-77/23 "Earthquake Simulator Tests of a Nine-Story Steel Frame with Columns Allowed to Uplift," by A.A. Huckelbridge - 1977 (PB 277 944)A09

UCB/EERC-77/24 "Nonlinear Soil-Structure Interaction of Skew Highway Bridges," by M.-C. Chen and J. Penzien - 1977 (PB 276 176)A07

UCB/EERC-77/25 "Seismic Analysis of an Offshore Structure Supported on Pile Foundations," by D.D.-N. Liou and J. Penzien 1977 (PB 283 180)A06

UCB/EERC-77/26 "Dynamic Stiffness Matrices for Homogeneous Viscoelastic Half-Planes," by G. Dasgupta and A.K. Chopra - 1977 (PB 279 654)A06

UCB/EERC-77/27 "A Practical Soft Story Earthquake Isolation System," by J.M. Kelly, J.M. Eidinger and C.J. Derham - 1977 (PB 276 814)A07

UCB/EERC-77/28 "Seismic Safety of Existing Buildings and Incentives for Hazard Mitigation in San Francisco: An Exploratory Study," by A.J. Meltsner - 1977 (PB 281 970)A05

UCB/EERC-77/29 "Dynamic Analysis of Electrohydraulic Shaking Tables," by D. Rea, S. Abedi-Hayati and Y. Takahashi 1977 (PB 282 569)A04

UCB/EERC-77/30 "An Approach for Improving Seismic - Resistant Behavior of Reinforced Concrete Interior Joints," by B. Galunic, V.V. Bertero and E.P. Popov - 1977 (PB 290 870)A06

UCB/EERC-78/01 "The Development of Energy-Absorbing Devices for Aseismic Base Isolation Systems," by J.M. Kelly and D.F. Tsztoo - 1978 (PB 284 978)A04

UCB/EERC-78/02 "Effect of Tensile Prestrain on the Cyclic Response of Structural Steel Connections, by J.G. Bouwkamp and A. Mukhopadhyay - 1978

UCB/EERC-78/03 "Experimental Results of an Earthquake Isolation System using Natural Rubber Bearings," by J.M. Eidinger and J.M. Kelly - 1978 (PB 281 686)A04

UCB/EERC-78/04 "Seismic Behavior of Tall Liquid Storage Tanks," by A. Niwa - 1978 (PB 284 017)A14

UCB/EERC-78/05 "Hysteretic Behavior of Reinforced Concrete Columns Subjected to High Axial and Cyclic Shear Forces," by S.W. Zagajeski, V.V. Bertero and J.G. Bouwkamp - 1978 (PB 283 858)A13

UCB/EERC-78/06 "Inelastic Beam-Column Elements for the ANSR-I Program," by A. Riahi, D.G. Row and G.H. Powell - 1978

UCB/EERC-78/07 "Studies of Structural Response to Earthquake Ground Motion," by O.A. Lopez and A.K. Chopra - 1978 (PB 282 790)A05

UCB/EERC-78/08 "A Laboratory Study of the Fluid-Structure Interaction of Submerged Tanks and Caissons in Earthquakes," by R.C. Byrd - 1978 (PB 284 957)A08

UCB/EERC-78/09 "Model for Evaluating Damageability of Structures," by I. Sakamoto and B. Bresler - 1978

UCB/EERC-78/10 "Seismic Performance of Nonstructural and Secondary Structural Elements," by I. Sakamoto - 1978

UCB/EERC-78/11 "Mathematical Modelling of Hysteresis Loops for Reinforced Concrete Columns," by S. Nakata, T. Sproul and J. Penzien - 1978

UCB/EERC-78/12 "Damageability in Existing Buildings," by T. Blejwas and B. Bresler - 1978

UCB/EERC-78/13 "Dynamic Behavior of a Pedestal Base Multistory Building," by R.M. Stephen, E.L. Wilson, J.G. Bouwkamp and M. Button - 1978 (PB 286 650)A08

UCB/EERC-78/14 "Seismic Response of Bridges - Case Studies," by R.A. Imbsen, V. Nutt and J. Penzien - 1978 (PB 286 503)A10

UCB/EERC-78/15 "A Substructure Technique for Nonlinear Static and Dynamic Analysis," by D.G. Row and G.H. Powell - 1978 (PB 288 077)A10

UCB/EERC-78/16 "Seismic Risk Studies for San Francisco and for the Greater San Francisco Bay Area," by C.S. Oliveira - 1978

UCB/EERC-78/17 "Strength of Timber Roof Connections Subjected to Cyclic Loads," by P. Gülkan, R.L. Mayes and R.W. Clough - 1978

UCB/EERC-78/18 "Response of K-Braced Steel Frame Models to Lateral Loads," by J.G. Bouwkamp, R.M. Stephen and E.P. Popov - 1978

UCB/EERC-78/19 "Rational Design Methods for Light Equipment in Structures Subjected to Ground Motion," by J.L. Sackman and J.M. Kelly - 1978 (PB 292 357)A04

UCB/EERC-78/20 "Testing of a Wind Restraint for Aseismic Base Isolation," by J.M. Kelly and D.E. Chitty - 1978 (PB 292 833)A03

UCB/EERC-78/21 "APOLLO - A Computer Program for the Analysis of Pore Pressure Generation and Dissipation in Horizontal Sand Layers During Cyclic or Earthquake Loading," by P.P. Martin and H.B. Seed - 1978 (PB 292 835)A04

UCB/EERC-78/22 "Optimal Design of an Earthquake Isolation System," by M.A. Bhatti, K.S. Pister and E. Polak - 1978 (PB 294 735)A06

UCB/EERC-78/23 "MASH - A Computer Program for the Non-Linear Analysis of Vertically Propagating Shear Waves in Horizontally Layered Deposits," by P.P. Martin and H.B. Seed - 1978 (PB 293 101)A05

UCB/EERC-78/24 "Investigation of the Elastic Characteristics of a Three Story Steel Frame Using System Identification," by I. Kaya and H.D. McNiven - 1978

UCB/EERC-78/25 "Investigation of the Nonlinear Characteristics of a Three-Story Steel Frame Using System Identification," by I. Kaya and H.D. McNiven - 1978

UCB/EERC-78/26 "Studies of Strong Ground Motion in Taiwan," by Y.M. Hsiung, B.A. Bolt and J. Penzien - 1978

UCB/EERC-78/27 "Cyclic Loading Tests of Masonry Single Piers: Volume 1 - Height to Width Ratio of 2," by P.A. Hidalgo, R.L. Mayes, H.D. McNiven and R.W. Clough - 1978

UCB/EERC-78/28 "Cyclic Loading Tests of Masonry Single Piers: Volume 2 - Height to Width Ratio of 1," by S.-W.J. Chen, P.A. Hidalgo, R.L. Mayes, R.W. Clough and H.D. McNiven - 1978

UCB/EERC-78/29 "Analytical Procedures in Soil Dynamics," by J. Lysmer - 1978

UCb/EERC-79/01 "Hysteretic Behavior of Lightweight Reinforced Concrete Beam-Column Subassemblages," by B. Forzani, E.P. Popov, and V.V. Bertero - 1979

UCB/EERC-79/02 "The Development of a Mathematical Model to Predict the Flexural Response of Reinforced Concrete Beams to Cyclic Loads, Using System Identification," by J.F. Stanton and H.D. McNiven - 1979

UCB/EERC-79/03 "Linear and Nonlinear Earthquake Response of Simple Torsionally Coupled Systems," by C.L. Kan and A.K. Chopra - 1979

UCB/EERC-79/04 "A Mathematical Model of Masonry for Predicting Its Linear Seismic Response Characteristics," by Y. Mengi and H.D. McNiven - 1979

UCB/EERC-79/05 "Mechanical Behavior of Light Weight Concrete Confined by Different Types of Lateral Reinforcement," by M.A. Manrique, V.V. Bertero and E.P. Popov - 1979

UCB/EERC-79/06 "Static Tilt Tests of a Tall Cylindrical Liquid Storage Tank," by R.W. Clough and A. Niwa - 1979

UCB/EERC-79/07 "The Design of Steel Energy Absorbing Restrainers and Their Incorporation Into Nuclear Power Plants for Enhanced Safety: Volume 1 - Summary Report," by P.N. Spencer, V.F. Zackay, and E.R. Parker - 1979

UCB/EERC-79/08 "The Design of Steel Energy Absorbing Restrainers and Their Incorporation Into Nuclear Power Plants for Enhanced Safety: Volume 2 - The Development of Analyses for Reactor System Piping," "Simple Systems" by M.C. Lee, J. Penzien, A.K. Chopra, and K. Suzuki "Complex Systems" by G.H. Powell, E.L. Wilson, R.W. Clough and D.G. Row - 1979

UCB/EERC-79/09 "The Design of Steel Energy Absorbing Restrainers and Their Incorporation Into Nuclear Power Plants for Enhanced Safety: Volume 3 - Evaluation of Commerical Steels," by W.S. Owen, R.M.N. Pelloux, R.O. Ritchie, M. Faral, T. Ohhashi, J. Toplosky, S.J. Hartman, V.F. Zackay, and E.R. Parker - 1979

UCB/EERC-79/10 "The Design of Steel Energy Absorbing Restrainers and Their Incorporation Into Nuclear Power Plants for Enhanced Safety: Volume 4 - A Review of Energy-Absorbing Devices," by J.M. Kelly and M.S. Skinner - 1979

UCB/EERC-79/11 "Conservatism In Summation Rules for Closely Spaced Modes," by J.M. Kelly and J.L. Sackman - 1979

UCB/EERC-79/12 "Cyclic Loading Tests of Masonry Single Piers Volume 3 - Height to Width Ratio of 0.5," by P.A. Hidalgo, R.L. Mayes, H.D. McNiven and R.W. Clough - 1979

UCB/EERC-79/13 "Cyclic Behavior of Dense Coarse-Grain Materials in Relation to the Seismic Stability of Dams," by N.G. Banerjee, H.B. Seed and C.K. Chan - 1979

UCB/EERC-79/14 "Seismic Behavior of R/C Interior Beam Column Subassemblages," by S. Viwathanatepa, E.P. Popov and V.V. Bertero - 1979

UCB/EERC-79/15 "Optimal Design of Localized Nonlinear Systems with Dual Performance Criteria Under Earthquake Excitations," by M.A. Bhatti - 1979

UCB/EERC-79/16 "OPTDYN - A General Purpose Optimization Program for Problems with or without Dynamic Constraints," by M.A. Bhatti, E. Polak and K.S. Pister - 1979

UCB/EERC-79/17 "ANSR-II, Analysis of Nonlinear Structural Response, Users Manual," by D.P. Mondkar and G.H. Powell - 1979

UCB/EERC-79/18 "Soil Structure Interaction in Different Seismic Environments," A. Gomez-Masso, J. Lysmer, J.-C. Chen and H.B. Seed - 1979

UCB/EERC-79/19 "ARMA Models for Earthquake Ground Motions," by M.K. Chang, J.W. Kwiatkowski, R.F. Nau, R.M. Oliver and K.S. Pister - 1979

UCB/EERC-79/20 "Hysteretic Behavior of Reinforced Concrete Structural Walls," by J.M. Vallenas, V.V. Bertero and E.P. Popov - 1979

UCB/EERC-79/21 "Studies on High-Frequency Vibrations of Buildings I: The Column Effects," by J. Lubliner - 1979

UCB/EERC-79/22 "Bond Deterioration of Reinforcing Bars Embedded in Confined Concrete Blocks," by S. Viwathanatepa, E.P. Popov and V.V. Bertero - 1979

UCB/EERC-79/23 "Shaking Table Study of Single-Story Masonry Houses, Volume 1: Test Structures 1 and 2," by P. Gülkan, R.L. Mayes and R.W. Clough - 1979

UCB/EERC-79/24 "Shaking Table Study of Single-Story Masonry Houses, Volume 2: Test Structures 3 and 4," by P. Gülkan, R.L. Mayes and R.W. Clough - 1979

UCB/EERC-79/25 "Shaking Table Study of Single-Story Masonry Houses, Volume 3: Summary, Conclusions and Recommendations," by R.W. Clough, P. Gülkan and R.L. Mayes

For sale by the National Technical Information Service, U. S. Department of Commerce, Springfield, Virginia 22161.

See back of report for up to date listing of EERC reports.